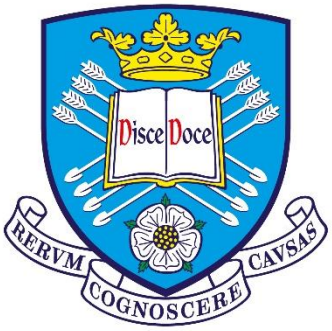

The University Of Sheffield.

Elucidating the role of NrCAM in the hypothalamic stem cell niche

A thesis submitted to the University of Sheffield

For the degree of Doctor of Philosophy

By

Alexander Moore

Department of Biomedical Science

October 2018

DECLARATION

I hereby declare that this thesis has not been and will not be submitted, in whole or in part, to another University for the award of any other degree.

Alexander Moore

ACKNOWLEDGEMENTS

The project has been made possible by the dedication of my supervisors, Prof Andrew Furley and Prof Marysia Placzek. Their wealth of knowledge and technical expertise has been invaluable for planning and troubleshooting experiments, and for contextualising results. Their hard work and patience has helped bring me to where I am today. My advisers Dr Freek van Eeden and Prof Peter Andrews have provided useful advice and consideration from an outside perspective that has assisted my research throughout its course. Additionally, this second edition would not be complete without giving thanks to my examiners Dr Jo Lewis and Dr Ivana Barbaric, who provided a rigorous and stimulating viva discussion.

Dr Sarah Brown and Dr Iain Stewart started my research and developed several of the ideas we have carried forward. Their discussions and advice during in my early studies guided the way I approached the project. I must also thank Basudha Basu, Pam Ellis, Travis Fu, and the other members of the D18 labs who have trained me, supported me, and cultured a welcoming environment to work in.

My friends have made this journey enjoyable. Whether you're from within the department, Sheffield, or the wider world, if we've shared a meaningful conversation or a few laughs over a pint, I want to thank you for being there for me. Extra special thanks go to my housemates from across the years – you've been fantastic.

I would not have my love of biology and science if it wasn't for my teachers at Desborough School. A special mention must go to Phil Mortimer, whose lessons on genetics and biotechnology brought biology to life.

My family, particularly my parents, can take a huge chunk of the credit for getting me to where I am today. They're always there to listen and provide sound advice. I'm sorry Debs, but the nerd talk at the dinner table has ended up being useful after all!

Finally, Rings. You've been amazing through and through. Thank you for loving me and suffering me in equal measures. Thank you for the support and the smiles and the patience to listen. You're the best.

ABSTRACT

Hypothalamic tanycytes are highly specialised glia that interface with the fenestrated capillaries of the median eminence, hypothalamic neurons, and the cerebrospinal fluid of the 3rd ventricle, serving a vital role in the regulation of homeostatic control. Stereotypically, tanycytes are divided into four subsets which express an array of different markers. Recent studies show that tanycytes in adult mice include a subset of neurogenic stem/progenitor cells, though reports conflict when identifying which subset is neurogenic. Furthermore, most reports focus on tanycytes in the medial hypothalamus, but do not discuss how their findings relate to tanycytes of anterior and posterior hypothalamic subregions.

In this study I characterise a variety of established tanycyte markers across the anterior-posterior axis of the hypothalamus, describe the cell adhesion molecule NrCAM as a new tanycyte marker, and show, for the first time, Sonic Hedgehog (Shh) expression in a tanycyte subset around the adult mouse 3rd ventricle. My results show that classic tanycyte subsets vary in dorso-ventral localisation across the anterior-posterior (A-P) hypothalamic axis, and suggest a new 3D model for tanycyte location that could improve on our understanding of tanycyte subset function. Based on the localisation of fibroblast growth factor 10 (Fgf10) and Shh in the adult posterior median eminence, I propose this region be further investigated as the site of a potential hypothalamic stem cell population.

I addition, I have begun to investigate the role of NrCAM by studying the hypothalamic phenotype in adult and embryonic mice lacking NrCAM. I show that loss of NrCAM induces a reduction of tanycytes and their embryonic radial-glial precursors. This is complemented by a decrease in hypothalamic dopaminergic neurons in adult mice, and an increase in the embryo. Together my work suggests a role for NrCAM in the development and/or maintenance of hypothalamic tanycytes and neuronal populations.

Publication and abstracts:

Elements of this work have been presented in a poster at the 2017 BSCB/BSDB/Genetics Society Spring Meeting (abstract below) and the KCL The Developing Brain in Health and Disease conference (2017).

This work has also been presented orally and as a poster for intra-departmental seminars.

Title 1: Is there a role for NrCAM in the hypothalamus? (BSDB/BSCB)

Title 2: Long term maintenance of hypothalamic tanycytes involves the function of neural cell adhesion molecules (KCL)

Alexander Moore, Andrew Furley, Marysia Placzek

The hypothalamus is a brain region dedicated to coordinating homeostasis. It consists of multiple discrete nuclei built around the third ventricle and above the median eminence. Recent research describes proliferative activity and de novo neurogenesis in the adult hypothalamus, and reveals that specialised radial glial-like cells called tanycytes derive from embryonic cells that maintain constitutive stem cell activity throughout life. Changes in local signals, and circulating levels of physiological signals can modulate a proliferative and neurogenic response in tanycytes, suggesting a plasticity that may be important postnatally.

Our work investigates whether the Neuronal Cell Adhesion Molecule (NrCAM) plays a role in the development and/or regulation of hypothalamic tanycytes. Our studies show that NrCAM is expressed on subsets of tanycytes and analysis of NrCAM knockout mice reveals abnormal tanycyte and neuron distribution in the adult hypothalamus. These observations point to a role for NrCAM in the regulation of hypothalamic stem cells.

TABLE OF CONTENTS

TABLE OF FIGURES AND TABLES

ABBREVIATIONS

3V – 3rd ventricle

A12/A13/A14/A15 – Dopaminergic cell groups

A-P – Anterior to posterior

AGRP – Agouti-related peptide

AHN – Anterior hypothalamic nucleus

AME – Anterior Median Eminence subregion

ARC – Arcuate nucleus

B27 – Neuronal cell culture supplement B27

BCIP – 5-bromo-4-chloro-3-indolyl-phosphate

BDNF – Brain derived neurotrophic factor

bFGF – Basic fibroblast growth factor

BMP – Bone morphogenetic protein

bp – Base pairs

BrdU – Bromodeoxyuridine

BSA – Bovine serum albumin

Ca – Calcium

CAM – Cell adhesion molecules

CHAPS – 3-[(3-Cholamidopropyl)dimethylammonio]-1-propanesulfonate hydrate

CHL1 – Close homologue of L1

Chk/*chokh* – Loss of function Rx3 zebrafish mutant

CNS – Central nervous system

CNTF – Ciliary neurotrophic factor

CO2/CO_2 – Carbon dioxide

CSF – Cerebrospinal fluid

CT – Computerised tomography scan

DAPI – 4′,6-diamidino-2-phenylindole blue-fluorescent DNA stain

DCX – Doublecortin

DEPC – Diethyl pyrocarbonate

DIG – Digoxigenin

DiI – DiIC18(3), fluorescent lipophilic cationic indocarbocyanine dye

DMEM – Dulbecco's modified Eagle medium

DMEM/F-12 – Dulbecco's modified Eagle medium with nutrient mixture F-12

DMN – Dorsomedial hypothalamic nucleus

DMSO – Dimethyl sulfoxide

DNA – Deoxyribonucleic acid

Drop-seq – mRNA sequencing from single cells suspended in droplets

E16 – Embryonic day 16

EDTA – Ethylenediaminetetraacetic acid

EGF – Epidermal growth factor

En1 – Engrailed homeobox 1

ELAV – Embryonic lethal abnormal visual system protein

Emx2 – Empty spiracles homeobox 2

FBS – Foetal bovine serum

FGF/Fgf – Fibroblast growth factor e.g. Fgf10

FGFR – Fibroblast growth factor receptor

FISH – Fluorescent *in situ* hybridisation

Foxg1 – Forkhead box G1

Foxd1 – Forkhead box D1

FSH – Follicle-stimulating hormone

GFAP – Glial fibrillary acidic protein

GFP – Green fluorescent protein

GHRH – Growth hormone-releasing hormone

GLAST – Glutamate aspartate transporter

GNP – Granule neuron precursor

GnRH – Gonadotropin-releasing hormone

HBSS – Hanks' Balanced Salt Solution

HCL – Hydrochloric acid

HEPES – 4-(2-hydroxyethyl)-1-piperazineethanesulfonic acid

HFD – High-fat diet

HuC/D – ELAV-like protein 3/4

HYP – Hypothalamus

IGF-1 – Insulin-like growth factor 1

IgSF CAM – Immunoglobulin superfamily cell adhesion molecule

IKKβ – Inhibitor of nuclear factor kappa-B kinase subunit beta

IR – Infundibular recess

Irx3 – Iroquois homeobox protein 3

ISH – *In situ* hybridisation

KO – Knock out

L1 – L1 cell adhesion molecule

L-15 – Leibovitz's 15 media

LepR – Leptin receptor

LH – Luteinising hormone

Lhx2 – LIM homeobox protein 2

LiCl – Lithium Chloride

MAP2 – Microtubule-associated protein 2

ME – Median Eminence

Mg – Magnesium

$MgCl_2$ – Magnesium chloride

MIP – Maximum intensity projection

MN – Mammillary nucleus

mRNA – Messenger ribonucleic acid

N – Number of samples

NaCl – Sodium Chloride

NaHCO3 – Sodium bicarbonate

NBT – 4-Nitro blue tetrazolium chloride

NF-κB – Nuclear factor kappa-B kinase subunit beta

NFASC - Neurofascin

Nkx2.1 – NK2 Homeobox 1

Nkx6.1 – NK6 Homeobox 1

NPY – Neuropeptide Y

NrCAM – Neuronal cell adhesion molecule/ NgCAM-related cell adhesion molecule

NSC – Neural stem cell

OC – Optic chiasm

OCT – Optimal cutting temperature compound

Opti-MEM – Reduced Serum Media modified from Eagle's minimum essential media

OS – Optic stalk

PB – Phosphate buffer

PBS – Phosphate buffered saline

PCR – Polymerase chain reaction

PFA PB – Paraformaldehyde solution in 0.12M phosphate buffer

p-H3 – Phospho-histone3

PHN – Posterior hypothalamic nucleus

PM – Prechordal mesoderm

PME – Posterior Median Eminence

POA – Preoptic area

POMC – Proopiomelanocortin

PS – Pituitary stalk

PVp – Periventricular hypothalamic nucleus (posterior part)

PVN – Paraventricular nucleus

PUFAs – polyunsaturated fatty acids

Rax – Retina and anterior neural fold homeobox gene

RDVM – Rostral diencephalic ventral midline

RGC – Radial glial cell

RIP – Antibody against 2',3'-cyclic nucleotide 3'-phosphodiesterase

RMS – Rostral migratory stream

RNA – Ribonucleic acid

RNA-seq – Ribonucleic acid sequencing

Rx3 – Retinal homeobox gene 3

SCN – Suprachiasmatic nucleus

SD – Standard deviation

SDS – Sodium dodecyl sulfate

Sema7a – Semaphorin-7a

SGZ – Subgranular zone

SMN – supramammillary nucleus

Shh/SHH – Sonic hedgehog

Six3 – Sine oculis homeobox homolog 3

Sox2 – SRY-box2

Sox3 – SRY-box3

SSC – Saline sodium citrate solution

SVZ – Subventricular zone

T3 – Triiodothyronine

T4 – Thyroxine

TAC – Transit amplifying cell

TAG1 – Transient axonal glycoprotein 1/Contactin 2

Tbx – T-box transcription factor

TGF-β – Transforming growth factor β

TH – Tyrosine hydroxlyase

TSHβ – Thyroid-stimulating hormone β

TRH – Thyrotropin-releasing hormone

VMN – Ventromedial hypothalamic nucleus

VZ – Ventricular zone

WT – Wildtype

YFP – Yellow fluorescent protein

ZO-1 – Zona occludens-1

CHAPTER 1: INTRODUCTION

1.1 The hypothalamus and tanycytes in coordination of homeostasis

1.1.1 Hypothalamic structure and function

The hypothalamus is a major regulator for organism-wide homeostasis and is found at the ventral border of the telencephalon and diencephalon. It is built around the 3rd ventricle (3V) and consists of multiple nuclei with different homeostatic roles (reviewed in Saper & Lowell, 2014). The hypothalamus can be split into roughly 4 regions along the anterior-posterior (rostro-caudal) axis: preoptic, anterior, tuberal, and mammillary (Fig 1.1 A). The preoptic region sits above the optic chiasm, and contains nuclei dedicated to thermoregulation, electrolyte balance, fertility and reproduction. The suprachiasmatic nucleus (SCN), which regulates sleep/wake cycle and circadian rhythms is shared between the preoptic region and the anterior region, which also contains the neurosecretory/neuroendocrine paraventricular nucleus (PVN). The tuberal region regulates feeding behaviour, energy balance, sexual behaviour, aggressiveness and stress, and lies above the median eminence and pituitary stalk. The median eminence is a unique structure found at the base of the third ventricle, bulging out of the hypothalamic pial surface (Yin and Gore, 2010). It contains one of the body's three portal capillary beds; the hypophyseal portal system, which connects the hypothalamus and the anterior pituitary gland. As such, the median eminence acts as the meeting place between the hypothalamic secretory neurons and the blood. Finally, the posterior region includes the mammillary bodies, and regulates arousal, wakefulness, and stress.

Figure 1.1 Overview of the hypothalamus

A – Sagittal schematic of the adult mouse hypothalamus. The hypothalamus has been divided into the 4 regions described: Preoptic (purple), Anterior (Blue), Tuberal/central (green), and Mammillary/posterior (orange). The grey vertical line bisecting the tuberal region indicates the section displayed in 1.1 B.

OC, Optic chiasm; POA, preoptic area; SCN, Suprachiasmatic nucleus; AHN, Anterior hypothalamic nucleus; SON, Supraoptic nucleus; PVN, Paraventricular nucleus; ARC, Arcuate nucleus; VMN, Venteromedial nucleus; DMN, Dorsomedial nucleus; ME, Median eminence; PS, Pituitary stalk; MN, Mammillary nucleus; SMN, Supramammillary nucleus; PHN, Posterior hypothalamic nucleus.

B – Coronal view of the central hypothalamus, through the section indicated in 1.1 A, outlining the various tanycyte subsets with respect to the local hypothalamic nuclei and the median eminence. α1-tanycytes project to the VMN, α2-tanyctes project to the ARC, β1- and β2-tanycytes project to the median eminence.

Figure 1.1

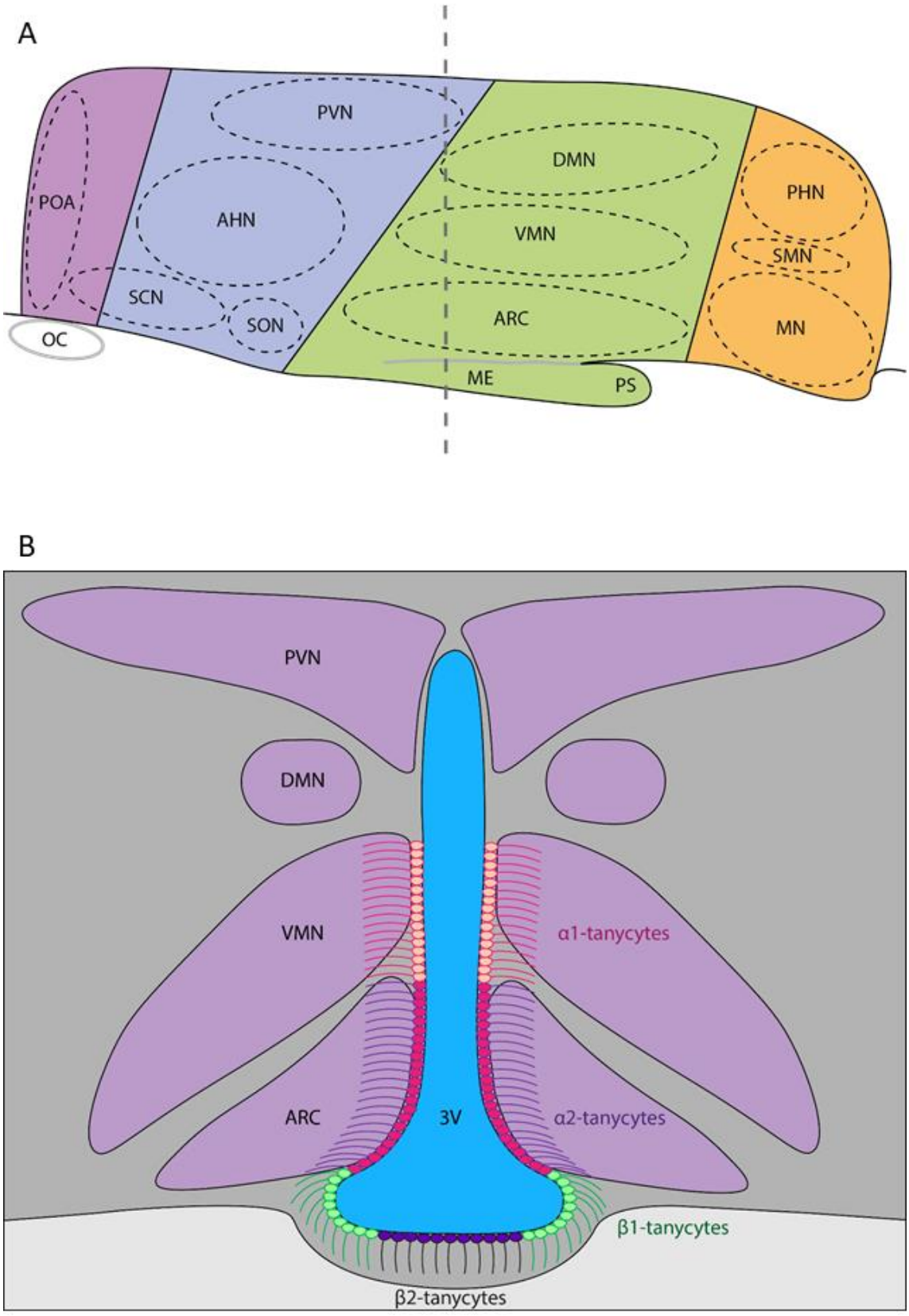
A
PVN
DMN
PHN
POA
AHN
VMN
SMN
SCN
ARC
MN
SON
OC
ME
PS
B
PVN
DMN
VMN
α1-tanycytes
ARC
3V
α2-tanycytes
β1-tanycytes
β2-tanycytes

To coordinate and integrate these processes, the hypothalamus monitors the blood via the fenestrated capillaries of the median eminence and the cerebral spinal fluid (CSF) of the 3rd ventricle. The fluctuations of various hormones and circulating molecules are interpreted by the corresponding nuclei which then coordinate a response. Outputs can be autonomic or endocrine in nature. In one such endocrine response, magnocellular neurons from the supraoptic nucleus and the PVN send projections through the pituitary stalk to the posterior pituitary, where they secrete hormones into the blood. An alternative output is through parvicellular neurons of the arcuate nucleus (ARC) and the PVN, which project to the median eminence, below the third ventricle. Here they contact the fenestrated hypophysial portal capillaries, outside the blood-brain barrier, and release hormones that travel directly to the anterior pituitary, initiating or inhibiting further hormone secretion.

1.1.2 Tanycytes: classification

Key to both the sensory input and parvicellular output are the specialised bipolar cells of the hypothalamus called tanycytes. Tanycytes resemble the radial-glial cell (RGC) progenitors of the developing brain (Anthony et al., 2004; Sild and Ruthazer, 2011; Tamamaki et al., 2001), and are situated around the lateral and ventral portions of the 3rd ventricle (Rodríguez et al., 2005). Their cell bodies line the line ventricle in the place of ependymocytes, and they have long processes that extend into the parenchyma of the brain. α-tanycytes are found along the lateral wall and project to various nuclei within the hypothalamus. β-tanycytes surround the median eminence and project to the fenestrated capillaries where they regulate hormone uptake and secretion (Rodríguez et al., 2005). At the distal end of these processes are structures known as tanycyte end-feet. The end-feet of β-tanycytes form part of the blood-brain barrier around the fenestrated capillaries and ensheath the neuronal terminals which release hormones into the bloodstream (Prevot et al., 2010; Rogers et al., 1997). The tanycyte subsets are further split into α1- and α2-, and β1- and β2-tanycytes, based on their dorso-ventral (D-V) location, their projections, and the markers they express (Fig 1.1B).

While this system of classification is widely accepted and used in the published literature, it is defined by fairly arbitrary metrics. To bolster the strength of these

classifications, and to investigate the properties of the different tanycyte subsets, research groups have identified and utilised a variety of markers that mark specific subsets. These include GLAST, GFAP, Fgf10, BLBP, and S-100β, as well as a variety of others (Goodman and Hajihosseini, 2015; Haan et al., 2013; Robins et al., 2013a). However, the expression domains of these markers often do not fit neatly into the established subsets, and as a consequence, different groups draw the boundaries between the tanycyte subsets in different places. For example, consider the diagrams in Figure 1.2 A and B, which are found in Robins et al., (2013) and Ebling & Lewis, (2018) respectively (reproduced here with author approval). Overall the diagrams are similar, however they differ over the boundary between the β/β1-tanycytes and the α2-tanycytes. In the diagram from Robins et al., (2013), α2-tanycytes have been split into ventral and dorsal α2-tanycytes based on results shown in the paper, and only α2-tanycytes project to the arcuate nucleus. The β-tanycytes are restricted to the ventral surface of the ventricle. In contrast, the Ebling & Lewis, (2018) review suggests that most of the tanycytes which project to the arcuate nucleus are in fact β1-tanycytes.

These differences are reflected in the experimental results of papers. For example, Figure 1.2 C and D are from Robins et al., (2013), and the authors are showing that addition of FGF2 increases neurogenesis. They use a BrdU pulse-chase experiment, in which mice are given an intraperitoneal injection of the radioactive nucleotide BrdU or EdU (the *pulse* phase). Cells undergoing S-phase of mitosis incorporate BrdU/EdU into the new DNA, labelling the dividing cell. For the *chase* phase, the investigators wait a specified time (in this case 6 weeks) then cull the mice and compare them to mice culled immediately after injection. Additional labelled cells in the *chase* samples are designated as progeny of the labelled cells.

Robins et al., (2013) say FGF2 induces neurogenesis in tanycytes, causing labelling of tanycyte nuclei by BrdU. They say these tanycytes are α2-tanycytes. Figure 1.2 E is adapted from a figure in Haan et al., (2013) (reproduced with author approval), in which the authors say Fgf10-expressing tanycytes (specifically the cells with their nuclei in the ventricular zone) are labelled by βgal, and some of these are proliferating and therefore co-label with EdU. They say these tanycytes are β-tanycytes. Side-by-side comparison of Figure 1.2 D

and E suggests the red BrdU-labelled cells overlap with the localisation of the green βgal-labelled cells, yet the groups claim they are different tanycyte subsets. These different interpretations lead to confusion and contradictory data when investigating tanycyte function and, in particular, neurogenesis (see section 1.2.3). This may be compounded by the reluctance of many research groups to thoroughly investigate the changes in tanycyte subsets in the more anterior and posterior aspects of the hypothalamus, instead treating this morphologically varied region as if it may all be represented by images from the medial hypothalamus (as shown in Fig 1.1 B and Fig 1.2 A-E, discussed further in section 1.2.3 and Chapter 4).

1.1.3 Tanycytes: function

Tanycytes have an array of functions important for hypothalamic regulation of homeostatic process (Prevot et al., 2018; Rodríguez et al., 2005). They monitor and conduct signals from the rest of the body, controlling their entry to the interstitial fluid of the hypothalamus via the median eminence or CSF. The anorexigenic (appetite suppressant) hormone Leptin produced by adipocytes controls food intake by activating the leptin receptors (LepR) in the hypothalamus, first in the arcuate nucleus and later in other nuclei regulating energy balance (Balland et al., 2014). When Leptin in the blood reaches the portal capillaries of the median eminence it is taken up by β-tanycyte end-feet, initiating p-STAT3 expression in the tanycyte processes and nuclei. The Leptin is transported from basal-apical within the tanycytes, and is released from the soma into the CSF. This release to the CSF is required for Leptin activate the mediobasal hypothalamic neurons (Balland et al., 2014). Tight junctions between β-tanycytes block the diffusion of molecules from the median eminence to the CSF and vice versa (Langlet et al., 2013a; Mullier et al., 2010), but the lack of tight junctions between α-tanycytes and ependymal cells allows the Leptin and other soluble to diffuse into the parenchymal tissue of the hypothalamus and activate the energy balancing homeostatic systems. In obese mice this transcellular trafficking pathway becomes inactive, whilst in fasting mice the tight junctions are reorganised to allow increased movement of metabolic factors between the median eminence, the CSF, and the parenchyma (Langlet et al., 2013b).

Figure 1.2 Comparison of tanycyte subsets in different publications

A – A model of tanycyte subsets adapted from Figure 1 in Robins et al., (2013) and reproduced here with author's permission. In this model, α2-tanyctes (which have been subdivided in ventral α2-tanyctes and dorsal α2-tanyctes) project to the arcuate nucleus.

B – A model of tanycyte subsets from Figure 1 in Ebling & Lewis, (2018) and reproduced here with author's permission. In this model, β1-tanycytes project to the arcuate, with α2-tanyctes projecting to only the dorsal most part of the arcuate nucleus.

C and D – Panels from Figure 4 in Robins et al., (2013) and reproduced here with author's permission. These panels show BrdU labelling after a BrdU pulse-chase with or without additional FGF2. Adding FGF2 leads to increased incorporation of BrdU, particularly in the lateral ventricular zone. The authors describe these BrdU-labelled ventricular zone cells as α2-tanyctes. Scale bars 100μm.

E and E' – Panels from Figure 4 in Haan et al., (2013) and reproduced here with author's permission. These panels show Fgf10-expressing cells labelled by βgal, and point out few cells that co-label for βgal and proliferation marker EdU. The authors describe all the βgal-labelled ventricular zone cells as β-tanycytes. This population appears to overlap with the red BrdU-labelled population in panel D, contradicting the subset localisation described by Robins et al., (2013). Scale bar in E 50μm. Scale bar in E' 5μm.

Figure 1.2

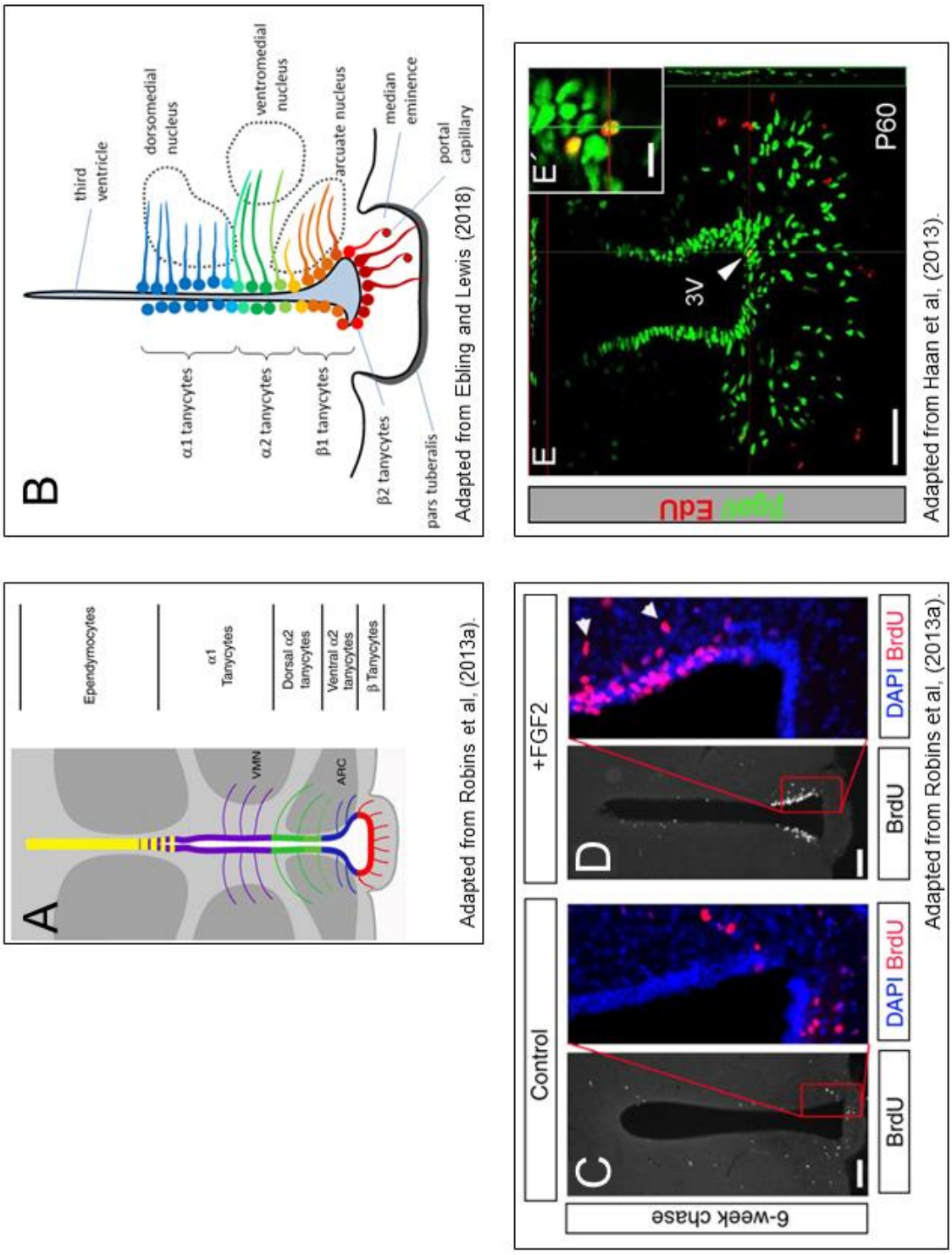
A
Ependymocytes
α1 Tanycytes
Dorsal α2 tanycytes
Ventral α2 tanycytes
β Tanycytes
VMN
ARC
Adapted from Robins et al. (2013a).
B
third ventricle
dorsomedial nucleus
ventromedial nucleus
arcuate nucleus
median eminence
portal capillary
α1 tanycytes
α2 tanycytes
β1 tanycytes
β2 tanycytes
pars tuberalis
Adapted from Ebling and Lewis (2018)
E
E'
3V
P60
EdU
Adapted from Haan et al. (2013).
6-week chase
Control
+FGF2
C
D
BrdU
DAPI BrdU
BrdU
DAPI BrdU
Adapted from Robins et al. (2013a).

As part of regulation of puberty and reproduction, Gonadotropin-releasing hormone (GnRH) is produced in the rostral hypothalamus and modulates the production of follicle stimulating hormone (FSH) and luteinising hormone (LH), which in turn regulate reproductive systems and behaviours. GnRH neurons project to the portal capillaries in the median eminence, but access to the portal capillaries is limited by β-tanycytes (Prevot et al., 2010; Rogers et al., 1997). Oestrogen is taken up by β2-tanycytes and, with TGF-β and IGF-1, it induces cytoskeletal remodelling to retract the tanycyte end feet from the capillaries (Baroncini et al., 2007; Hiney et al., 1996; Prevot et al., 2000, 2003; Seranno et al., 2010). This allows GnRH to be released into the capillaries to travel to the anterior pituitary and regulate LH and FSH.

A similar system is in place to regulate thyroid activity. Circulating thyroid hormone T4 (Thyroxine) is taken up by both α- and β-tanycytes where it is converted by DIO2 to the more active T3(Triiodothyronine) (Bolborea and Dale, 2013). This T3 is thought to affect the regulation of neuropeptide Y (NPY) neurons in the arcuate nucleus, and the paraventricular nucleus (PVN) production and release of Thyrotropin-Releasing Hormone (TRH) (Coppola et al., 2008; Fekete et al., 2014). β2-tanycytes may respond to T3 by retracting their end-feet and allowing TRH secreted by PVN neuronal projections to be released into the median eminence capillaries (Yamamura et al., 2006). TRH then travels to the anterior pituitary where it promotes TSHβ release, which in turn causes thyroid hormone release from the thyroid. The β2-tanycytes also express pyroglutamyl peptidase II, which breaks down TRH, in response to T3 (Sanchez et al., 2009), and allows regulation of circulating TRH in response to levels of T3, through interaction at the neuronal terminals and tanycyte end-feet. This feedback system is thought to help regulate responses to seasonal changes in photoperiod including modulation of energy expenditure.

In addition to trafficking hormones into and out of the hypothalamus, tanycytes have been shown to act as glucose sensors and to change vascular permeability in response to changes in circulating blood glucose (Frayling et al., 2011). As additional functions continue to be found, it becomes clear that tanycytes are vital for hypothalamic homeostatic control. Recent work investigating an adult population of hypothalamic neurogenic cells has brought further interest to this special glial cell population.

1.2 Neurogenesis in the adult hypothalamus

1.2.1 Discovery of adult mammalian neurogenic populations

Over the past three decades, a plethora of published studies have investigated neurogenic neural stem cell (NSC) populations retained in the adult brain (Ming and Song, 2011). Following the observation of new-born neurons in the adult songbird brain, and the identification of a NSC population, researchers quickly turned to look for similar populations in mammals (Alvarez-Buylla et al., 1990b, 1990a; Goldman and Nottebohm, 1983; Lois and Alvarez-Buylla, 1993; Nottebohm, 1980). It was well known that lesions to the mammalian peripheral nervous system (PNS) or central nervous system (CNS) formed glial scars, and regeneration did not appear to occur. On this basis, it was assumed that adult neural tissues were not neurogenic. This dogma was shown to be false when a neurogenic population was found in the subventricular zone (SVZ) of the lateral ventricle in the adult mouse brain, first by utilising *in vitro* cultures, and then through the use of lineage-tracing (Lois and Alvarez-Buylla, 1993; Reynolds and Weiss, 1992; Richards et al., 1992). It was found, quite unexpectedly, that NSCs of the SVZ constitutively give rise to neuroblasts that migrated to the olfactory bulb where they differentiated into new olfactory neurons (Doetsch et al., 1999; Lois and Alvarez-Buylla, 1994). This substantial pilgrimage is now known as the rostral migratory stream (RMS).

Following these successes, researchers were keen to determine whether other neurogenic populations existed. It was not long before an additional population was identified in the subgranular zone of the dentate gyrus (Gage et al., 1998; Kuhn et al., 1996; Palmer et al., 1997; Ray et al., 1993; Suhonen et al., 1996). Proliferation of these NSCs has been linked to learning and memory, and blocking neurogenesis impairs memory-based learning (Deng et al., 2010; Shors et al., 2001). In recent years, headlines were made by studies linking reduced hippocampal proliferation to depressive symptoms, and investigations in mice suggest that increasing hippocampal proliferation may relieve depression and anxiety (Hill et al., 2015; Sahay and Hen, 2007).

1.2.2 The structure of the neurogenic niche

A vital part of understanding the regulation and function of these two NSC

populations has come from studies investigating their neurogenic niches. The term ‘stem cell niche’ refers to the microenvironment in which the self-renewing multipotent stem cells reside (Li and Xie, 2005). Niches for different stem cell populations are varied, but many share common features. The stem cells often reside in close proximity to blood vessels, which may provide signals that affect proliferation behaviour. Signals affecting proliferation and behaviour may also come from cells found locally, such as from support cells that are often found in direct contact with stem cells. Also within the niche, there may be found transit amplifying cells (TACs) and immature daughter cells. Stem cells are regarded as slow-dividing, often quiescent, long-lived cells, capable of unrestricted division to self-renew and give rise to different daughter cells. These daughter cells are often TACs: short-lived, fast-dividing cells, which rapidly produce new immature cells. Immature cells migrate to their target location and differentiate into mature cells capable of fulfilling the function of the tissue. Through the actions of the cells and molecules in the stem cell niche microenvironment, a balance of proliferation and differentiation will retain the stem cell population throughout life, whilst maintaining the tissue in which it resides.

In the SVZ, the NSC population is comprised of cells with astrocytic morphology, so-called B1 cells, which lie just below the lateral ventricle ependymal layer, and have a projection that squeezes between the ependymal cells to contact the CSF (Fig 1.3A) (Decimo et al., 2012; Doetsch, 2003; Doetsch et al., 1999). These cells can be labelled with the astrocyte marker glial-fibrillary acidic protein (GFAP), the transcription factor Sox2, and an intermediate filament protein Nestin. B1 cells divide to produce a $Nestin^{+}$ daughter TAC termed a C cell which acts as a fast-dividing neuronal precursor. These precursors yield the migratory neuroblasts, known as A cells, which express the immature neuron-associated doublecortin protein (DCX) and migrate along the RMS to the olfactory bulb (Gleeson et al., 1999). The niche also includes stellate astrocytes that are not in contact with the ventricle (B2 cells), and overall is surrounded by blood vessels. The endothelial cells of the blood vessels remain in contact with the B cell astrocytes, which receive signals from the blood and CSF that regulate proliferation/differentiation behaviours (Silva-Vargas et al., 2013, 2016).

The SGZ NSC niche is similar but distinct from the SVZ (Fig 1.3 B) (Decimo et

al., 2012; Doetsch, 2003). Rather than lying next to the ventricle, the SGZ GFAP$^+$ Sox2$^+$ Nestin$^+$ B-like cells are radial cells that sit next to blood vessels, and send apical projections through the granule layer of the dentate gyrus (Palmer et al., 2000; Seri et al., 2001). These slow-dividing stem cells produce DCX$^+$ daughters, termed D cells, that are functionally similar to the TAC C cells of the SVZ, but multiply at a slower rate, giving rise the immature granule neurons (IG) (Seri et al., 2001, 2004).

Investigating the niche of the SVZ and SGZ NSC populations has uncovered processes regulating of these populations, and has provided clues about the characteristics that might be found in other adult neurogenic niches. Since the discovery of the SVZ and SGZ NSC populations, researchers have also begun to describe neurogenic populations in the amygdala, cortex, spinal cord, and hypothalamus (Barnabé-Heider et al., 2010; Gould, 2007; Ming and Song, 2011).

1.2.3 Neurogenesis in the adult hypothalamus

The first evidence for a neurogenic population in the adult mammalian hypothalamus came in 2001, when Pencea and colleagues injected brain-derived neurotrophic factor (BDNF) and the cell proliferation marker bromodeoxyuridine (BrdU) into the lateral ventricle of rats and saw incorporation of BrdU into cells of the hypothalamic parenchyma (Pencea et al., 2001). Another group of researchers used a 4th ventricle injection of the lipophilic label DiI to mark 3rd and 4th ventricle ependymal cells, and showed that the ependymal layer of the 3V yields DiI-labelled *in vitro* neurosphere cultures (Xu et al., 2005b). The neurosphere assay is used to identify tissues containing cells capable of long-term self-renewal, a property of stem cells (discussed further in Chapter 7.1) (Reynolds and Weiss, 1992). In this context, the DiI labelled neurospheres suggested that the hypothalamic ependymal layer contained self-renewing cells. Xu et al., (2005) built upon this result by injecting BrdU and basic fibroblast growth factor (bFGF/FGF2) into the 3V and observing co-labelling of Nestin$^+$/GFAP$^+$ tanycytes with BrdU. Through lineage-tracing they were able to show that tanycytes gave rise to BrdU$^+$ neurons in the

Figure 1.3 Neurogenic niches

A – Diagram of the SVZ neurogenic niche. Stem cells (B1) send projections through the ependymal layer (E) to reach the lumen (L), and apically project toward the blood vessels (BV). B1 cells self-renew and give rise to transit amplifying cells (C), which in turn give rise to neuroblasts (A).

B – Diagram of the SGZ neurogenic niche. Stem cells (B) sit next to the blood vessels (BV) and divide to self-renew and give rise to transit amplifying daughter cells (D). These daughter cells give rise to immature granule neurons (IG), which mature into granule neurons (G) and extend apical and basal projections.

C – Diagram of the hypothalamus niche. Tanycytes (T) lie next to the lumen and self-renew or give rise to neuronal and glial offspring. It is unclear whether an intermediate cell exists, or whether cells from the parenchyma modulate tanycyte proliferation. New neuronal and glial cells are thought to migrate out to the ARC and broader hypothalamic parenchyma.

Figure 1.3

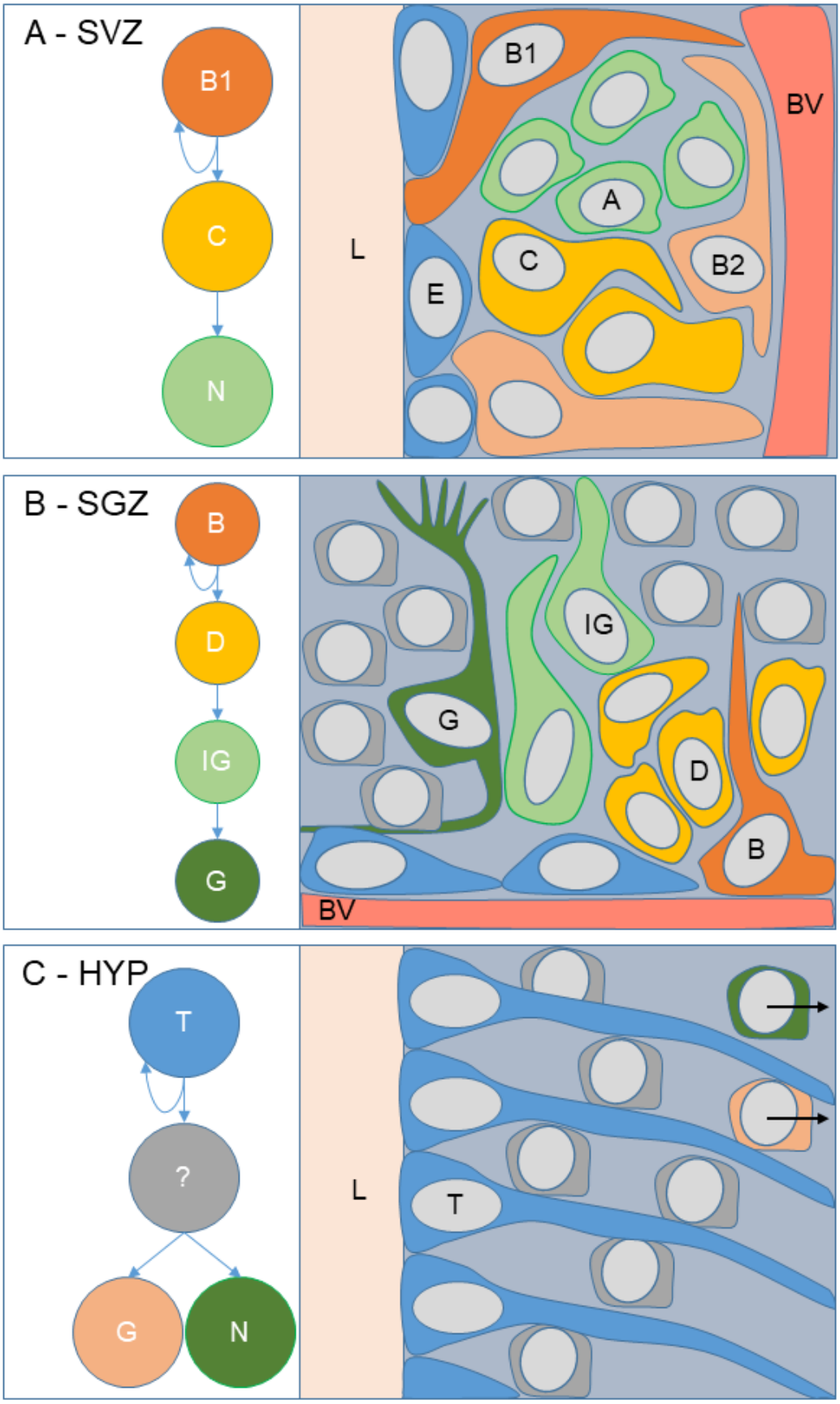

hypothalamic parenchyma, thus identifying tanycytes as including a neural progenitor population.

Lineage-tracing is an umbrella term for a range of experimental techniques that allow you to mark a cell or groups of cells with a persistent label that will be retained in the original cell/s, any cells derived from them, or their subsequent progeny (referred to as their lineage). BrdU pulse-chase is a crude version of this type of experiment, but the label is “diluted” or “washed out” by repeated divisions, which can lead to loss of labelling over time. More robust experimental protocols involve inducing genetic changes in the original cell/s, which are then passed onto the progeny causing permanent change in their lineage. Xu et al., (2005) used an adenovirus vector carrying the DNA sequence for GFP injected into the 4^{th} ventricle which after 48-hours lead to the GFP-labelling of ventricular zone cells (including tanycytes), but not parenchymal cells. After 2-4 weeks, GFP-labelled cells were also found in the hypothalamic parenchyma. A similar pattern was seen when using the BrdU pulse-chase experiment. Tanycytes, but not parenchymal cells, were labelled by BrdU 1 week after injection, but after a one month chase they also observed BrdU cells in the hypothalamic parenchyma and which were labelled by the neuronal marker Hu. Together these experiments show that Tanycytes proliferate to give rise to parenchymal cells including neurons.

Other studies using BrdU injection into the 3V showed that the murine hypothalamus contains constitutively proliferative cells that yield parenchymal neurons, though they did not specify tanycytes as the source (Kokoeva et al., 2005, 2007). Furthermore, they showed that the weight loss induced by ciliary neurotrophic factor (CNTF) in obese rodents is dependent upon increased hypothalamic proliferation, suggesting hypothalamic neurogenesis may be regulated to modulate homeostatic processes in health and disease (Kokoeva et al., 2005).

In recent years, further studies have identified tanycytes as a likely source of adult neurogenesis. Bennett et al., (2009) used a Nestin-GFP reporter to show GFP expression in both tanycytes and hypothalamic neurospheres. This experiment built upon the previous DiI labelling experiment that suggested the 3V ependymal layer is neurogenic (Xu et al., 2005b), and strongly suggests that

the ependymal tanycytes are the likely source of adult neurogenesis. A later study with an inducible Nestin-reporter line (Nestin:CreER^{R26stopYFP}) that labels tanycytes and their progeny showed directly that tanycytes give rise to hypothalamic neurons in juvenile mice, and that feeding adult mice a high-fat diet (HFD) quadrupled the rate of proliferation (Lee et al., 2012). Blocking neurogenesis with CT-guided irradiation focussed on the median eminence drastically reduced proliferation and slowed weight gain. These results further support the hypothesis that hypothalamic neurogenesis is responsive to physiological signals, and that the proliferative response leads to changes in neural circuitry that impact homeostatic processes.

The HFD and the feeding-circuitry of the hypothalamus have been useful for further probing the hypothalamic neurogenic population in response to external signals, however the results have not always been consistent. The HFD induces apoptosis in agouti-related peptide$^+$ (AGRP$^+$) NPY$^+$ neurons found in the feeding circuits of the ARC, and specific loss of these neurons, through induced mitochondrial dysfunction in AGRP$^+$ neurons, has been shown to increase hypothalamic proliferation and generation of replacement neurons (Moraes et al., 2009; Pierce and Xu, 2010; Xu et al., 2005a). Another group showed that n-3 polyunsaturated fatty acids (PUFAs), a dietary component that has been associated with an array of health benefits, cause an increase in neurogenesis of the feeding circuit proopiomelanocortin (POMC) neurons, which are anorexigenic/appetite suppressant, but not orexigenic/appetite stimulating NPY neurons (Millington, 2007; Nascimento et al., 2016; Ruxton et al., 2007). They suggest a preliminary link between PUFA supplementation and reduced weight gain. One group observed that embryonic AGRP/NPY neurons of the hypothalamus are replaced by new-born neurons in the juvenile period, showing hypothalamic proliferation may make developmentally important changes in hypothalamic circuitry (McNay et al., 2012). They also showed that HFD produces a greater quantity of neurosphere producing (neurospherogenic) cells and, in contrast to previous studies, reduced the rate of proliferation *in vivo* (McNay et al., 2012). In a further contradictory twist, Gouazé et al., (2013) saw increased proliferation after the HFD, like Lee et al., (2012), but then found that pharmacologically blocking neurogenesis accelerated obesity onset, rather than reducing weight. Additional studies have suggested the response may be

sexually dimorphic (Lee et al., 2014), and, consistent with this, a recent study has shown HFD to increase neurogenesis in female mice, though neurogenesis is decreased when the HFD is combined with oestrogen treatment (Bless et al., 2016). These conflicting reports serve to highlight that further research is required to understand the complicated factors affecting proliferation in response to changes in homeostasis, and also to determine what the effects of the changes in neurogenesis are.

To explore these ideas further, researchers have investigated other physiological signals. These include showing that voluntary exercise (Niwa et al., 2016), moderate heat exposure (Matsuzaki and Katakura, 2009; Matsuzaki et al., 2017), seasonal changes in photoperiod (Batailler et al., 2014, 2016; Butruille et al., 2018; Migaud et al., 2011, 2015), and a variety of growth and neurotrophic factors all modulate tanycyte neurogenesis. In addition to the previously mentioned studies on CNTF and BDNF (Kokoeva et al., 2005; Pencea et al., 2001), IGF-1, inflammatory pathways via IKKβ/NF-κB , and FGFs have also been shown to moderate proliferation in the resident tanycyte population (Bless et al., 2016; Chaker et al., 2016; Haan et al., 2013; Li et al., 2012; Pérez-Martín et al., 2010; Robins et al., 2013a; Xu et al., 2005b). The effects of the FGF family are of particular note as Fgf10 and Fgf18 have been shown to be endogenously expressed by various tanycyte subsets (Haan et al., 2013; Hajihosseini et al., 2008; Robins et al., 2013a). The $Fgf10^{+}$ tanycytes have been lineage-traced to show contribution to parenchymal neuron populations, and Fgf2 supplementation promotes α2-tanycyte proliferation in hypothalamic slice culture and long-term self-renewal in neurosphere culture (Haan et al., 2013; Robins et al., 2013a).

In addition to the debate over the effects of HFD, there is also debate between research groups over the location of the neurogenic population within tanycyte subsets. Papers investigating the response of tanycytes to IGF-1 have suggested α1-tanycytes contain a neurogenic population (Pérez-Martín et al., 2010), whilst others investigating the HFD and Fgf10 lineage-tracing have suggested the β-tanycytes are proliferative (Haan et al., 2013; Lee et al., 2012). Previous studies from our lab traced the lineages of α1- and α2-tanycytes using a tamoxifen-inducible GFP-reporter under the Glutamate aspartate transporter (GLAST) promoter, grew hypothalamic slice-cultures, and grew neurospheres

from the different tanycyte subsets, to generate compelling data suggesting the α2-tanycytes contain a responsive, self-renewing, and proliferative population (Robins et al., 2013a). Reasons for these apparently conflicting results may include using mice of different ages, mice of different sex, using different markers to identify tanycytes (as outlined above in section 1.1.2), and failing to account for anterior-posterior (A-P) differences in hypothalamic populations.

For example, Lee et al., (2012) use postnatal day 19 (P19) pre-adolescent mice to investigate the hypothalamic neurogenic population and identify β2-tanycytes as the prime candidates. This identification is not as clear as they suggest. While the image shown in the main body of the paper does appear to highlight $BrdU^+$ VZ cells in only the domain where β2-tancytes are found, the supplementary figures show a range of A-P hypothalamic sections with $BrdU^+$ VZ cells in what some would describe as the β1-tanycyte domain. A lack of clear β1-, and β2-tancytes markers makes distinguishing between these populations difficult.

When Lee et al., (2012) examine the effect of a HFD on proliferation they use adult mice. They measure this effect by describing increased new neurons labelling for BrdU, but do not comment on BrdU in tanycytes. They do not show pictures of the increased proliferation in mice fed a HFD (instead showing it graphically). By omitting these images, the reader cannot see whether BrdU still labels only the β2-tanycytes, or also labels other tanycyte subtypes. This is important information, particularly when considering that labs looking at adult mice and rats have since shown that α-tanycytes may proliferate (Pérez-Martín et al., 2010; Robins et al., 2013a).

They then claim to show that the β2-tanycytes give rise to the neurons through lineage-tracing under a Nestin promoter. After induction by tamoxifen at P4, Yellow fluorescent protein (YFP) is induced in both cells that express Nestin and their progeny. While they do show that new neurons express YFP, this alone is not sufficient to support their hypothesis. As all tanycytes express Nestin this lineage-tracing is not specific to β2-tanycytes, and the new neurons may be derived from any tanycyte population. Similarly, they use focal irradiation to specifically target the ventral medial hypothalamus, which includes tanycytes, and show that this causes reduced proliferation and reduced weight

gaining, supporting their hypothesis that tanycyte neurogenesis is required for producing new neurons in response to the HFD, which in turn leads to weight gain. However, the region that was irradiated (and labels strongly for DNA damage), includes β2-, β1-, and α2-tanycytes, and as a consequence one cannot conclude this effect was specifically because proliferation was reduced in β2-tanycytes. While it is fair to conclude that β-tanycytes may be proliferative at P19, and that tanycyte proliferation is involved in the neurogenic response to a HFD, one cannot conclude from the data presented that β2-tanycytes specifically are the source of the new neurons.

Other papers investigating the HFD in the hypothalamus, either fail to mention tanycytes, make vague assumptions about tanycyte neurogenesis, or fail to show images where tanycyte neurogenesis can properly be assessed. J. Li et al., (2012) claim dietary change reduces hypothalamic neurogenesis, but also claim tanycytes are only a small proportion of the hypothalamic neural stem cells. They assume that because Sox2 labels other neural stem cell populations, all the Sox2-labelled hypothalamic cells must be hypothalamic stem cells, despite not showing whether this true. When McNay et al., (2012) investigated the neurogenic effects of the high-fat diet in adult mice they did not specifically look at tanycytes and saw reduced *in vivo* proliferation. From their images it appears as though α2- and/or β1-tanycytes label for BrdU. However, the boundary between these two regions is disputed and the images presented cut off the β2-tanycyte domain. A review by Bolborea & Dale, (2013) identifies the BrdU cells in the McNay et al., (2012) study as α- or β1-tanycytes, and suggests the result contrasts with the Lee et al., (2012) report, however they do not acknowledge that the papers do not show comparable images of the various tanycyte populations in mice of similar ages. Furthermore, no markers are used in either paper to distinguish tanycyte subsets, which frustrates attempts to draw specific conclusions about which subsets are neurogenic.

Other studies that investigate the effect of the HFD on hypothalamic neurogenesis also appear to show BrdU labelling in the α2- and/or β1-tanycyte domains, however they do not comment on it specifically (Bless et al., 2016; Gouazé et al., 2013). As no studies consistently show comparable sections with tanycyte markers, at comparable life stages, and using comparable HFD protocols, we cannot come to any firm conclusions about how HFD affects

tanycyte neurogenesis in mice.

A variety of markers have been used to describe the various tanycyte subsets in the published literature (described in detail in Goodman & Hajihosseini, (2015)). However, many of these markers are expressed by multiple tanycyte subsets, and this makes it difficult to distinguish precisely which tanycyte subset is being discussed (see section 1.1.2). A further complication is introduced by the morphological changes that occur along the anterior-posterior (A-P) axis of the hypothalamus. The majority of papers that discuss tanycyte neurogenesis use stereotypical hypothalamic sections including the median eminence that resemble the Figure 1.1 B and Figure 1.2 A-E to support their conclusions. However, tanycytes can be found lining the hypothalamic ventricle from anterior to the median eminence, through the region containing the median eminence, to more posterior regions overlying the pituitary stalk (discussed further in Chapter 3). Few papers describe tanycyte markers over more anterior and posterior hypothalamic regions, but where they do it becomes apparent that established tanycyte α- and β- subsets do not necessarily occupy the same dorsal-ventral domains as in the widely used medial sections (Haan et al., 2013; Hendrickson et al., 2018; Mirzadeh et al., 2017; Robins et al., 2013a). Given how little we know about the properties of tanycytes beyond those in the medial, stereotypical, median eminence-containing domain that is routinely displayed in publications, one may question how confident we can be in the assertions about neurogenesis occurring in specific tanycyte subsets.

Despite more than 15 years investigating neurogenesis in the adult hypothalamus, we still know relatively little about the neurogenic population. We do not know precisely which subset/s of tanycytes may be neurogenic. We have little information regarding the A-P localisation of these subsets and the potential neurogenic population. Furthermore, when we compare the hypothalamus to other stem cell-containing tissues in the body, or even to the neurogenic niches within the CNS, we find that we have scant details about the usual stem cell niche components (Fig 1.3 C). Tanycytes are located in the proximity of the 3V and median eminence blood vessels, but we do not have knowledge of local support cells or whether daughter cells constitute a population of transit amplifying cells. It is likely that this knowledge deficit has been exacerbated by the conflicting reports of neurogenic tanycyte subsets and

inconsistent use of tanycyte markers, spreading the focus of interested research groups. These concerns must be addressed if we are to understand the physiological functions of adult hypothalamic neurogenesis, and the role tanycytes may play as a stem or progenitor population.

1.3 Evidence for a stem cell from the developing hypothalamus

In parallel to studying neurogenesis in the adult hypothalamus, we may be able to uncover related mechanisms of proliferative control by studying the pathways directing the growth and differentiation of the hypothalamus during development. Adult stem cells and regenerative targets are often thought to re-engage developmental protocols, and in the hypothalamus we know that the mitogen Fgf10 is involved both in developmental growth and specification, and in guiding adult neurogenesis (Fu et al., 2017; Haan et al., 2013; Robins et al., 2013a). With this in mind I will discuss the systems and signals that build the embryonic hypothalamus, and, where appropriate, compare them to those known to be at work in the adult mouse hypothalamus. The large proportion of studies studying the early hypothalamus use chicks as a model, as the egg is a tractable system that, unlike the mouse embryo, can be easily manipulated, imaged, and tracked over time, yet remains relatable to the development of the mammalian hypothalamus. The cited literature in the following section refers to complimentary studies using both mouse and chick models.

1.3.1 Patterning and growth in the early hypothalamus

In the early neural plate, the transcription factor Six3 is expressed in the presumptive avian and mammalian hypothalamus, (Kobayashi et al., 2002; Oliver et al., 1995) and primes cells to respond to Shh (Ahlgren et al., 2003; Geng et al., 2008; Kobayashi et al., 2002; Lagutin et al., 2003; Newman et al., 2018; Sanchez-Arrones et al., 2012) (Fig 1.4 A). The prechordal mesoderm (PM) sits below the midline of the presumptive hypothalamus, and provides a source of Shh, inducing cells termed rostral diencephalic ventral midline (RDVM). These cells co-express Shh and Six3 (Geng et al., 2008; Jeong et al., 2008; Manning et al., 2006; Zhao et al., 2012). Shh deriving from the PM and RDVM cells establishes an early dorso-ventral pattern in the nascent hypothalamus. In the PM, Shh is rapidly replaced by BMPs and, after the initial

patterning of the hypothalamus by Shh, these BMPs induce a change in RDVM cells so that they upregulate BMP2/4/7 and Fgf10 (Manning et al., 2006). Thus a set of progenitor cells is induced that co-express Shh, Fgf10 and BMP7.

Fate-mapping studies show that this progenitor population has the characteristics of a stem-like cell: it gives rise to descendants that grow extensively and contribute to the anterior hypothalamus, then the mammillary hypothalamus and finally the infundibulum (Fu et al., 2017). As this occurs, both Shh^+ 'anterior' progenitors and $Fgf10^+$ 'tuberal' progenitors are generated and a Shh^+Fgf10^+ cell(s) appears to be retained at boundary between these zones.

The mechanism that mediates these events is in-part understood. As BMPs are upregulated in RDVM cells, they induce Tbx2, and Tbx3. These downregulate Shh expression and upregulate Fgf10 (Alvarez-Bolado et al., 2012; Ellis et al., 2015; Manning et al., 2006; Ohyama et al., 2008; Pearson et al., 2011; Trowe et al., 2013). Timing of Shh downregulation is important, as loss of Shh too early leads to reductions in anterior and tuberal hypothalamic domains (Fu et al., 2017; Muthu et al., 2016; Shimogori et al., 2010; Zhao et al., 2012). Following the downregulation of Shh in the RDVM, the remaining $Fgf10^+$ cells constitute a tuberal hypothalamus progenitor population that give rise first to the Shh^+ anterior hypothalamus progenitors, and then to the $Emx2^+$ mammillary hypothalamus progenitors (Fu et al., 2017) (Fig 1.4 B). However, initial unpublished results appear to indicate a handful of cells at the anterior and posterior boundaries of the Fgf10 domain may retain Shh, and these $Fgf10^+Shh^+$ cells may forming the driving front of developmental growth and proliferation (Placzek/Towers, unpublished).

In addition to the signals Shh and Fgf10, the transcription factor Rax has been implicated in early patterning and growth of the hypothalamus. Rax is expressed from early in embryonic development where it engages in a complex promotion/repression feedback loop with Shh, leading to the specification of the

Figure 1.4 Signals governing the developing hypothalamus

A – Schematic of hypothalamic induction from signals in the prechordal mesoderm. Shh in the prechordal mesoderm (PM, blue) induces Shh in the $Six3^+$ RDVM that will become the hypothalamus (HYP, green). Shh in the PM is then replaced by BMPs (red), which then induces BMP2/4/7 and Fgf10 in the prospective hypothalamus (red). OS, Optic stalk.

B – Sagittal schematic of developmental hypothalamic growth based on (Fu et al., 2017). Following the demarcation of Anterior (Shh^+, green), Tuberal ($Fgf10^+$, red), and Posterior ($Emx2^+$, blue) domains, cells of the tuberal domain give rise to anterior migrating Shh+ progenitors, followed by posterior migrating Emx2+ progenitors.

C – Feedforward/Feedback model of Shh and Rx3 expression by anterior/tuberal progenitors in the developing zebrafish (*danio rerio*) hypothalamus. Adapted from (Muthu et al., 2016).

D – Hypothesised model of stem cells at the anterior/tuberal boundary during developmental growth of the hypothalamus. In the model, $Fgf10^+Shh^+$ stem cells at the tuberal boundary divide to produce a Shh^+ anterior progenitor and an $Fgf10^+$ tuberal progenitor. Shh-signalling from the anterior progenitor re-induces Shh and Rax/Rx3 in the $Fgf10^+$ tuberal progenitor. The cycle is repeated, and the $Fgf10^+Shh^+Rax^+$ stem cell divides to self-renew and yield a Shh^+ anterior progenitor. This new anterior progenitor displaces the previous Shh^+ cell at the boundary, which will express P57 when it begins to differentiate.

Figure 1.4

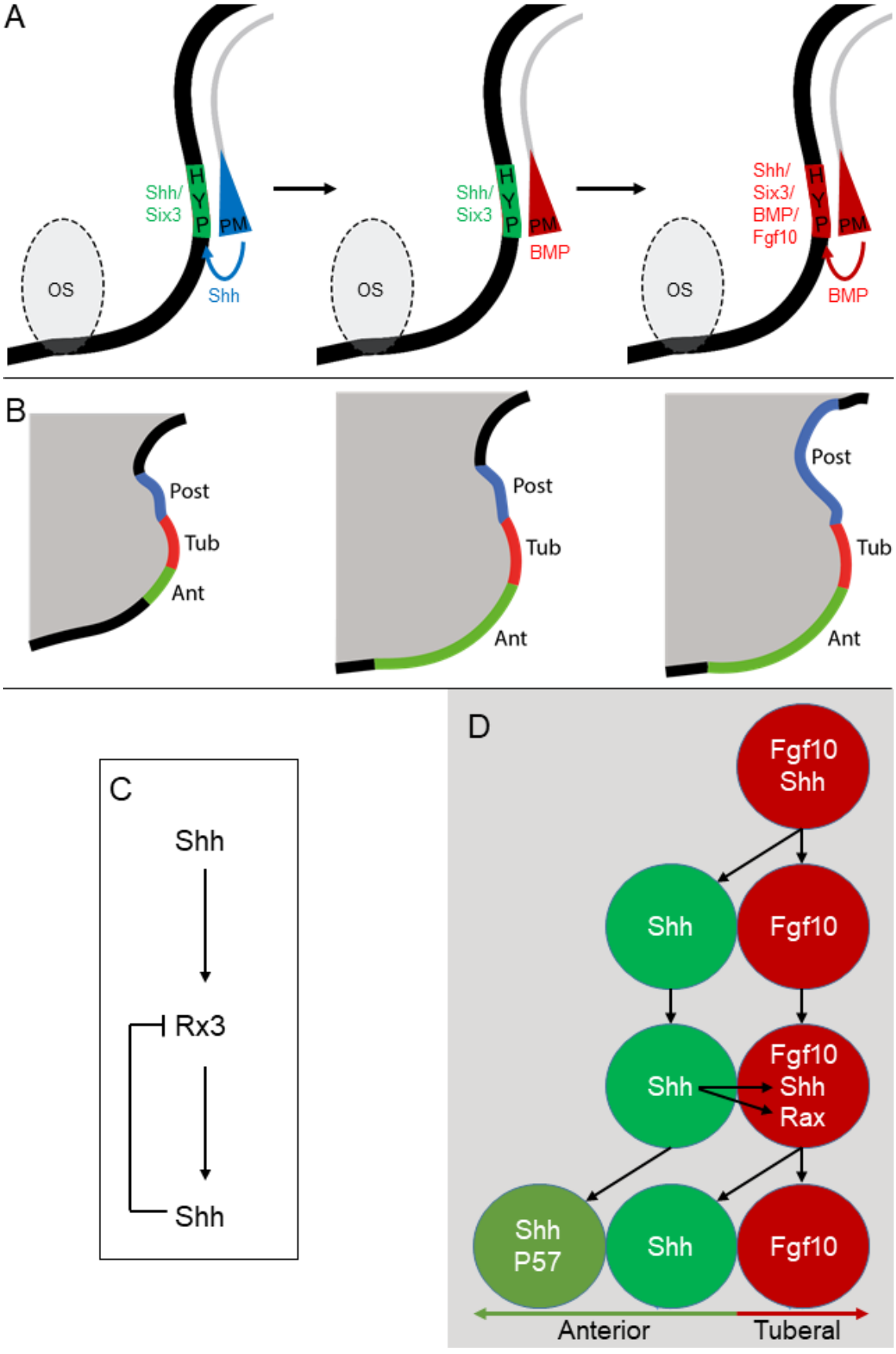
A
Shh/
Six3
HYP
PM
Shh
OS
Shh/
Six3
HYP
PM
BMP
OS
Shh/
Six3/
BMP/
Fgf10
HYP
PM
BMP
OS
B
Post
Tub
Ant
Post
Tub
Ant
Post
Tub
Ant
C
Shh
Rx3
Shh
D
Fgf10
Shh
Shh
Fgf10
Shh
Fgf10
Shh
Rax
Shh
P57
Shh
Fgf10
Anterior
Tuberal

prospective anterior/tuberal hypothalamic domains, including the development of the ARC and VMN (Furukawa et al., 1997; Lu et al., 2013; Orquera et al., 2016; Wataya et al., 2008). Early conditional KO of Rax in the hypothalamus phenocopies loss of the Shh^+ anterior progenitors, i.e. leading to a lack of neurons characteristic of the anterior/tuberal hypothalamus and a failure of infundibular formation. This appears to be because normally Rax maintains Shh expression while the hypothalamic domain is specified (Lu et al., 2013; Orquera et al., 2016). Zebrafish *chokh* (chk) mutants lack functional Rx3 (homologue of Rax), and as a consequence they do not display the normal anterior Shh^+ domain (Muthu et al., 2016). These mutants also display an increase in progenitors expressing the *Rx3* missense mRNA transcript, either due to disrupted neuronal/glial differentiation or apoptosis, and which is thought to be caused by the loss of Shh. As a consequence, an array of anterior/tuberal neuronal populations are lost, or diminished in number, including the $POMC^+$ and dopaminergic tyrosine hydroxylase-expressing (TH^+) neurons of the ARC. To explain this complex phenotype, Muthu et al., (2016) suggested the following model (Fig 1.4 C):

1. Shh induces Rx3 in the anterior/tuberal progenitors,
2. Rx3 maintains Shh expression in these progenitors,
3. This maintained Shh expression turns off Rx3, allowing for differentiation.

Based on the models of proliferation and growth from Fu et al., (2017), Muthu et al., (2016), and as yet unpublished work from the Placzek lab group, one can consider the hypothetical model outlined in Figure 1.4 D. An $Fgf10^+Shh^+$ stem-like cell divides to produce a Shh^+ 'anterior' progenitor daughter and an $Fgf10^+$ progenitor daughter cell. Shh from the anterior progenitor re-induces Shh in the tuberal daughter via the transcription factor, Rax/Rx3. These $Fgf10^+Shh^+Rax^+$ cells would be competent to repeat this processes, i.e. establishing self-renewing progenitors whilst producing a stream of Shh^+ anterior progenitors that drive the previously described anisotropic anterior growth (Fu et al., 2017). Posterior growth appears to follow a similar pattern to that of the anterior domain, once the anterior domain has finished expanding. If this is the case, and the proposed model for the anterior/tuberal progenitors is correct, then we may expect to see a similar population at the posterior boundary to the $Fgf10^+$ domain.

A key element of this model is the presence of a self-renewing, multipotent population, displaying the defining characteristics of stem cells, and expressing Fgf10, Shh and Rax. Whether such cells persist into the adult is not clear. Although Shh expression has not been reported in the adult mouse hypothalamus, the expression of Fgf10 on neurogenic tanycytes has, and FGFs are known to drive proliferation in this tissue, both *in vivo* and *in vitro* (Alvarez-Buylla and Lim, 2004; Bless et al., 2016; Haan et al., 2013; Robins et al., 2013a; Xu et al., 2005b). Based on the conserved function of FGFs to drive proliferation in both the embryonic and adult hypothalamus, one may hypothesise that a stem cell population established to drive growth and differentiation in the developing hypothalamus is retained into the adult hypothalamus, where it can undergo proliferation in response to changes in response to external cues, allowing the reprogramming of homeostatic circuitry.

1.3.2 Rax is a master regulator of tanycytes

In addition to its role establishing anterior and tuberal progenitors in the early hypothalamus, Rax is also necessary for the establishment of the tanycyte population (Miranda-Angulo et al., 2014; Salvatierra et al., 2014). While these specified progenitors are driving neurogenesis in the hypothalamus from E10-E14 (Shimada and Nakamura, 1973), Rax induces Lhx2 in the ventricular zone (VZ) of the 3V (Salvatierra et al., 2014). By E15, and coinciding with the end of the hypothalamic expansion, Rax is downregulated throughout the hypothalamus except in radial glial cells (RGCs) of the VZ, where Lhx2 now acts to maintain its expression (Lu et al., 2013; Muthu et al., 2016; Salvatierra et al., 2014). Both Lhx2 and Rax are retained into adulthood, where they are required to confer tanycyte identity (Miranda-Angulo et al., 2014; Salvatierra et al., 2014). Through study of Rax heterozygote mice (to avoid lethality in Rax KOs caused by absence of the hypothalamus, craniofacial defects, and anophthalmia), Miranda-Angulo et al., (2014) showed that haploinsufficiency leads to a depleted tanycyte population in adult mice, and ventral extension of the dorsally located ependomycytes into the normal tanycyte domain.

The requirement for Rax for anterior/tuberal hypothalamic patterning and for maintaining adult tanycytes, thought to contain the adult hypothalamic stem/progenitor population, fits directly into the hypothesis that the $Fgf10^{+}$ stem

cell population is retained from early hypothalamic development into adult. To determine whether this is accurate, one must trace Rax and Fgf10 expression through development and into adulthood, as the retained stem cell hypothesis requires they are co-expressed in the proliferative population. Furthermore, it must be established that the expression of Rax in adult tanycytes is linked to the identified proliferative and/or differentiation behaviour.

1.4 Cell adhesion molecules in the stem cell niche

As noted above, one hindrance to the study of hypothalamic stem cells is the availability of markers that delineate hypothalamic stem cell identity, particularly markers that can be used to identify and purify live cells, thus making the identification of cell surface molecules specific to tanycytes a priority. Increasing evidence suggests that cell surface components are critical to progenitor and stem cell behaviour, interacting with intracellular signalling pathways and transcription factors to regulate proliferation and differentiation (Hynes, 2002; Marthiens et al., 2010). In what may be the best described stem cell niches, those in *Drosophila melanogaster* gonads, cell adhesion molecules (CAMs) of the cadherin and integrin families are required to provide the correct anchorage within the niche for the stem and support cells respectively (Fuller and Spradling, 2007; Jin et al., 2008; O'Reilly et al., 2008; Song and Xie, 2002; Tanentzapf et al., 2007). These adhesions are also vital for successfully conducting asymmetric cell division, by facilitating appropriate spindle orientation (Yamashita et al., 2003, 2007). Similar attachments have been described in mammalian haematopoietic and endothelial niches, with some going as far as to state that α6 and β1 integrins are markers of human neural stem cells (Hall et al., 2006; Zhang et al., 2003). Such observations have also been made in the RGC niche throughout the developing CNS, where it is believed integrins, cadherins, F3/contactin and its cousin TAG1, and tight-junction proteins like Zonula occludens-1 (ZO-1) are important for correct RGC positioning at the basal and apical surfaces, survival within the niche, and guiding symmetric/asymmetric cell division (Bizzoca et al., 2012; Haubst et al., 2006; Junghans et al., 2005; Kadowaki et al., 2007; Kosodo et al., 2004; Loulier et al., 2009; Marthiens and Ffrench-Constant, 2009; Okamoto et al., 2013; Radakovits et al., 2009).

While several studies have investigated the roles of various CAMs in tanycytes, these have been with regard to their homeostatic functions. For example, β1 integrins enable β2-tanycytes to respond to Sema7a, coordinating the ensheathment of GnRH nerve terminals by the tanycyte end-feet (Messina and Giacobini, 2013; Parkash et al., 2015). Tight junction proteins such as ZO-1 and occludin are expressed in β- and α2-tanycytes, though this expression changes depending on fasting status, adapting the permeability of the tanycyte/CSF barrier (Langlet et al., 2013a; Mullier et al., 2010; Neuwelt et al., 2011; Rodriguez et al., 1979). Connexins form gap junctions between tanycytes, and from tanycyte end-feet to axon varicosities in the median eminence (Szilvásy-Szabó et al., 2017). Cadherins have been identified on a variety of tanycyte subsets, but their roles have not been thoroughly studied (Peruzzo et al., 2000; Rodríguez et al., 2005). These studies are proving useful for understanding the roles of tanycytes in homeostatic and reproductive control, but they have not yet been investigated in the hypothalamus with the specific goal of learning more about the adult stem/progenitor population and its niche. To address this, our lab has identified NrCAM, of the immunoglobulin-superfamily (Ig-SF CAMs), related to and a binding partner of both TAG1 and F3/contactin, as a protein with a potential role in tanycyte proliferation or maintenance.

1.4.1 L1-family CAMs in neurogenesis

The Ig-SF CAMs are so named because their extracellular domains contain a series of Ig-like repeats, which are followed by a series of fibronectin type III domains proximal to the plasma membrane (reviewed in Katidou et al., 2008). A prominent Ig-SF CAM subgroup is the L1-like family of CAMs, which are grouped based on their similarity to the defining member L1. This family each have six extracellular immunoglobulin domains and five fibronectin type III domains, as well as a highly conserved intracellular domain. This domain contains ankyrin binding sites, allowing the L1-family members to attach to the actin cytoskeleton (Bennett and Baines, 2001). L1-proteins exhibit an array of homophilic and heterophilic interactions with other L1-family and Ig-SF CAMs, as well as with integrins, netrins, extracellular matrix proteins, and signalling receptors (Brümmendorf and Rathjen, 1996; Castellani et al., 2004; Felding-habermann et al., 1997; Katidou et al., 2008; Maness and Schachner, 2007; Rougon and Hobert, 2003; Silletti et al., 2000). Through these interactions, L1

CAMs play a wide range of roles in neuronal outgrowth, migration/guidance, axon fasciculation, ion channel organisation, and node of Ranvier formation (Brümmendorf and Lemmon, 2001; Brümmendorf and Rathjen, 1996; Buchstaller et al., 1996; Castellani et al., 2004; Dang et al., 2012; Dzhashiashvili et al., 2007; Kamiguchi et al., 1998; Kunz et al., 1998; Lustig et al., 2001a; Sakurai, 2012; Salzer, 2003; Silletti et al., 2000).

In addition to these roles, L1 CAMs, and those from the related F3/contactin-family, have been found to have roles in modulating proliferation and differentiation behaviours in the developing nervous system. TAG1 has been shown to be important for anchorage of the basal end-feet of RGCs, loss of which severely disrupts normal neurogenesis (Okamoto et al., 2013). F3/contactin misexpressed under the promoter of related molecule TAG1 in the developing cortex promotes SVZ progenitor proliferation (Bizzoca et al., 2012), and leads to increased hippocampal size with related improvements in memory and synaptic potentiation (Gulisano et al., 2017; Puzzo et al., 2013, 2015). When it is misexpressed in the developing cerebellum it inhibits the proliferation of granule neuron precursors (GNPs) (Bizzoca et al., 2003). The L1-family members NrCAM (NgCAM-related cell adhesion molecule/neuronal cell adhesion molecule), CHL1 (Close homologue of L1), and L1 itself cause slight reductions cerebellar lobe sizes when mutated, outlining an importance in the development of this neuronal tissue (Heyden et al., 2008; Sakurai et al., 2001; Zonta et al., 2011). Moreover, the combined loss of L1 and NrCAM in a double mutant leads to major reductions in the size of the cerebellum, indicating that L1 and NrCAM function is redundant in the development of the cerebellum. F3/contactin is a ligand for NrCAM and L1, and its loss causes severe disruption of cerebellar architecture (Berglund et al., 1999). Based on these observations, our group has further interrogated the roles of these CAMs in the control of progenitor proliferation, particularly in cerebellar development.

GNPs grown *in vitro* and treated with a cross-linked soluble version of F3 (F3-fc) showed a reduced proliferative response to SHH, the key GNP mitogen in cerebellar development, and increased differentiation, but this activity is blocked by the addition of TAG1 (Xenaki et al., 2011). F3/contactin and TAG1 thus appear to act antagonistically on GNPs *in* vitro, and perhaps in cells of the middle external germinal layer of the developing cerebellum *in vivo*.

F3/contactin binds NrCAM on these cells and NrCAM is required in GNPs in order for F3/contactin to have its inhibitory effect on SHH-induced proliferation (Xenaki et al., 2011). Recent unpublished *in vitro* studies indicate that loss of NrCAM leads to a failure of the SHH receptor Patched (Ptch) to leave the primary cilium upon SHH stimulation, which is normally required to activate the SHH pathway (Chen and Yang, 2018).

Together these studies strongly implicate L1-family members, and their contactin-family binding partners, in the control of neural progenitor cell proliferation and differentiation. A role for NrCAM in controlling cell proliferation is further implied from its involvement in tumorigenesis, where it has been linked to poor prognosis and increased proliferation and motility in melanoma and colorectal cancer (Chan et al., 2011; Conacci-Sorrell et al., 2002, 2005). This research warrants further investigation of this family of CAMs with respect to developmental and adult neurogenesis.

1.4.2 NrCAM labels tanycytes and hypothalamic neurospheres

Preliminary work exploring NrCAM expression throughout the nervous system has identified NrCAM in the ventricular zone (VZ) of developing (Lustig et al., 2001b) and adult mouse hypothalamus (Allen brain atlas[1]), where RGCs and tanycytes are located. Furthermore, NrCAM KO mice (line establishment described in section 2.1.1) have reduced body weight and length and display abnormal sleep behaviour, and genomic association studies have linked NrCAM with addiction and autism, conditions associated with hypothalamic abnormalities (Moré *et al.*, 2001; Ishiguro *et al.*, 2006; Sakurai *et al.*, 2006; Jackson laboratory[2]). Though NrCAM KO mice have mild body size abnormalities, cerebellar lobe abnormalities, sleep behaviours abnormalities, and increased cataract formation, they have no overt, obvious phenotype (Moré et al., 2001; Sakurai et al., 2001, Jackson laboratory[3]). Our lab set out to confirm its expression in the hypothalamus and determine whether it may be involved in modulating proliferation and differentiation behaviours in this niche. MSc student Sarah Brown confirmed that NrCAM is expressed by Nestin$^+$

[1] Displayed in the Allen Brain Atlas http://mouse.brain-map.org/gene/show/106439
[2] Data displayed at http://www.mousephenotype.org/data/genes/MGI:104750#order2
[3] Data displayed at http://www.mousephenotype.org/data/genes/MGI:104750#order2

tanycytes in the adult hypothalamus, and that hypothalamic neurospheres are NrCAM$^+$ (Fig 1.5 A,B; unpublished). This corroborates previous data suggesting these neurospheres are derived from tanycytes (Bennett et al., 2009; Robins et al., 2013a; Xu et al., 2005b). Furthermore, preliminary analysis suggested NrCAM KO mice displayed an abnormally thin VZ (Fig 1.5 C; unpublished).

A thin VZ with fewer tanycytes may indicate that the proliferative capacity of tanycytes is compromised, and that they can no longer self-replenish (Robins et al., 2013a). Where reduced Rax leads to fewer tanycytes, it was observed that the barrier function in tanycytes appeared to be compromised (Miranda-Angulo et al., 2014). Additionally, lean and hypermetabolic Gnasxl-deficient mice to have fewer α-tanycytes, and Holmes et al., (2016) highlight potential impacts upon tanycyte neurogenesis and tanycyte transport of nutrients from the CSF to hypothalamic networks managing energy homeostasis. The pilot study conducted in our lab demonstrates a need to further explore CAMs such as NrCAM in the hypothalamus with respect to the tanycyte stem/progenitor niche.

1.5 Thesis aims and hypotheses

The data I have described indicate tanycytes as a likely stem or progenitor population in the adult hypothalamus, though little is known about the neurogenic niche. Recent embryonic studies have shown that hypothalamic A-P growth is driven by progenitors at the boundaries of the tuberal Fgf10$^+$ domain, and this may be accomplished by Fgf10$^+$Shh$^+$ stem cells. It is not known whether A-P dynamics affect adult neurogenesis, as studies tend to use stereotypical sections from central hypothalamic sections. Preliminary work shows NrCAM on tanycytes in the hypothalamus and hints at a phenotypic change in tanycytes when NrCAM is absent. In other neural tissues, NrCAM has been identified as a modulator of Shh signalling and its proliferation/differentiation outcomes. Based on these observations I outline the aims for my thesis below.

First aim: I will investigate tanycytes and the neurogenic niche along the A-P axis of the hypothalamus. This will include examining the localisation of hypothalamic neurons with respect to the tanycytes they are thought to arise from. I will also examine the localisation of the embryonic growth signals Fgf10

and Shh. I will investigate the various markers used to describe the tanycyte subtypes, and discuss how these subtypes are represented across the axis. I hypothesise that tanycyte markers and signals will vary with the changes in morphology across the hypothalamic A-P axis, and that this will correlate with differences in neurogenic potential.

Second aim: I will establish whether NrCAM marks tanycytes, and if so which specific subsets. Given the roles of NrCAM and L1-family members in proliferation/differentiation behaviour, I will investigate whether NrCAM has a role in these behaviours in the adult and developing hypothalamus by examining NrCAM mutant mice and comparing proliferation and differentiation competency *in vitro*. I hypothesise that NrCAM is expressed by tanycytes and regulates their proliferation/differentiation behaviour.

Figure 1.5 NrCAM expression in the adult hypothalamus
Figures from S Brown MSc Dissertation used with permission

A – NrCAM co-localises with Nestin on Tanycytes. Immunofluorescence image collected at 10x magnification of a medial hypothalamic section showing expression of NrCAM (green), Nestin (red), and the nuclear marker DAPI (blue), with 100µm scale bar. Boxed inserts I and ii show 20x magnification z-stacks displayed as maximum intensity projections (MIP) with 20µm scale bars. Insert I shows the α1-tanycyte domain, and insert ii shows the α2-tanycyte domain.

B – Immunofluorescence image showing NrCAM (red) is expressed on 7th passage hypothalamic neurospheres. Scale bar 20µm

C – DAPI labelling of the α1-tanycyte domain in wild type and NrCAM KO mice. The VZ appears thinner in the NrCAM KO sections. Scale bars 20µm

D – Average nuclei in the VZ of images from wild type and NrCAM KO medial hypothalamic sections. Ten sections were quantified and error bars show the standard error of the mean. NrCAM KO mice have significantly reduced number of cells lining the VZ ($p<0.0001$).

Figure 1.5

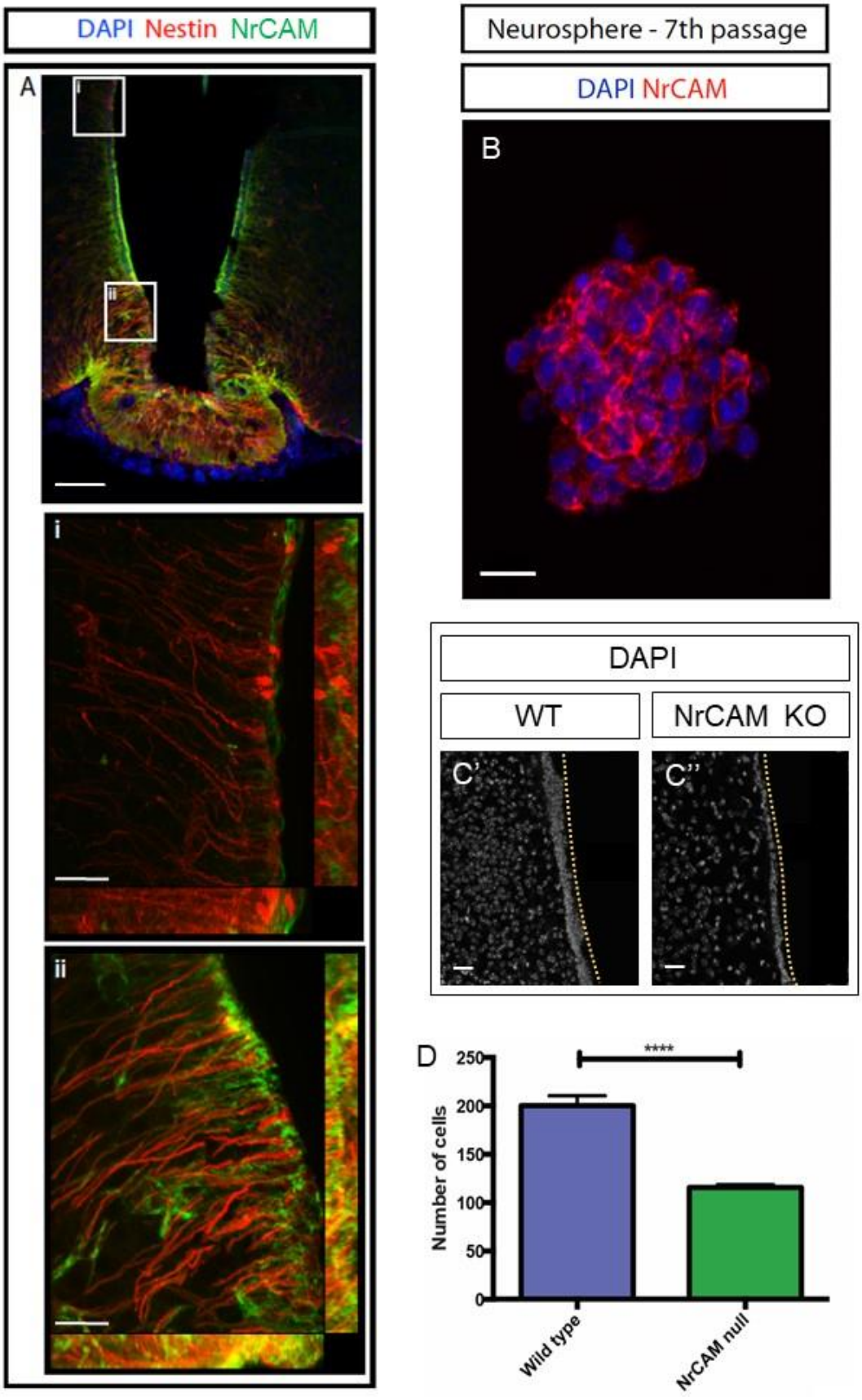
DAPI Nestin NrCAM
A
i
ii
i
ii
Neurosphere - 7th passage
DAPI NrCAM
B
DAPI
WT
NrCAM KO
C'
C''
D
****
Number of cells
250
200
150
100
50
0
Wild type
NrCAM null

CHAPTER 2: MATERIALS AND METHODS

2.1 Mice

2.1.1 Strains

Adult mice used in this study were 8-12 week old females. Embryonic mice of both sexes were sacrificed at E16. Wild type refers to C57Bl/6J mice. NrCAM knock-out (KO) ($Nrcam^{tm1Gmt}/Nrcam^{tm1Gmt}$) transgenic mice were previously constructed (Sakurai et al., 2001) and kept on a C57Bl/6J background. The NrCAM KO line was originally derived by replacing the second exon with a neomycin cassette, removing the ATG translation initiation codon. The modified NrCAM construct was electroporated into the W4 mouse embryonic stem cell line, and three clones were used to establish mouse chimeras through morula aggregation. Two clones successfully transmitted into the germline and then established into outbred lines. Wild type and NrCAM KO mice used for phenotypic comparison were bred within an $NrCAM^{+/-}$ colony and age matched at time of analysis.

All studies were approved by the University of Sheffield Ethical Review Board and were carried out in accordance with the UK Animals (Scientific Procedures) Act of 1986 (project license PPL PPL 40/3724, personal license PIL 80/2451).

2.1.2 Conditions

Mice were kept in standard conditions for the duration of the study. They received continuous access to fresh water and an 18% protein rodent diet. Cages were housed in a 12 hour light/dark cycle, at 19-23°C with 55% (±10%) humidity and 15-20 air changes per hour.

2.1.3 Genotyping

2.1.3.1 DNA Extraction

Mice in our colony were identified and genotyped by earclips collected by Biological Services staff. After sacrifice genotypes were confirmed from tail clips. Embryonic mice were genotyped after collection using limb tissue

samples. Samples were stored in 100% ethanol (437433T; VWR International) prior to analysis.

The DNA extraction protocol was adapted for from the Jackson Laboratory Phenol/chloroform extraction from mouse tail biopsies[4]. Approximately 1mm of tail or limb, or a single ear clip were removed, briefly washed in fresh Milli-Q Type 1 water, and placed in polypropylene microfuge tubes with 0.2mL DNA digestion buffer (50mM Tris-HCL pH8.0 (0497; Amresco), 100mM EDTA pH8.0 (D/0750/50; Fisons), 100mM NaCl (102415K; BDH), 1% SDS (301754L; BDH), 0.5mg/mL proteinase K (25530-049; Fisher Scientific)). Samples were incubated at 55°C overnight. The following day, 0.28mL neutralized phenol/chloroform/iso-amyl alcohol (25:24:1) (P2069-100ML; Sigma) was added and mixed vigorously on a shaker platform at room temperature for 1 hour. Tubes were spun at 16000G for 5 minutes and the aqueous DNA-containing upper phase was carefully drawn off and to a new microcentrifuge tube containing 0.5mL 100% ethanol, watching for evidence of DNA precipitation. Tubes were spun at 16000G for 5 minutes and the supernatant was removed and replaced with 0.5mL 70% ethanol chilled at -20°C. Tubes were inverted several times to wash the pellet and were then spun once again at 16000G for 5 minutes. The supernatant was immediately removed, taking care with last few µL not to disturb the pellet. Tubes were placed in a heat block at 55°C with their lids open until the remaining liquid evaporated. The DNA pellet was resuspended by incubation at 65°C for 15 minutes in 0.2mL TE buffer (10mM Tris pH8.0 (0497; Amresco) and 1mM EDTA (D/0750/50; Fisons) in DEPC-treated Milli-Q Type1 water adjusted to pH7.5). DNA yield was quantitated using a NanoDrop Spectrophotometer ND-1000 and samples were stored at 4°C until genotyping.

2.1.3.2 Genotyping

To genotype the collected DNA, the NrCAM gene sequence was amplified by PCR with primers for the NrCAM gene or the neomycin cassette inserted in the KO. DNA samples (200-500ng) and primers (0.2µM, supplied by Integrated DNA Technologies) for either the wild type or KO gene were mixed with 10µL

[4] https://www.jax.org/jax-mice-and-services/customer-support/technical-support/genotyping-resources/dna-isolation-protocols

BioMix (BIO-25012, Bioline) in PCR tubes (781320; SLS), and made up to a final volume of 20µL with fresh Milli-Q Type1 water. An MJ Research PTC-200 thermocycler was used for the PCR amplification using the following protocol, with a 55°C annealing temperature for NrCAM primers, and a 59°C annealing temperature for Neo primers:

Table 2-1

Primer:	Detection	Primer Sequence
Nr Int 3:	NrCAM WT	GCT CAG GAT GGT TGC GCC
Nr MP1:	NrCAM WT	CTT CCT GTG CCA GAT GAT CA
NEO F1:	NrCAM KO	TGG AGA GGC TAT TCG GCT ATG AC
NEO B5:	NrCAM KO	AGC AAG GTG AGA TGA CAG GAG ATC

94°C	5 min	
94°C	30 sec	x 30 cycles
55/59°C	30 sec	
72°C	1 min	
72°C	10 min	
4°C	hold	

The PCR products were visually assessed by gel electrophoresis on a 2% agarose gel (A9539; Sigma) and compared to bands from established NrCAM$^{+/+}$, NrCAM$^{+/-}$, and NrCAM$^{-/-}$ DNA samples. The expected PCR products are 340bp for NrCAM and 260bp for Neo.

2.1.4 Embryonic mouse collection

Embryonic mice were collected in accordance with Schedule 1 methodology. After removal from the mother, embryos were immersed in ice cold Leibovitz's 15 (L-15) media (11415-049; GIBCO) and decapitated. Tissue of the head was removed leaving the intact skull which was immersed in 4% paraformaldehyde (P6148; Sigma) in 0.12M Phosphate buffer (4% PFA PB) overnight at 4°C. The

following day the brain was removed from the skull and fixed in 4% PFA PB for a further 3 hours at 4°C before transfer to 30% sucrose (S0389; Sigma) in 0.2M phosphate buffer. These were kept at 4°C on a rocker overnight before washing in 1X phosphate buffered saline (PBS) (P4417; Sigma) and mounting in OCT (361603E; VWR International). Mounted brains were frozen on dry ice and transferred to -80°C for storage.

2.1.5 Adult mouse collection

To collect fixed brain tissue adult mice were sacrificed by inhalation of isoflurane anaesthetic (B506; Abbott) and perfused with 4% PFA PB. After perfusion the mice were decapitated and the brains removed. Brains were stored in 4% PFA PB at 4°C overnight. The following day they were transferred to 30% sucrose (S0389; Sigma) in 0.2M phosphate buffer and kept on a rocker at 4°C for 3 days until the brains stopped floating and sank to the bottom of the solution. For mounting the anterior forebrain, hindbrain, and cerebellum were removed in 1X PBS. The remaining medial portion of the brain containing the hypothalamus was orientated in OCT and frozen on dry ice before storage at -80°C.

2.2 Immunostaining

2.2.1 Cryosectioning

Adult sections were collected on a cryostat (OTF5000; Bright) as 15µm floating sections (unless stated otherwise) in 1X PBS. Embryonic sections and explant were collected as 15µm sections directly onto superfrost slides. Sections collected directly onto slides were air-dried then immersed in 1X PBS.

2.2.2 Immunostaining procedure

Samples were washed three times for 5 minutes in 1X (PBS) then immersed in blocking buffer for 1 hour at room temperature. If antigen retrieval (2.2.1) was required it was done after the washes and prior to blocking. Blocking buffer contained 1X PBS containing 0.5% TritonX-100 (T8787; Sigma) and 5% heat-inactivated goat serum (16210-072; GIBCO) for adult tissue, and 0.1% TritonX-100 and 1% heat-inactivated goat serum for embryonic tissue. For differentiation cultures (outlined in 4.3) blocking buffer was made using 0.05%

TritonX-100 and 1% heat inactivated goat serum in 1X PBS. Following the 1 hour block, samples were labelled with primary antibody diluted in blocking buffer at 4°C overnight. After primary antibody binding, the samples were washed three times for five minute in 1X PBS and labelled with secondary antibody diluted in the appropriate blocking buffer for 1 hour at room temperature protected from light. For adult tissue DAPI (D9542-10MG; Sigma) was added at 100ng/mL to the secondary antibody solution. This was followed by an additional three by 5 minute washes in 1x PBS to remove unbound secondary antibody. Floating sections were then mounted on slides by careful manipulation with forceps and fine paintbrushes in a small quantity of 0.5X PBS. Excess liquid was removed from slides and two drops of fluoroshield mounting media were added to allow coverslipping (22x64mm Cover Glass; 631-0880; VWR International). For adult tissue fluoroshield without DAPI (F6182; Sigma) was used, and for embryonic tissue and differentiated neurospheres fluoroshield with DAPI (F6057; Sigma).

2.2.3 Antigen retrieval

For observable labelling of some antigens in adult mouse sections a citrate buffer antigen retrieval was required. Paraformaldehdye fixation causes protein cross-linking which can mask antigen binding sites and cause poor fluorescent labelling or false-negative results. The following treatment is designed to break the cross-linkages, opening the antigen binding sites for antibody labelling. All antibodies used in this study were tested with and without antigen retrieval. Antigen retrieval was not seen to reduce the signal for any antigens, but was seen to elicit a marked improvement in labelling in adult sections for primary antibodies derived from a mouse host. In keeping with these observations, all experiments on adult brain sections using a mouse-derived primary antibody included the following antigen retrieval steps.

Sections were collected as described in section 2.1 (onto slides or floating) and the initial three by 5 minute 1X PBS washes from section 2.2 were performed. Before the blocking step, slides were transferred to coplin jars containing Citrate Buffer (10mM Citric Acid (277804I; BDH), 0.05% Tween 20 (P9416; Sigma), pH 6.0) and incubated at 90°C for 1 hour. Sections were then cooled for 20 minutes

Table 2-2

Primary antibody	Host	Dilution	Source	Catalogue #	Reference:
GFAP	Mouse IgG	1:50	BD Pharmingen	556330	(Pegram et al., 1983)
GHRH	Rabbit	1:600	Chemicon	AB1751 (Disc)	(Bloch et al., 1983)
Islet1	Mouse IgG	1:20	DSHB	4D5.61	(Tsuchida et al., 1994)
HuC/D (16A11)	Mouse IgG	1:70	Molecular Probes	A21271	(El-Yazbi et al., 2008)
MAP2	Mouse IgG	1:1000	Sigma-Aldrich	M9942	(Yan et al., 2001)
Nestin [2Q178]	Mouse IgG	1:200	Abcam	Ab6142	(Robins et al., 2013a)
NPY	Rabbit	1:1000	Immunostar	22940	(Xu et al., 2004)
NrCAM	Rabbit	1:1000	Lustig et al, 2001	838	(Lustig et al., 2001b)
phospho-H3	Rabbit	1:1000	Millipore	06-570	(Hendzel et al., 1997)
RIP	Mouse IgG	1:10	DSHB	AB_531796	(Song et al., 2002)
Six3	Rabbit	1:10000	Eurogentec	3826	Custom antibody for Placzek lab. Sequence: RLQ-HQA-IGP-SGM-RSL-AEP-GC
Sox2	Rabbit	1:200	Abcam	Ab97959	(Mukouyama et al., 2006)
TH	Rabbit	1:1000	EMD Millipore	Ab152	(Tompkins et al., 1997)

Table 2-3

Secondary antibody	Host	Dilution	Source	Catalogue #
α-Rabbit Alexa488	Goat	1:500	Molecular Probes	A11034
α-Rabbit Alexa594	Goat	1:500	Molecular Probes	A11012
α-MouseIgG Alexa488	Goat	1:500	Molecular Probes	A11001
α-MouseIgG Alexa594	Goat	1:500	Molecular Probes	A11005

before washing in 1X PBS three times for 5 minutes. The protocol from 2.2 was then resumed and the sections were immersed in blocking buffer for 1 hour at room temperature.

2.2.4 Antibodies

Antibodies were used at dilutions previously described in academic literature referenced by the manufacturers.

2.2.5 Image acquisition and analysis

2.2.5.1 Fluorescence acquisition, controls, and analysis

Images of samples labelled by immunofluorescence were captured using a Zeiss Axioimager Z1 with Apotome.2 attachment and viewed in the Zeiss Zen 2 image acquisition software. Images were collected at 10x and 20x magnification using air objectives and at 40x using oil objectives. Where required, z-stacks were created by imaging slices at evenly-spaced intervals between the upper and lower limits of focus for each section. For further analysis, z-stacks were flattened into maximum intensity projections (MIP) except were otherwise outlined. Exposure was kept consistent during acquisition for images used in comparison or quantification.

To ensure the fluorescent labelling was not a product of non-specific background labelling by the fluorescently-tagged secondary antibodies, control samples were prepared following the protocol described in 2.2.2, but with the primary-antibody step replaced by an equivalent incubation in blocking buffer. Images from labelled samples and secondary antibody-only controls were

compared during imaging to ensure no background labelling was included in the analysis.

Where antibodies were used for the first time, we compared the resulting images to those in the published literature to ensure the pattern of labelling was correct. While the anti-NrCAM antibody has been used widely before (Lustig et al., 2001b), it had not previously been used in the adult hypothalamus. To ensure the antibody was specifically labelling NrCAM in the hypothalamus, we compared labelling by the antibody in wildtype and NrCAM KO mice. No labelling was observed in the NrCAM KO mice, indicating that the labelling observed in the wildtype brains was specific to the localisation of the NrCAM molecule.

Where appropriate, brightness and contrast were adjusted to produce representative and comparable images, and to improve cell identification during manual quantification. To ensure consistency within each experiment an optimal adjustment profile was made manually, and then applied to all the images collected. Raw data files were exported as .TIF files for viewing in ImageJ. Cell or process quantifications were conducted manually using the ImageJ counting tool and the resulting data were statistically analysed using GraphPad Prism 7. Statistical tests used are outlined in the appropriate figure legends and results text.

2.2.5.2 Fluorescence quantification

To quantify Nestin^{+} processes in adult and E16 hypothalamic sections 20x magnification z-stacks were collected, flattened, and split into single channel images. For every section, processes on each side of the ventricle were counted separately yielding two replicates. Processes were counted from ventral to dorsal, beginning with the ventral most processes projecting the lateral flexures of the ME and continuing dorsally to those extending to the dorsal arcuate (Fig 2.1). Counts were made manually by opening the files in ImageJ, identifying the processes by eye, and marking with the multipoint tool. To maintain consistency, and to ensure no processes were counted twice, they were marked where they first extend into SVZ from the VZ. To control for differences in the countable region in each image, a curve was drawn round the counted region of the ventricle and the length was measured. The total number

Figure 2.1 Example of Nestin+ tanycyte process identification for quantification

Identical images showing Nestin+ tanycyte processes (white fluorescent labelling [left] or coloured [right]) extending from the VZ (dashed yellow line). Images were collected at 20x magnification and enlarged on screen to allow Nestin+ process quantification. Identified processes have been false coloured in the right hand image as an example. Identified processes were counted, then density was calculated by dividing by the length of the VZ against the tanycyte-containing domain that was counted.

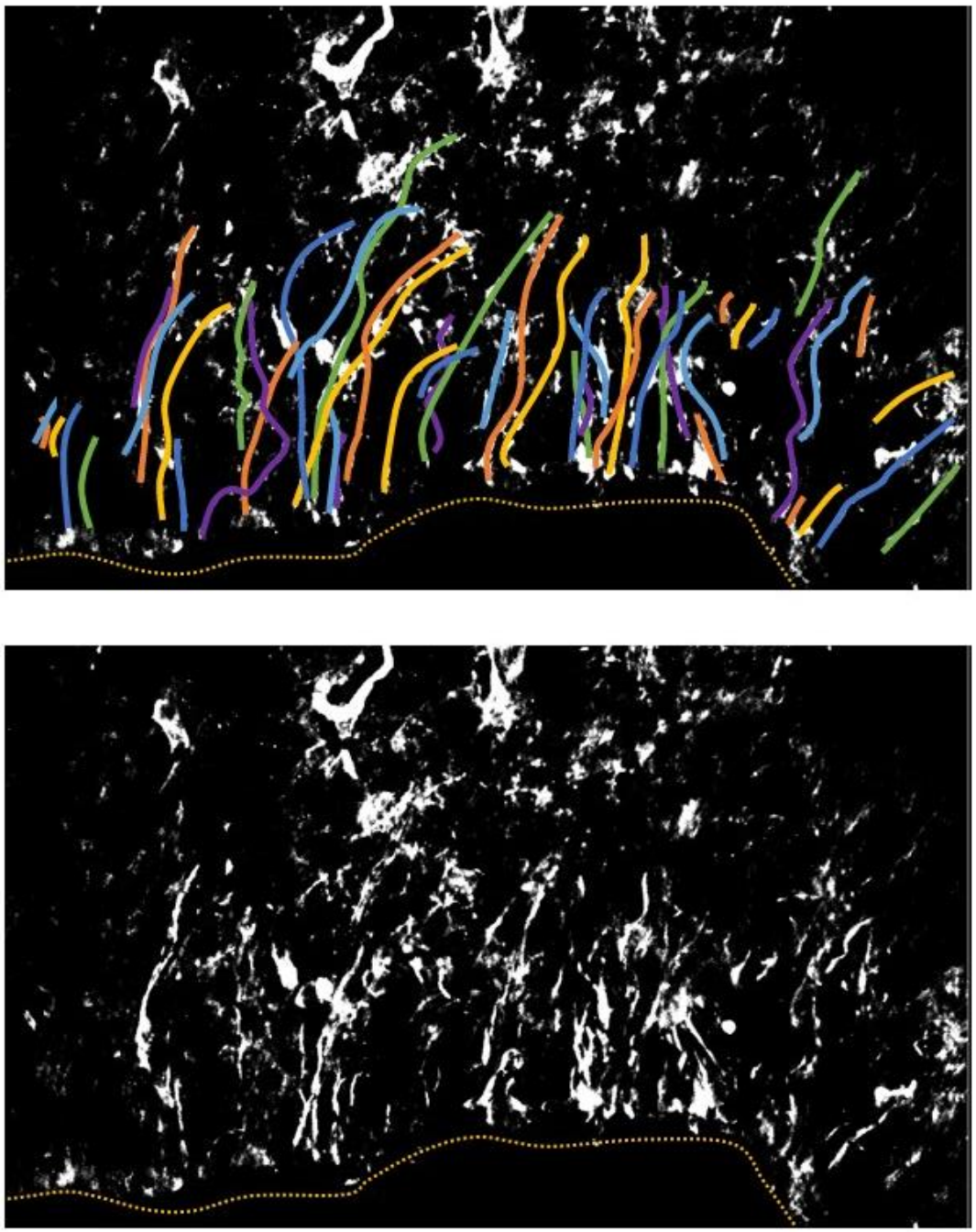

of processes counted was divided by the counted distance, giving a measure of process density (processes per µm) along the ARC-adjacent 3V. Section counts were pooled into AME, ME, PME, and P subgroups for comparison, as well as into a single pool to compare overall differences in process density between WT and NrCAM KO mice. This method was repeated multiple times on the same sections whilst blinded and following a delay of days to establish consistency.

To quantify TH^+ cells in adult and E18 hypothalamic sections, 10x magnification images were collected and split into single channel images. For every section, TH^+ cells on each side of the ventricle were counted separately yielding two replicates. TH^+ cells were counted from ventrolateral to mediodorsal across the ARC. Counts were made manually by opening the files in ImageJ, identifying the TH^+ cell bodies by eye, and marking with the multipoint tool. To be counted the TH^+ cells bodies must be distinctly rounded and equal to or greater in size to nuclei. In the few instances where I was unsure whether the label showed a cell body, or if I was unsure whether the label showed two cells in close proximity, I compared the single channel image to a combined DAPI/TH image and identified whether one or more nuclei were present in the queried area of signal. Section counts were pooled into A, AME, ME, PME, and P subgroups for comparison, as well as into a single pool to compare overall differences in process density between WT and NrCAM KO mice. This method was repeated multiple times on the same sections whilst blinded and following a delay of days to establish consistency.

To quantify TH^+, HuC/D^+, and phospho-$H3^+$ cells in hypothalamic explant sections, 20x magnification images were collected and split into single channel images. Counts were made manually by opening the files in ImageJ, identifying the TH^+, HuC/D^+, and phospho-$H3^+$ cell bodies by eye, and marking with the multipoint tool. To be counted the cell bodies must distinctly rounded and equal to or greater in size to nuclei. In the few instances where I was unsure whether the label showed a cell body, or if I was unsure whether the label showed two cells in close proximity, I compared the single channel image to a combined DAPI/TH image and identified whether one or more nuclei were present in the queried area of signal. Where sections covered multiple images, cells in each image were counted and then combined.

2.3 *In situ* Hybridisation

2.3.1 Probes and probe-making

To generate probes from plasmid stocks a standard plasmid linearization and probe synthesis protocol was followed. Both antisense and sense probes were made and used during ISH to ensure specificity of chromogenic labelling (see 2.3.5).

Table 2-4

Probe	Antisense RE/polymerase	Sense RE/polymerase	Dilution	Source
Rax	SalI/T7	NotI/Sp6	1:50	Geneservices
Shh	HindIII/T3	NotI/T7	1:50	D. Epstein
Fgf10	BamHI/T3	PstI/T7	1:50	S. Bellusci

2.3.2 Restriction enzymes and RNA polymerases

T3 (M0378; New England Biolabs), T7 (M0251; New England Biolabs), Sp6 (M0207; New England Biolabs). NotI (R0189; New England Biolabs; Buffer 3.1 (B7203; New England Biolabs)), SalI (R0138; New England Biolabs; Buffer 3.1), PstI (R0140; New England Biolabs; Buffer 3.1), HindIII (R3104; New England Biolabs; Cutsmart Buffer (B7204; New England Biolabs)), BamHI (R602A; Promega; Buffer E (R005A; Promega)).

2.3.3 Probe linearization and synthesis

Rax, Shh, Fgf10 probes were made from previously established plasmid stocks. The probe linearization reactions for antisense and sense probes were setup with 20µg DNA in the relevant restriction enzyme and associated restriction buffer, 1 µL BSA (R396D; Promega), and diethyl pyrocarbonate (DEPC; D5758; Sigma)-treated Milli-Q Type 1 water. Reaction samples were incubated at 37°C for 3 hours and an aliquot was kept to run on a 1% agarose (A9539; Sigma) gel to confirm linearization was successful. Linearised DNA was cleaned up using a miniprep kit (27014; Qiagen) and a sample was collected to run on the gel.

Probes were synthesised by combining 1µg linearised DNA with reaction buffer

(#B9012S; New England Biolabs), DIG (11277073910; Roche) or fluorescein labelling mix (11685619910; Roche), RNase inhibitor (#M0314S, New England Biolabs), Milli-Q Type 1 water (Millipore), and the appropriate RNA polymerase for a sense or antisense probe. An additional reaction setup without RNA polymerase was used to provide a control for the confirmatory gels. This mixture was incubated for 2 hours at 37°C, with additional polymerase added after the first hour. At this point a sample for running on a gel was collected from each reaction.

To precipitate probes the reaction mixture was made up to 90mM LiCl in 65% ethanol (437433T; VWR International) added and was stored at -20°C overnight. On the following day, probes were spun down in a 4°C centrifuge at 16000G for 30 minutes. All supernatant was immediately removed and the pellet was washed in 70% ethanol (clean for RNA work). The mixture was vortexed and spun for 5 minutes at 4°C and all the supernatant was removed. The pellet was dried in a heating block at 50 degrees for 10 minutes. The pellet was returned to suspension in 50µL DEPC-treated Milli-Q Type 1 water by mixing with repeated expulsion of liquid through a pipette and heating at 65°C in a water bath. A final sample for the confirmatory gel was taken and 50µL formamide (47670; Sigma) was added to the resuspended probe.

Success in generating probes was determined by running the outlined samples on a 1% agarose gel. Samples from the no-RNA polymerase control were checked for a single band of linearised DNA, whilst the post-synthesis and post-precipitation samples were checked for a shorter RNA band and the longer linearised DNA band.

2.3.4 Cryosectioning

Adult and embryonic (E16) mouse brain 15µm serial sections were collected on a cryostat (OTF5000; Bright) directly onto superfrost slide and air dried before storage at -80°C.

2.3.5 ISH procedure

The chromogenic *in situ* hybridisation protocol used in this study was adapted from a protocol received from the Blackshaw lab, where it was used for the analysis of Rax expression in the adult mouse hypothalamic ventricular zone

(Miranda-Angulo et al., 2014).

Slides were removed from -80°C, thawed, briefly air dried, and post-fixed in 4% PFA PB for 10 minutes at room temperature. They were then washed 3 times in 1X PBS for 5 minutes and permeabilised in PBS containing 0.1% TritonX-100 for 30 minutes at room temperature. An acetylation mixture containing 1.3% triethanolamine (90279; Sigma), 2.1M HCl (H/1150/PB17; Fisher Scientific) and 0.25% acetic anhydride (added last) (A6404; Sigma) in DEPC Milli-Q Type1 water was applied to samples for 10 minutes at room temperature to decrease background signal and inactivate any RNases present. This was followed by three 5 minutes washes in 1X PBS.

Slides were then placed in hybridisation chambers, coated with 500µL pre-hybridisation solution containing 50% formamide, 5X saline-sodium citrate buffer (SSC), 2% blocking reagent (11096176001;Roche), 0.1% TritonX-100, 0.5% CHAPS (C-3023; Sigma), 1mg/mL yeast RNA (109 223; Roche), 5mM EDTA (D/0750/50; Fisons), and 50µg/mL heparin (H3149; Sigma) in DEPC Milli-Q Type1 water. Slides were then coated with coverslip-sized parafilm slices (NOVIX2-10; Iwaki) to ensure slides retained their pre-hybridisation solution covering. The chamber floor was moistened with tissue soaked in 5X SSC and the pre-hybridisation reaction was allowed to occur for 2 hours at room temperature. Pre-hybridisation solution was removed and replaced with 250µL an identical hybridisation solution containing a dilution of RNA probe. Slides were coverslipped and the hybridisation chambers were sealed with waterproof tape and incubated overnight at 68°C.

Coverslips were removed and slides were transferred to coplin jars of 0.2X SSC at 68°C for 1 hour on a rocking tray. This wash was repeated before slides were removed from coplins and given a further 5 minute 0.2X SSC wash at room temperature. Slides were washed in B1 buffer (0.1M Tris pH7.5 (0497; Amresco) and 0.15M NaCl (102415K; BDH) in DEPC-treated Milli-Q Type1 water) for 5 minutes at room temperature. To equilibrate sections for antibody binding they were immersed in B2 buffer (B1 with 5% heat-inactivated goat serum) for 1 hour at room temperature. Alkaline phosphatase conjugated anti-DIG or anti-Fluorescein antibodies were diluted 1:2000 in B2 and applied to the slides. Slides were covered with coverslip-sized parafilm slices to ensure

antibody solution was retained and were incubated overnight at 4°C in the humidified chambers.

The following day slides were washed 3 times with B1 buffer for 5 minutes. They were then equilibrated overnight at 4°C in B3 Buffer (0.1M Tris pH9.5, 0.1M NaCl, 50mM $MgCl_2$, and 1% Tween20 in DEPC-treated Milli-Q Type1 water, 0.45µm filtered). After equilibration the development reaction was initiated by pooling slides with B4 buffer (B3 containing 3.375 µL/mL NBT (11383213001; Roche) and 3.5µL/mL BCIP (1138221001; Roche)). Slide were kept in the dark at room temperature and checked every 3 hours for development and B4 was replaced. Where necessary, slides were stored in fresh B3 to 4°C overnight, slowing the reaction until developing could be continued on the following day.

Once the chromogenic signal had sufficiently developed slides were rinsed with TE buffer (10mM Tris pH8.0 and 1mM EDTA in DEPC-treated Milli-Q Type1 water adjusted to pH7.5) then DEPC-treated Milli-Q Type1 water. Slides were mounted with 2 drops of fluoroshield (without DAPI) per slide and coverslipped (22x64mm Cover glass).

To ensure the chromogenic labelling identified during ISH was specific to the location of the target mRNA, antisense and sense probes were used on serial sections. Antisense probes target the desired mRNA sequence, while sense probes target the complimentary sequence and are used as a negative control. Labelling by sense probes is off-target or non-specific labelling, and sense probe labelling, whether in a pattern or as background labelling, must be discounted from analysis of the antisense probe.

Such comparisons were important for determining the labelling of Fgf10 and Shh. ISH for Fgf10 produces very weak specific-labelling over the course of many days. Comparison to the sense probe allowed me to identify the specific labelling against the background labelling. ISH for Shh labels a very small number of cells in the adult mouse, so comparison from mouse to mouse, and comparison to the sense probe was required to show that labelling was specific and not an artefact caused by non-specific labelling, ventricle folding, or crystal formation.

Comparison to these negative controls allowed me to be confident that the labelling I was observing was specific, and that the small changes I observed in NrCAM KO mice are not a product of changes in non-specific labelling. As an additional control, ISH for WT and NrCAM KO mice was conducted in pairs, probing for the same markers by conducting the protocol at the same time, with the same solutions, and developing the chromogenic labelling for precisely the same amount of time. This ensured the ISH chromogenic labelling was comparable in the paired WT and NrCAM KO samples, and changes in the intensity of that labelling represent of differences in expression levels of the target mRNA.

2.3.6 Image acquisition and quantification

Images of samples labelled by chromogenic *in situ* hybridisation were captured using an Olympus BX60 with QIClick 01-QICLICK-R-F-M-12 camera and viewed in Q-Capture Pro 7.0 software (Q-Imaging). Images were collected at 10x and 20x with an air objective.

2.3.6.1 Quantification of the length of chromogenic ISH labelled ventricular zone

Images of Rax, Fgf10, and Shh, labelled sections from adult and E16 brains were opened ImageJ. The segmented line tool was used to draw along the ventricle surface lined by chromogenically labelled cells, and the length measurement for the line was collected.

Measurements were taken from paired wild type and NrCAM$^{-/-}$ mouse sections from in order from anterior to posterior, with three biological replicates for each A-P position. The measurements were statistically analysed in GraphPad Prism 7.04 using the Wilcoxon matched-pairs signed rank test.

2.3.6.2 Quantification of chromogenic ISH signal intensity

Images of Rax, Fgf10, and Shh, labelled sections from adult and E16 brains were opened ImageJ. The segmented line tool was used to draw a one-pixel line profile through the centre of the VZ, round the entire chromogenically labelled domain, and the mean grey value was measured. A control measurement was collected from a line profile through the adjacent non-

labelled parenchyma, and the mean grey value of the labelled domain was adjusted so that it was normalised relative to the background signal. Mean grey value describes the mean brightness of the pixels in the line profile, with a readout between 0-256 (back-white). For chromogenic ISH, a lower mean grey value represents a darker, stronger signal, indicative of more target mRNA.

Measurements were taken from paired wild type and NrCAM$^{-/-}$ mouse sections from in order from anterior to posterior, with three biological replicates for each A-P position. The measurements were statistically analysed in GraphPad Prism 7.04 using the Wilcoxon matched-pairs signed rank test.

2.3.6.3 Quantification of individual chromogenic ISH labelled cells

To quantitate isolated Shh^{+} cells in the VZ, or Rax^{+} cells in the median eminence parenchyma, images of labelled sections were opened in ImageJ, and the cells were individually recorded with the multi-point tool. Measurements were taken from paired wild type and NrCAM$^{-/-}$ mouse sections from in order from anterior to posterior.

To compare Rax^{+} median eminence cells, three biological replicates were collected for each A-P position. The measurements were statistically analysed in GraphPad Prism 7.04 using the Wilcoxon matched-pairs signed rank test. As few sections over one subregion contained Shh^{+} cells in the VZ, measurements from three biological replicates were pooled and statistically analysed in GraphPad Prism 7.04 using an unpaired t-test with Welch's correction.

2.4 Neurosphere culture

Neurosphere culture is a method of investigating neural stem and progenitor cells *in vitro* (Reynolds and Weiss, 1992). This study uses a protocol derived from Robins et al, (2013), in which the assay was used to assess capacity for long-term self-renewal in adult hypothalamic tissue.

2.4.1 Hypothalamus dissection

Adult mice were sacrificed by inhalation of isoflurane anaesthetic (Zoetis) and cervical dislocation in accordance with Schedule 1 procedures. Mice were decapitated and the brains removed into ice-cold Leibovitz's 15 (L-15) media

(11415-049; GIBCO). The ventral surface meninges and exposed optic nerve including the optic chiasm were removed. Small cuts were made into the ventral surface of the brain anterior, posterior, and lateral to the hypothalamus and the hypothalamus was removed. Tissue of two hypothalamus were pooled and minced using forceps. The tissue was centrifuged at 145G for 5 minutes, supernatant was removed, and the tissue was trypsinised (TrypLE solution, 12604013, Life Technologies) at 37°C for 10 minutes. An equal volume of 4°C trypsin inhibitor solution (0.01M HEPES (H3375; Sigma), 0.3% BSA solution (A8412; Sigma), and 140µg/mL trypsin inhibitor (T6522-25MG Sigma) in L-15) was added to stop the reaction with 40µl DNAse solution (1mg/mL DNAse 1 (D4527-10KU Sigma) in Ca^{2+}/Mg^{2+} free HBSS). The tissue was centrifuged at 145G for 5 minutes then resuspended in dissociation solution (0.3% BSA solution in DMEM:F12 (21331; GIBCO)) and 40µl DNAse solution. To manually dissociate the cells, the suspension was triturated through the tip of a P1000 pipette for 90 seconds. The solution was centrifuged and additional time at 145G for 5 minutes and the supernatant was replaced with neurosphere culture media (DMEM/F-12 (21331; GIBCO) supplemented with 100U/mL penicillin/streptomycin (11578876: Fisher Scientific), 2mM L-Glutamine (25030024; GIBCO), 1X B27 (17504-044; Life Technologies), 5µg/ml heparin, 10µM transferrin (T0665; Sigma), 20nM progesterone (P7556; Sigma), 30nM selenite (S5261; Sigma), 100µM putrescine (P5780; Sigma), 50ng/mL IGF-1 (I8779-50UG; Sigma), 20ng/mL bFGF (13256029; Life Technologies), and 20ng/mL EGF (PHG0314; Life Technologies)). Primary neurosphere cultures were maintained at 37°C and 5% CO2 for 7 days in Corning Costar Ultra-Low attachment 24 well plates (3473 SLS).

2.4.2 Neurosphere quantification and passaging

Where comparison of neurosphere numbers was required, neurospheres in the wells of rows 2 and 3 were counted using a 4x magnification objective and averaged prior to passaging.

To passage the neurospheres, the contents of all wells were pooled and centrifuged at 145G for 5 minutes then resuspended in TrypLE trypsin solution an trypsinised for 10min at 37°C. An equal volume of 4°C trypsin inhibitor solution with 40µl DNAse solution was added to stop the reaction and the

samples were centrifuged at 145G for 5 minutes. The supernatant was removed and the pellet was resuspended in dissociation solution with 25µl DNAse solution. To manually dissociate the cells, the suspension was triturated through the tip of a P1000 pipette for 90 seconds. The solution was centrifuged and additional time at 145G for 5 minutes and the supernatant was replaced with neurosphere culture media. Cell concentration was quantified using a haemocytometer and cells were re-plated at a concentration of 10000 cells/mL and cultured at 37°C and 5% CO2 for 6 days. Cultures from first passage onwards were fed with neurosphere media every other day.

Additional cells yielded by passaging were cultured in T25 flasks (690175; Greiner Bio-One) containing neurosphere culture media for 1 day before transfer to cryovials (E3090-6212) for freezing in neurosphere culture media containing 10% DMSO (D2650; Sigma) and storage at -80°C. To re-establish cultures from frozen neurosphere stock, cryovials were thawed at 37°C in a water bath and quickly combined with pre-warmed dissociation solution. Cell suspensions were centrifuged at 145G for 5 minutes and the supernatant was replaced with neurosphere culture media. Re-established cells were cultured in T25 flasks at 37°C and 5% CO2 for 6 days and fed with neurosphere culture media every other day.

2.4.3 Neurosphere differentiation

Neurospheres were differentiated in Nunc Lab-Tek 8-well Permanox chamber slides (C7182; Sigma) coated with poly-D-lysine (P1024; Sigma) for 1 hour and fibronectin (10042682; Fisher Scientific) for 4 hours. Differentiation media was made to the same specification as neurosphere culture media but without IGF-1, EGF, reduced bFGF (10ng/mL), and with B27 supplement replaced with B27 minus insulin (A1895601; Thermo Fisher). Differentiation media was equilibrated in the coated chamber slides for 1 hour. One neurosphere was added to each well and cultured at 37°C and 5% CO2 for 14, 21, or 28 days as specified. Differentiation cultures were fed every two days.

Once the end of the culture duration was reached, media was removed and cells were fixed for 20 minutes in 4% PFA PB. Chambers were peeled off and the Permanox slides were washed three times for 5 minutes in 1X PBS followed by one was in 0.05% TritonX-100 in 1X PBS. The immunostaining protocol for

neurosphere differentiation cultures is described in section 2.2.

2.5 Explant culture

2.5.1 Hypothalamus dissection

Adult mouse brains where removed into ice cold Leibovitz's 15 (L-15) media (11415-049; GIBCO). Careful dissection removed the forebrain and hindbrain, leaving only the area of interest. These chunks containing hypothalamus were mounted coronally on a McIlwain tissue chopper and chopped into 100µm sections. Tungsten needles were used to separate the venteromedial regions of the ventricle from the lateral parenchyma, and to split the ventricle into three parts: the two lateral walls and the ME.

2.5.2 Explant culture

Explant culture in collagen was adapted from Placzek & Dale (1999). Collagen from rat tails was extracted with glacial acetic acid at 4°C for 24-36 hours and then dialyzed against 0.1X DMEM, pH 4.0, without bicarbonate at 4°C for 3 days. This preparation was conducted by another member of our lab group. 90µL collagen solution was mixed with 10 µL 10x DMEM (Sigma, D2429) and 6µL 0.8M NaHCO3 and vortexed until the solution turned light pink. 25µL collagen solution was pipetted into the centre of each well in 4-well multidishes (176740; Thermo Scientific) and left to set at room temperature for 20 minutes. Explants were transferred to each collagen cushion carefully using a Pasteur pipette and overlayed with 25µL collagen, before being left to set for 40 minutes. Explants were covered with 0.5mL culture media of Opti-MEM (31985070; Fisher Scientific) with 100U/mL penicillin/streptomycin (11578876; Fisher Scientific), 2mM L-Glutamine (25030024; GIBCO), and 4% FBS (10042682; Fisher Scientific) (Placzek et al., 1993) supplemented with 3nM Shh (1845-SH; R&D Systems), as used in Ohyama *et al* (2005) to promote hypothalamic neuron differentiation from prospective hypothalamic tissue. Controls were fixed in 300µL 4% PFA PB immediately without addition of media. Cultured explants were incubated at 37°C and 5% CO2 for 7 days, feeding on alternate days. Following culture, explants were fixed in 300µL 4% PFA PB for 2 hours at 4°C. Fixative was replaced with PBS (P4417; Sigma) for bright field imagining of the explants. After imaging, the PBS was replaced with

30% sucrose (S0389; Sigma) and incubated at 4°C overnight. The following day, explants in collagen were mounted in OCT (361603E; VWR International). The collagen matrices were by carefully detached from the base of each well and placed on chucks topped with OCT. Once settled, a final thin coat of OCT was added and the chucks were placed on dry ice to freeze.

2.5.3 Explant bright field imaging

Bright field images of explants were collected after culture and prior to sectioning to characterise and compare the shape and extent of outgrowth. Images were collected at 10x and 8x magnification using a Leica M165FC with mounted Leica 10447367 0.63x camera. Images were processed using LAS X software.

2.6 Statistical analysis

In the main body of text in this thesis I collected data for statistical analysis from three biological replicates (3 pairs of wildtype and NrCAM KO mice), and pooled these data to increase the number of measurements in each analysis. The aim when doing this was to increase the sensitivity of the statistical analysis to differences with a small effect size. Data sets were classed as paired when serial sections were collected, allowing direct matching between wildtype and NrCAM KO sections. Data sets were classed as unpaired when sections could not be directly matched following the collection of floating sections.

I have checked the distribution of data, and where the data was shown to be normally distributed I have used an unpaired t-test with Welch's correction (where unequal variance was observed) or Mann-Witney U test for. Where data were paired but distribution was not normal a Wilcoxon signed rank test was used. Unpaired data have been shown using scatterplots for the whole hypothalamus or grouped into subregions. Scatter plots display every data point and have bars indicating the mean and standard deviation of the measurements to describe the variance within the data. Paired data could be assigned a position along the A-P axis of the hypothalamus, and as a consequence they have been plotted as line graphs. As each A-P position contains only 3 data points for each genotype, bars have been added to show the range of the values around the mean value depicted by the line.

The best statistical method for analysing much of my data was unclear. For each biological replicate (pairs of individual wildtype and NrCAM KO mice) there were dozens of measurements, each corresponding to a different A-P positions. Analysing the data from all biological replicates together and chunking the data based on the subregion allowed me to simplistically assess the differences in subregions between wildtype and NrCAM KO mice. However, this analysis did not account for variation between biological replicates from the same genotype. It also did not represent the pairing of wildtype and NrCAM KO mice. For adult mice, these pairs were selected from within a single litter (at least one pair per experiment), or from closely age-matched mice within the inbred $NrCAM^{+/-}$ breeding colony. Pairs of embryonic mice were littermates. To determine whether the analyses I have conducted are representative of differences between every pair of wildtype and NrCAM KO mice, each of these pairs need to be statistically analysed.

Since writing this thesis, we have sought to address this issue so that we can prepare the data for publication. Through discussion with biostatistician we have elected to change the way the analysis on this data is conducted. Details of this reanalysis and examples of its use have been included in an appendix (Chapter 9), and compared to the results described in the main body of the thesis. As we continue this analysis in preparation for publication we will continue our discussion with the biostatistician, ensuring the analysis is appropriate for the investigations we have conducted.

CHAPTER 3: DEFINING THE HYPOTHALAMIC NEUROGENIC NICHE

3.1 Introduction

The adult hypothalamic neurogenic niche has been the focus of many studies over the past decade (Butruille et al., 2018; Haan et al., 2013; Hendrickson et al., 2018; Kokoeva et al., 2005, 2007; Lee et al., 2014; Pellegrino et al., 2017; Pierce and Xu, 2010; Robins et al., 2013a; Wang et al., 2012). While various local populations have been investigated as sources of neurogenesis, the brunt of the research has been focussed on tanycytes. (Haan et al., 2013; Hendrickson et al., 2018; Lee et al., 2014; Li et al., 2012; Robins et al., 2013a). Lineage-tracing studies reveal that tanycytes can give rise to neurons of the ARC in response to physiological changes (Bless et al., 2016; Chaker et al., 2016; Haan et al., 2013; Kokoeva et al., 2005; Lee et al., 2012; Pierce and Xu, 2010; Robins et al., 2013a). In this capacity, tanycytes are thought to be important for long-term maintenance or changes in particular ARC neuronal populations, in particular those that co-ordinate feeding and energy metabolism (see Introduction). Generally, most studies on the neurogenic niche therefore investigate tanycytes that occupy the median eminence (ME) – the region that harbours the ARC. However a few studies have shown that tanycytes are found over a much greater length along the A-P axis. The limits of tanycytes along the A-P axis (and therefore, potentially, the limits of the neurogenic niche) are poorly-defined, and in fact, no study has examined whether tanycyte and ARC nucleus position correlate precisely along the A-P axis. A first aim of this chapter was therefore to better characterise the neurogenic niche, by examining consecutive sections along the anterior-posterior (AP) axis in terms of morphology, tanycyte occupancy and markers of the ARC.

A second and linked aim was to examine expression of developmental-like signalling molecules in tanycytes along the A-P axis. As outlined in the Introduction, tanycyte-driven neurogenesis can be stimulated by physiological signals such as feeding behaviour and photoperiod (Batailler et al., 2016; Lee et al., 2012). In addition, a range of signalling molecules, including Fgf1, Fgf2, IGF1 and NFκβ can stimulate

tanycyte proliferation and differentiation (Bless et al., 2016; Chaker et al., 2016; Haan et al., 2013; Li et al., 2012; Pérez-Martín et al., 2010; Robins et al., 2013a). The finding that Fgf10 and Fgf18 are expressed in tanycytes around the median eminence raises the possibility, therefore, that endogenous FGF signalling may govern tanycyte behaviour. Intriguingly, members of the FGF signalling family, including Fgf10 are expressed in the hypothalamus from the earliest stages of development. Here, Fgf10 interacts with Shh, both to maintain a stem-like cell and to initiate its differentiation towards $Shh^{+}Fgf10^{-}$ and $Shh^{-}Fgf10^{+}$ progenitors (see Introduction 1.3.1 and Fig.1.3C). An outstanding question is therefore whether Fgf10 and Shh are ever detected in close proximity, or even in the same subregion in the adult hypothalamus. This might reveal the location of a 'stem-like' hypothalamic cell that is set up in the embryo and retained throughout life. This is an important question: while many authors suggest the existence of a stem cell within the neurogenic niche, no study has yet distinguished *in vivo* between a self-renewing stem cell versus progenitor cells with more limited potential. Currently, no study has detected expression of Shh within adult mouse tanycytes, although some expression has been noted in other mammals (Lomet et al., 2018; Traiffort and Charytoniuk, 1999). To address this second aim, I have performed a systematic analysis of Fgf10 and Shh expression within the adult hypothalamus, to ask (a) whether I could detect Shh expression and (b) whether, in any region, Fgf10 and Shh lie adjacent to one another, or even appear to overlap.

3.2 Results

3.2.1 Morphology of the hypothalamus along the A-P axis

Figure 3.1 shows an atlas of every 15µm section collected through the hypothalamus labelled with DAPI, over a 1.2mm region, centred around the ME. In anterior-most regions (A) the ventricle is a long thin structure, which extends towards the ventral pial surface, eventually coming close to it in posterior sections (red arrowhead). DAPI-labelling reveals the beginning of the ARC and VMN. More posteriorly the ventricle begins to widen and assume a rectangular conformation, indicating the transition to the median eminence (ME) region. In contrast to A subregion, ME regions have a nuclei-dense ventral pial region called the pars tuberalis (green arrowhead). I defined two subregions within the ME, the Anterior Median Eminence

(AME) and the Central Median Eminence (ME). Although their precise border cannot easily be defined, the ME itself shows the characteristic bulbous-shaped median eminence (grey arrowhead) (ie the median eminence increases in depth), the out-pocketings of the infundibular recesses (IR: purple arrowheads) and the wider base of the 3rd ventricle (yellow arrowhead). The ME ends when the ends of the median eminence extend further dorsal than the ventral base of the IR (orange arrowhead), which begins to narrow bringing the sides of the ventricle closer together. I find that in posterior parts of the ME (ME^{P}) the coalescing nuclei that define the ARC and VMN can no longer be detected.

The ME region is followed by a short domain in which the median eminence continues to round off and the base of the ventricle narrows entirely to a point. The median eminence fully encircles itself, cutting itself off from the ventral surface of the hypothalamus and forming the pituitary stalk (white arrowhead). I refer to this region as the Posterior Median Eminence (PME). Continuing further posterior (P) the 3rd ventricle decreases in size until it is lost entirely. Adjacent to the PME and P subregions, nuclei within the parenchyma cannot be clearly allocated to defined nuclei.

These five regions (A, AME, ME, PME and P) will be used throughout the remaining chapters of my thesis to help describe the changes in the cell populations and molecular markers that occur along the A-P axis of the hypothalamus. Where I need to describe anterior or posterior differences within a region, I will use nomenclature such as AME^{A} or AME^{P}.

3.2.2 Nestin^{+} tanycytes along the A-P axis

Previous reports have shown that tanycytes occupy the ME region of the hypothalamus, but have not systematically analysed their distribution along the A-P axis. I therefore analysed consecutive sections with Nestin, previously described as labelling all tanycyte subsets (Hendrickson et al., 2018; Robins et al., 2013a; Wei et al., 2002).

In the A hypothalamus, Nestin^{+} tanycytes, with short but defined processes are first seen in the ventral tip of the 3V, close to the A-AME^{A} subregion boundary (Fig 3.2 A, B). Their appearance correlates with the ARC and they appear to project towards it.

Figure 3.1 Atlas of coronal sections from anterior to posterior through the hypothalamus

Images at 10x magnification of coronal cross-sections, labelled with DAPI to show cell nuclei, centred on the base of the 3V and the ME. 15µm sections displayed in order from anterior to posterior with labels describing the position of the sections as Anterior, Anterior Median Eminence (AME), Median Eminence (ME), Posterior Median Eminence (PME), and Posterior. Every section along the axis has been collected and displayed, including those that are damaged or folded which have been marked by a white asterisk. The AME-P region is 945µm long (63x15µm sections). Red arrowhead, A subregion ventricle extension; green arrowhead, AME/ME nuclei-dense pial region; grey arrowhead, pars tuberalis; purple arrowheads, infundibular recesses; yellow arrowhead, broad base of ME 3V; orange arrowhead, ME extends beyond ventral 3V surface; white arrowhead, ME forms the pituitary stalk. Atlas is representative of all mice studied. Scale bars 100µm.

Figure 3.1

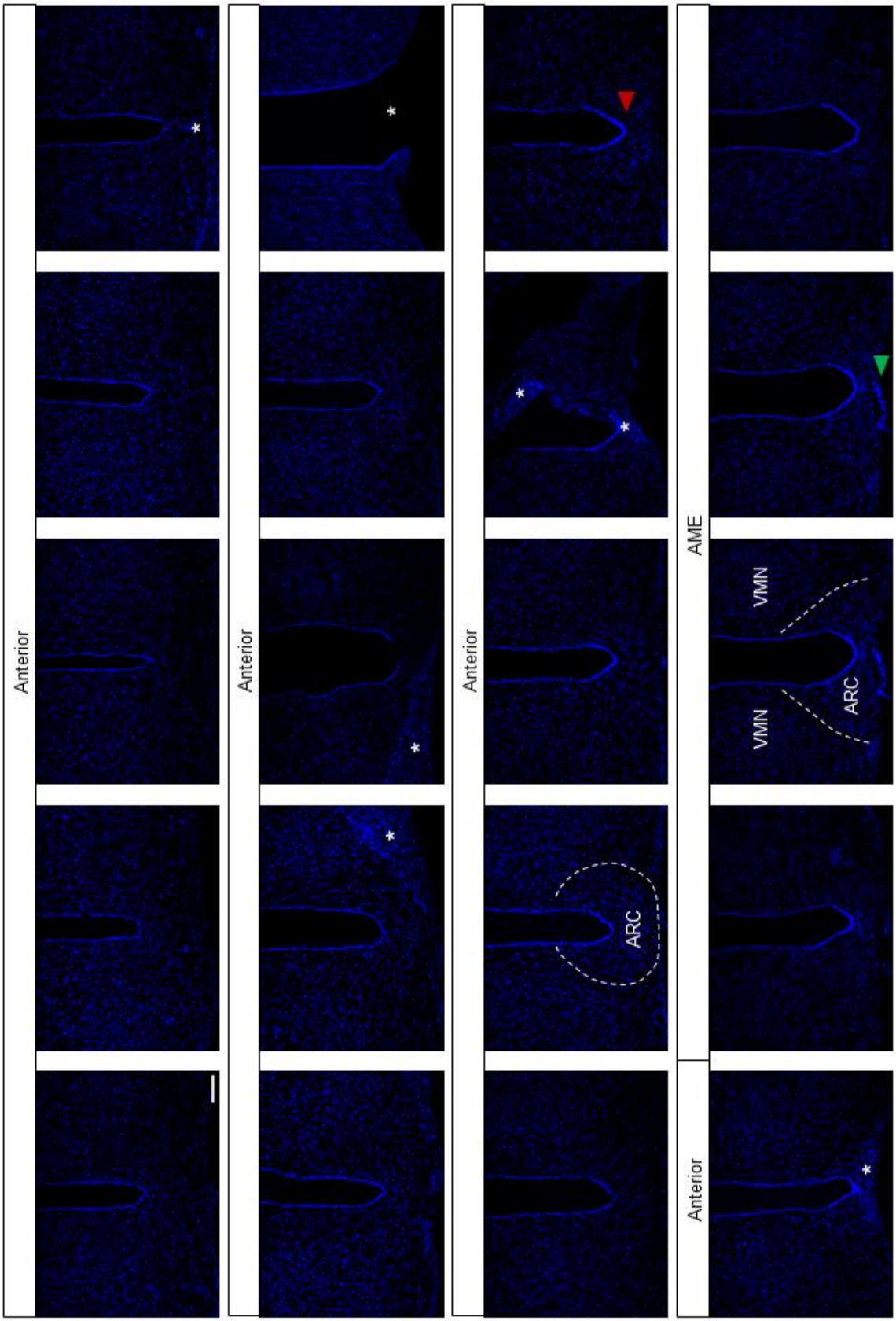

Figure 3.1

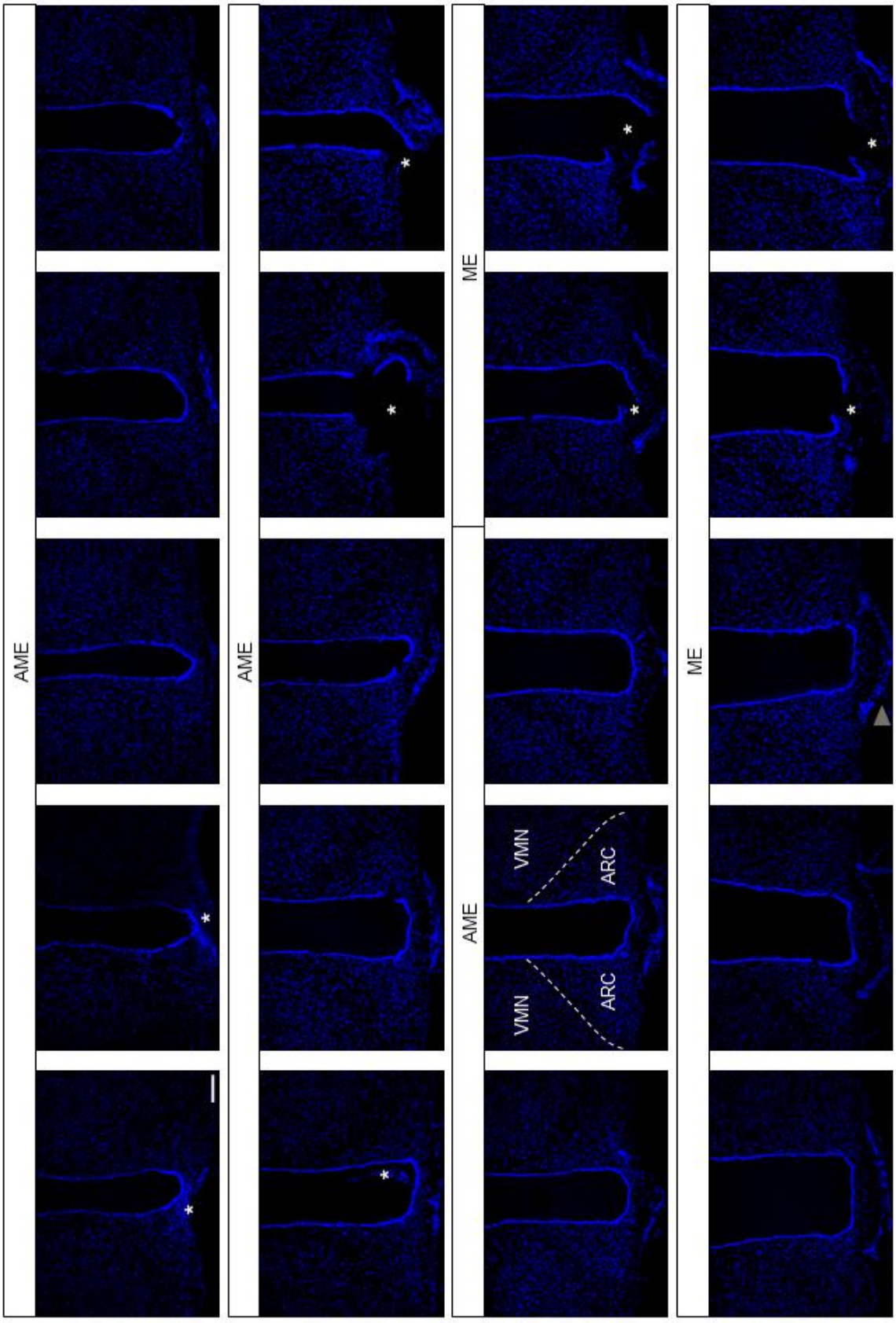

Figure 3.1

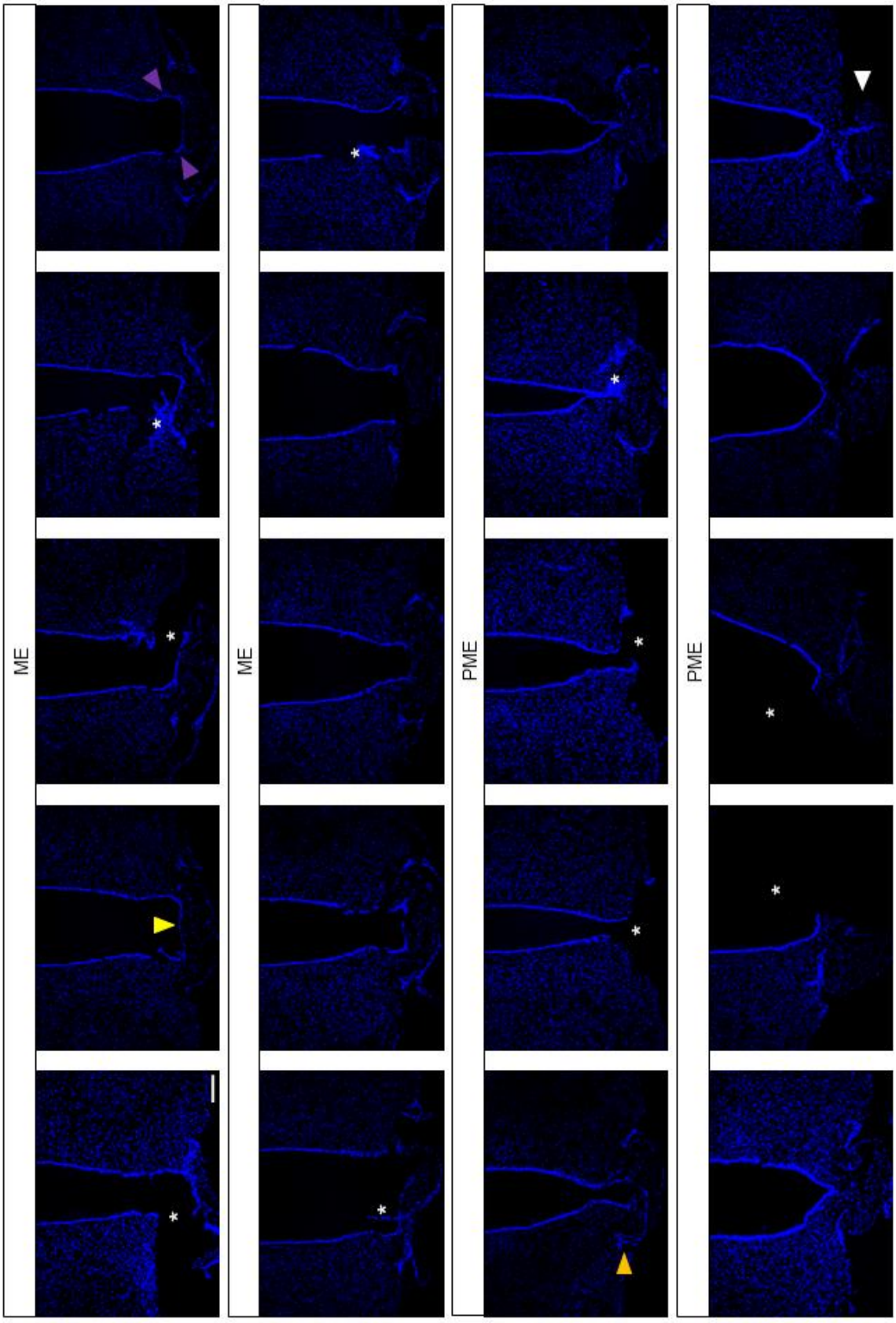

Figure 3.1

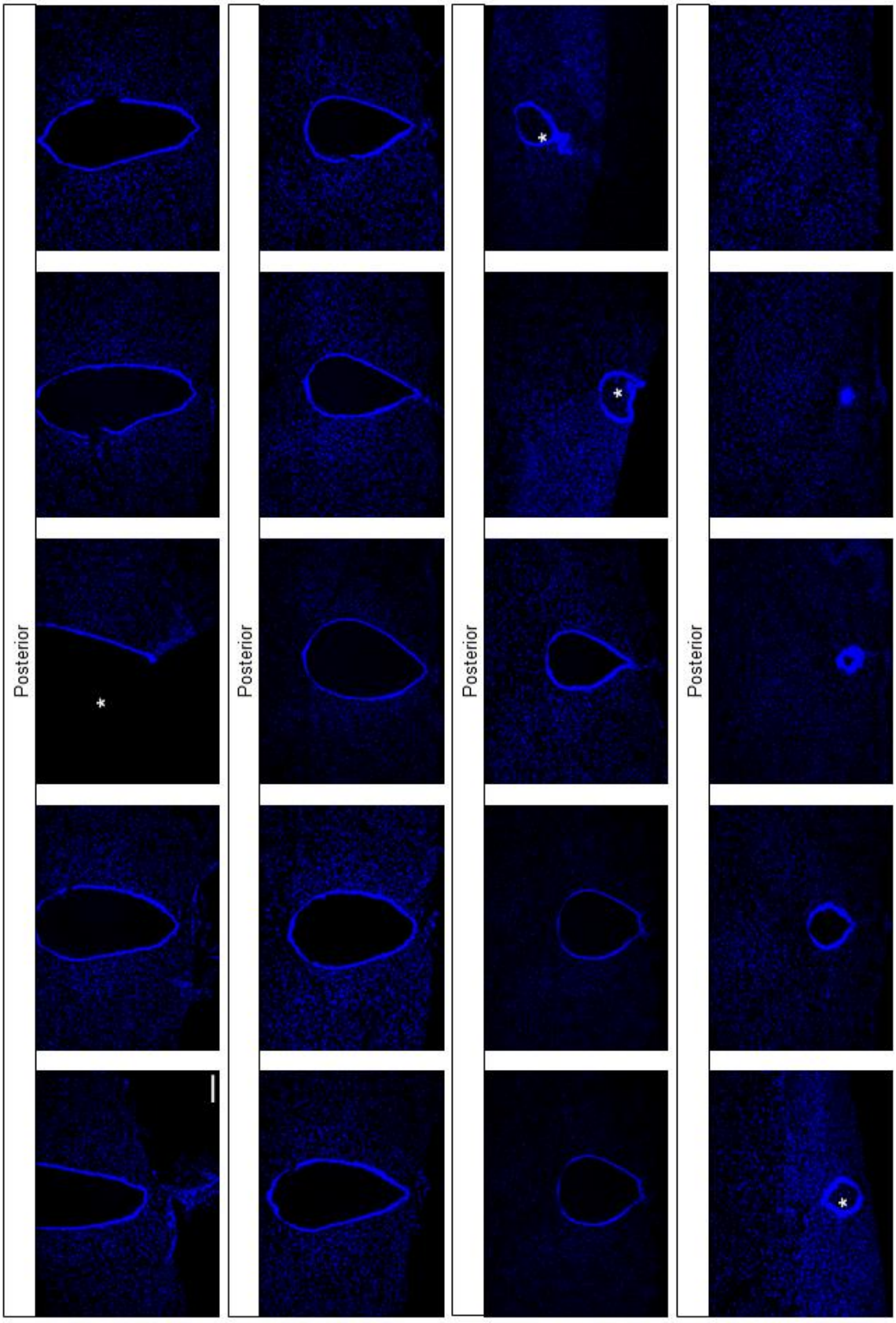

Through the AME, Nestin^{+} tanycytes spread more dorsally around the VZ (Fig 3.2 Bii). In the ME, Nestin is expressed strongly in ventral tanycytes and more weakly in more dorsal tanycytes (Fig 3.2 Ci,Cii,Di,Dii). Classically, ventral-tanycytes are termed β-tanycytes and dorsal-tanycytes are termed α-tanycytes. Label intensity increases in the ME^{P} (Fig 3.2 Di,Dii). Strong expression is also detected in PME and P sections, where Nestin^{+} tanycytes are present in large numbers and extend throughout the ventral half of the 3rd ventricle (Fig 3.2 E-F). Finally, I noted that in addition to expression in tanycytes, Nestin is expressed by non-tanycyte ependymocytes in the dorsal roof in A, AME and ME^{A} subregions.

Together, my study shows that Nestin^{+} tanycytes extend for approximately 1.1mm along the A-P axis and are centred around the ME, with greatest density in the ME^{P}-P subregions. In AME-ME^{A} regions, tanycyte position correlates with the ARC. In ME^{P}-P regions, tanycytes lie adjacent to parenchymal regions where the ARC is not well-defined. This distribution forms the basis of the schematic I outline in Figure 4.9.

3.2.3 ARC neuronal markers along the A-P axis of the hypothalamus

I next asked whether ARC neurons are restricted to the morphologically-defined ARC or can in fact, be detected outside of the ARC, i.e. within the parenchyma in ME^{P} to P regions.

3.2.3.1 NPY

NPY/AGRP and POMC neurons coordinate feeding and hunger (Aponte et al., 2011; Hahn et al., 1998; Lin et al., 2000; Reddy et al., 1999). Many previous studies have used NPY expression as a marker of neurons within the ARC nucleus (Aujla et al., 2013; Hahn et al., 1998; Lee et al., 2012; Lin et al., 2000; Ma et al., 2015; Yee et al., 2009), although notably, others have suggested a wider distribution along the A-P axis (Ebling et al., 1998; J. Everitt et al., 1986; Reddy et al., 1999). Immunohistochemical analysis confirms that NPY is detected in the ARC, and additionally, confirms that the ARC nucleus is obvious in AME and ME sections (Fig 3.3). However, in support of earlier studies (Ebling et al., 1998; J. Everitt et al., 1986; Reddy et al., 1999), NPY is additionally expressed in more posterior regions (Fig.3.3). Thus, although NPY decorates neurons of the ARC,

Figure 3.2: Nestin expression in the tuberal hypothalamus along the anterior-posterior axis
Image composites (A-F) at 10x magnification of coronal cross-sections showing Nestin expression (red) by immunofluorescence in relation to the 3V, ME, and hypothalamic parenchyma along the A-P axis with nuclear DAPI staining (blue) in an adult wild type mouse. Box inserts (i and ii for each cross section) indicate corresponding image z-stacks collected at 20x magnification and converted to maximum intensity projections (MIPs) (Ai/Aii-Fi). Scale bars for all images 100µm. Images representative of n=6 mice.

Nestin expression is present at the anterior/AMEA boundary in the 3V with few processes beginning to extend beyond the ventricle at the most ventral point (A). Nestin+ processes extend from the ventral 3V to the ME and parenchyma from the AME (B) with increasing intensity and dorsal extension toward the posterior hypothalamic 3V (C-F).

Figure 3.2

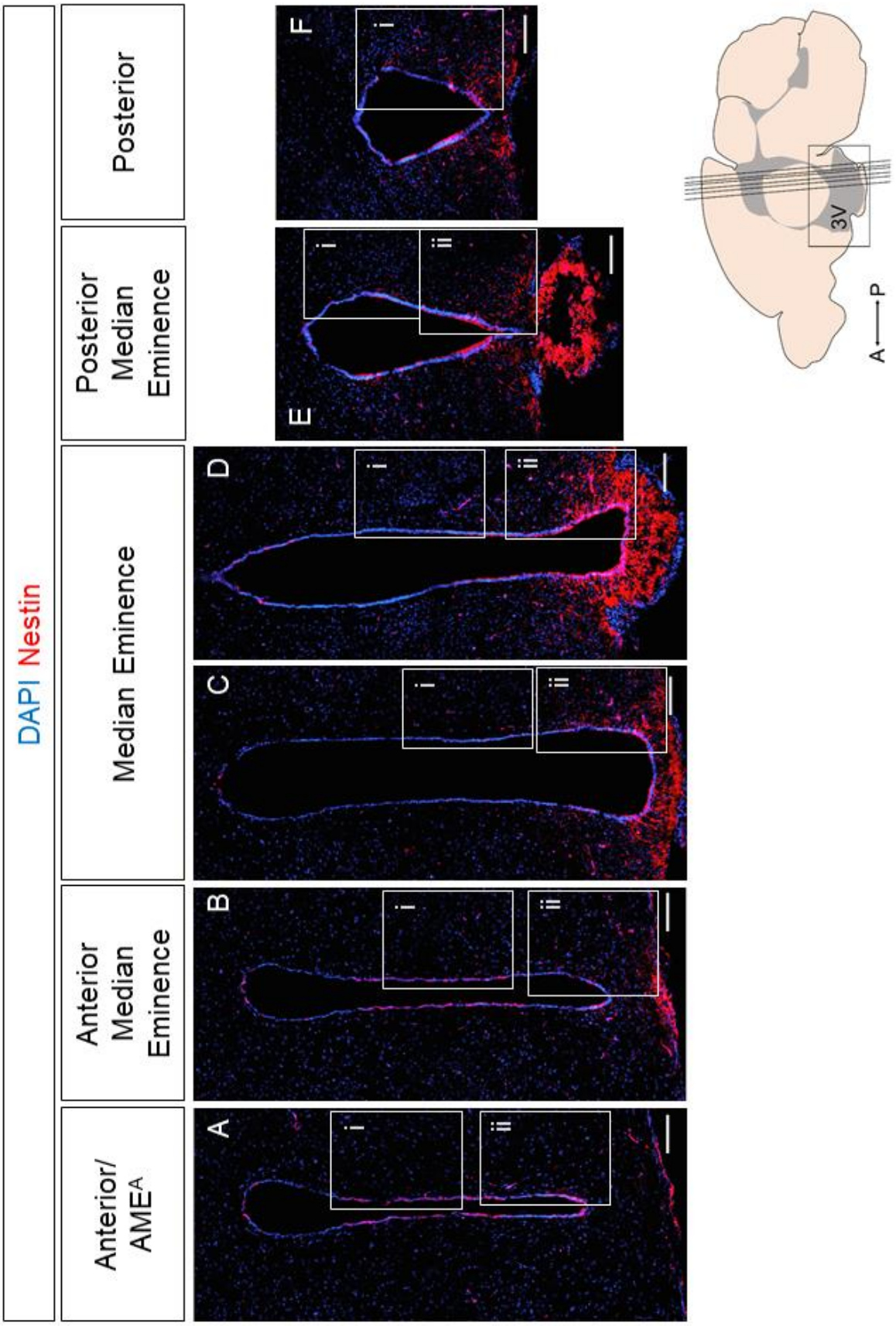
DAPI Nestin
Anterior/ AME^A
Anterior Median Eminence
Median Eminence
Posterior Median Eminence
Posterior
A
B
C
D
E
F
i
ii
3V
A
P

Figure 3.2

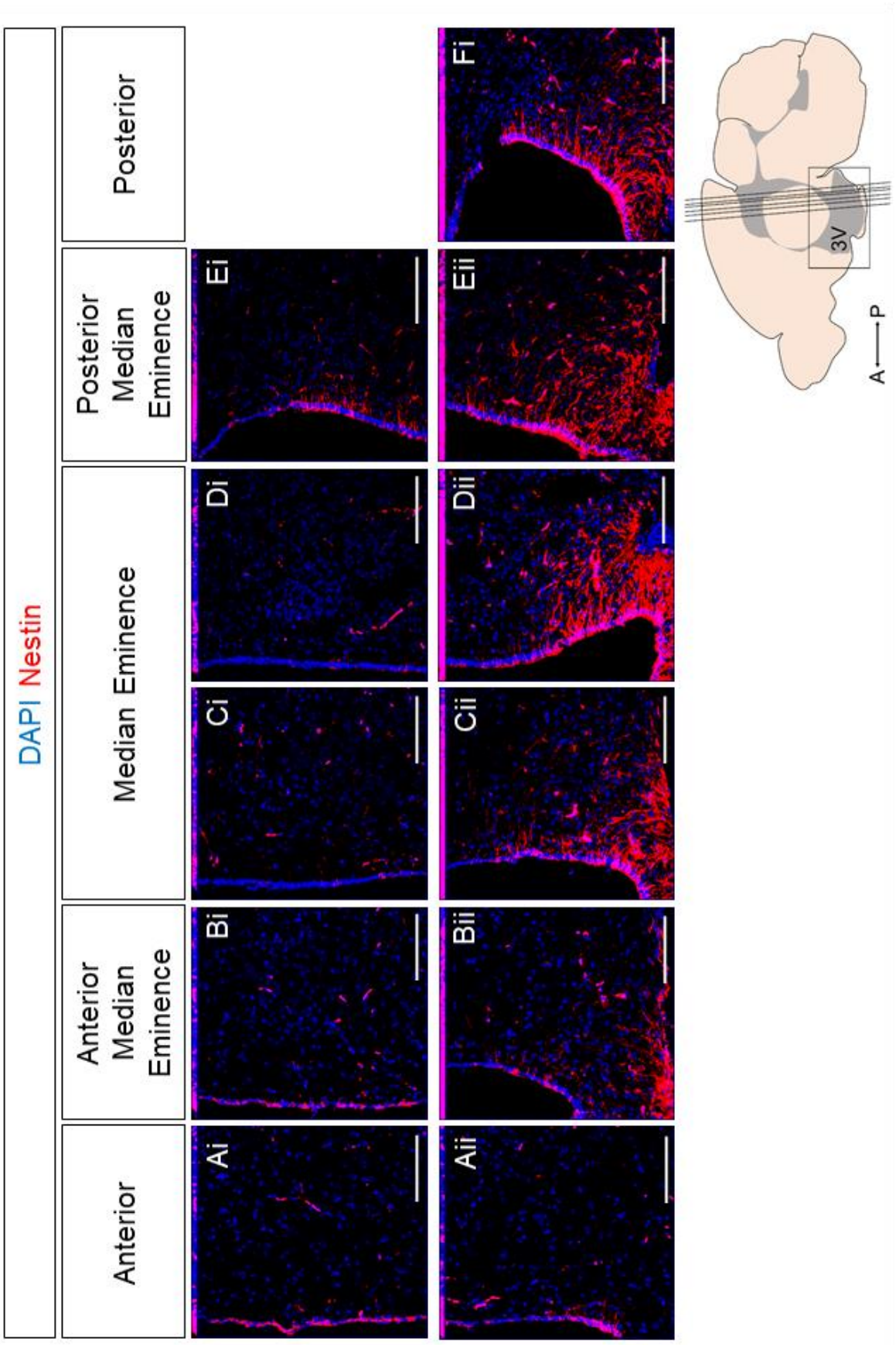
DAPI Nestin
Anterior
Anterior Median Eminence
Median Eminence
Posterior Median Eminence
Posterior
Ai
Aii
Bi
Bii
Ci
Cii
Di
Dii
Ei
Eii
Fi
3V
A
P

it is also expressed in cells in wider, ill-defined territories throughout the parenchymal region, including PME and P regions, where there are abundant tanycytes.

3.2.3.2 GHRH

GHRH neurons, which control GH release from the pituitary (Smith et al., 1997), have been described along the hypothalamic A-P axis in past studies (J. Everitt et al., 1986), and my analysis concurs. GHRH is expressed in the ARC, where its labelling again confirms the position of the ARC in AME and ME regions (Fig 3.4 Aii-Fi). It is also detected in neurons of the PVN in A subregions (Fig 3.4 Ai), and in neurons of the VMN and DMN in AME and ME regions (Fig 3.4 Ci-Ei). Similar to NPY, in PME and P subregions, GHRH labels cells in wide, ill-defined territories throughout the parenchyma.

3.2.3.3 TH

The A12 population of TH neurons occupy the ARC along its A-P axis (Fig 3.5 B-E) and constitute a subset of GHRH neurons (Bouyer et al., 2007; J. Everitt et al., 1986; Marin et al., 2005; Meister et al., 1986) that regulate prolactin secretion (Ben-Jonathan and Hnasko, 2001). The population is spatially distinct from the more anterior and dorsal A14 population (Fig 3.5 A,Ai), the Zona Incerta A13 population seen dorsolateral to the ventricle in AME sections (Fig 3.6 B), and the ventrolateral A15 population (J. Everitt et al., 1986). ARC TH neurons are found in highest quantities in the AME and ME (Fig 3.5 Bi,Ci). However, small numbers of TH^+ neurons can also be detected in A and PME regions, although in these regions, the cells do not coalesce within the defined ARC nucleus (Fig 3.5 Di-Fi).

My analyses confirm that the ARC nucleus occupies AME and ME^A subregions. Additionally they show that in ME^P, PME, and P subregions, ARC-type neurons can be detected, even though they do not coalesce into a clear nucleus. In these subregions, ARC-type neurons lie close to regions of the VZ with abundant Nestin+ tanycytes.

Figure 3.3: NPY expression in the tuberal hypothalamus along the anterior-posterior axis
Image composites (A-F) at 10x magnification of coronal cross-sections showing NPY expression (green) by immunofluorescence in relation to the 3V, ME, and hypothalamic parenchyma along the A-P axis with nuclear DAPI staining (blue) in an adult wild type mouse. Box inserts (Ai-Fi) indicate corresponding images collected at 20x magnification. Scale bars for all images 100µm. n=1 mouse: A single mouse was used to confirm this labelling which has been previously reported (Ebling et al., 1998; J. Everitt et al., 1986; Reddy et al., 1999).

NPY is expressed in diffuse dendritic projections and cell bodies of the parenchyma lateral to the ventral 3V along the A-P axis of the tuberal hypothalamus (A-F), with greatest expression over the posterior ME/PME subregion (D-E). It is additionally expressed sparsely in diffuse dendrites lateral to the dorsal 3V, with strongest expression anterior to the ME (A), and lateral to the medial 3V over the AME-PME subregions (B-E) with greatest expression in the PME sections (E).

Figure 3.3

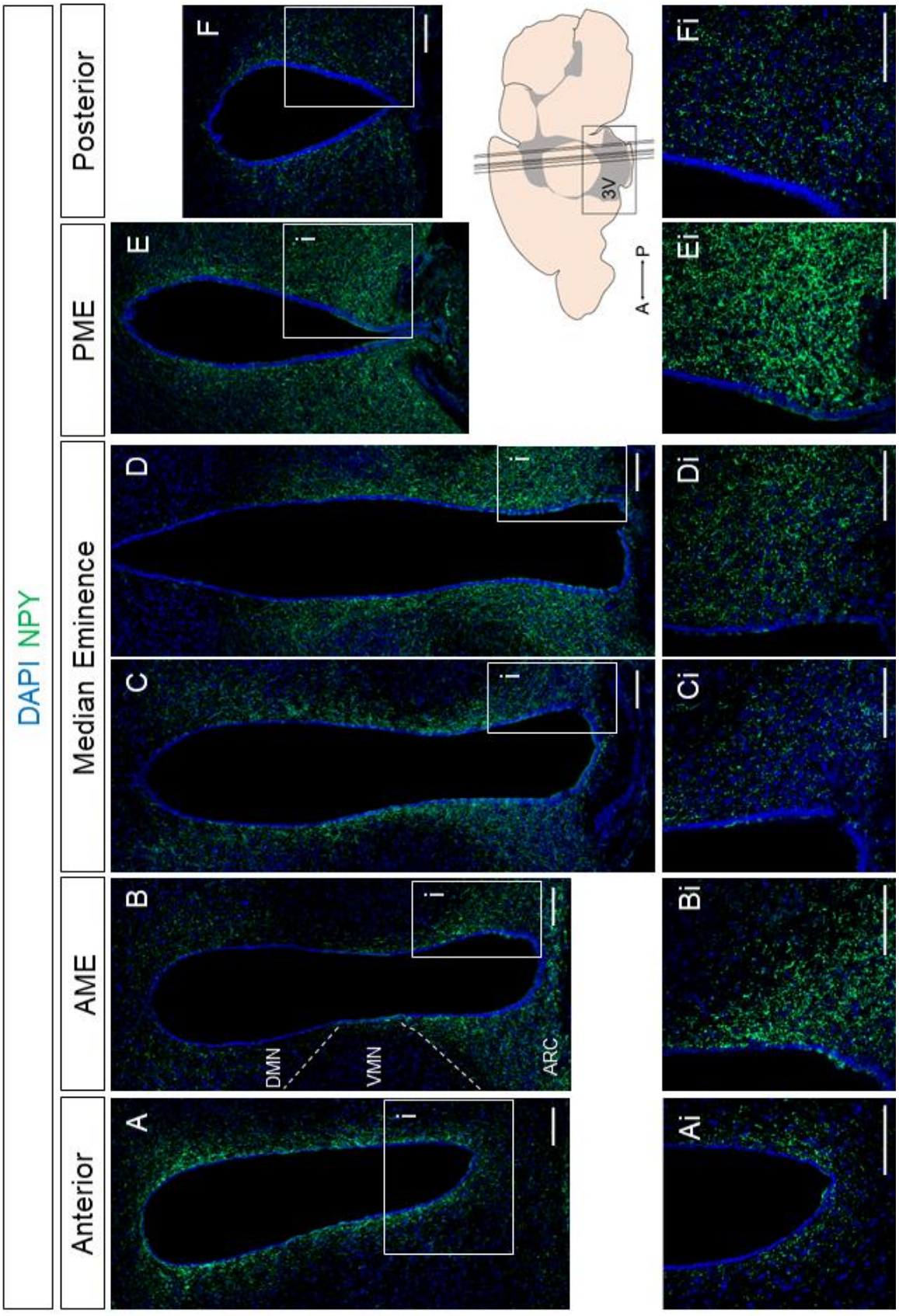
DAPI NPY
Anterior
AME
Median Eminence
PME
Posterior
A
B
C
D
E
F
Ai
Bi
Ci
Di
Ei
Fi
i
DMN
VMN
ARC
3V
A
P

Figure 3.4: GHRH expression in the tuberal hypothalamus along the anterior-posterior axis
Image composites (A-F) at 10x magnification of coronal cross-sections showing GHRH expression (green) by immunofluorescence in relation to the 3V, ME, and hypothalamic parenchyma along the A-P axis with nuclear DAPI staining (blue) in an adult wild type mouse. Box inserts (i and ii for each cross-section) indicate corresponding image z-stacks collected at 20x magnification and converted to maximum intensity projections (MIPs) (Ai/Aii-Fi). Scale bars for all images 100µm. n=1 mouse: A single mouse was used to confirm this labelling which has been previously reported (Ebling et al., 1998; J. Everitt et al., 1986; Reddy et al., 1999).

GHRH is expressed in cells of the parenchyma lateral to the ventral 3V along the A-P axis of the tuberal hypothalamus (A-F), with greatest expression over the ME subregion (C-D). It is additionally expressed sparsely in cells lateral to the dorsal 3V, with strongest expression anterior to the ME (A), and lateral to the medial 3V over the AME-PME subregions (B-E) with greatest expression in the anterior ME sections (C).

Figure 3.4

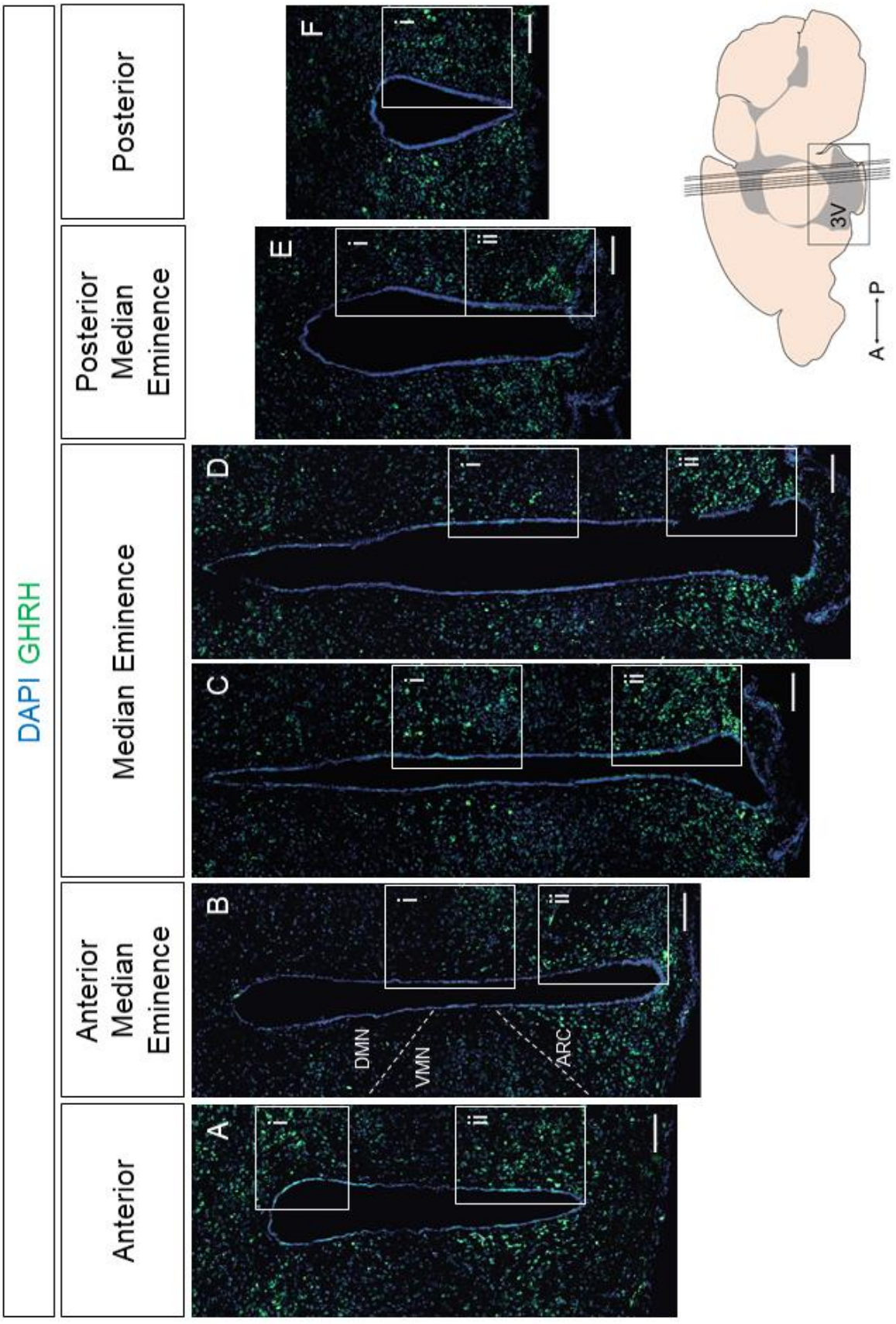
DAPI GHRH
Anterior
Anterior Median Eminence
Median Eminence
Posterior Median Eminence
Posterior
A
B
C
D
E
F
i
ii
DMN
VMN
ARC
3V
A
P

Figure 3.4

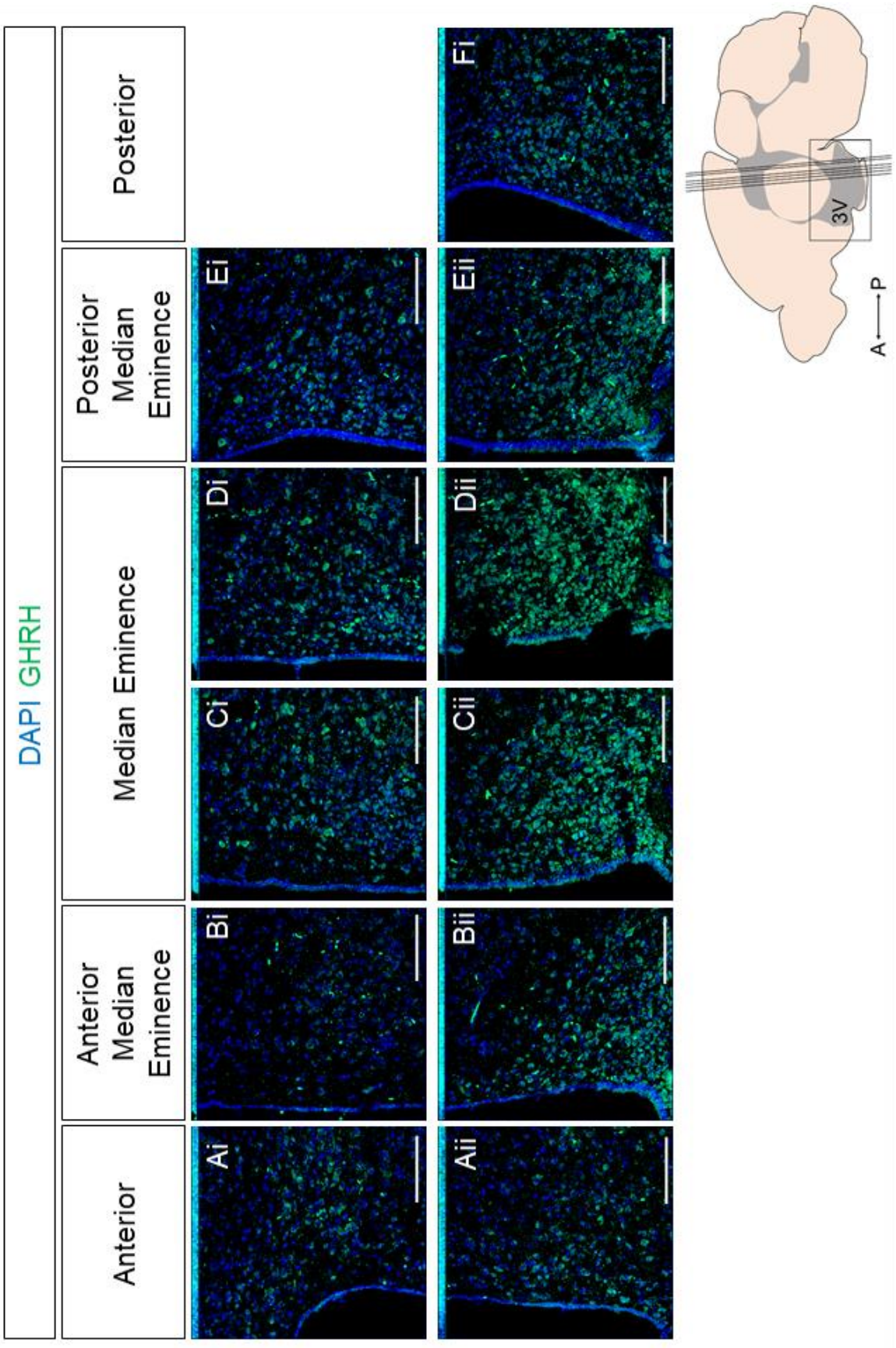
DAPI GHRH
Anterior
Anterior Median Eminence
Median Eminence
Posterior Median Eminence
Posterior
Ai
Bi
Ci
Di
Ei
Fi
Aii
Bii
Cii
Dii
Eii
Fii
3V
A
P

Figure 3.5: TH expression in the ventral tuberal hypothalamus along the anterior-posterior axis

Images (A-F) at 10x magnification of coronal cross-sections showing TH (red) expression by immunofluorescence in relation to the ventral 3V and hypothalamic parenchyma along the A-P axis with nuclear DAPI staining (blue) in an adult wild type mouse. 3V shown centrally (A, B) or to the left hand side (C-F) to emphasise extent of lateral TH expression in the parenchyma. Box inserts (i and ii for each cross-section) indicate corresponding image z-stacks collected at 20x magnification and converted to maximum intensity projections (MIPs). Scale bars for all images 100µm. TH expression representative of n=6 mice.

In sections anterior to the ME (A) TH is expressed in scattered cells of the parenchyma toward the dorsal aspect of the image with few further toward the ventral aspect of the 3V and none ventral to the VZ. In AME and the anterior portion of ME sections (B, C) many TH^+ cells are seen predominantly in parenchyma lateral to the ventral aspect of the 3V in the ARC, with few cells further dorsal. Moving posteriorly (D-E) TH^+ cells decrease in number and become sparsely distributed until few remain (F).

Figure 3.6: TH expression in the dorsal tuberal hypothalamus along the anterior-posterior axis

Images (A-E) at 10x magnification of coronal cross-sections showing TH (red) expression by immunofluorescence in relation to the dorsal 3V (left) and hypothalamic parenchyma along the A-P axis with nuclear DAPI staining (blue) in an adult wild type mouse. 3V shown to the left hand side. Scale bars for all images 100µm. Labelling representative of n=6 mice.

TH^+ cells are absent from the parenchyma lateral to the dorsal 3V in sections anterior to the ME (A). TH^+ cells are expressed in great numbers in a cluster dorsal and lateral to the 3V in AME sections (B). Through the ME and PME (C-E) 1-3 cells are seen in this subregion.

Figure 3.5

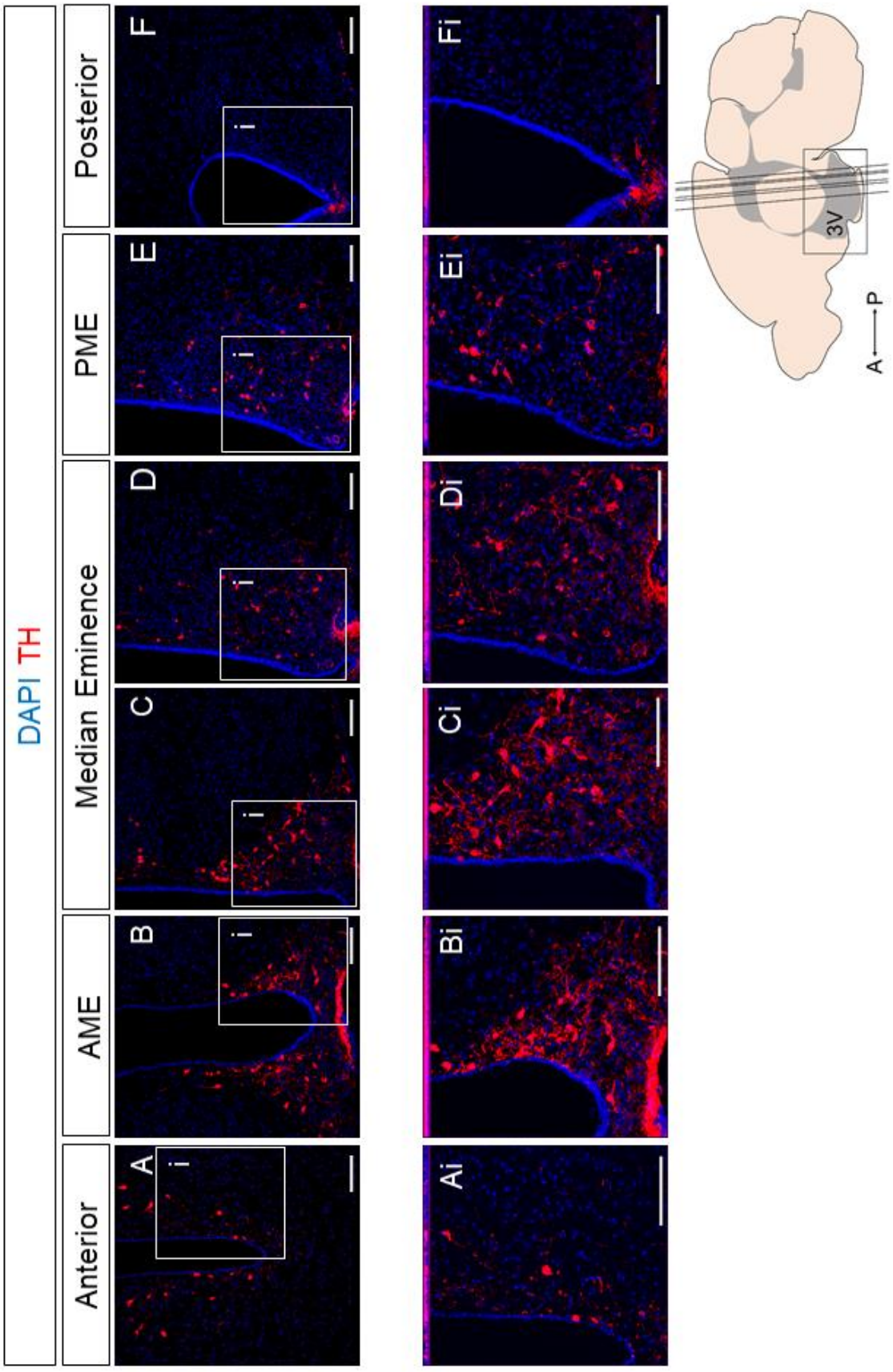
DAPI TH
Anterior
AME
Median Eminence
PME
Posterior
A
B
C
D
E
F
Ai
Bi
Ci
Di
Ei
Fi
i
3V
A
P

Figure 3.6

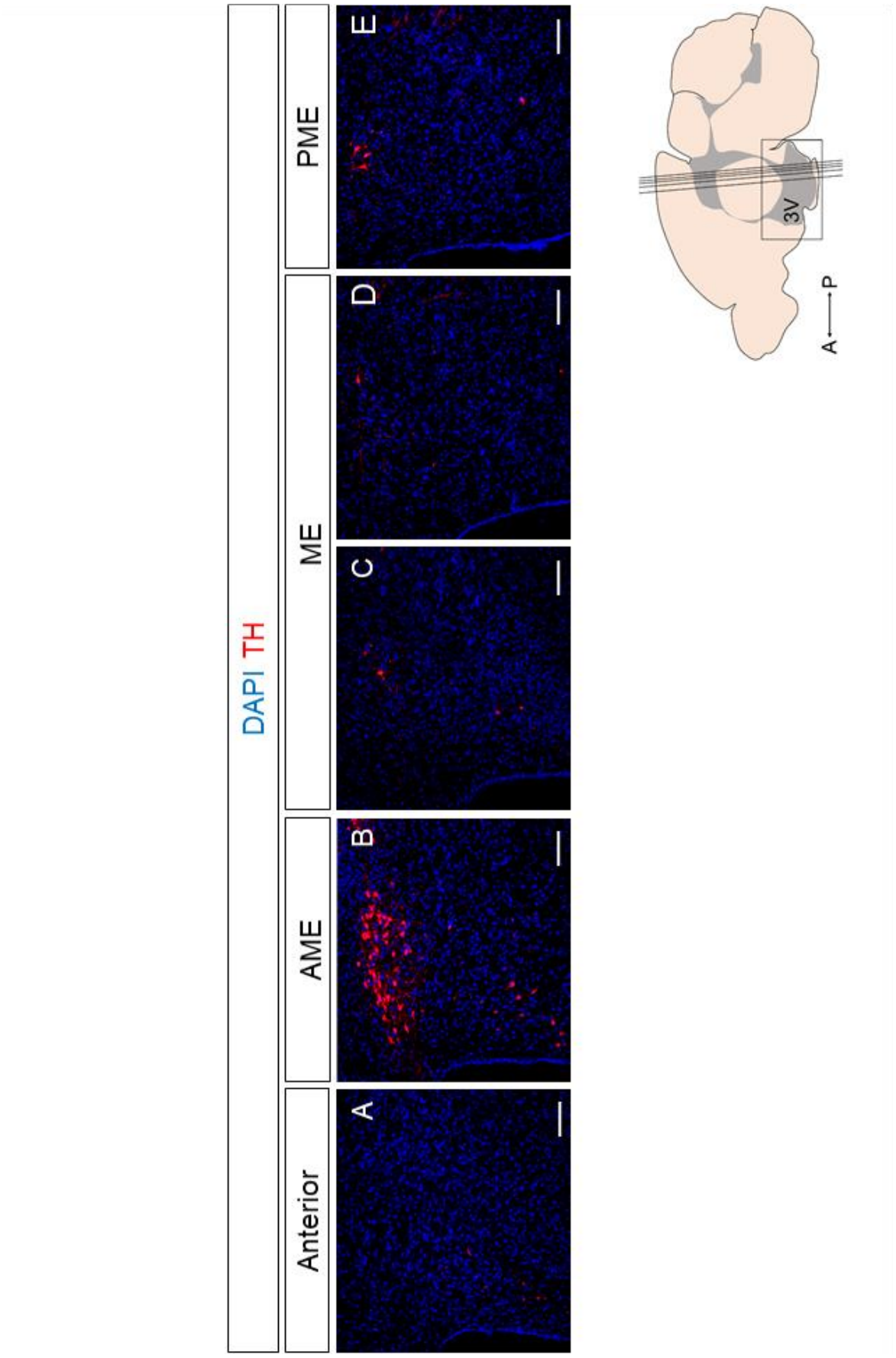

3.2.4 Spatially-restricted expression of signalling molecules within the adult neurogenic niche

On this platform, I next analysed expression of Fgf10 and Shh.

3.2.4.1 Fgf10

Fgf10 mRNA is absent in the A subregion (not shown), with expression initiating in the ventral tip of the VZ in the AME^{A} (Fig 3.7 A,Ai). Through the AME and ME Fgf10 mRNA labelling spreads dorsally to tanycytes that lie adjacent to the ARC (Fig 3.7 B,Bi,C,Ci) (Robins et al., 2013a). Intriguingly, in the ME^{P} and PME^{A}, *Fgf10* expression is not uniform at the base of the 3V: little/no expression can be detected in the medial-most regions containing β2 tanycytes (Fig 3.7 Ci, Di; Fig 1.1B). In PME and P regions, *Fgf10* is again detected in the ventral tip of the 3V (Fig 3.7 D,Di,E,Ei). No expression is detected in ependymocytes in any subregion, but in the P subregion, expression is detected in the lateral recesses (arrowheads, Fig 3.7 F,Fi).

3.2.4.2 Shh

Using *in situ* hybridisation on slide sections, a sensitive method of detection, I have observed, for the first time, that Shh mRNA is expressed in the adult mouse hypothalamus. Expression is limited to scant cells (1-5 cells per section) in the base of the 3V in ME^{P} and PME^{A} subregions (Fig 3.8). Intriguingly, analysis of serial adjacent sections shows that these cells are detected in the *Fgf10*$^{-}$ region of the ME^{P} and PME^{A} (Fig 3.8 B-F). No expression is detected in the A, AME, or P subregions (not shown), but in PME sections, expression is detected in cells at the tip of the 3V. Together this means that in ME^{P} and PME^{A} regions *Shh*$^{+}$ and *Fgf10*$^{+}$ cells appear to abut, while in PME sections, a small set of cells at the ventral tip of the 3V appear to co-express *Shh* and *Fgf10*.

3.3 Discussion

I have built upon previous investigations to analyse the hypothalamic neurogenic niche. My studies suggest that the niche may occupy a 1.1mm-long domain, at least as determined by the presence of Nestin^{+} tanycytes. Interestingly, the densest tanycytes are not located in the ME region, but instead are located in posterior parts of the niche, in the PME/P subregions. These tanycytes lie posterior to the ARC

itself, but in regions where ARC-type neurons are diffusely distributed.

In addition, I have built on previous studies that document the localisation of Fgf10 in the hypothalamic niche. As described previously I detect expression of *Fgf10* in tanycytes (Haan et al., 2013; Robins et al., 2013a). However, my studies show that *Fgf10* shows heterogeneous expression in tanycytes along the A-P axis. In particular, *Fgf10* is not detected (or is expressed at low levels) in β2 tanycytes in ME^{P} and PME^{A} regions. To my knowledge, this is the first description of an Fgf that distinguishes β2 and β1 tanycytes. Additionally, I have described *Fgf10* in the transition zone between tanycytes and ependymal cells in P sections. This has not been reported previously, but weak $Fgf10^{+}$ labelling at the transition zone of posterior sections can be identified in Robins et al. (2013) and Haan et al. (2013).

My studies are the first to show that *Shh* is expressed in adult tanycytes. Intriguingly, in the ME, Shh^{+} cells appear to occupy the $Fgf10^{-}$ β2-tanycyte domain. The scant expression suggests either that these cells constitute a smaller spatially-restricted tanycyte subset within this defined group, that Shh is temporarily/cyclically expressed in β2-tanycytes, or that Shh may be expressed in a previously undescribed non-tanycyte cell population in these subregions. Further investigation with previously described tanycyte markers can address whether the Shh^{+} cells are indeed tanycytes.

The *Shh* expression pattern differs drastically from that reported in the adult rat and sheep hypothalamus, where it appears to be expressed in the α2- and β1- domain (Lomet et al., 2018; Traiffort and Charytoniuk, 1999). In the sheep hypothalamus, this expression shows seasonal changes and has been linked to thyroid stimulating hormone (TSH) regulation (Lomet et al., 2018). Shh was strongly expressed in May, when the photoperiod is long, and was diminished in November, when the photoperiod in short. As inbred strains of mouse used in the lab have lost such seasonally-regulated pathways, any such changes in expression would be absent from our results. Although *Shh* and *Fgf10* appear to abut around the 3V base in ME regions, in a small set of cells in the PME, they appear to overlap (schematic, Fig.4.9). To try and push this investigation further, I looked for expression of *Shh* and *Fgf10* together in the tanycyte subsets proposed by Campbell et al, (2017) following Drop-seq analysis of the hypothalamus. They propose two β2 tanycyte subsets, one

Figure 3.7: Fgf10 expression in the tuberal hypothalamus along the anterior-posterior axis
Image composites (A-F) at 10x magnification of coronal cross-sections showing Fgf10 mRNA expression (purple) by *in situ* hybridisation in relation to the 3V, ME, and hypothalamic parenchyma along the A-P axis in an adult wild type mouse, with corresponding 20x magnification images of the ventral 3V(Ai-Fi). Scale bars 100µm. Images representative of n=3 mice.

Inspecting sections along the A-P axis, Fgf10 mRNA is found in the ventral-most cells of 3V VZ in the AME^{A} (A). Through the ME, Fgf10 mRNA spreads dorsally up the VZ and the signal increases in its intensity (B-C). Through the PME Fgf10 label decreases in intensity (D-E), and in the posterior 3V it is absent through the VZ except in a few cells in the ventral most point and at the lateral recesses (arrowheads) where the dorsal rounding of the ventricle meets the steep ventral edges (F). Fgf10 mRNA labelling appears to be diminished in the floor of the IR (C-D).

Figure 3.8: Shh expression in the Median Eminence
Image composites (A-F) at 10x magnification of coronal cross-sections showing Shh mRNA expression (purple) by *in situ* hybridisation in relation to the 3V from A-P through the ME and PME in an adult wild type mouse, with corresponding 20x magnification images of the ventral 3V(Ai-Fi). Scale bars 100µm. Images representative of n=3 mice.

Shh expression is restricted to a subset of sections from midway through ME sections until the IR is lost from the ME in late PME sections (B-F). This domain is between 375-450µm in length. Shh is absent from more anterior and posterior sections (A, G). In this ME/PME subregion, Shh is expressed in 1-5 cells of the IR floor per section.

Figure 3.7

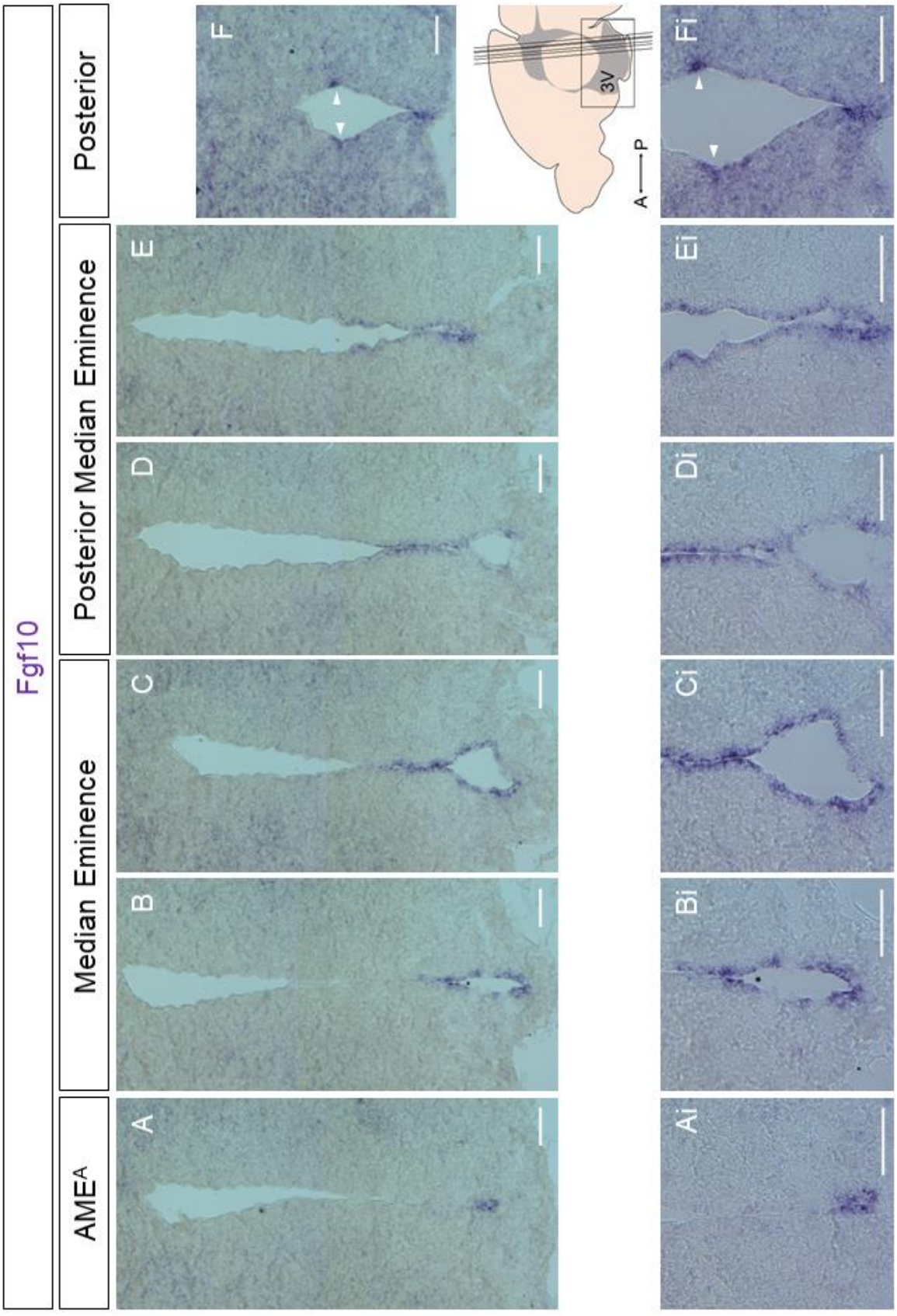
Fgf10
AME^A
Median Eminence
Posterior Median Eminence
Posterior
A
B
C
D
E
F
Ai
Bi
Ci
Di
Ei
Fi
3V
A
P

Figure 3.8

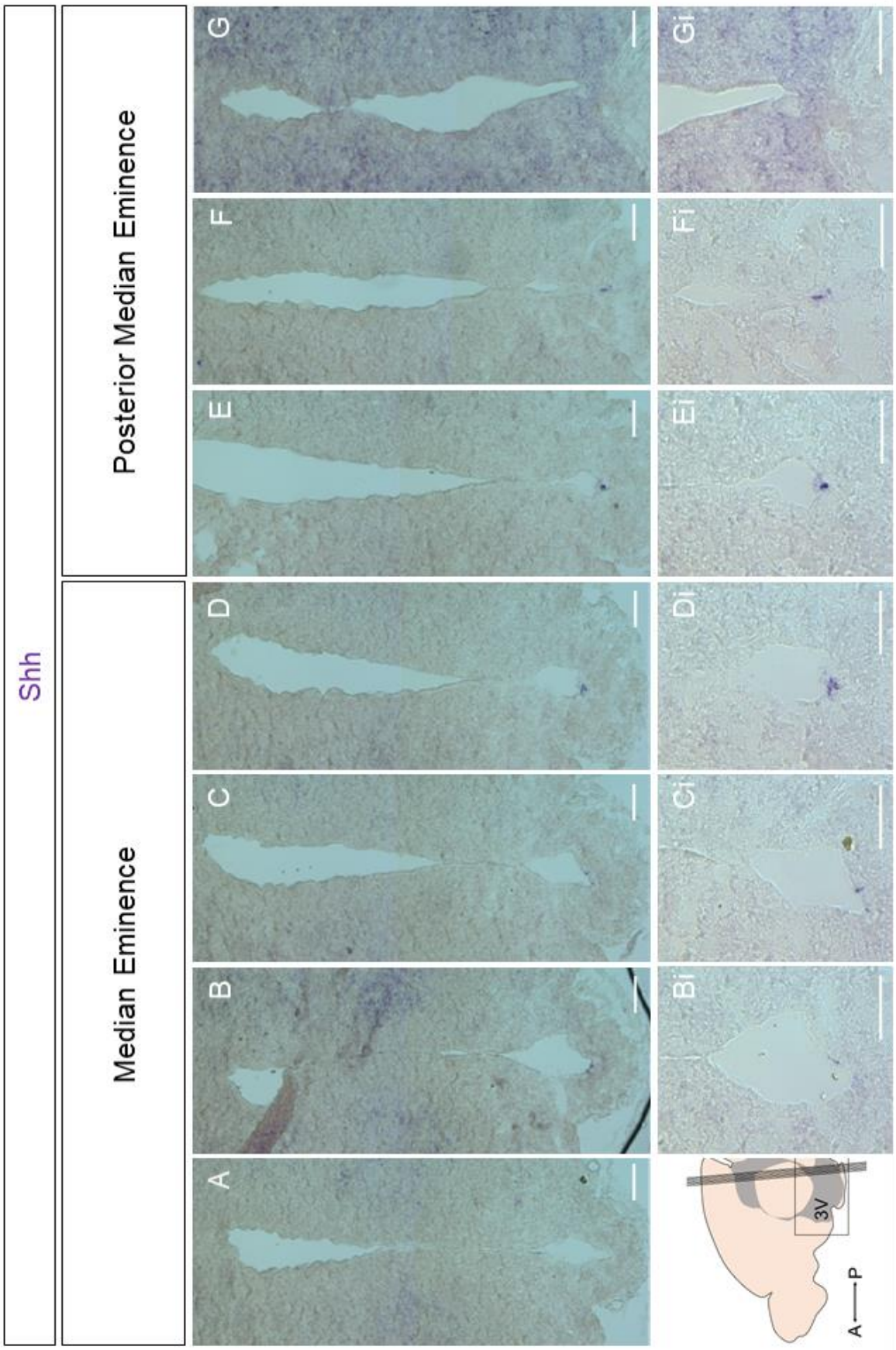
Shh
Median Eminence
Posterior Median Eminence
A
B
C
D
E
F
G
Bi
Ci
Di
Ei
Fi
Gi
3V
A
P

that is *Fgf10*$^{+}$*Shh*$^{-}$, and one that is *Fgf10*$^{+}$*Shh*$^{+}$. This analysis suggests my observation that there are cells expressing both Shh and Fgf10 is correct. The lack of a *Shh*$^{+}$*Fgf10*$^{-}$ tanycyte population in this analysis either suggests that there is no such population, they exist but are not tanycytes, or that they exist but were not identified/picked out as a separate cluster in this experiment. Double *in situ* hybridisation experiments examining *Fgf10* and *Shh* expression together should be performed in future to confirm this localisation. This could be performed using one DIG-containing probe and one Fluorescein-containing probe, followed by either successive chromogenic and Fast Red labelling, or by double fluorescent labelling. Alternative options include double immunofluorescence labelling, or post-*in situ* immunofluorescence labelling. However, immunofluorescence labelling is most successful with abundant proteins, and I have not successfully identified Shh from immunofluorescence labelling with the anti-Shh 5E1 antibody.

The localisation of *Shh* and *Fgf10* I have observed are reminiscent of *Shh* and *Fgf10* expression during hypothalamic development. Reciprocal expression of *Fgf10* and *Shh* at the anterior border of the tuberal domain in the developing hypothalamus guides the fate decisions of the anterior progenitors (Fu et al., 2017). *Fgf10*$^{+}$ progenitors give rise to *Fgf10*$^{-}$*Shh*$^{+}$ anterior progenitors, which in turn initiate transcriptional and behavioural changes that lead to the development of the anterior hypothalamus. However, the stem cell is thought to co-express *Shh* and *Fgf10* (Fig 1.4 C). If these signals do prove to be similar to those seen in the embryo, then potentially, a similar system to that described in development is seen in the adult hypothalamus, where an *Fgf10*$^{+}$*Shh*$^{+}$ cell is a stem cell, while *Shh*$^{+}$*Fgf10*$^{-}$ and *Shh*$^{-}$*Fgf10*$^{+}$ cells are progenitors. Notably, the *Fgf10*$^{+}$*Shh*$^{+}$ cells in the adult are in the region of the hypothalamus that contains the densest distribution of Nestin^{+} tanycytes. Tentatively, therefore, I suggest that heart of the neurogenic niche – i.e. potentially, a region containing a stem cell – lies in the PME region, rather than the generally-accepted ME region. In support of this idea, cells in both the ME and PME regions are neurospherogenic, whereas cells in the anterior hypothalamus are not (Robins et al., 2013).

CHAPTER 4: DEFINING TANYCYTE SUBSETS ALONG THE ANTERIOR-POSTERIOR HYPOTHALAMIC AXIS

4.1 Introduction

My observation that tanycytes differ in density and expression of molecular markers along the A-P axis, together with my tentative hypothesis that tanycytes of the PME may harbour a stem-like population, prompted me to examine expression of a wider set of tanycyte markers along the A-P axis. In the past, various markers have been used to study tanycyte subsets along the dorso-ventral axis at the level of the median eminence. Commonly-used markers include Nestin, Vimentin, Rax, Sox2 and GFAP (Hendrickson et al., 2018; Lee et al., 2012; Miranda-Angulo et al., 2014; Pellegrino et al., 2017; Robins et al., 2013a; Wei et al., 2002). Through these studies, a spatial map of tanycytes in/around the median eminence has been developed: β2-tanycytes are located ventro-medially, followed by β1-, α2-, and α1- subsets (Figure 1.1B). Functional studies have gone on to suggest that 'stemness' is associated with median eminence α2-tanycyte populations that express high levels of Rax, and GFAP (Miranda-Angulo et al., 2014; Robins et al., 2013; S. Blackshaw pers comm). At present there is no proof that either of these two molecules is key to stemness in the adult. However, in the embryo, high levels of Rax may drive hypothalamic stemness, while lower levels are required for stem cells to differentiate to progenitors (Muthu et al., 2016). The first aim of this chapter was therefore to determine the distribution of GFAP and Rax along the A-P axis. At the same time I analysed Sox2 (previously implicated as a hypothalamic stem cell marker (Li et al., 2012)) and Six3, a transcription factor that governs Shh expression in the embryonic hypothalamus (Geng et al., 2008; Jeong et al., 2008). I wanted to test the hypothesis that *Shh*$^{+}$*Fgf10*$^{+}$ tanycytes in the PME express high levels of GFAP, Rax, Sox2 and Six3.

A second aim of this chapter was to analyse expression of the cell adhesion molecule NrCAM in tanycytes along the A-P axis. As outlined in the Introduction (Chapter 1.4.2), unpublished studies in our lab had shown that NrCAM is expressed in tanycytes at the level of the median eminence. I wanted to expand on this observation, to ask whether NrCAM is expressed in all

Figure 4.1: Comparison of tanycyte associated markers and signals in the tuberal hypothalamus

Image composites at 10x magnification showing a coronal cross-section of the 3V, ME, and hypothalamic parenchyma in adult wild type mice labelled for various markers associated with tanycytes in previous literature. Scale bars 100µm.

A –Nestin (red) immunofluorescence labelling with nuclear DAPI staining (blue). Image representative of n=6 mice investigated.

B – Sox2 (green) and GFAP (red) immunofluorescence labelling with nuclear DAPI staining (blue). n=1 mouse for Sox2 and n=2 for GFAP. A single mouse was used to confirm this labelling as it has been previously described: Sox2 (Li et al., 2012), GFAP (Campbell et al., 2017; Robins et al., 2013a).

C – Six3 (green) immunofluorescence labelling with nuclear DAPI staining (blue). Image representative of n=3 mice investigated.

D – Rax mRNA labelled by chromogenic in situ hybridisation (blue). Image representative of n=6 mice investigated.

E – Fgf10 mRNA labelled by chromogenic in situ hybridisation (blue). Image representative of n=3 mice investigated.

Figure 4.1

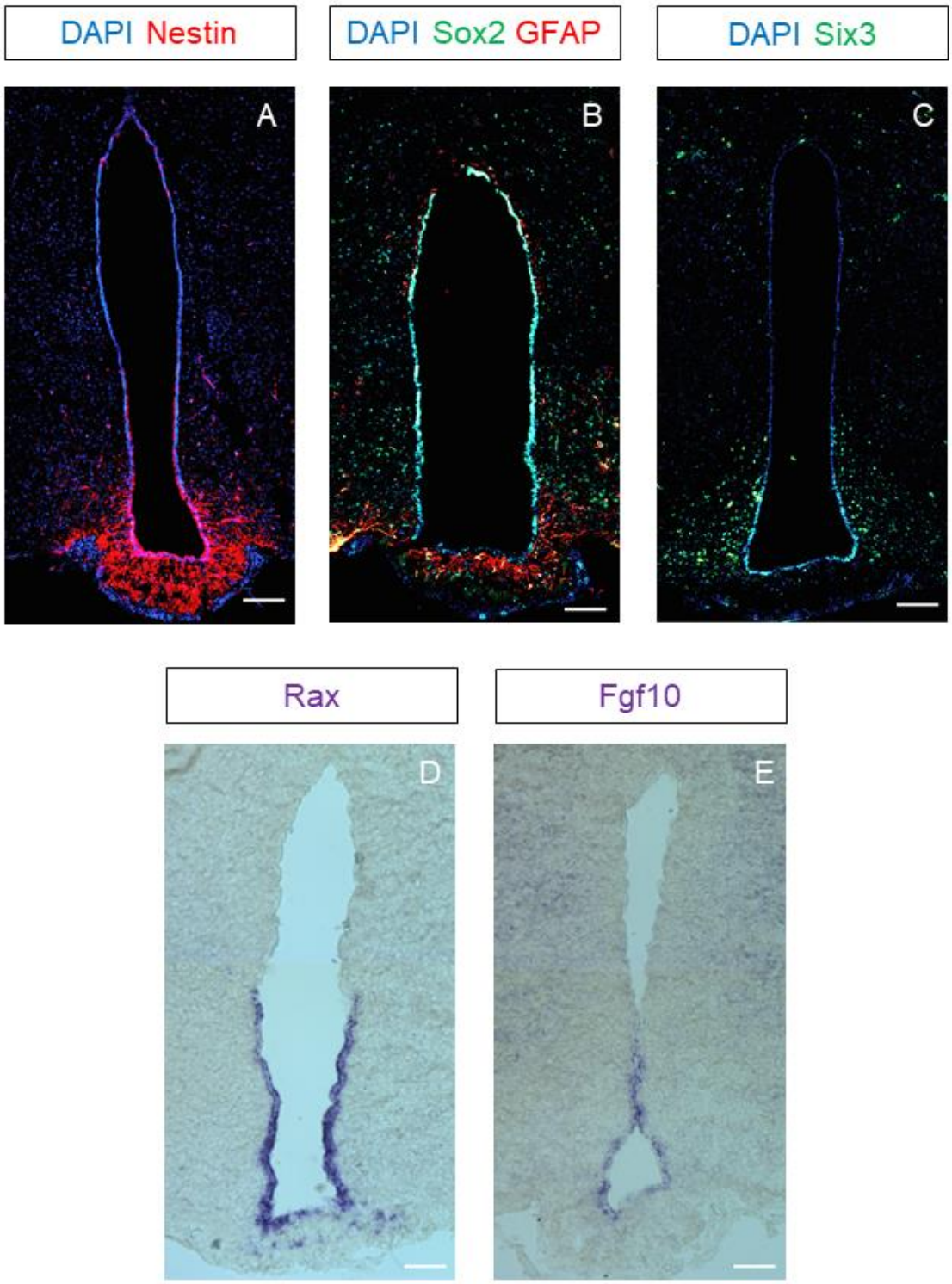

tanycytes, or in subsets, and to ask if NrCAM expression is particularly high in the PME.

4.2 Results

I first confirmed the expression patterns of Sox2, GFAP, Six3, *Rax* and NrCAM in central ME hypothalamic sections. Sox2 is expressed in a 'salt and pepper' manner by tanycytes lining the ventricle, but is also expressed in dorsal ependymocytes, and in parenchymal cells of the ARC, DMN, and VMN (Fig 4.1 B) (Haan et al., 2013; Li et al., 2012; Robins et al., 2013a). The intermediate filament protein, GFAP, is expressed in α-tanycytes (Fig.4.1 B, Fig 4.3) but additionally is detected on astrocytes in the parenchyma, most notably around the dorsal ependymal cell domain and around β-tanycytes (Robins et al., 2013). The transcription factor Six3 demonstrates nuclear localisation in β1- and α2-tanycytes; it does not extend dorsally into the α1-tanycyte domain and appears to be expressed weakly in β2 tanycytes (Fig 4.1 C). Six3 is also expressed in cells of the parenchyma in the ARC and DMN. *Rax* is localised to α- and β-tanycyte cell bodies (Fig 4.1 D). Similar to *Fgf10* and Six3, *Rax* is expression is week or absent in medial-most β2 tanycytes. In addition to tanycyte expression, distinct Rax^{+} nuclei can also be detected in the median eminence parenchyma. This profile matches that described by Miranda-Angulo et al (2014).

Analysis of ME sections show that, as previously reported in the lab (S.Brown, MSc, unpublished), NrCAM is expressed on tanycyte cells bodies at the VZ and on their processes extending to the median eminence and ARC (Fig 4.2 A,B). Like Nestin, NrCAM appears to label both β- and α-tanycyte subsets (Fig.4.2 and 4.3). Indeed, NrCAM and Nestin appear to be expressed together in all tanycytes and to co-label multiple processes (one prominent process highlighted by the yellow arrow head). Unlike Nestin, NrCAM additionally decorates tanycyte cell bodies at the VZ, so that a honeycomb-like expression is observed at the 3V. This expression is similar to that of various tight junction proteins (occludin, ZO-1, claudin 5) that allow tanycytes to form a barrier between the CSF of the 3V and the hypothalamic parenchyma (Mullier et al., 2010). In the parenchyma, NrCAM is not detected on cell bodies. Some expression is detected on circular structures (Figure 4.2, 4.3.) Similar

Figure 4.2: NrCAM is expressed in the ventricular zone of the third ventricle in the tuberal hypothalamus

NrCAM expression in coronal cross-sections at the ME shows expression in the 3V VZ and on projections extending to the ME and parenchyma. Labelling in the parenchyma close to VZ in C and Ci may be on cells bodies, structures made by VZ processes, or blood vessels.

A – NrCAM (red) immunofluorescence labelling with nuclear DAPI staining (blue). 30µm section thickness 20x magnification with 50µm scale bar. Image representative of n=9 mice investigated.

B – NrCAM (white) immunofluorescence labelling. 30µm section thickness 20x magnification with 50µm scale bar. Image representative of n=9 mice investigated.

C – NrCAM (red) immunofluorescence labelling with nuclear DAPI staining (blue). 15µm section thickness 10x magnification with 50µm scale bar. Image representative of n=9 mice investigated.

Ci – NrCAM (red) immunofluorescence labelling. 30µm section thickness 20x magnification with 50µm scale bar. Image representative of n=9 mice investigated.

Figure 4.2

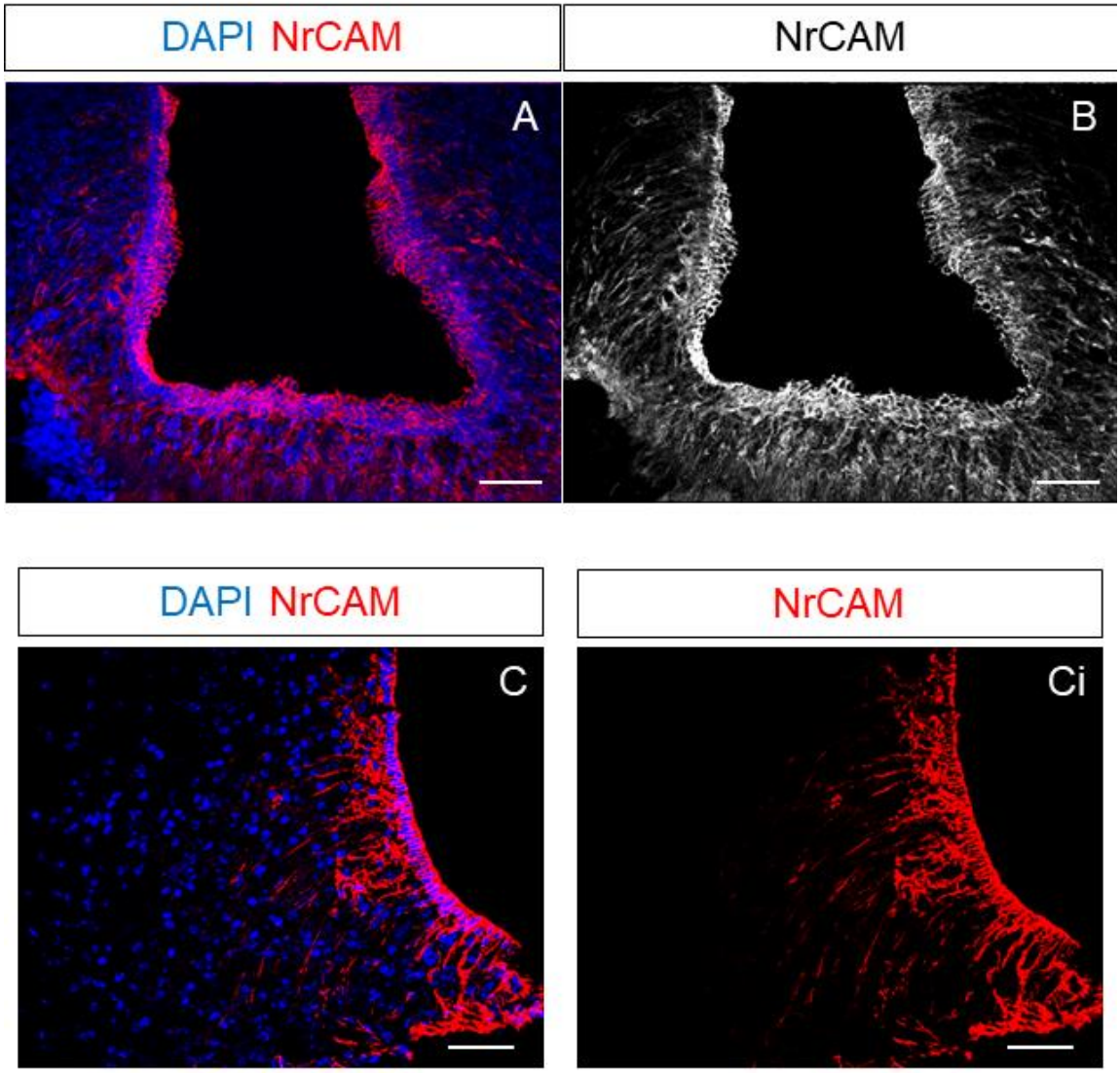

Figure 4.3: NrCAM and Nestin label tanycytes processes in the tuberal hypothalamus

NrCAM and Nestin are expressed in the VZ of the 3V and in processes extending to toward the ME and the parenchyma. NrCAM expression and Nestin expression appear to overlap, suggesting NrCAM is expressed by tanycytes.

A – Nestin (green) and NrCAM (red) immunofluorescence labelling with nuclear DAPI staining (blue) on a coronal cross-section at the ME. Region in box is shown in B, Bi, Bii. 10x magnification with 50µm scale bar. Image representative of n=6 mice investigated.

B – Nestin (green) and NrCAM (red) immunofluorescence labelling with nuclear DAPI staining (blue). 20x magnification image of region outlined in A. Bi and Bii show Nestin and NrCAM expression respectively (white). Overlapping expression is labelled yellow in B, with yellow arrow heads highlighting one process in the three panels. 50µm scale bar. Image representative of n=6 mice investigated.

C – Stylised depiction of tanycytes in a comparable section to that in A, B.

Figure 4.3

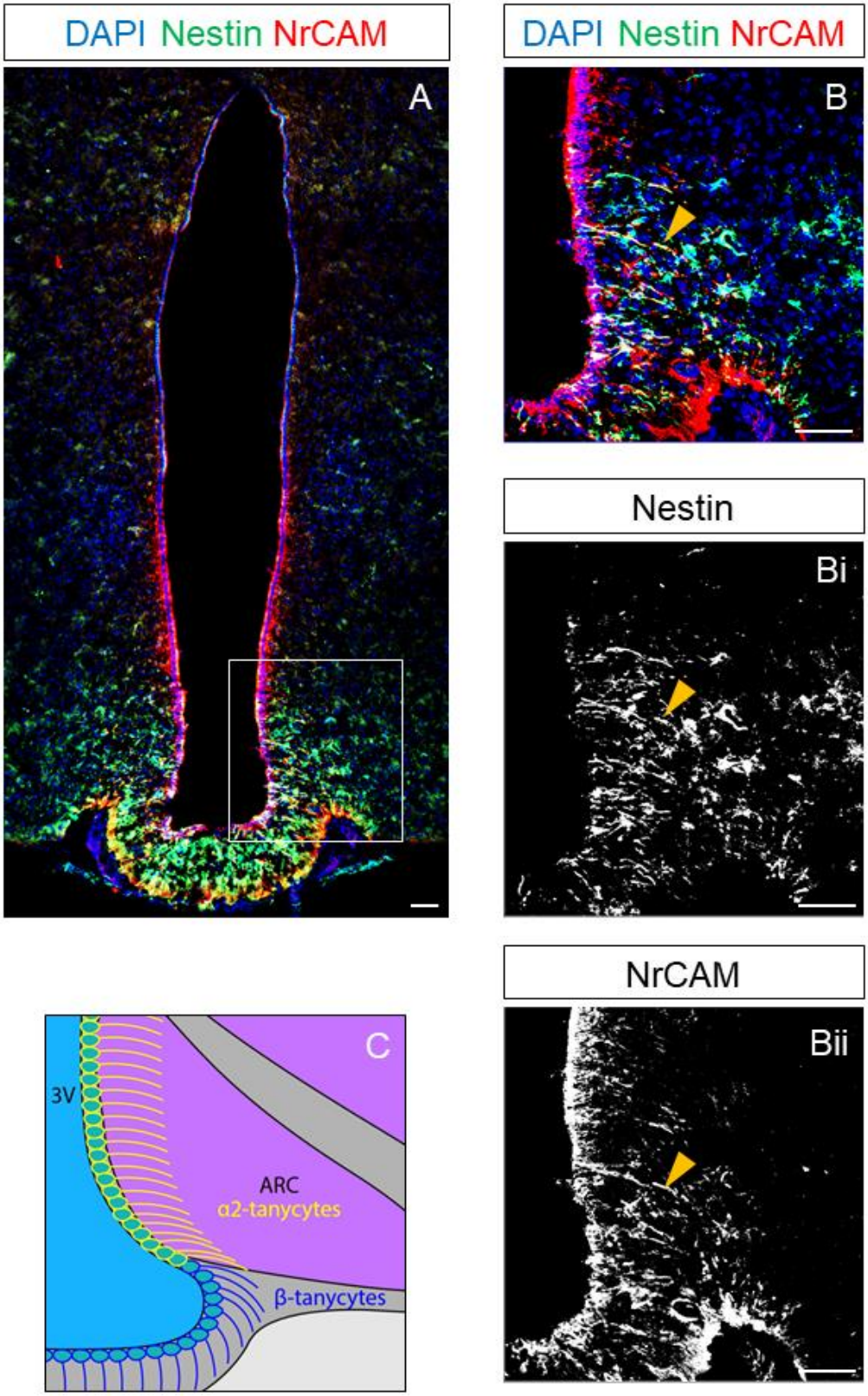
DAPI Nestin NrCAM
A
DAPI Nestin NrCAM
B
Nestin
Bi
NrCAM
Bii
C
3V
ARC
α2-tanycytes
β-tanycytes

configurations have previously been observed in tanycyte processes surrounding the endothelial cells of hypothalamic blood vessels (Norsted et al., 2008). These observations of NrCAM in the VZ, on processes that extend to the ARC/median eminence, and surrounding periventricular blood vessels, suggest NrCAM may be a marker specific to tanycytes.

Having established that I could recapitulate profiles described previously, I next analysed expression of these markers along the A-P axis.

4.2.1 GFAP

Analyses of consecutive sections shows that GFAP$^+$ tanycytes are first detected in ventral-most regions of the 3rd ventricle in the A/AME^A subregion (Fig.4.4.A), the same region where Nestin$^+$ tanycytes are first detected. More posteriorly, abundant GFAP$^+$ tanycytes are detected in the AME and ME^A: in both regions they appear to label α2-, but not β–tanycytes, and their processes project to the upper ARC and the VMN (Fig 4.4 Bii). In the ME^P, GFAP$^+$ tanycytes cannot be detected (Fig 4.4 Cii,Dii), but in the PME, strongly labelled GFAP$^+$ tanycytes are detected at the base of the 3V, ie in the same position as *Fgf10*$^+$ *Shh*$^+$ tanycytes. No GFAP$^+$ tanycytes are detected in P subregions.

In addition to expression on tanycytes, GFAP is expressed on astrocytic-like cells that lie adjacent to ependymal cells/tanycytes in dorsal and ventral regions, particularly clustered around the dorsal roof of the 3V (Campbell et al., 2017; Robins et al., 2013a). My investigation of GFAP shows this dorsal cluster is greatest in the A and AME (Fig 4.4 A,B), diminishing posteriorly until a small population remain directly dorsal to the Nestin$^+$ population of ependymal cells in the roof of the 3V (Fig 4.4C,D,E,F).

4.2.2 Sox2

In all A-P regions, Sox2 is expressed throughout the 3V and in cells of the parenchyma (Figure 4.4). Double-label analysis with GFAP suggests that some tanycytes are GFAP$^+$ Sox2$^+$. Given its prevalence throughout the region, its expression does not provide any additional information for investigating tanycyte subtype distribution.

Figure 4.4: GFAP and Sox2 expression in the tuberal hypothalamus along the anterior-posterior axis

Image composites (A-F) at 10x magnification of coronal cross-sections showing Sox2 (green) and GFAP (red) expression by immunofluorescence in relation to the 3V, ME, and hypothalamic parenchyma along the A-P axis with nuclear DAPI staining (blue) in an adult wild type mouse. Box inserts (i and ii for each cross-section) indicate corresponding image z-stacks collected at 20x magnification and converted to maximum intensity projections (MIPs) (Ai/Aii-Fi). Scale bars for all images 100µm. n=1 mouse for Sox2 and n=2 for GFAP. A single mouse was used to confirm this labelling as it has been previously described: Sox2 (Li et al., 2012), GFAP (Campbell et al., 2017; Robins et al., 2013a).

Sox2 expression is present throughout the VZ of the 3V and in cells of the parenchyma from anterior to posterior. Ventrally, GFAP is expressed on astrocytes and processes extending from the VZ. Dorsally, GFAP appears to be expressed on astrocytes clustered around the VZ ependymocyte domain. Expression is strongest in anterior and AME sections (A-B), then decreasing until it is almost absent in PME and posterior sections (E-F), except where strong GFAP is seen in the base of the 3V in the PME (white arrowhead, E,Eiii).

Figure 4.4

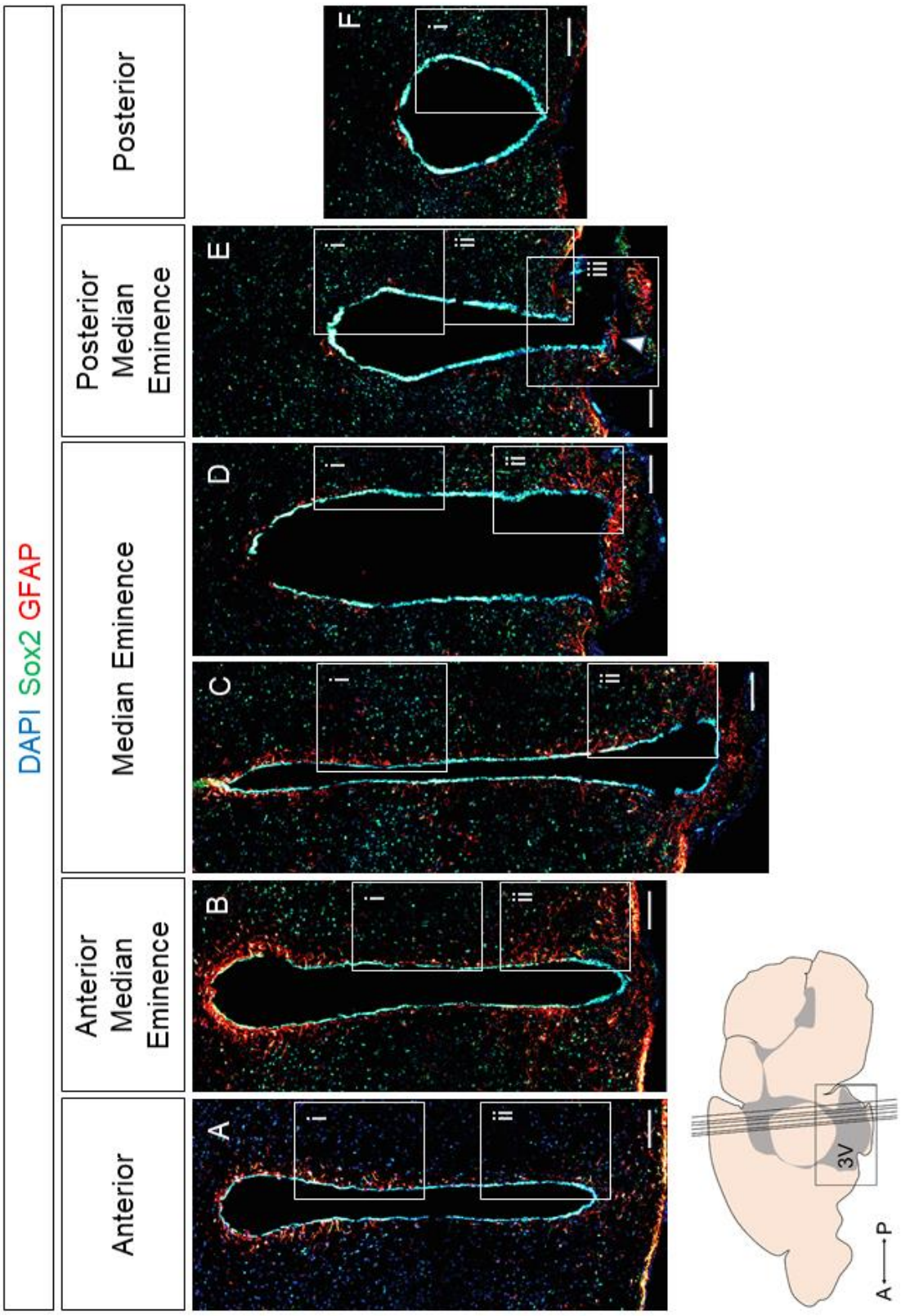
DAPI Sox2 GFAP
Anterior
Anterior Median Eminence
Median Eminence
Posterior Median Eminence
Posterior
A
B
C
D
E
F
i
ii
iii
3V
A
P

Figure 4.4

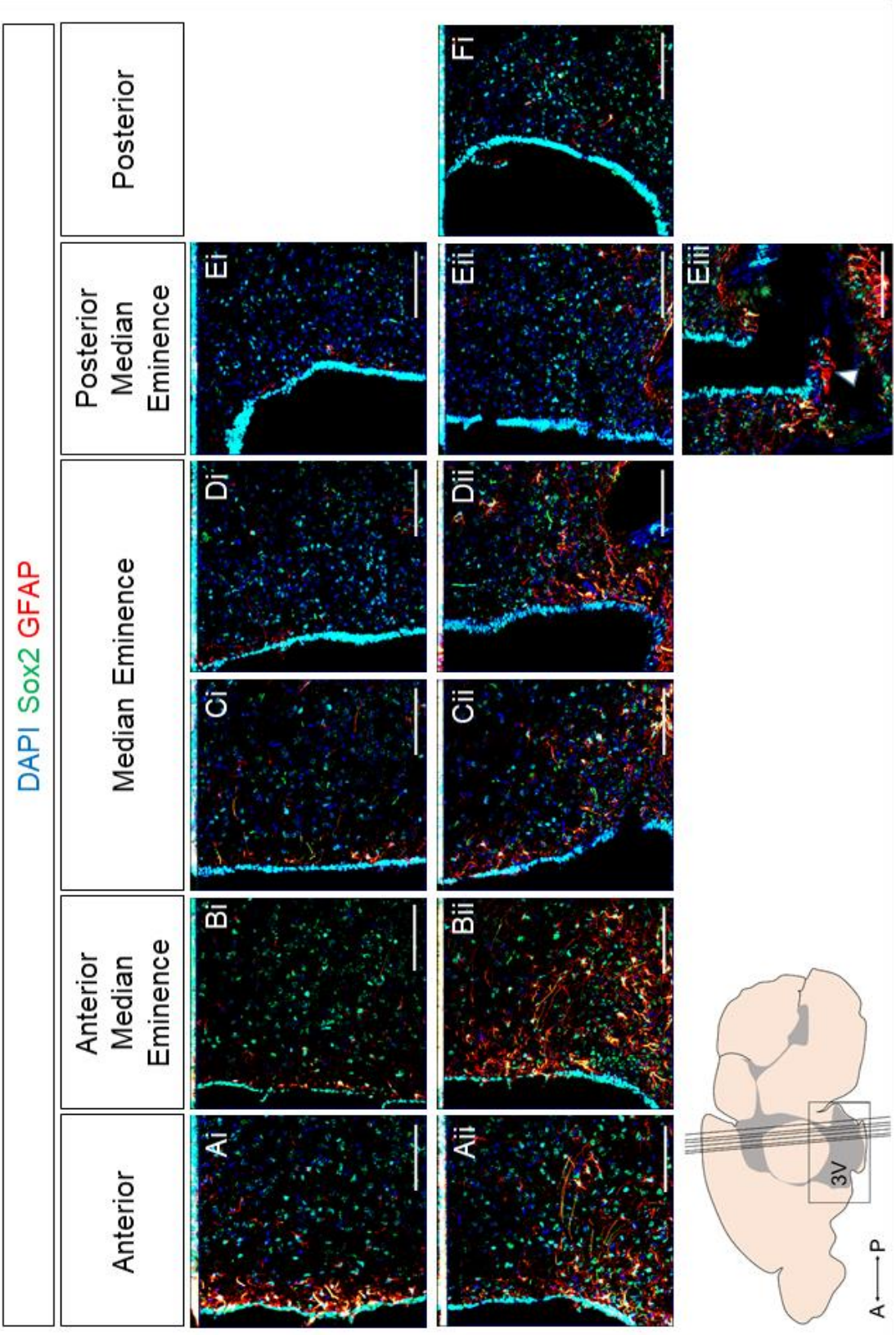
DAPI Sox2 GFAP
Anterior
Anterior Median Eminence
Median Eminence
Posterior Median Eminence
Posterior
Ai
Bi
Ci
Di
Ei
Fi
Aii
Bii
Cii
Dii
Eii
Eiii
3V
A
P

4.2.3 Six3

In development, Six3 interacts with Rax and Shh to induce and pattern the hypothalamus (reviewed in Yoo & Blackshaw, 2018, and discussed in Chapter 1.3.1 and 6.1), however, investigation of Six3 in the adult hypothalamus has been limited (Conte et al., 2005). Analysis along the A-P axis reveals that, like *Fgf10* and GFAP, Six3 is expressed within a subset of Nestin^{+} tanycytes (Fig 4.5 and schematised in Fig 4.9). Expression appears to be nested within and below that of GFAP. Similar to GFAP and *Fgf10*, expression diminishes/cannot be detected in β2 tanycytes of the median eminence (Figure 4.5 C,D), but is detected at highest levels in ventral-most tanycytes of the PME (Figure 4.5E). No expression is detected in the P region (Fig 4.5 F).

Six3 can also be detected in the parenchyma. Anteriorly, Six3 is observed in scattered nuclei of the PVN and ARC (Fig 4.5 A,Ai,Aii). In the AME and ME^{A}, Six3 can be detected in the ARC (Fig 4.5 B,Bii,C,Cii) and weakly in the DMN (Fig 4.5 Bi,C,Ci,D,Di).

4.2.4 Rax

Expression of Rax mRNA, like Nestin and GFAP, initiates at the A/AME^{A} boundary (Fig 4.6 A). Through the AME and ME, *Rax* expression spreads dorsally into the α2- and α1-tanycyte domains (Fig 4.6 B,C). The extent of its expression is maintained through the ME, PME, and P (Fig 4.6 D,E,F). However, similar to GFAP, *Fgf10* and Six3, expression is reduced/barely detected in medial-most ME cells – most likely β2-tancytes. Strong expression is then detected in the PME and P regions. Unlike other markers examined, *Rax* is also clearly detected in distinct cells scattered through the median eminence of the ME and PME subregions (Fig 4.6 Ci-Ei).

4.2.5 NrCAM as a marker of tanycytes

To investigate whether NrCAM labels all tanycytes, or a subset, I compared NrCAM and Nestin expression, performing double immunolabelling in sections taken along the A-P axis (Fig 4.7). As in the ME, NrCAM and Nestin appear to be expressed together in all tanycytes. This suggests that NrCAM labels all tanycytes, and not any particular subset. Similar to my observations with Nestin, NrCAM label intensity, or NrCAM^{+} tanycyte density, increases posteriorly

Figure 4.5: Six3 expression in the tuberal hypothalamus along the anterior-posterior axis

Image composites (A-F) at 10x magnification of coronal cross-sections showing Six3 (green) expression by immunofluorescence in relation to the 3V, ME, and hypothalamic parenchyma along the A-P axis with nuclear DAPI staining (blue) in an adult wild type mouse. Box inserts (i and ii for each cross section) indicate corresponding image z-stacks collected at 20x magnification and converted to maximum intensity projections (MIPs) (Ai/Aii-Fi). Scale bars for all images 100µm. Images representative of the n=3 mice investigated.

Six3 expression is present in cells of the parenchyma from anterior to posterior and in the ventral VZ of the 3V from AME to PME (B-E), with strongest expression in the AME and anterior-most portion of the ME (B-C).

Figure 4.5

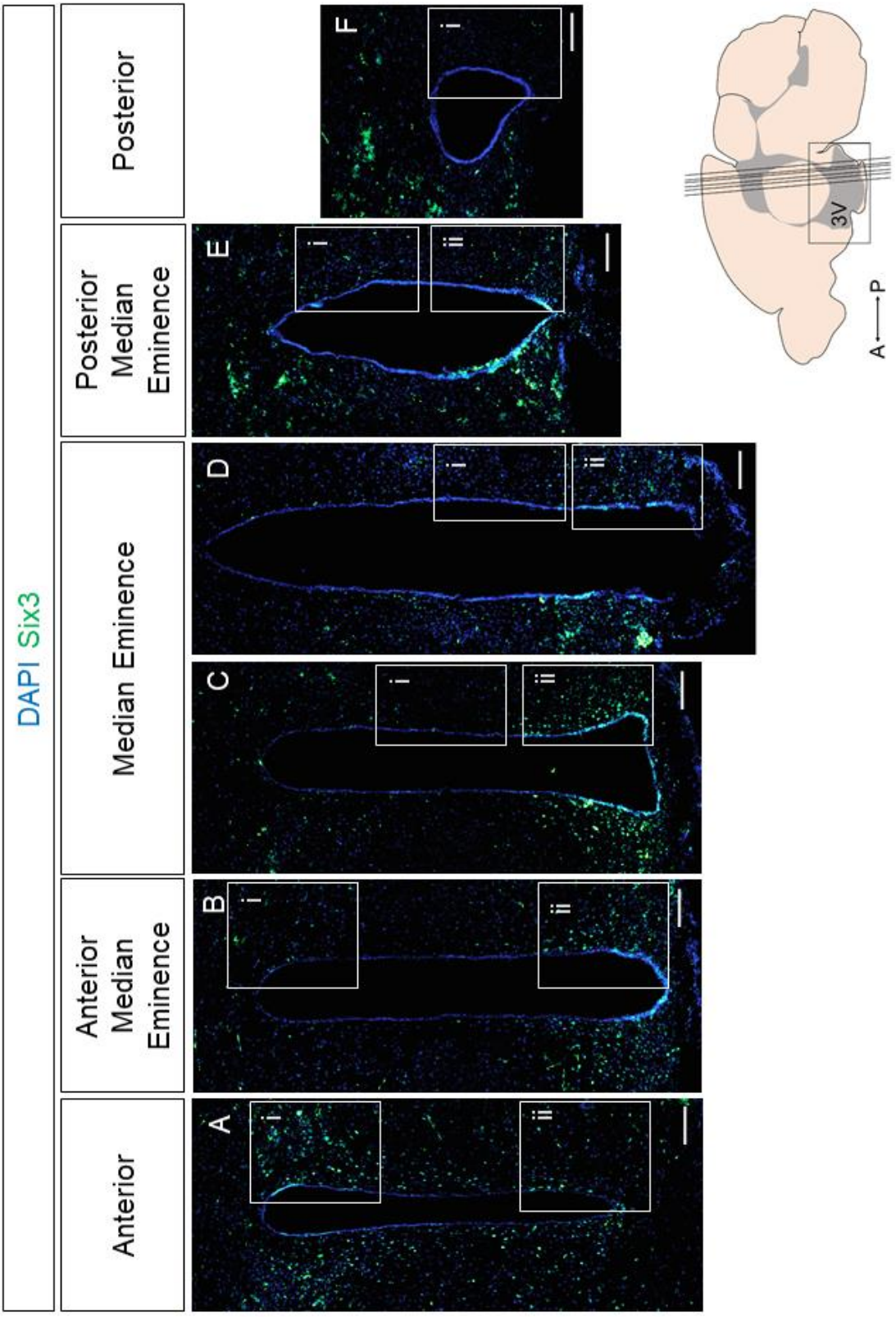
DAPI Six3
Anterior
Anterior Median Eminence
Median Eminence
Posterior Median Eminence
Posterior
A
B
C
D
E
F
i
ii
3V
A
P

Figure 4.5

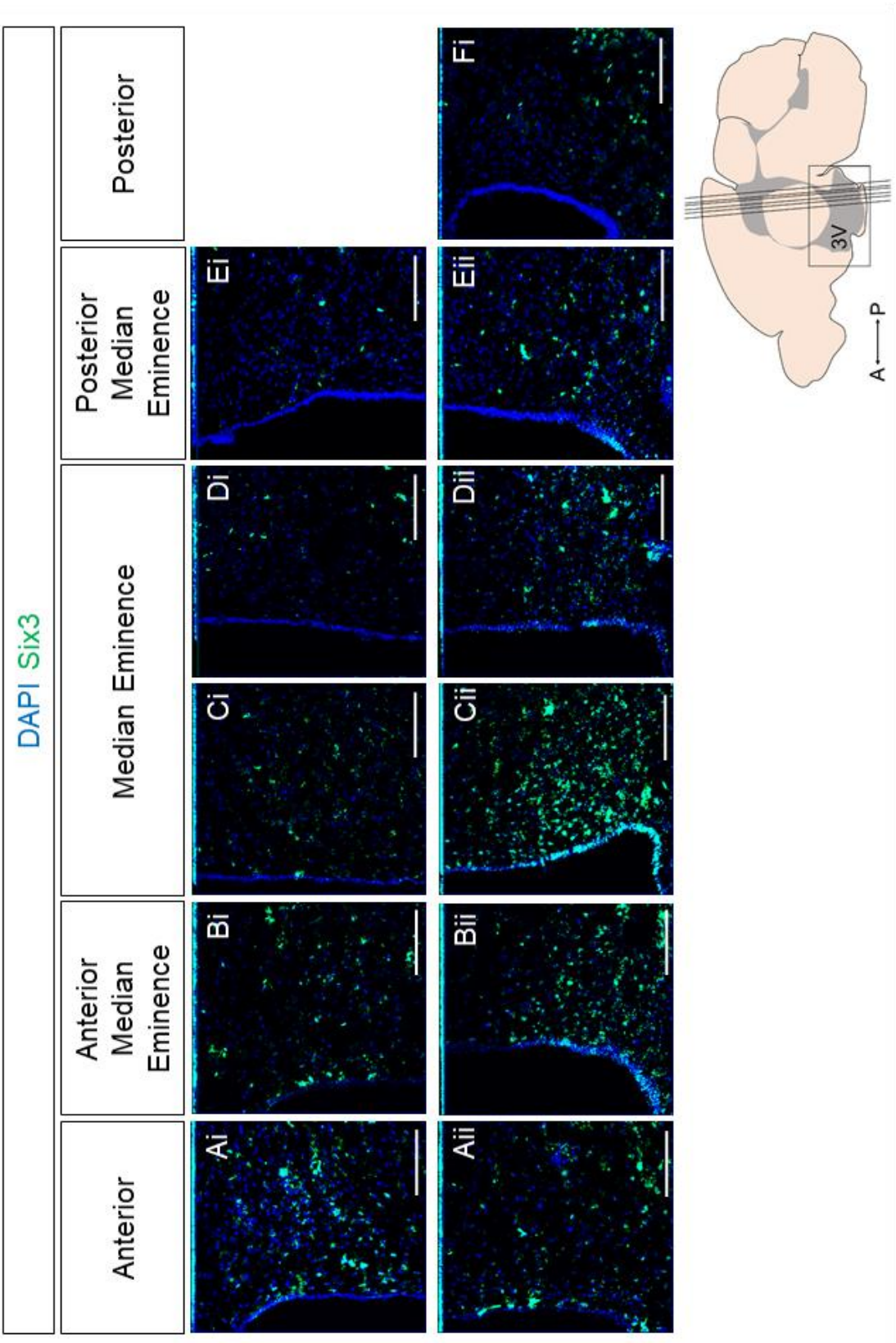
DAPI Six3
Anterior
Anterior Median Eminence
Median Eminence
Posterior Median Eminence
Posterior
Ai
Bi
Ci
Di
Ei
Fi
Aii
Bii
Cii
Dii
Eii
Fii
3V
A
P

Figure 4.6: Rax expression in the tuberal hypothalamus along the anterior-posterior axis

Image composites (A-F) at 10x magnification of coronal cross-sections showing Rax mRNA expression (purple) by *in situ* hybridisation in relation to the 3V, ME, and hypothalamic parenchyma along the A-P axis in an adult wild type mouse, with corresponding images of the median eminence (Ci-Ei). Scale bars 100µm. Images representative of the n=5 mice investigated.

Rax expression initiates in the ventral most region of the 3V VZ at the Anterior/AME^{A} boundary. Expression progresses dorsally and increases in intensity through to the posterior aspect of the hypothalamic 3V. In ME and PME sections Rax expression is seen in cells of the ME (C-E).

Figure 4.6

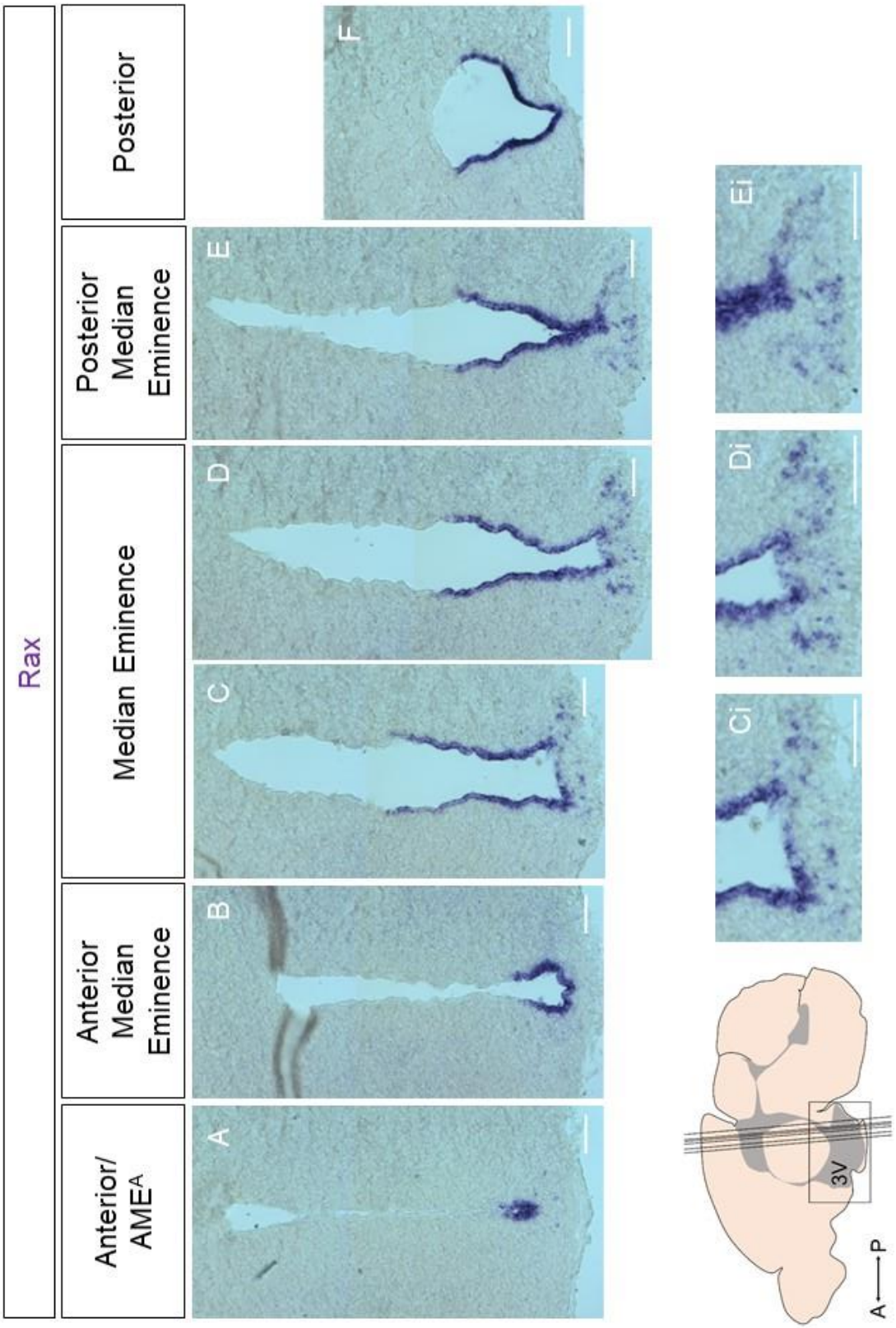
Rax
Anterior/ AME^A
Anterior Median Eminence
Median Eminence
Posterior Median Eminence
Posterior
A
B
C
D
E
F
Ci
Di
Ei
3V
A
P

Figure 4.7: NrCAM and Nestin expression in the tuberal hypothalamus along the anterior-posterior axis

Image composites (A-F) at 10x magnification of coronal cross-sections showing Nestin (green) and NrCAM (red) expression by immunofluorescence in relation to the 3V, ME, and hypothalamic parenchyma along the A-P axis with nuclear DAPI staining (blue) in an adult wild type mouse. Box inserts (i and ii for each cross-section) indicate corresponding image z-stacks collected at 20x magnification and converted to maximum intensity projections (MIPs) displayed as combined and separate channel images (Bi/Bii-Fi/Fii). Scale bars for A-F 100µm and for inserts 50 µm. Images representative of the n=6 mice investigated.

Nestin and NrCAM expression appears similar along the A-P axis the 3V in the tuberal hypothalamus. Low NrCAM expression is seen along the apical surface of the ventricle of anterior sections and is expressed in the VZ ventrally where Nestin expression first appears through the A-P axis of the tuberal hypothalamus. Both are expressed strongly in α2-tanycyte processes from the AME, with intensity of expression increasing with posterior progression (Bii-Fii). NrCAM expression is more apparent in the VZ than Nestin, and more clearly marks the α1-tanycytes that have comparatively weak NrCAM and Nestin expression in processes (Bi-Fi). No significant difference observed between $NrCAM^+$ and $Nestin^+$ processes counted over 62 20x images of 31 sections (left and right of the lower ventral ventricle) in 1 adult wild type mouse ($p=0.8824$).

Figure 4.7

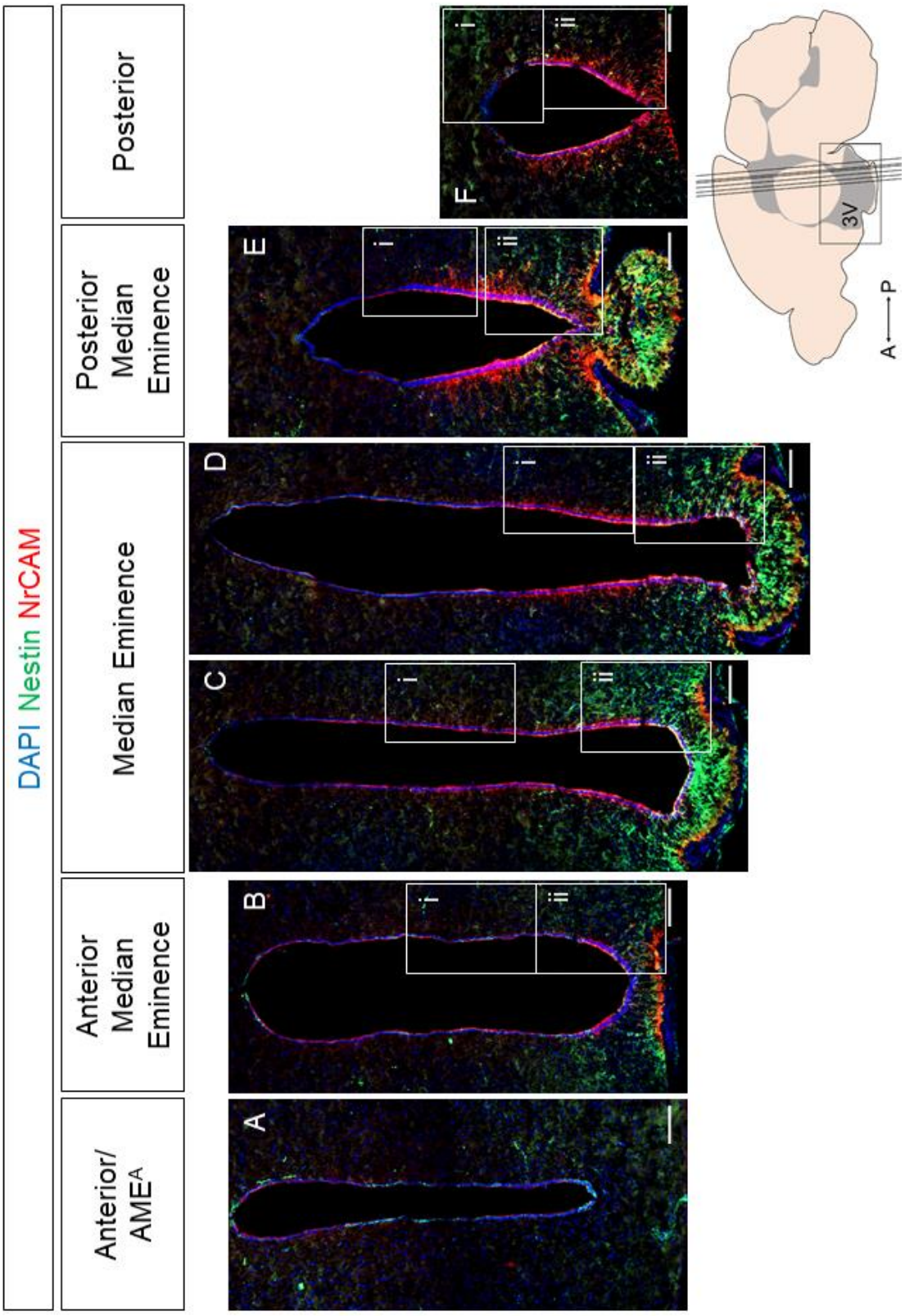
DAPI Nestin NrCAM
Anterior/ AME^A
Anterior Median Eminence
Median Eminence
Posterior Median Eminence
Posterior
A
B
C
D
E
F
i
ii
3V
A
P

Figure 4.7

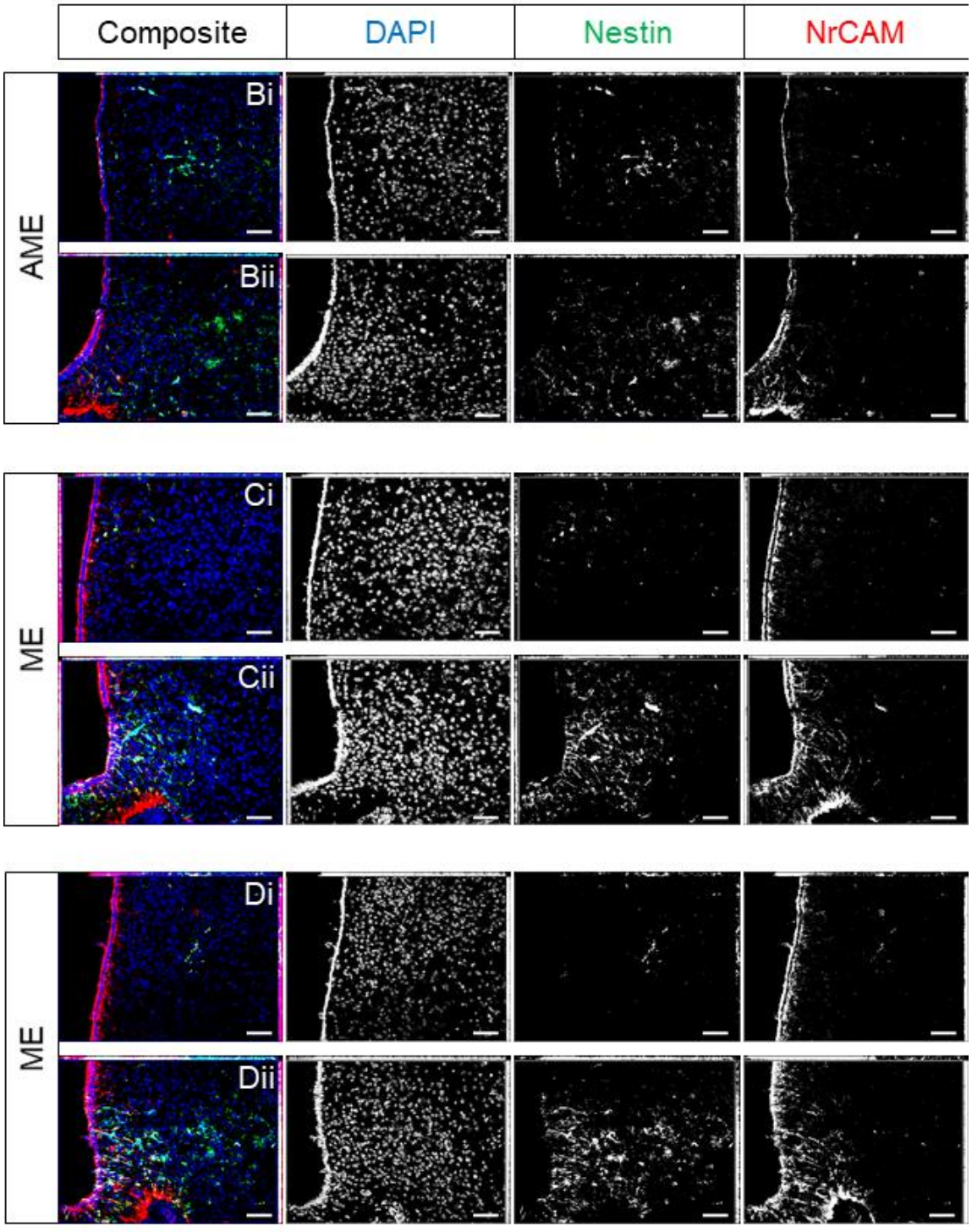

Figure 4.7

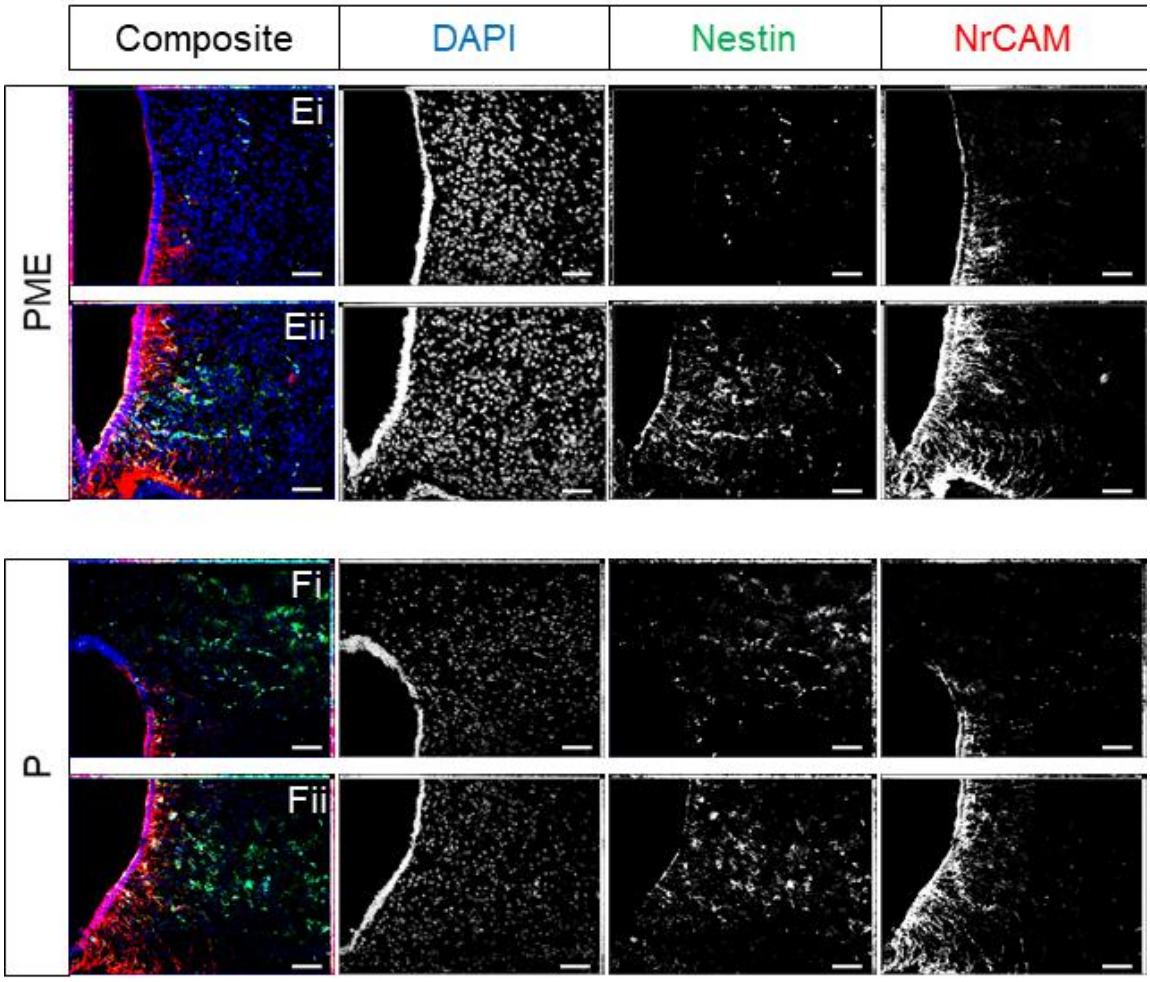

through the hypothalamus (Fig 4.7 Eii,Fii). Again, this suggests that tanycyte density is greatest in the ventral part of the 3V in the PME. Direct comparison of NrCAM and GFAP, through double immunohistochemical labelling, confirms the strongly-expressing $GFAP^+$ $NrCAM^+$ tanycytes in the ventral PME (Fig 4.8).

4.3 Discussion

In this chapter I set out to describe the expression of NrCAM, relative to other tanycyte markers, and to ascertain if tanycytes in the ventral part of the 3V in the PME express high levels of tanycyte markers, especially *Rax* and GFAP, both previously implicated as markers of stem-like tanycytes.

My work suggests that, similar to Nestin, Sox2, and *Rax*, NrCAM labels all tanycyte subsets (Fig 4.9). Its expression pattern correlates with the expression on Rax mRNA on tanycyte cell bodies in the VZ. Previous research has suggested that both Rax and Nestin are expressed in all tanycyte subsets (Miranda-Angulo et al., 2014; Robins et al., 2013a), and the overlap of NrCAM and Nestin throughout the hypothalamus indicates NrCAM may similarly mark all subsets.

NrCAM and Nestin do not appear to co-label the same subcellular domains within tanycytes: NrCAM is largely localised to the cell surface, whereas Nestin is an intermediate filament protein and so internally localised. The cell surface labelling of NrCAM may provide an explanation for why NrCAM labels tanycytes more robustly than does Nestin. Not only is labelling robust, but NrCAM also appears to label cells in a more specific manner than either Nestin or Sox2, suggesting that it may be a more useful general marker. Thus, I detect Nestin both in tanycytes and in cells of the dorsal 3V roof, while I detect Sox2 in tanycytes, as well as parenchymal cells. These findings resonate with recent single cell Drop-seq analysis of the arcuate hypothalamus and median eminence, which reveal high expression of Nestin in tanycytes, and lower expression in ependymal cell, endothelial cell, and mural cell clusters, and reveal expression of Sox2 in oligodendrocytes, astrocytes, ependymocytes, tanycytes, and some neurons (Campbell et al., 2017). This promiscuous expression severely limits the usefulness of either Nestin or Sox2 as a marker for tanycytes. By contrast, I detect NrCAM only in tanycytes, suggesting that it

Figure 4.8: NrCAM and GFAP expression in the tuberal hypothalamus along the anterior-posterior axis

Image composites (A-F) at 10x magnification of coronal cross-sections showing NrCAM (green) and TH (red) expression by immunofluorescence in relation to the 3V, ME, and hypothalamic parenchyma along the A-P axis with nuclear DAPI staining (blue) in an adult wild type mouse. Box inserts (Ai-Fi) indicate corresponding image z-stacks collected at 20x magnification and converted to maximum intensity projections (MIPs). Scale bars for all images 100µm. This comparison has been made on sections from one mouse (n=1), but GFAP has been described here in two mice (n=2), and NrCAM in nine mice (n=9).

NrCAM and GFAP expression presents as previously described. GFAP appears to be expressed on astrocytes and processes with strongest expression in anterior and AME sections with expansive expression round the dorsal ependymocyte domain. NrCAM expression is mostly absent from anterior sections, with strong expression restricted to the ventral VZ and processes in the AME, before spreading dorsally and increasing in intensity with posterior progression through the ME and beyond. GFAP and NrCAM expression appear as though in an inverse gradient across the A-P axis of the tuberal hypothalamus, with limited overlap, if any, in the anterior aspect of the ME (C, Ci, Cii).

Figure 4.8

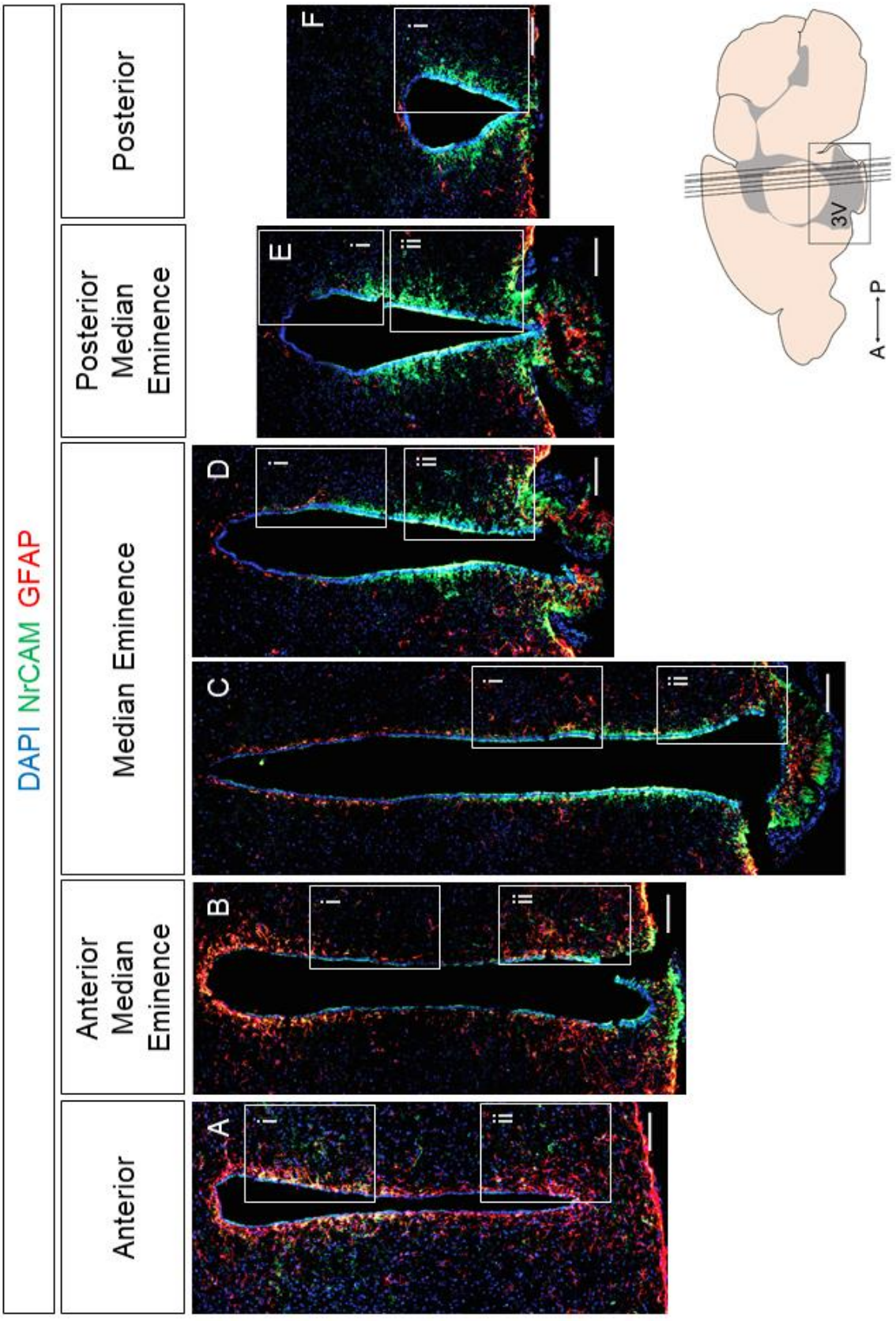
DAPI NrCAM GFAP
Anterior
Anterior Median Eminence
Median Eminence
Posterior Median Eminence
Posterior
A
B
C
D
E
F
i
ii
3V
A
P

Figure 4.8

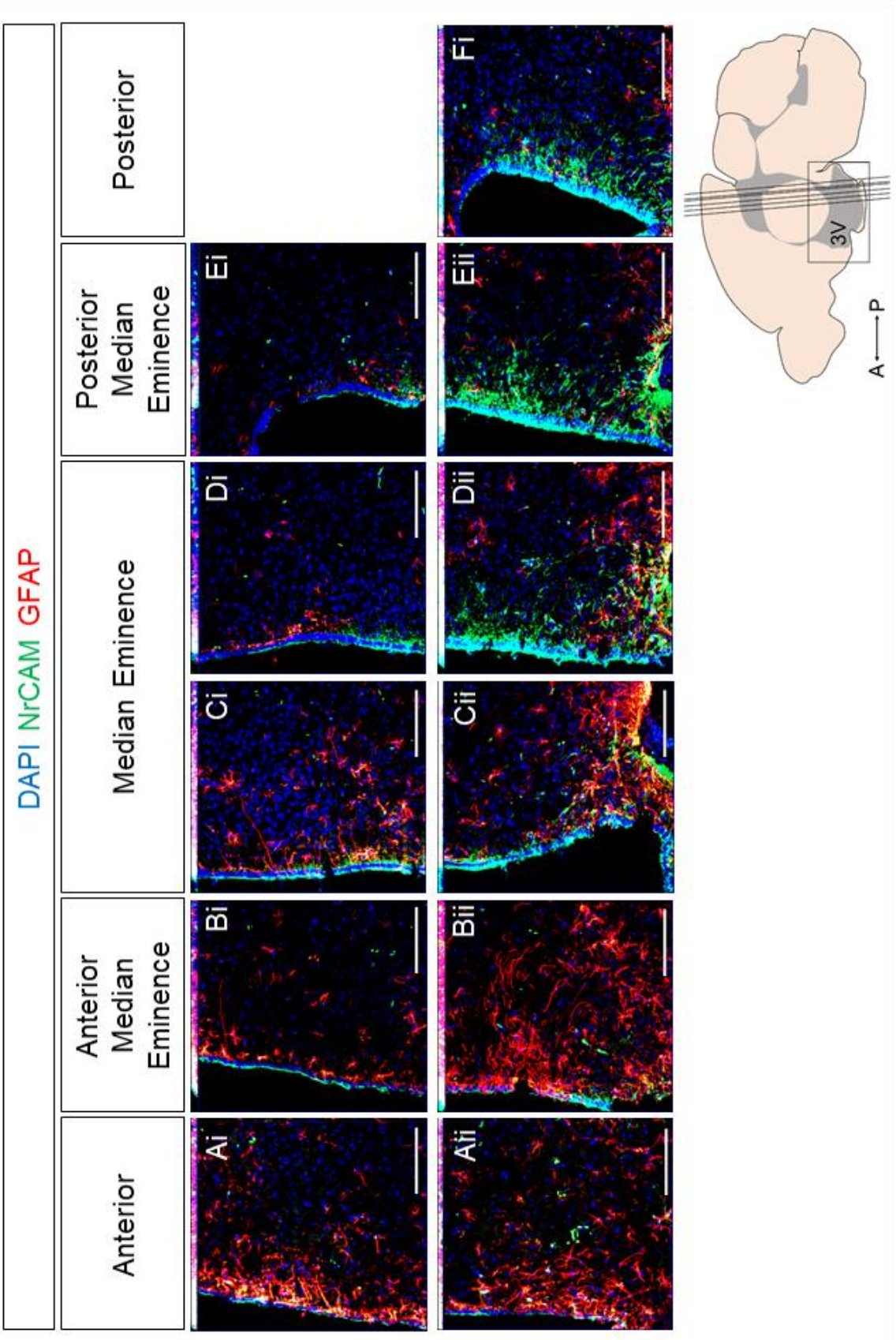
DAPI NrCAM GFAP
Anterior
Anterior Median Eminence
Median Eminence
Posterior Median Eminence
Posterior
Ai
Aii
Bi
Bii
Ci
Cii
Di
Dii
Ei
Eii
Fi
3V
A
P

Figure 4.9 Comparative expression of tanycyte markers and signalling molecules along the anterior-posterior axis of the hypothalamus

Schematic illustrations of coronal cross-sections from anterior to posterior through the hypothalamus highlighting expression of Nestin, NrCAM, Rax, Six3, GFAP, Fgf10, and Shh. Tanycytes are labelled by colour for the markers they express. Ependymal cells are shown in blue, and Nestin^{+} ependymal cells at the dorsal tip of the 3V are in single purple circles. Hypothalamic nuclei ARC, DMN, VMN, PVp, PVN, and the median eminence are labelled to show whether they include cells that express Six3, GFAP, or Rax. The anterior cross-section is representative of sections collected at approximately Bregma -1.4mm, directly anterior to the AME where tanycyte are first observed and their projections do not meet the ventral surface of the brain.

Figure 4.9

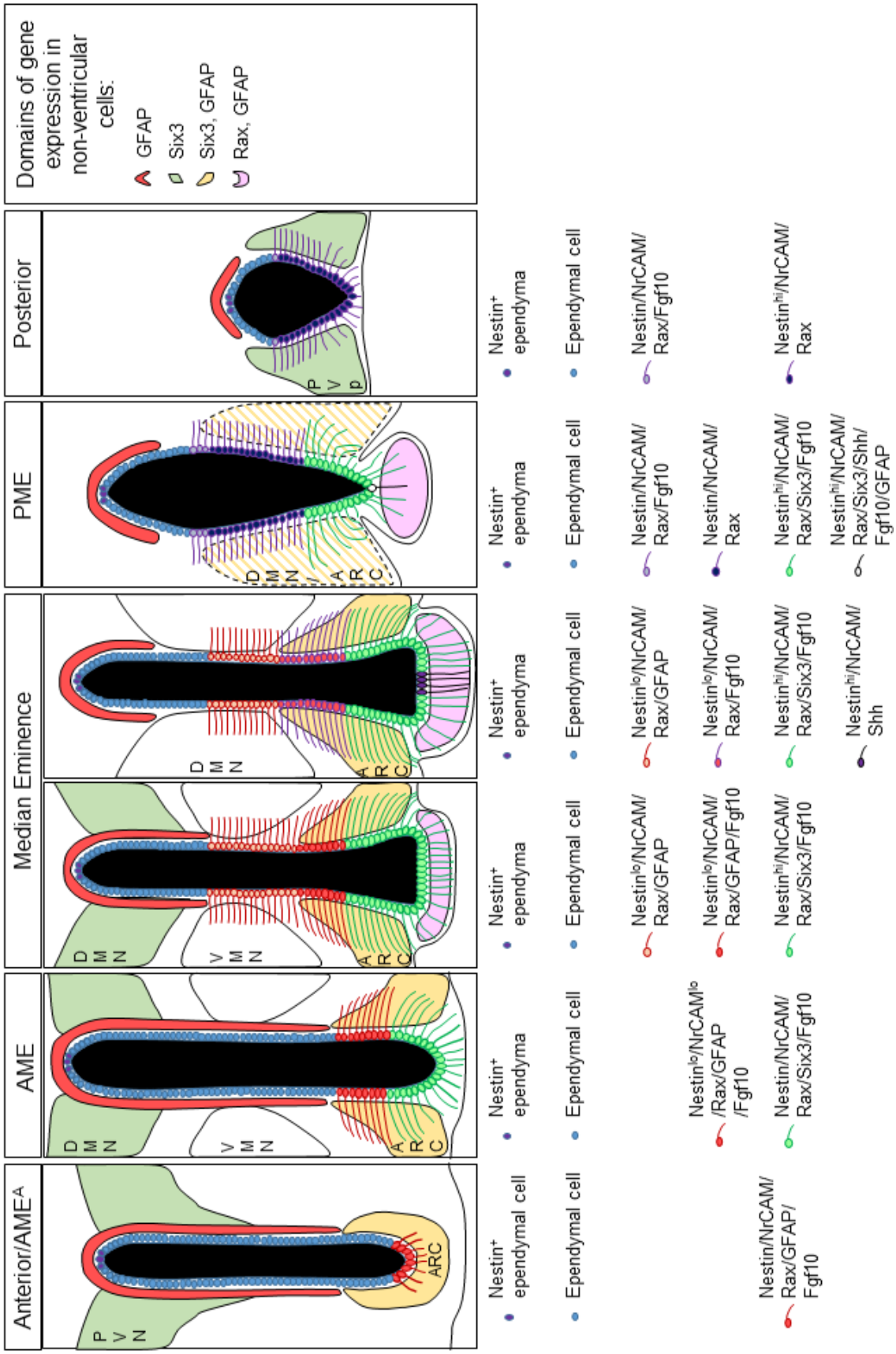
Anterior/AME^A
AME
Median Eminence
PME
Posterior
Domains of gene expression in non-ventricular cells:
GFAP
Six3
Six3, GFAP
Rax, GFAP
P V N
D M N
V M N
A R C
ARC
D M N
A R C
D M N
A R C
P V P
Nestin+ ependymal cell
Ependymal cell
Nestin+ ependyma
Nestin/NrCAM/ Rax/GFAP/ Fgf10
Nestin/NrCAM/ Rax/Six3/Fgf10
Nestinlo/NrCAM/ Rax/GFAP
Nestinlo/NrCAM/ Rax/GFAP/Fgf10
Nestinlo/NrCAM/ /Rax/GFAP /Fgf10
Nestinlo/NrCAM/ Rax/Fgf10
Nestin/NrCAM/ Rax/Fgf10
Nestinhi/NrCAM/ Rax/Six3/Fgf10
Nestin/NrCAM/ Rax
Nestinhi/NrCAM/ Shh
Nestinhi/NrCAM/ Rax/Six3/Shh/ Fgf10/GFAP

may be a more specific marker. Further experiments, nonetheless, are required to prove this. Drop-seq analysis suggests NrCAM is expression is upregulated in both tanycytes and astrocytes, but it is not clear whether this is due to the more sensitive methodology, or reflects a contamination (Campbell et al., 2017).

One question raised by the expression of NrCAM in tanycytes is what purpose its serves. NrCAM enacts a variety of roles throughout the nervous system, from clustering Na^+ channels at nodes of Ranvier, to modulating Shh-induced proliferation in cerebellar granule neuron progenitors (Lustig et al., 2001a; Sakurai, 2012; Xenaki et al., 2011). The diversity of NrCAMs roles in other cell types, coupled with the diverse cellular behaviours of tanycytes, mean that NrCAM could have a role in a whole host of intracellular or extracellular activities. To explore this further, I have investigated the effects of NrCAM KO on the hypothalamus in Chapter 5.

My analyses of tanycyte markers along the A-P axis suggest 4 conclusions. First, tanycyte subsets should not be categorised according to the simple dorso-ventral nomenclature used currently. My analyses suggest that tanycytes of similar molecular profile occupy nested semi-circles, around the PME (Fig.4.10 schematic), such that in A/AME/PME/P subregions, these lie ventrally at the 3V, while in the ME, they occupy a more dorso-lateral position. Double-label studies will be required in future to compare the precise profiles, but overall, *Rax* appears to be widely expressed, while GFAP and Six3 appear to be nested within the *Rax* domain, each in a more restricted ventro-posterior domain. I suggest that tanycyte nomenclature should be defined on the basis of marker expression, rather than dorso-ventral position: for instance in the AME subregion, $GFAP^+$ Rax^+ $Fgf10^+$ $Six3^+$ tanycytes that occupy the ventral part of the 3V are more likely to be similar to α2 tanycytes of the ME region than to β2 tanycytes. This idea has support from other studies: Mirzadeh et al (2017) suggested that the biciliated α-tanycytes seen in ventral parts of the ME are replaced in the PME and P by unicilitated tanycytes: in the ME, such uniciliated tanycytes are detected more dorsally. My model of tanycyte position is shown in the schematics in Figures 4.9 and 4.10.

Second, my work indicates that β2 tanycytes are a very distinctive population, molecularly, that do not express/express low levels of *Rax*, *Fgf10*, GFAP and

Six3. While double in situ hybridisation studies are needed to prove this, my experiments suggest that this population may instead express *Shh* (Chapter 3 Fig 3.8, Fig 4.9).

Intriguingly, my studies suggest a third conclusion, namely that particularly high levels of GFAP, *Rax* and Six3 are detected in tanycytes of the PME. Intriguingly, these are the tanycytes that appear to also express *Fgf10* and *Shh*, and are the tanycytes that are most densely distributed, as judged through Nestin and NrCAM labelling. Although functional studies are required, these observations support the hypothesis I suggest in Chapter 3, i.e. that stem-like tanycytes may exist in ventral most parts of the 3V at the level of the PME. Finally, my work confirms previous studies, showing scattered *Rax*$^{+}$ cells within the parenchyma of the median eminence. It is unclear what these cells are, though Miranda-Angulo et al (2014) showed they also express GPR50 and speculated that they may be a form of astrocytic tanycytes that were first observed through Golgi staining over 40 years ago (Millhouse, 1971). Drop-seq analysis suggests Rax is expressed specifically in tanycytes, which may suggest these *Rax*$^{+}$ cells cluster with tanycytes by expression (Campbell et al., 2017). Previous studies investigating hypothalamic proliferation have observed BrdU^{+} cells in this region following stimulation, though it is unknown whether these are derived from dividing parenchymal cells or tanycytes (Kokoeva et al., 2005, 2007; Lee et al., 2012; McNay et al., 2012). It has not been investigated whether these *Rax*$^{+}$ cells also express GFAP (which marks many astrocytes in this region). Further characterisation with tanycyte and non-tanycyte markers is required.

Figure 4.10 – Schematic model of tanycyte marker distribution from sagittal and ventral views.

Model of tanycyte marker distribution based on our observations. In this model, a population of PME tanycytes at the base of the 3V are $Fgf10^{+}$ and Shh^{+}, as well as strongly expressing other tanycyte markers associated with stem/progenitor behaviour, such as GFAP, Six3, Rax. Our hypothesis suggests this population contains a stem cell population retained from the embryonic growth of the hypothalamus, and this population. In this model, tanycytes in closer proximity to this stem population retain more of the markers associated with progenitors: Ventral ME and AME^{P} tanycytes express GFAP/Six3/Rax/Fgf10, whilst the more distant AME and dorsal ME^{A} tanycytes express GFAP/Rax/Fgf10 but not Six3. The white region demarcates the $Fgf10^{-}Rax^{-}Six3^{-}GFAP^{-}$ population at base of the 3V. The PME stem cells are slow dividing capable of long-term self-renewal, whilst the ventral AME^{P} and ME tanycytes are progenitors capable of proliferating in response to stimuli, generating new tanycytes, neurons, and glia. It is so unclear whether the Rax^{+} median eminence parenchymal cells and the $Shh^{+}Fgf10^{-}$ cells at the base of the 3V play roles in the stem/progenitor behaviour observed in the hypothalamus.

Figure 4.10

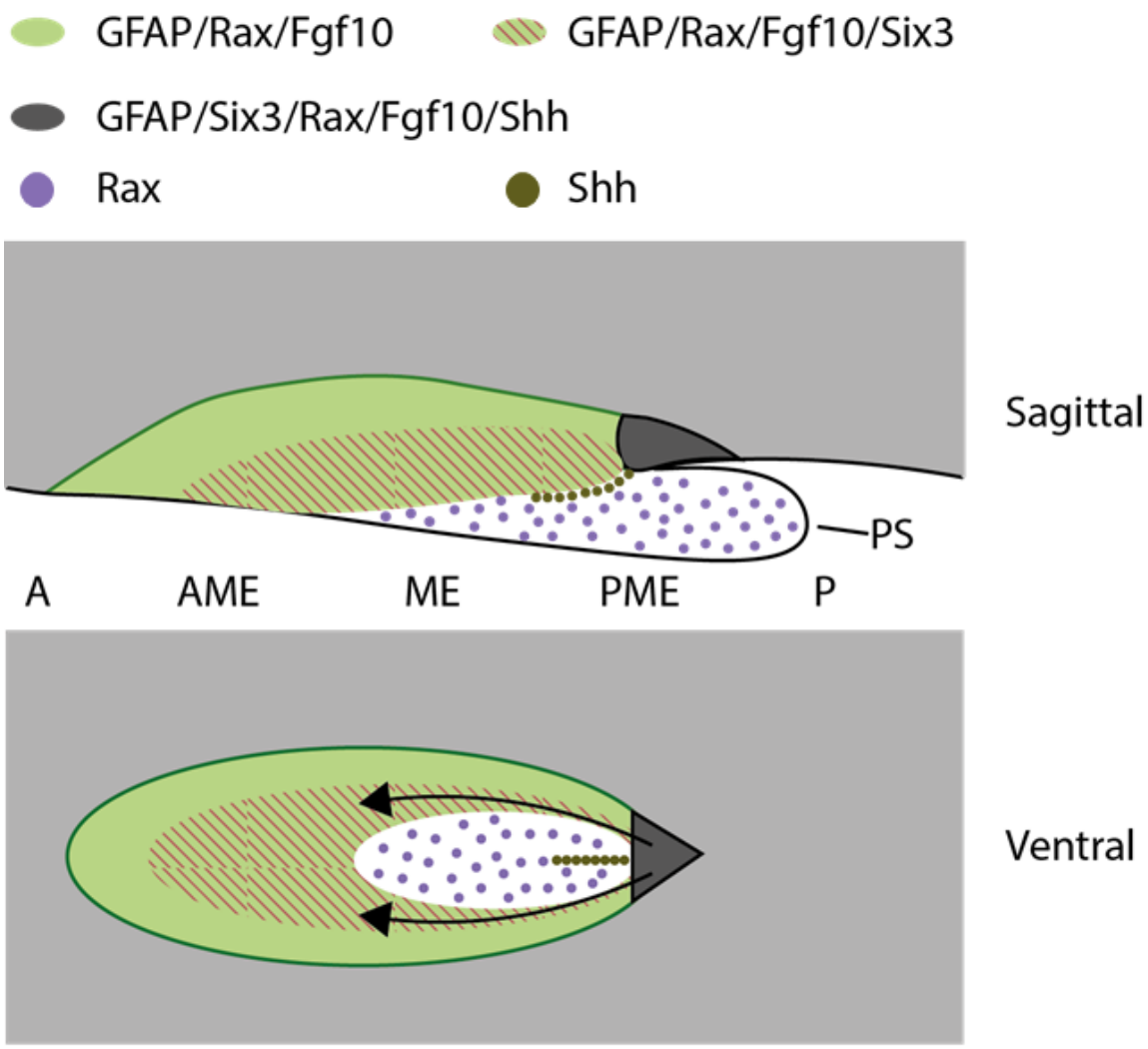
GFAP/Rax/Fgf10
GFAP/Rax/Fgf10/Six3
GFAP/Six3/Rax/Fgf10/Shh
Rax
Shh
Sagittal
PS
A
AME
ME
PME
P
Ventral

CHAPTER 5: COMPARISON OF HYPOTHALAMIC CELLS IN ADULT WILDTYPE AND NRCAM KO MICE

5.1 Introduction:

In Chapter 4 I defined the expression of NrCAM in tanycytes, and argued that its specific expression in tanycytes within the hypothalamus makes it a useful marker for further tanycyte research. Beyond its use as a marker, expression of NrCAM by tanycytes raises questions about its function in these cells. As previously discussed, NrCAM has an array of roles and interactions, including functions in cell-cell adhesion, ion channel and receptor localisation, receptor trafficking, and signal modulation (Demyanenko et al., 2014; Lustig et al., 2001a; Sakurai, 2012; Sakurai et al., 2001; Xenaki et al., 2011). Previous studies have linked NrCAM to tumourigenicity in melanomas, colon carcinomas, and papillary thyroid carcinomas, with suggestions that it promotes motility and proliferation (Conacci-Sorrell et al., 2002, 2005; Górka et al., 2007). IgSF-CAMs have also been explored in relation to proliferation and differentiation behaviours in the CNS. NrCAM, TAG1, and F3/contactin are known to modulate Shh-induced proliferation and differentiation behaviour in cerebellar granule neuron precursors (Xenaki et al., 2011), and F3/contactin and TAG1 are associated with cerebral and hippocampal neurogenesis (Bizzoca et al., 2003, 2012, Puzzo et al., 2013, 2015).

The roles of NrCAM and related proteins in neurodevelopmental processes, including proliferation and differentiation behaviours, provide motivation for further studying NrCAM in the hypothalamus. The expression on tanycytes hints at potential involvement with the previously described tanycytic stem/progenitor populations (Bless et al., 2016; Chaker et al., 2016; Haan et al., 2013; Lee et al., 2014; Pierce and Xu, 2010; Robins et al., 2013a). Furthermore, at E16 NrCAM is expressed by hypothalamic RGC progenitors that give rise to neurons, tanycytes, and other glia (see Chapter 6) (Edwards et al., 1990; Lustig et al., 2001b; Noctor et al., 2001; Sild and Ruthazer, 2011; Tamamaki et al., 2001). NrCAM$^{-/-}$ mice have abnormalities in adult body mass (Moré et al., 2001), as well as variety of other growth, metabolic, and neurological changes that may be linked to hypothalamic processes (see

Figure 5.1 Nestin^{+} Median Eminence tanycytes in wild type and NrCAM KO adult mice

Image composites at 10x magnification of coronal cross-sections showing Nestin (green) expression by immunofluorescence with nuclear DAPI staining (blue) in an adult wild type mouse (A) and NrCAM KO mouse (B) (age-matched (P73) half-siblings from NrCAM$^{+/-}$ colony). Box inserts indicate corresponding Nestin (white) image z-0stacks (Ai, Bi) collected at 20x magnification and converted to maximum intensity projections (MIPs). Scale bars for all images 50µm. Scale bars for all images 50µm. Images representative of the n=6 mice investigated.

Figure 5.1

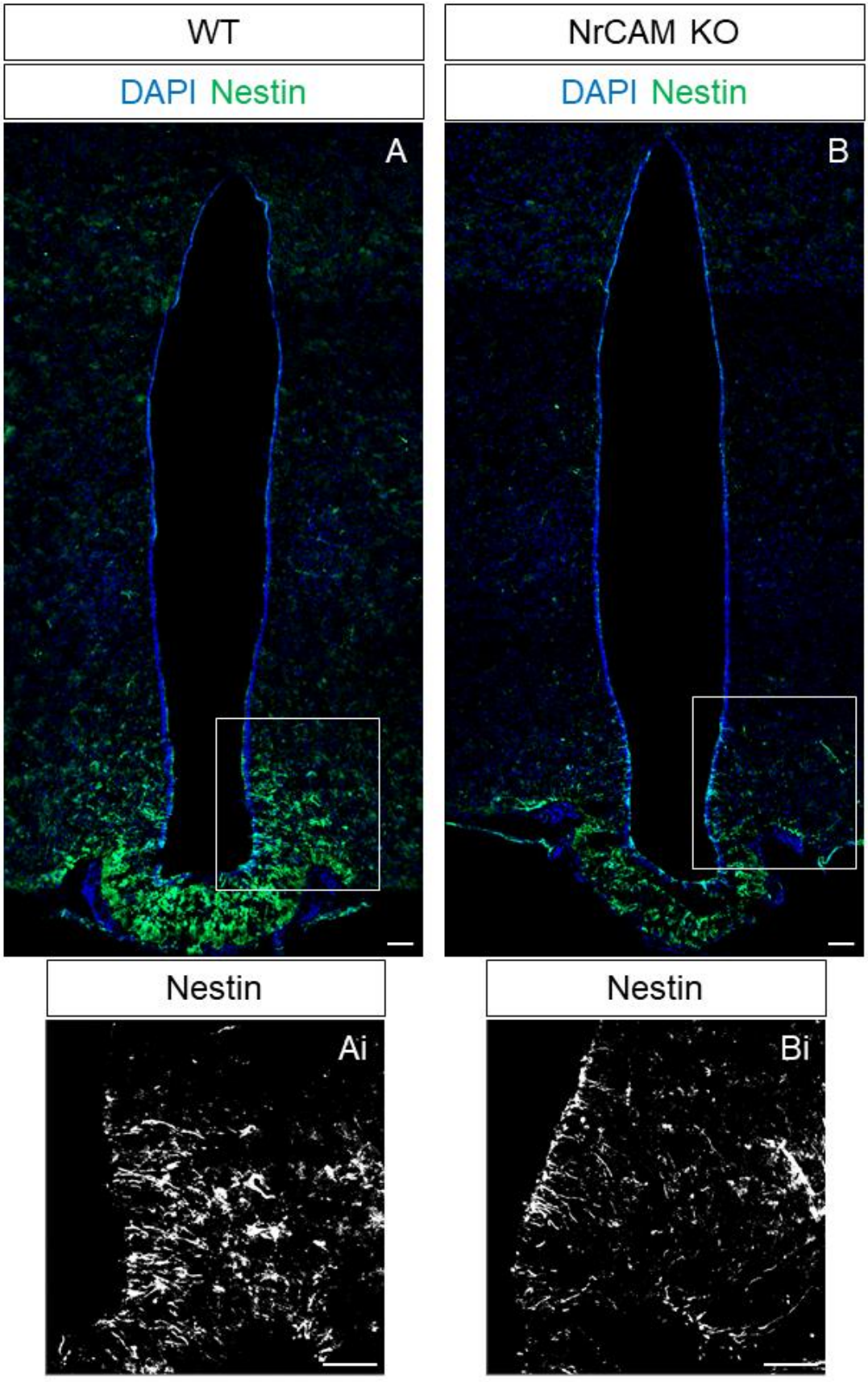

Figure 5.2 Nestin expression and quantification along the anterior-posterior axis of the hypothalamus for wild type and NrCAM KO adult mice.

Image composites (A-L) at 10x magnification of coronal cross-sections showing Nestin (green) expression by immunofluorescence in relation to the 3V, ME, and hypothalamic parenchyma along the A-P axis with nuclear DAPI staining (blue) in adult wild type (A-F) and NrCAM KO (G-L) mice. Box inserts (i and ii for each cross section) indicate corresponding image z-stacks collected at 20x magnification and converted to maximum intensity projections (MIPs) displayed as combined channel and Nestin only images (Bi/Bii-Fi/Fii, Hi/Hii-Li,Lii). Scale bars for 10x images 100µm, and 20x images 50 µm. Images representative of the n=3 pairs of mice investigated.

M – Quantification of Nestin^{+} process density for β1 and α2 tanycytes in all tanycyte containing sections along the A-P axis of the tuberal hypothalamus in three pairs of wild type and NrCAM KO adult mice. Each icon represents a single measurement, collected as described in Chapter 2.2.5.2. Bars show 1 SD either side of the mean value. Analysis by unpaired t-test showed a significant reduction of Nestin^{+} tanycyte density in NrCAM KO adult mice ($P<0.0001$).

N – Quantification of Nestin^{+} process density for β1 and α2 tanycytes in AME, ME, PME, and P subregions in three pairs of wild type and NrCAM KO adult mice. Each icon represents a single measurement, collected as described in Chapter 2.2.5.2. Bars show 1 SD either side of the mean value. Analysis by unpaired t-test showed significant reductions of Nestin^{+} tanycyte density in NrCAM KO adult mice in every A-P subregion (AME $P=0.0007$; ME $P=0.0013$; PME $P=0.0105$; P $P<0.0001$).

Figure 5.2

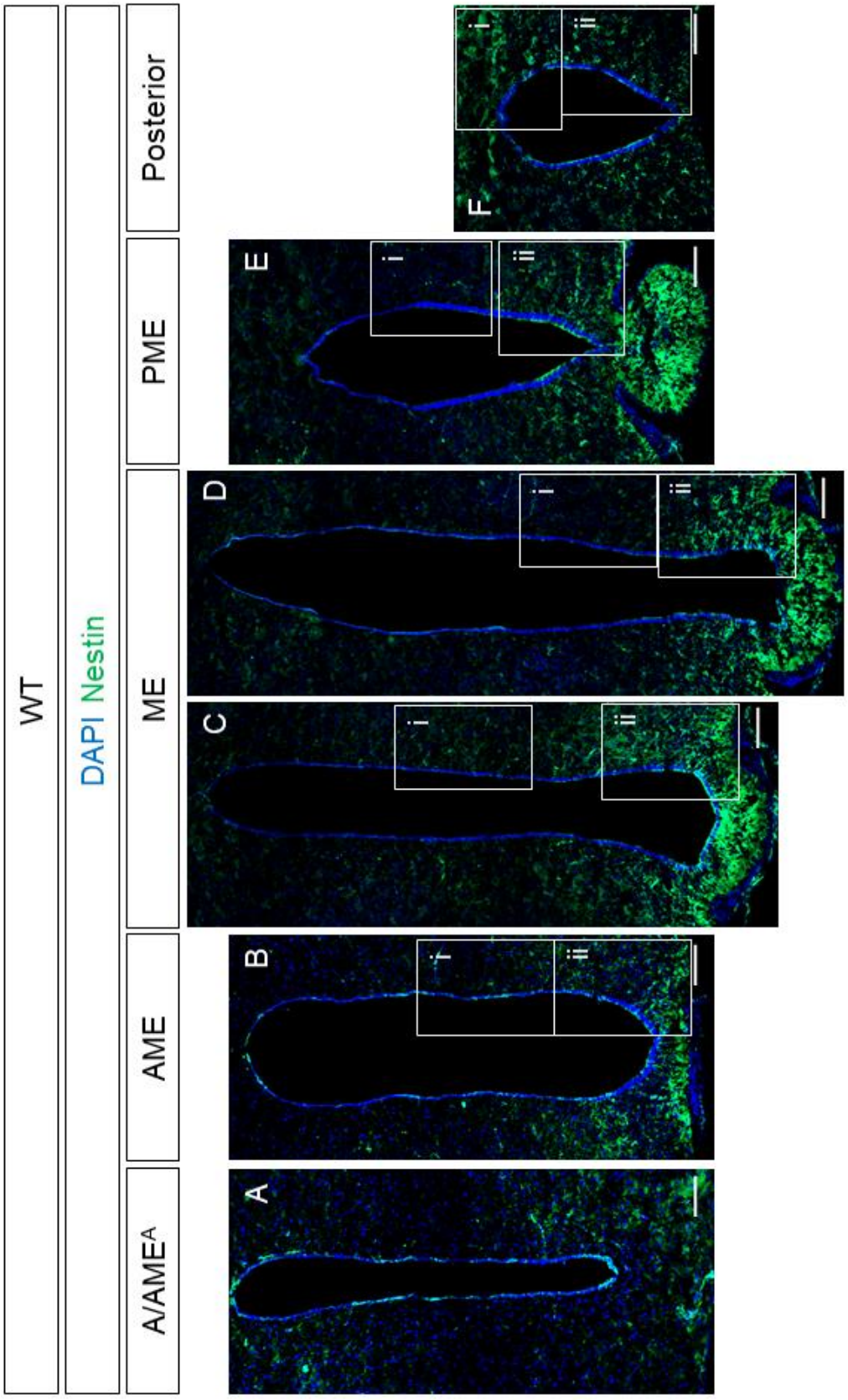

Figure 5.2

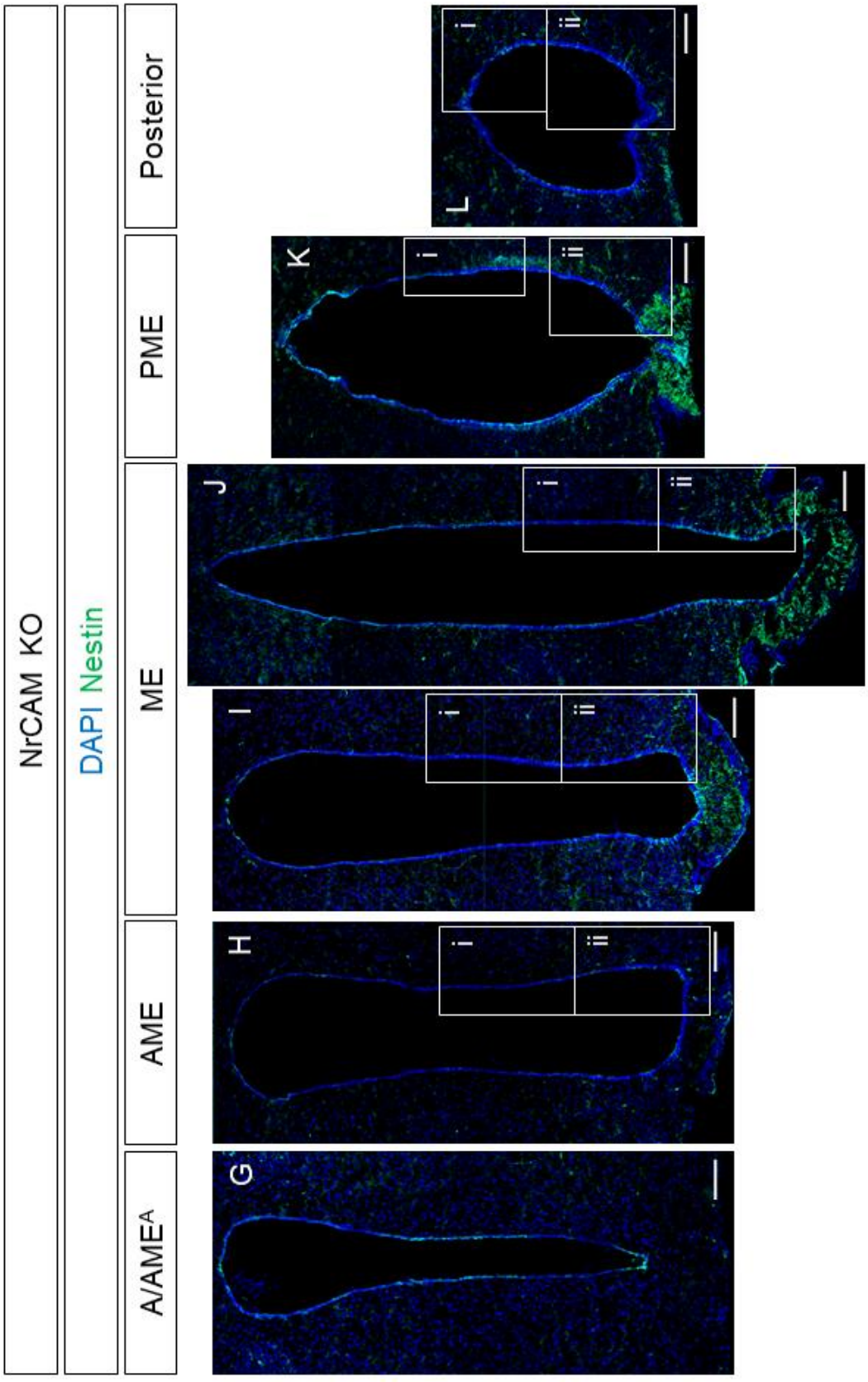

Figure 5.2

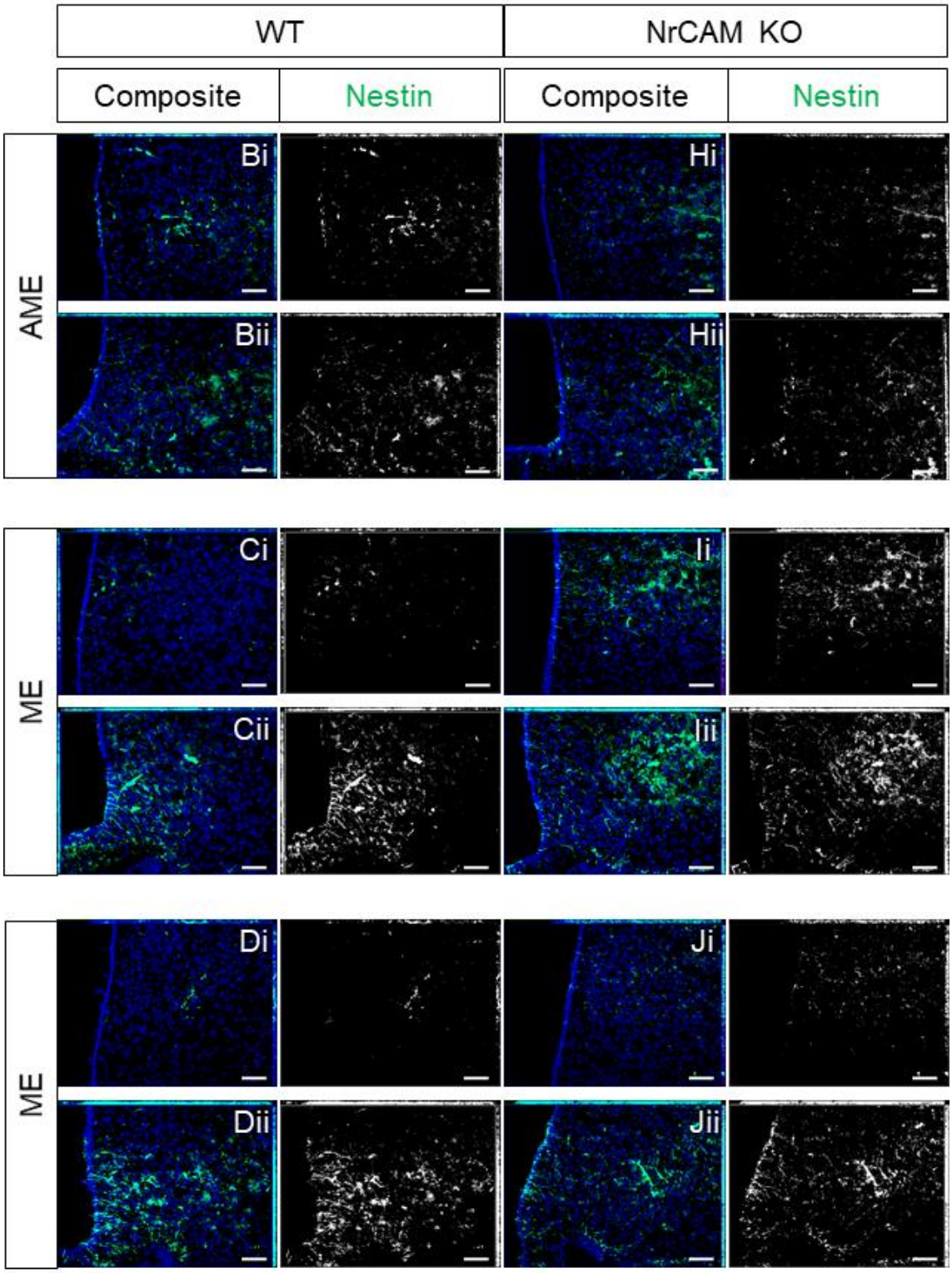
WT
NrCAM KO
Composite
Nestin
Composite
Nestin
AME
Bi
Hi
Bii
Hii
ME
Ci
Ii
Cii
Iii
ME
Di
Ji
Dii
Jii

Figure 5.2

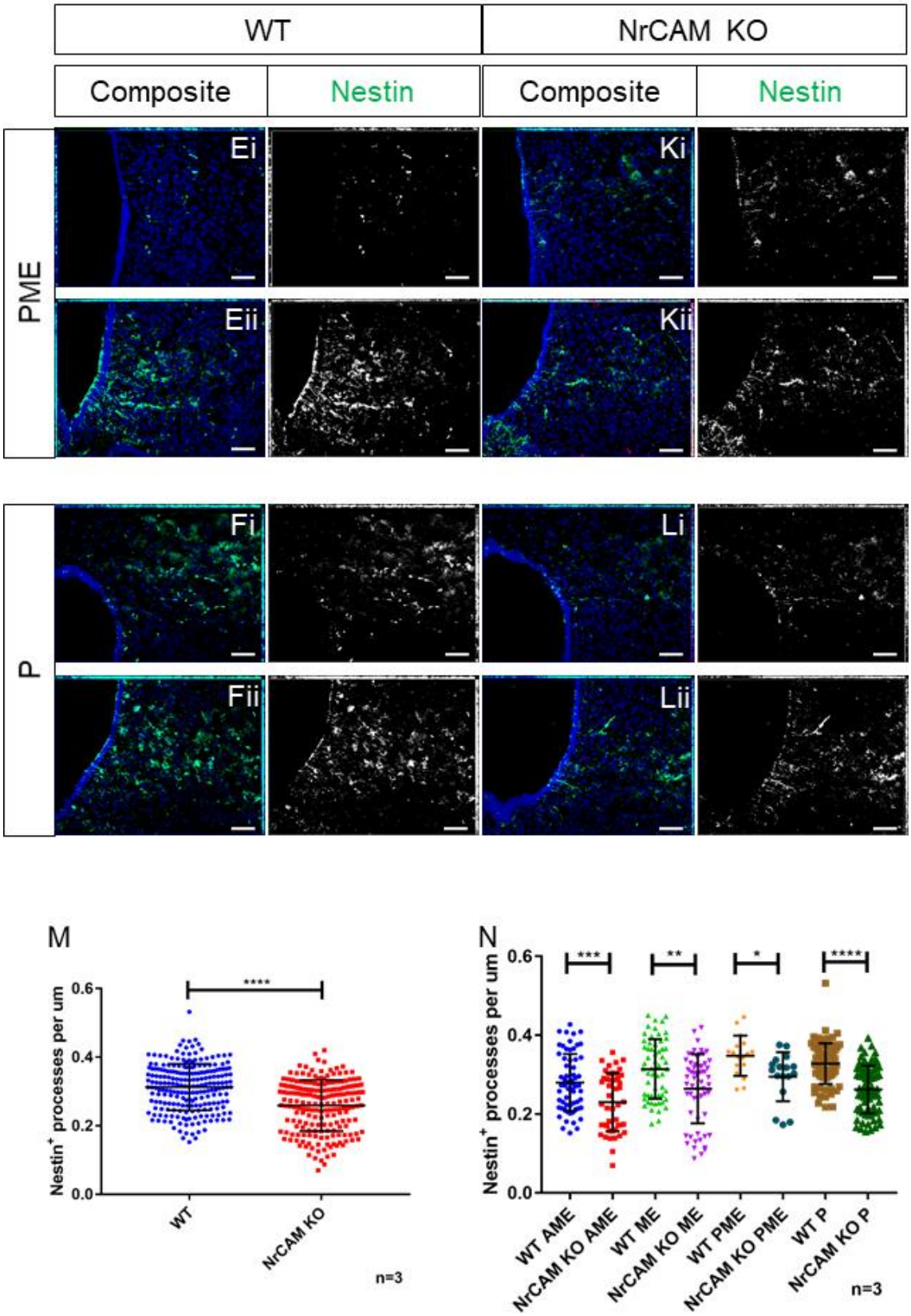
WT
NrCAM KO
Composite
Nestin
Composite
Nestin
PME
Ei
Ki
Eii
Kii
P
Fi
Li
Fii
Lii
M
Nestin+ processes per um
0.6
0.4
0.2
0.0
****
WT
NrCAM KO
n=3
N
Nestin+ processes per um
0.6
0.4
0.2
0.0
***
**
*
****
WT AME
NrCAM KO AME
WT ME
NrCAM KO ME
WT PME
NrCAM KO PME
WT P
NrCAM KO P
n=3

Final Discussion: analysis by The Jackson Laboratory[5]). As discussed in Chapter 1.4.2, preliminary work from within our lab has suggested that NrCAM KO mice may have reduced tanycytes at the VZ. In this chapter I will begin to characterise the effect of NrCAM KO on hypothalamic cells in adult mice.

5.2 Results

5.2.1 Nestin

To begin the comparison of tanycytes in wild type and NrCAM$^{-/-}$ mice I analysed expression of Nestin in ME sections (Fig 5.1). There is a marked reduction in Nestin expression in the vicinity of the VZ, ME, and ARC in the NrCAM$^{-/-}$ hypothalamus (Fig 5.1 A,B). Higher magnification imaging indicate that the Nestin^{+} tanycyte processes are less densely packed than in wild type (Fig 5.1 Ai,Bi).

Analysis of Nestin^{+} tanycytes across the hypothalamic A-P axis shows that Nestin expression appears diminished in all subregions in NrCAM$^{-/-}$ animals when compared to similar sections from wild type mice (Fig 5.2 A-L). Qualitative analyses suggest fewer β- and α2-tanycyte processes in the AME, ME, PME, and P regions (Fig 5.2 Bii-Lii). Quantification showed a statistically significant decrease in the process density across the whole hypothalamus (Fig 5.2 M); consistently, each subregion showed a 20% decrease in the number of Nestin^{+} processes (Fig 5.2 N). Nestin labelling of dorsal/α1-tanycytes was weak in both wild type and NrCAM$^{-/-}$ mice, and tanycyte processes were not quantified (Fig 5.2 Bi-Li). The decrease in β- and α2-tanycyte density suggests that loss of NrCAM leads to either a reduction in the generation or maintenance of tanycytes, or the expression of Nestin. The number of sections collected over the hypothalamus was consistent between the wild type and NrCAM KO mice.

5.2.2 Rax

As outlined in the Introduction, the paired box gene, Rax, is required for tanycyte development. Adult Rax$^{+/-}$ mice have fewer tanycytes and a thinner VZ than wild type littermates (Miranda-Angulo et al., 2014). The reduction in

[5] Data displayed at http://www.mousephenotype.org/data/genes/MGI:104750#order2

Figure 5.3 Rax expression along the anterior-posterior axis of the hypothalamus in wild type and NrCAM KO adult mice.

Image composites at 10x magnification of coronal cross-sections showing Rax mRNA expression (purple) by *in situ* hybridisation in relation to the 3V, ME, and hypothalamic parenchyma along the A-P axis in adult wild type (A-F) and NrCAM KO (G-L) mice, with corresponding images of the median eminence (Ci-Ei, Ii-Ki). Scale bars 100µm. Images representative of the n=3 pairs of mice investigated.

Figure 5.3

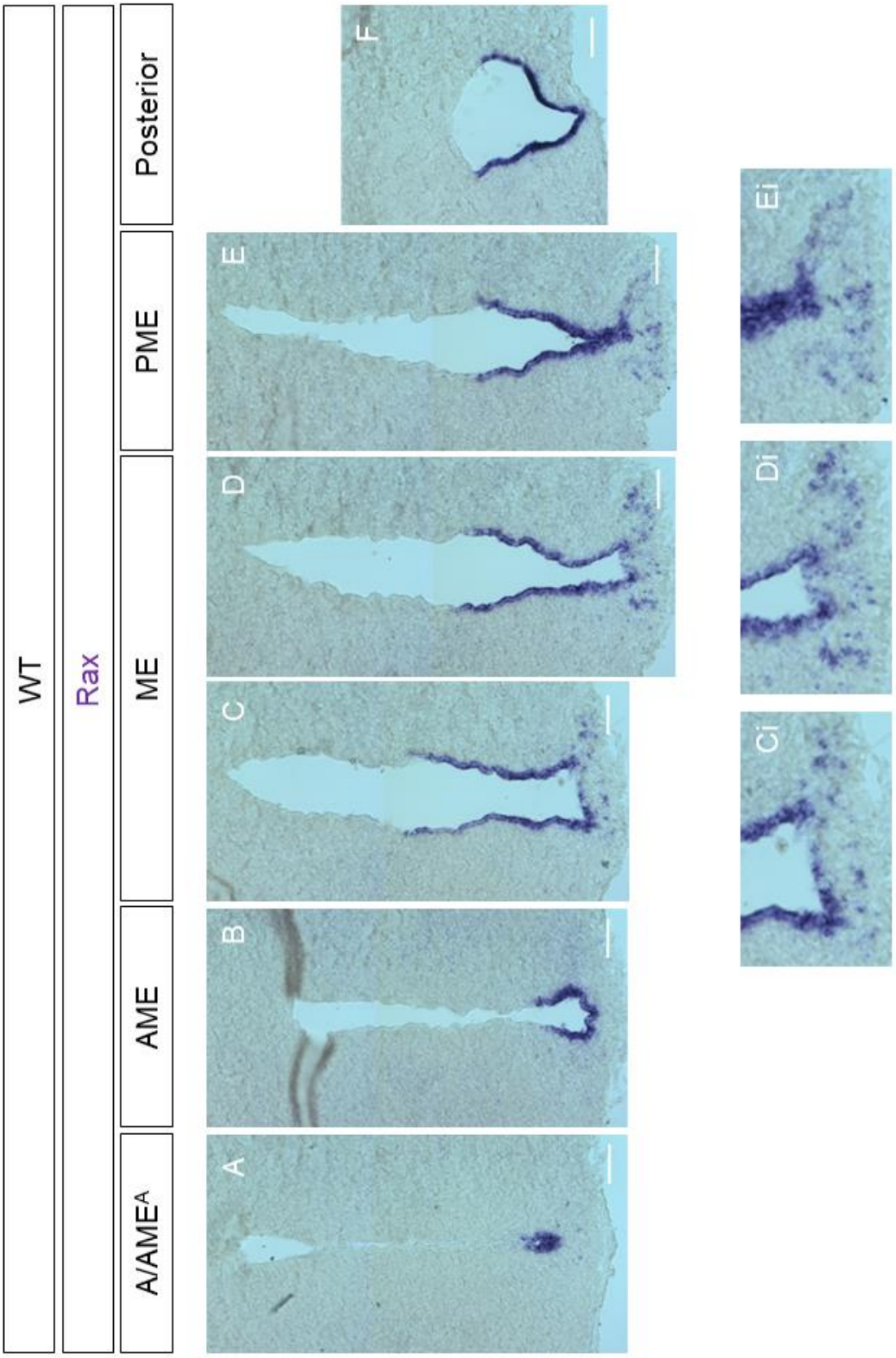

Figure 5.3

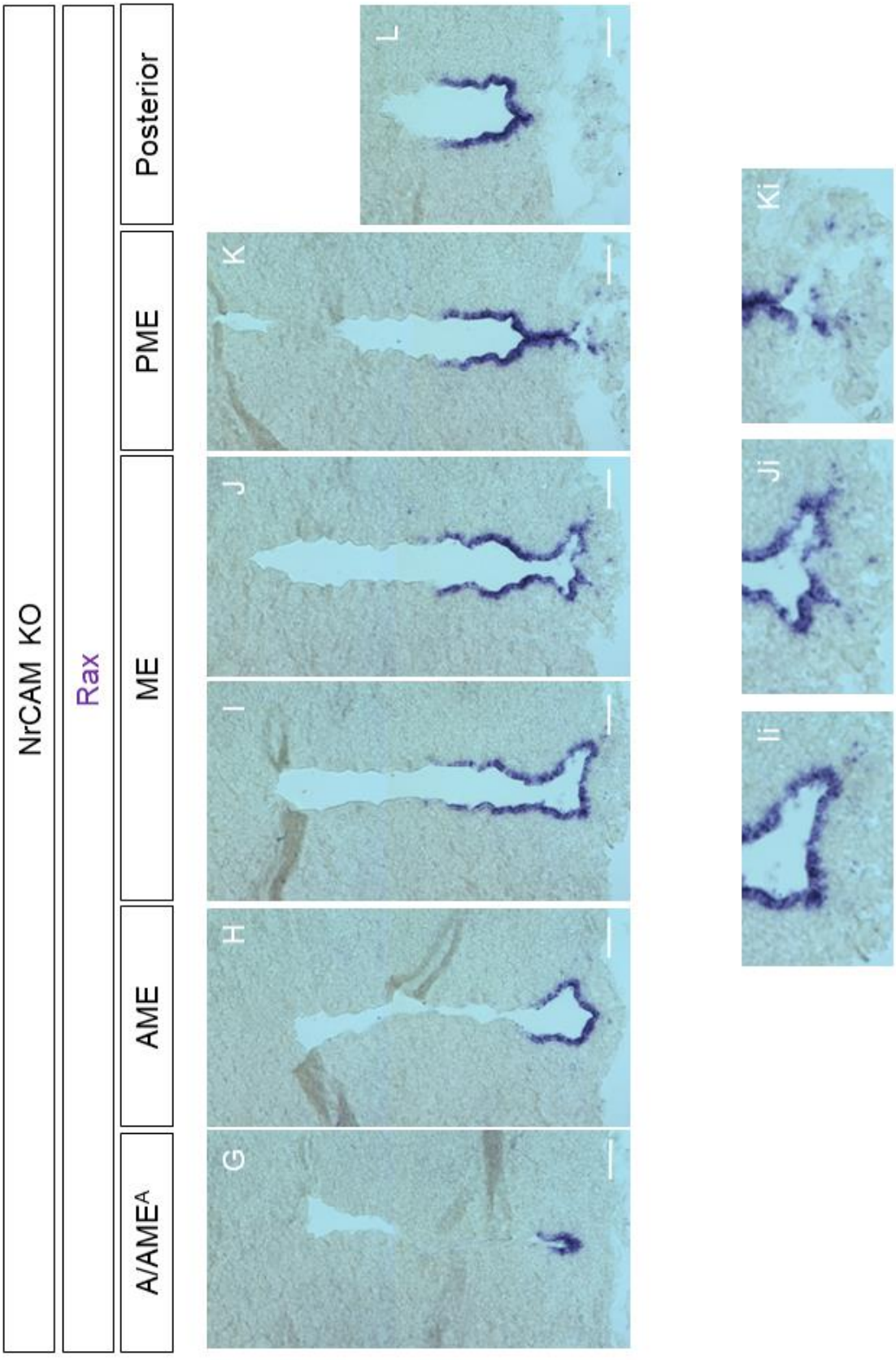

Figure 5.4 Quantification of Rax expression along the anterior-posterior axis of the hypothalamus for wild type and NrCAM KO adult mice.

A – A graph comparing the length of the Rax-expressing domain round the ventral 3V in adult wild type (blue) and NrCAM KO (red) mice. The plotted value at each marked position is the mean of three biological replicates, with the bars showing the range. Using the Wilcoxon signed rank test, no significant difference was observed when values across the whole Rax-expressing domain in the wild type and NrCAM KO were compared. When the AME, ME, PME, and P subregions were individually assessed, the Rax-expressing VZ was shown to be significantly longer in the ME subregion of wild type mice ($p=0.0273$).

B – A graph comparing the chromogenic signal intensity of the Rax-expressing domain round the ventral 3V in adult wild type (blue) and NrCAM KO (red) mice. The plotted value at each marked position is the mean of three biological replicates, with the bars showing the range. The mean gray value gives a readout between 0 (black) and 256 (white) that represents the chromogenic signal intensity, and has been normalised against the background. A lower mean gray value (closer to black) represents a stronger signal strength. Using the Wilcoxon signed rank test, the mean gray value of the Rax+ VZ was shown to be significantly lower in the wild type mouse than the NrCAM KO ($p=0.0018$). This indicates a stronger chromogenic signal in the wild type mouse than in the NrCAM KO mouse. When the AME, ME, and PME/P subregions were assessed, the mean gray value of the Rax-expressing VZ was shown to be significantly lower in only the PME/P subregions of wild type mice ($p=0.0024$).

C – A graph comparing the percentage change in relative Rax signal strength in the NrCAM KO when compare to the wild type at each position along the A-P axis. The plotted value at each marked position is the mean of three biological replicates, with the bars showing the range. For each replicate, the normalised mean gray value for Rax in an NrCAM KO section was subtracted from the normalised mean gray value in the paired wild type section and converted to a percentage.

D – A graph comparing the number of the Rax+ cells in the ME of adult wild type (blue) and NrCAM KO (red) mice across the A-P axis of the hypothalamus. The plotted value at each marked position is the mean of three biological

replicates, with the bars showing the range. Using the Wilcoxon signed rank test, significantly fewer Rax+ cells were observed in the ME of the NrCAM KO compared to wild type mice (p=0.0010).

Figure 5.4

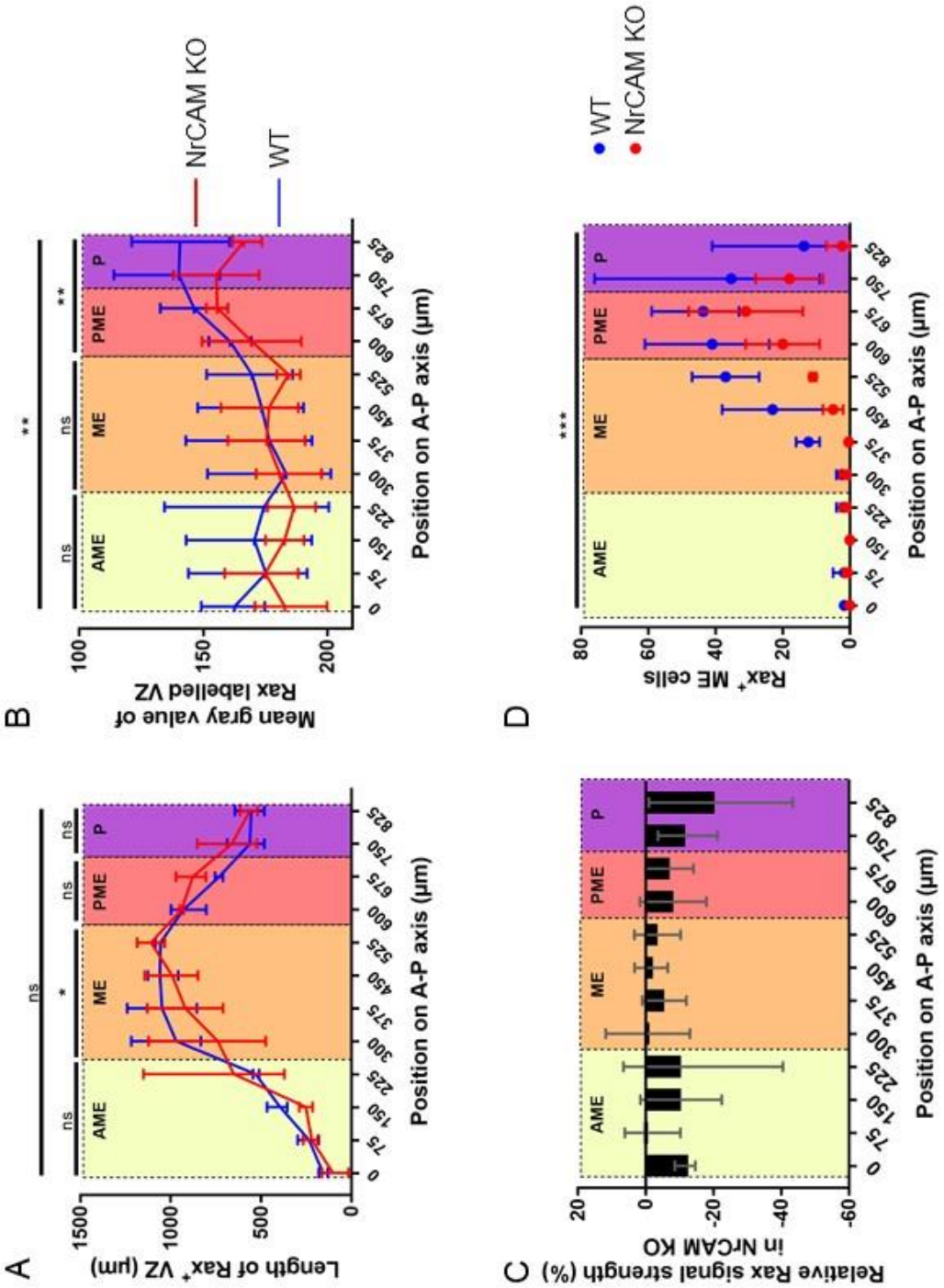

tanycytes is particularly marked along the dorso-ventral axis, and ependymal cells extend into regions normally occupied by alpha-tanycytes (Miranda-Angulo et al., 2014). My data describing decreased Nestin^{+} tanycyte density in the NrCAM$^{-/-}$ mouse was reminiscent of the Rax$^{+/-}$ mouse phenotype. I therefore hypothesised that NrCAM may be acting upstream of Rax and that Rax expression may be altered in the NrCAM$^{-/-}$ mouse.

In situ hybridisation for Rax mRNA in the NrCAM$^{-/-}$ mouse reveals expression across the same A-P region as in wild type mice (Fig 5.3 A-L). To determine whether, as in Rax$^{+/-}$ mice, tanycytes are more restricted along the dorso-ventral axis, I measured the total length of the *Rax*$^{+}$ VZ in each subregion. There was no significant difference in length in AME, PME, or P subregions, however, the *Rax*$^{+}$ VZ was significantly shorter in the ME subregion of NrCAM$^{-/-}$ mice compared to wild type mice (Fig 5.4 A).

I next compared levels of Rax mRNA by quantifying from the chromogenic signal (Chapter 2.3.6.2). The Rax mRNA signal across the hypothalamus was significantly weaker in NrCAM$^{-/-}$ mice (Fig 5.4 B,C). Analysis of the AME and ME showed no significant difference in these subregions, but a significant reduction in the chromogenic labelling for Rax mRNA was observed in the PME/P subregions. It is unclear whether these decreases are due to a change in the number of cells or the level of *Rax* expression within each cell.

In addition to quantitating the expression of *Rax* in tanycytes at the VZ, I also quantitated the number of *Rax*$^{+}$ cells in the ME. These *Rax*$^{+}$ cells are identifiable in both the wild type (Fig 5.3 Ci-Ei) and NrCAM$^{-/-}$ mice (Fig 5.3 Ii-Ki). Quantification of these cells across the hypothalamus in paired sections revealed a significant decrease in the NrCAM$^{-/-}$ mouse relative to the wild type (Fig 5.4 D).

5.2.3 Fgf10

Having identified a decrease in Nestin^{+} tanycytes and mRNA of the tanycyte regulator Rax, I next investigated expression of Fgf10 mRNA. Its roles in establishing the progenitor populations of the developing hypothalamus (discussed in Chapter 1.3.1 and Chapter 6.1)(Fu et al., 2017), as a regulator of postnatal tanycyte proliferation (discussed in Chapter 1.2.3

Figure 5.5 Fgf10 expression along the anterior-posterior axis of the hypothalamus in wild type and NrCAM KO adult mice.

Image composites at 10x magnification of coronal cross-sections showing Fgf10 mRNA expression (purple) by in situ hybridisation in relation to the 3V, ME, and hypothalamic parenchyma along the A-P axis in adult wild type (A-F) and NrCAM KO (G-L) mice, with corresponding 20x magnification images of the ventral 3V(Ai-Li). Lateral recess in wild type marked by arrowheads (F,Fi). Scale bars 100µm. Images representative of the n=5 pairs of mice investigated.

Figure 5.5

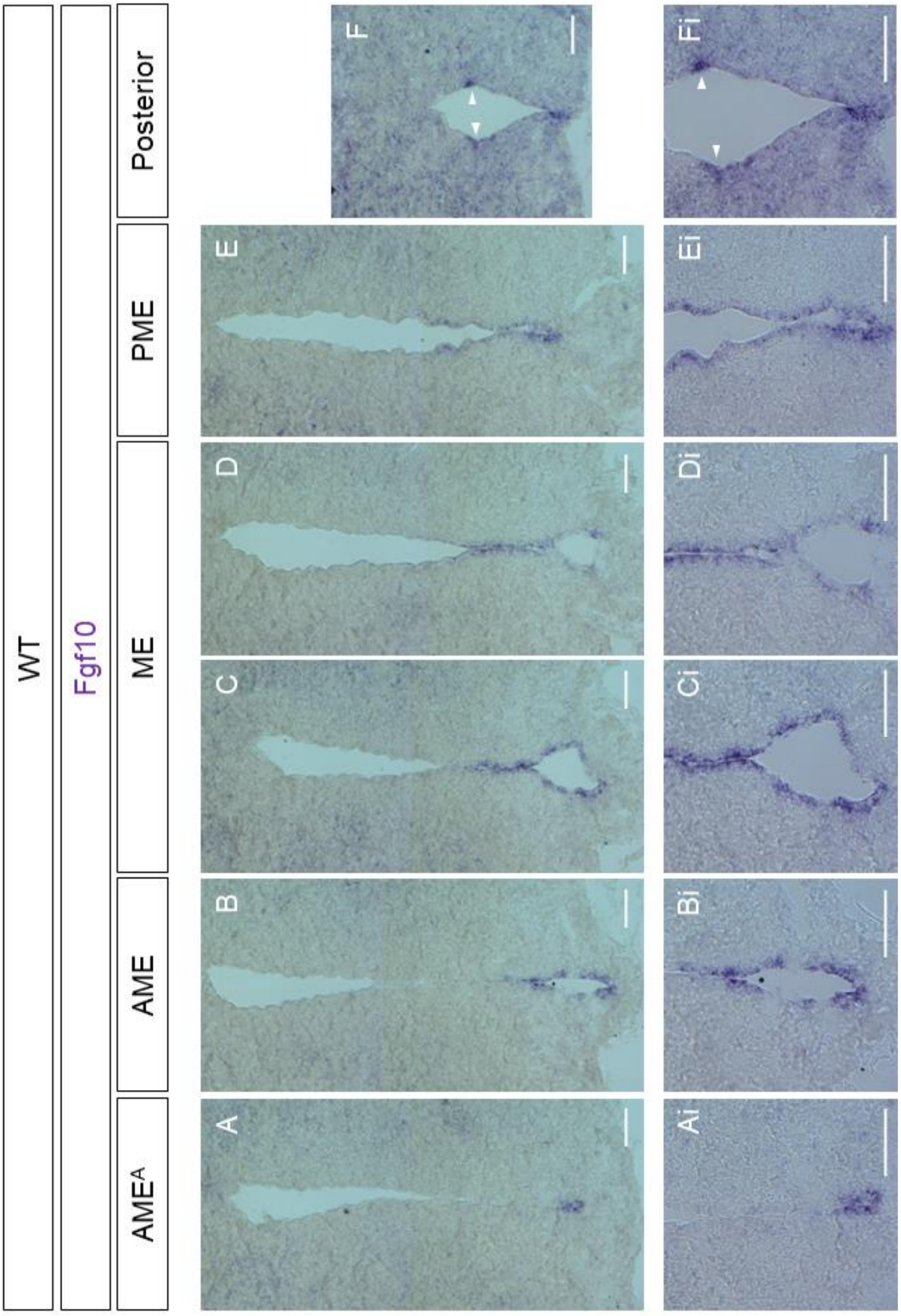

Figure 5.5

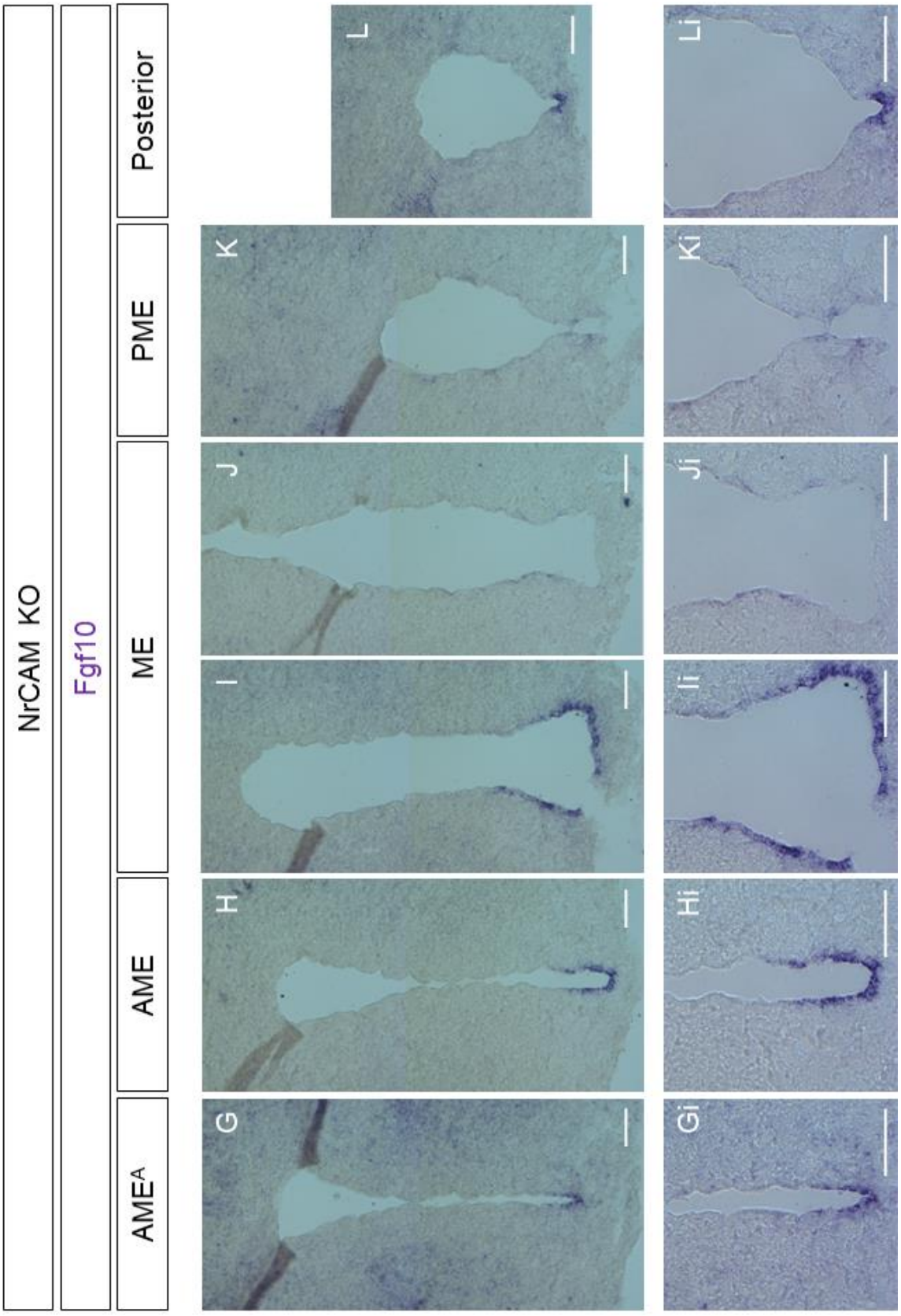
NrCAM KO
Fgf10
AME^A
AME
ME
PME
Posterior
G
H
I
J
K
L
Gi
Hi
Ii
Ji
Ki
Li

Figure 5.6 Quantification of Fgf10 expression along the anterior-posterior axis of the hypothalamus for wild type and NrCAM KO adult mice.

A – A graph comparing the length of the Fgf10-expressing domain round the ventral 3V in adult wild type (blue) and NrCAM KO (red) mice. The plotted value at each marked position is the mean of three biological replicates, with the bars showing the range. Using the Wilcoxon signed rank test, no significant difference was observed when values across the whole Fgf10-expressing domain in the wild type and NrCAM KO were compared. When the AME, ME, PME, and P subregions were individually assessed, the Fgf10-expressing VZ was shown to be significantly longer in the AME subregion of wild type mice ($p=0.0273$).

B – A graph comparing the chromogenic signal intensity of the Fgf10-expressing domain round the ventral 3V in adult wild type (blue) and NrCAM KO (red) mice. The plotted value at each marked position is the mean of three biological replicates, with the bars showing the range. The mean gray value gives a readout between 0 (black) and 256 (white) that represents the chromogenic signal intensity, and has been normalised against the background. A lower mean gray value (closer to black) represents a stronger signal strength. Using the Wilcoxon signed rank test, no significant difference was observed when values across the whole Fgf10-expressing domain in the wild type and NrCAM KO were compared. When the AME, ME, and PME/P subregions were assessed, the mean gray value of the Fgf10-expressing VZ was shown to be significantly lower in only the PME/P subregion of wild type mice ($p=0.0010$). This indicates a stronger chromogenic signal for the PME/P subregion of the wild type mouse than of the NrCAM KO mouse.

C – A graph comparing the percentage change in relative Fgf10 signal strength in the NrCAM KO when compare to the wild type at each position along the A-P axis. The plotted value at each marked position is the mean of three biological replicates, with the bars showing the range. For each replicate, the normalised mean gray value for Fgf10 in an NrCAM KO section was subtracted from the normalised mean gray value in the paired wild type section and converted to a percentage..

Figure 5.6

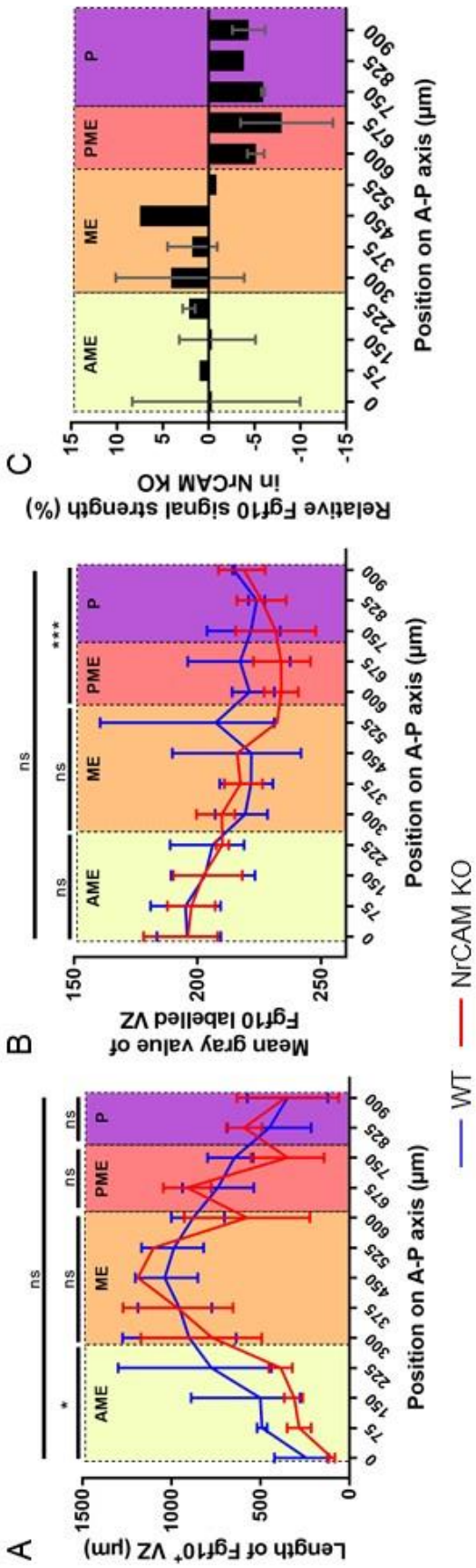
A
Length of Fgf10+ VZ (μm)
1500
1000
500
0
*
ns
ns
ns
ns
AME
ME
PME
P
0
75
150
225
300
375
450
525
600
675
750
825
900
Position on A-P axis (μm)
WT
NrCAM KO
B
Mean gray value of Fgf10 labelled VZ
150
200
250
ns
ns
ns
***
AME
ME
PME
P
Position on A-P axis (μm)
C
Relative Fgf10 signal strength (%) in NrCAM KO
15
10
5
0
-5
-10
-15
AME
ME
PME
P
Position on A-P axis (μm)

and Chapter 4.1)(Haan et al., 2013; Robins et al., 2013a), and as a marker (with *Shh*) of a potential adult stem-like population (Chapter 3) make it a target of interest for investigating the loss of tanycytes.

Chromogenic ISH analysis in the NrCAM$^{-/-}$ mouse reveals that expression is detected in the same region as in wild type mice (Fig 5.5 A-L). There was no significant difference in length in ME, PME, or P subregions. However, the dorso-ventral extent of the *Fgf10*$^{+}$ VZ was significantly shorter in the AME subregion of NrCAM$^{-/-}$ mice compared to wild type mice (Fig 5.6 A). The *Fgf10*$^{+}$ VZ length profiles were erratic, and unlike *Rax* there was no significant decrease in ME subregion. Further repeats would be beneficial for determining whether these are real, or artefacts of the experiment or quantification.

Quantification of *Fgf10* (through analysis of chromogenic signal) reveals that, in contrast to *Rax*, the Fgf10 mRNA signal was not significantly different in NrCAM$^{-/-}$ mice across the hypothalamus (Fig 5.6 B,C). However, quantitative analysis of individual regions showed that, while the AME and ME showed no significant difference, there is a significant reduction in the chromogenic labelling for Fgf10 mRNA in the PME/P regions of NrCAM$^{-/-}$ mice, as was seen for *Rax* (Fig. 5.6 B, C). It is unclear whether these decreases are due to a change in the number of cells or the level of *Fgf10* expression within each cell.

Finally, in wild type mice *Fgf10* is retained at the lateral recesses between the tanycyte and ependymal cell domain in the P subregion (Fig 5.5 Fi, arrowheads), however this is not seen in the NrCAM$^{-/-}$ mice (Fig 5.5 L,Li).

5.2.4 Shh

The reduction in *Fgf10* and *Rax* expression within PME but not more anterior ME or AME regions is an interesting observation, given my hypothesis that Fgf10/Rax mark a stem-like cell in the PME region of the hypothalamus. In Chapter 3 I provided evidence that *Shh* is also expressed within these cells, as well as more anterior (β2?) tanycytes. I have asked whether *Shh* expression might also be specifically downregulated in the PME of NrCAM$^{-/-}$ mice, by ISH labelling hypothalamic sections from NrCAM$^{-/-}$ mice and comparing them to wild type sections. Shh mRNA^{+} cells are seen in both NrCAM$^{-/-}$ and wild type mice in the β2-tanycyte domain of ME^{P} sections (Figure 5.7).

Figure 5.7 Shh expression along the anterior-posterior axis of the hypothalamus in wild type and NrCAM KO adult mice.

Image composites at 10x magnification of coronal cross-sections showing Shh mRNA expression (purple) by in situ hybridisation in relation to the 3V from A-P through the ME and PME in adult wild type (A-G) and NrCAM KO (H-N) mice, with corresponding 20x magnification images of the ventral 3V(Bi-Gi, Ii-Ni). All distinct Shh^{+} cells were observed in or adjacent to the VZ in both wild type and NrCAM KO mice. Cell-like dark patches in the parenchyma of 10x images were confirmed to be non-cellular crystalline artefacts when viewed at higher magnification. Scale bars 100µm. Images representative of the n=5 pairs of mice investigated.

Figure 5.7

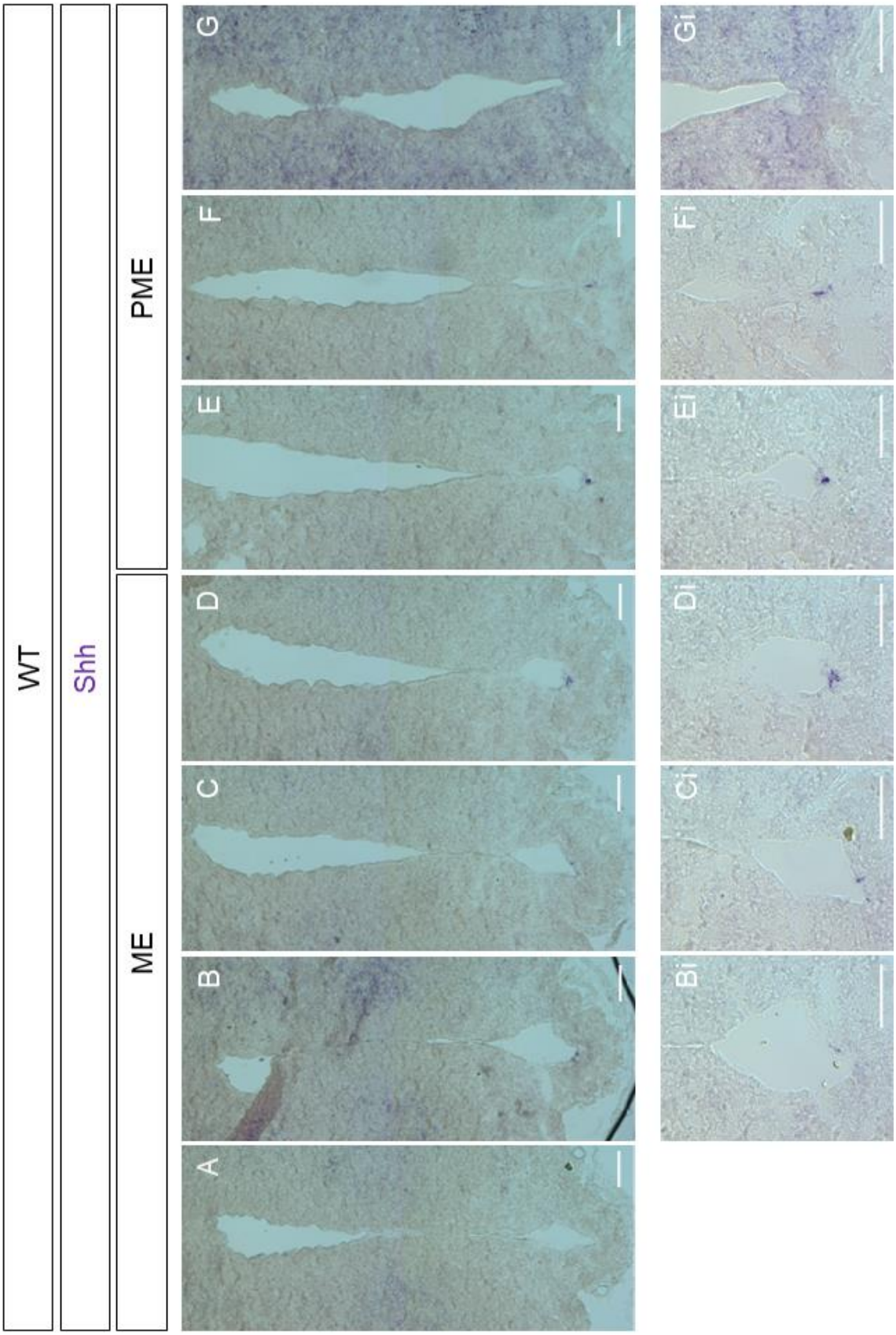

Figure 5.7

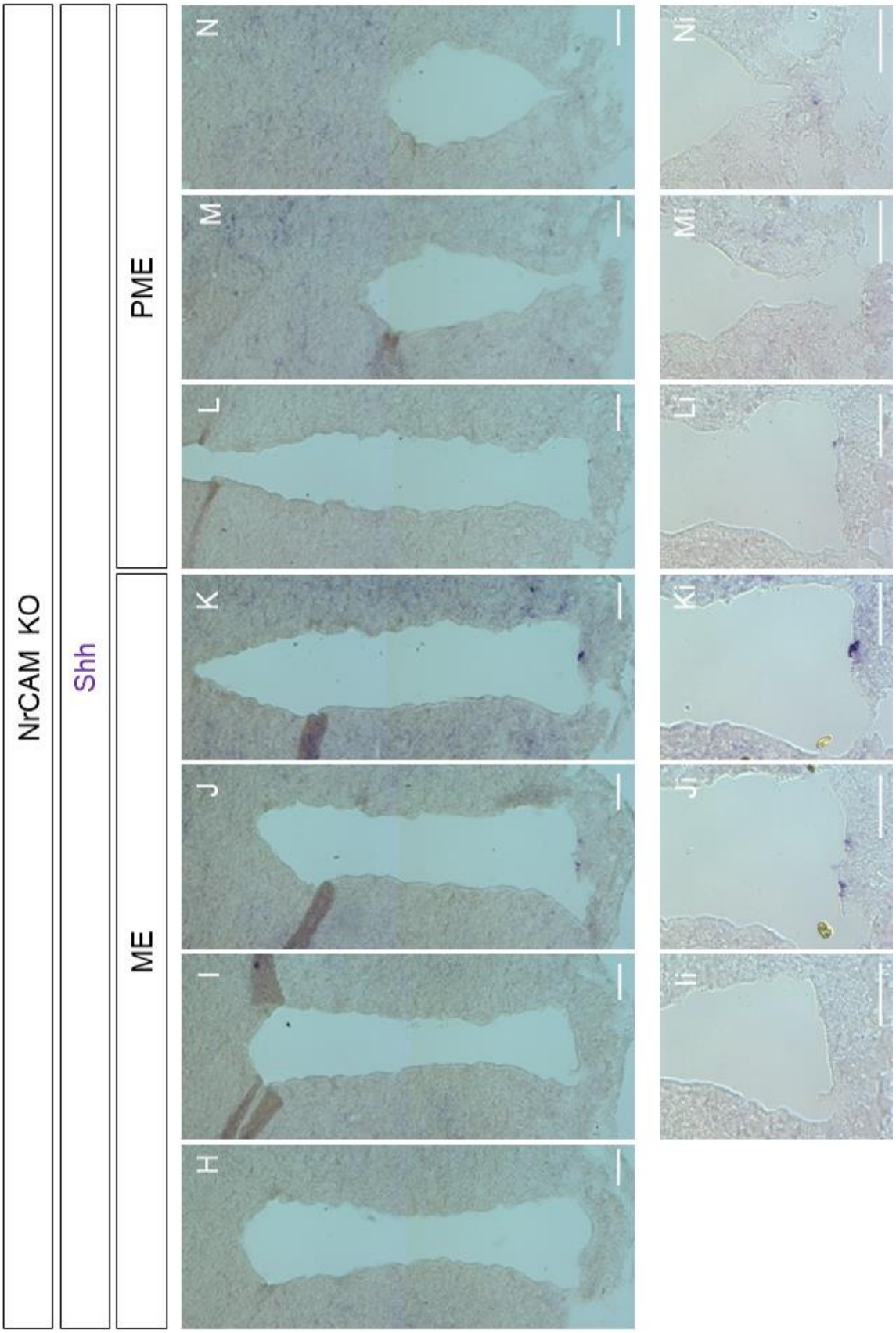

Figure 5.8 Quantification of Shh expression along the anterior-posterior axis of the hypothalamus for wild type and NrCAM KO adult mice.

The number of Shh^+ cells in the VZ of wild type and NrCAM KO adult mice were counted along the A-P axis of the hypothalamus. Cells were counted on 15µm sections, collected at 75µm intervals. The total number of cells in three biological replicates were compared for wild type and NrCAM KO using an unpaired t-test. No significant difference was observed (p=0.0550).

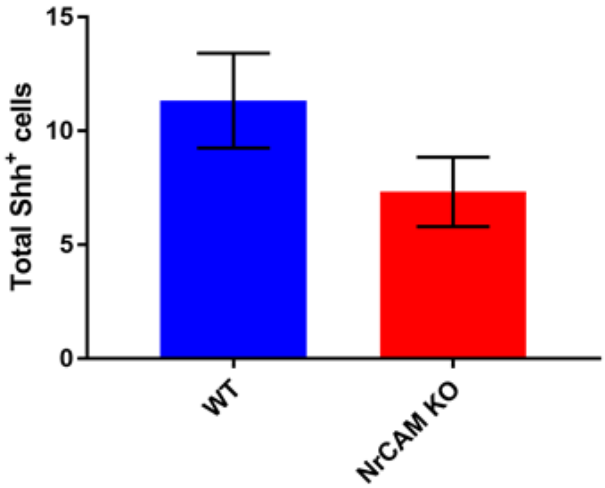

However, few/no *Shh*$^{+}$ cells were detected in PME regions of NrCAM$^{-/-}$ mice (Figure 5.7 L,M). Quantitative analyses of *Shh*$^{+}$ cells through the entire hypothalamus showed that the number of *Shh*$^{+}$ cells was not significantly different in NrCAM$^{-/-}$ mice relative to wild type mice, though a negative trend that approached significance was observed (p=0.0550). The Shh mRNA^{+} cells occur in very low numbers and on few sections, giving attempts at statistical analysis low power. Repeated analysis on more mice and using every section, rather than sections at 75µm intervals, may improve accuracy and reliability of results, and determine whether the observed trend is likely to be representative. Although subtle and weak, the alterations in expression of *Shh*, *Fgf10* and *Rax*, specifically in the PME region of the hypothalamus, together with reduced numbers of Nestin^{+} tanycytes, raise the intriguing possibility that a hypothalamic stem-like cell might exist in the PME, and is de-regulated in the NrCAM$^{-/-}$ mice.

5.2.5 TH^{+} neurons are reduced in NrCAM$^{-/-}$ mice

I next asked whether TH^{+} ARC-type neurons show altered numbers in NrCAM$^{-/-}$ mice, focusing on these as their small numbers can be easily quantified. Before asking whether TH number is affected by loss of NrCAM, I first examined the relative expression patterns of NrCAM^{+} tanycytes and TH^{+} neurons in wild type mice.

5.2.5.1 TH^{+} DA neurons lie close to NrCAM^{+} tanycytes

Previous analysis of NrCAM suggested it is not expressed in cells of the ARC (Fig 4.2), and in keeping with this observation, no overlap is seen between TH and NrCAM in the A12 population using double-label immunofluorescence (Fig 5.9 Bi-Fi). NrCAM and TH labels both localise to the external layer of the median eminence where tanycytes and neurons interact with the fenestrated capillaries, however this is not indicative of localisation within single cells (Fig 5.9 Bi). NrCAM and TH labels appear to overlap round circular blood vessels in ME/PME sections, where tanycytes surround endothelial cells (Fig 5.9 Di,Ei). The expression of NrCAM and TH at these locations appear similar but sufficiently different to suggest that they may be in different cells in close proximity to one another.

5.2.5.2 TH in NrCAM$^{-/-}$ mice

ARC TH^{+} neurons can be observed in NrCAM$^{-/-}$ mice over the same region they are seen in wild type mice (Fig 5.10 A-L). Nevertheless, over the A, AME, ME, and PME there is striking reduction in the number of ARC TH^{+} neurons in the NrCAM$^{-/-}$ mouse when compared to wild type (Fig 5.10 M). Analysis of the individual subregions showed this reduction was present throughout the A, AME, ME, and PME subregions (Fig 5.10 N). No significant difference was observed in the P subregion where TH^{+} neurons are sparse (Fig 5.10 N).

To determine whether this observation affected TH^{+} neurons globally, or was specific to A12 ARC TH^{+} neurons , I quantified the TH^{+} neurons of the zona incerta (A13)(Fig 5.10 O-Q). I found no significant difference in the zona incerta TH^{+} neuron population between the wild type and NrCAM$^{-/-}$ mice (Fig 5.10 Q). This suggests the reduction in ARC TH^{+} neurons in NrCAM$^{-/-}$ mice is not common to all TH^{+} populations, or all TH^{+} neurons in the vicinity of the hypothalamus.

5.3 Discussion

My preliminary analysis of tanycytes, progenitor cells and TH^{+} neurons outlines a subtle but significant effect of NrCAM KO across the adult hypothalamus. Although the length of the hypothalamus appears the same in wild-type and NrCAM$^{-/-}$ mice, I detect a uniform reduction of Nestin^{+} tanycytes and TH^{+} neurons across the hypothalamus, and a reduction of *Rax*$^{+}$ astrocytic-like cells in the median eminence. These changes are accompanied by subregion-specific reductions in expression of *Rax*, *Fgf10*, and potentially of *Shh.*

The reduction of Nestin^{+} tanycytes in the NrCAM$^{-/-}$ mouse was seen across the whole hypothalamic domain in which tanycytes are located, and indicates that NrCAM is either important for the developmental generation of tanycytes, for the maintenance of tanycytes in the adult mouse, or for both processes. As this is not a conditional KO for NrCAM, the identified phenotype could present at any time in the lives of the mice before the 8-12 week postnatal timepoint analysed in these studies.

Figure 5.9: TH and NrCAM expression in the ventral tuberal hypothalamus along the anterior-posterior axis

Images (A-F) at 10x magnification of coronal cross-sections showing NrCAM (green) and TH (red) expression by immunofluorescence in relation to the ventral 3V and hypothalamic parenchyma along the A-P axis with nuclear DAPI staining (blue) in an adult wild type mouse. 3V shown centrally (A, B) or to the left hand side (C-F) to emphasise extent of lateral TH expression in the parenchyma. Box inserts (i and ii for each cross-section) indicate corresponding image z-stacks collected at 20x magnification and converted to maximum intensity projections (MIPs) displayed as combined and separate channel images. Scale bars for all images 100µm. TH expression n=6 mice, NrCAM/TH double immunofluorescence n=1 mouse.

Signal in the red and green channels appear to overlap round the interior surface of ME (B-E) where tanycytes and ARC neurons are known to interact with fenestrated capillaries. Overlap is also seen on circular structures enclosing a single nucleus adjacent to the VZ in the bottom left of panels Di and Ei. These structures are morphologically similar to blood vessels. Segregation of signal from the green and red channels on cell bodies and processes in the VZ and parenchyma suggest a lack of overlapping cellular expression for NrCAM and TH.

Figure 5.9

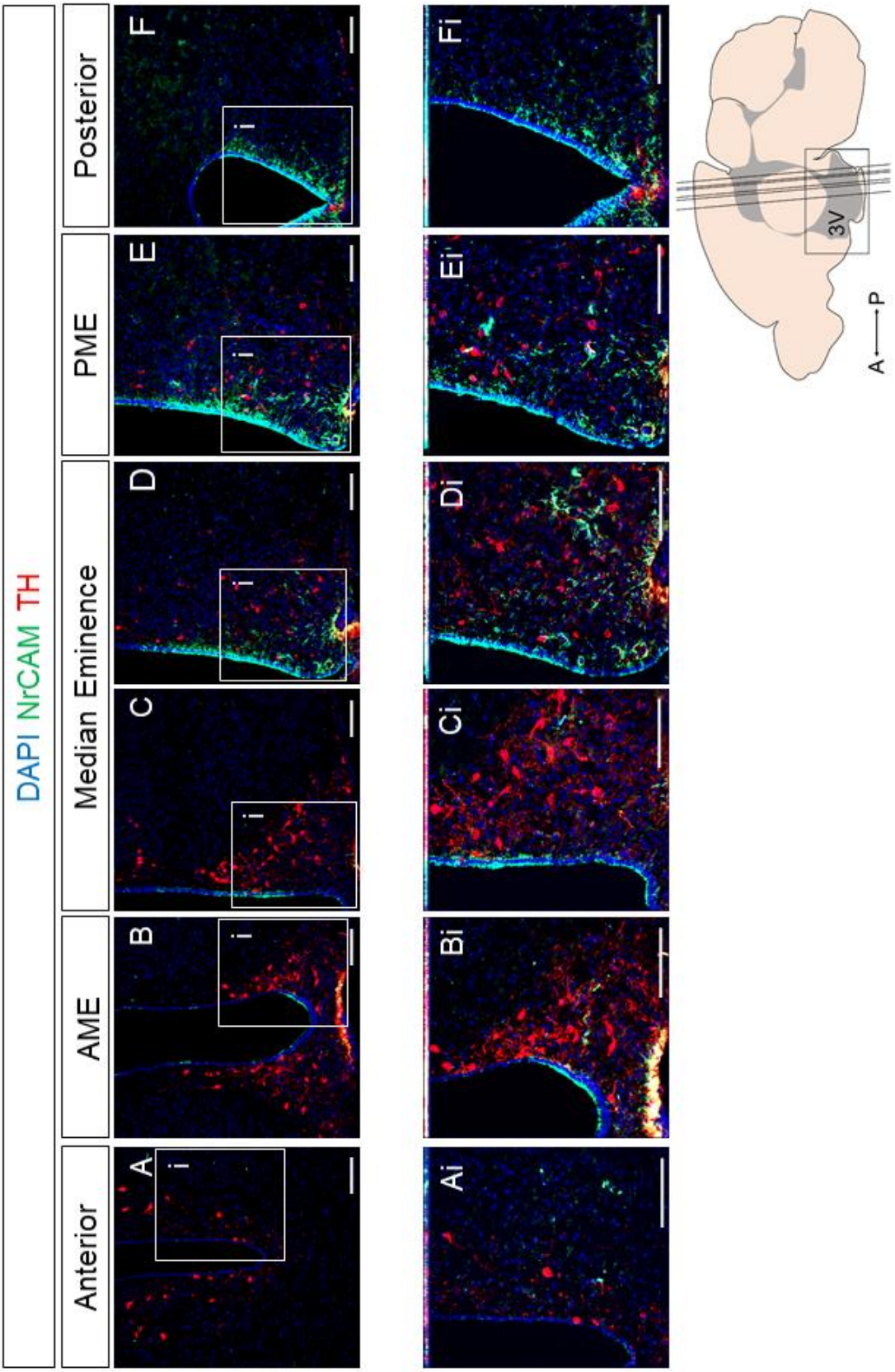
DAPI NrCAM TH
Anterior
AME
Median Eminence
PME
Posterior
A
B
C
D
E
F
Ai
Bi
Ci
Di
Ei'
Fi
i
3V
A
P

Figure 5.9

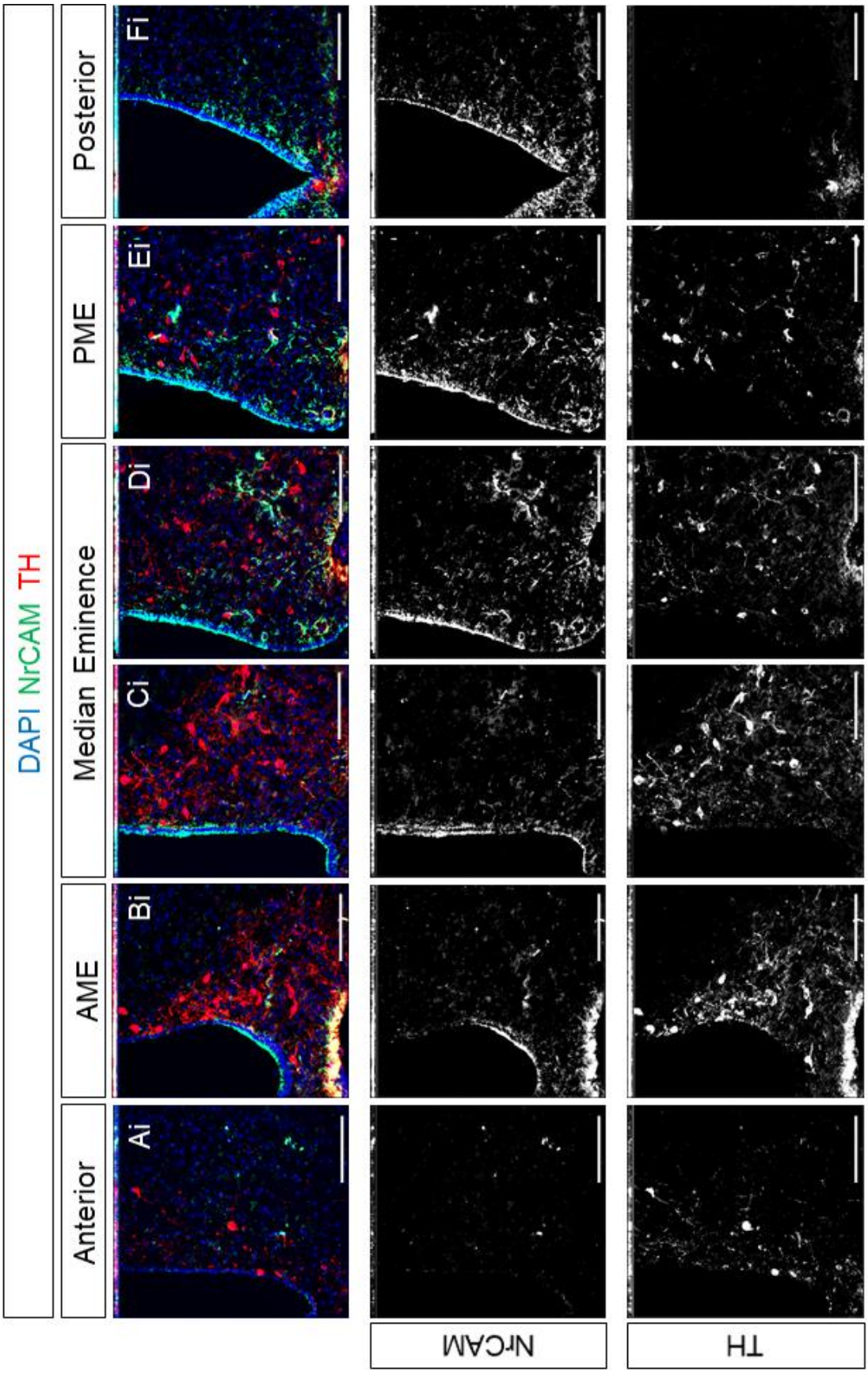
DAPI NrCAM TH
Anterior
AME
Median Eminence
PME
Posterior
Ai
Bi
Ci
Di
Ei
Fi
NrCAM
TH

Previous studies have, in fact, reported NrCAM expression in the E16 hypothalamus (Lustig et al., 2001b), where it is expressed by radial glial cells (RGCs: tanycyte-precursors) (Noctor et al., 2001; Sild and Ruthazer, 2011; Tamamaki et al., 2001). If NrCAM has a function in modulating RGC proliferation, differentiation, generation, or survival, its removal could cause the observed phenotypes in adult mice. An alternative hypothesis is that NrCAM is important for maintenance of the adult tanycyte population, either by impacting on survival, or through modulation of the stem-like behaviours.

The observed reductions of *Rax*$^{+}$ astrocytic cells in the median eminence and of the TH^{+} A12 ARC dopaminergic population could similarly reflect a developmental effect or an effect on adult cell maintenance. However, whereas NrCAM is expressed in tanycytes, or their precursors (Marc Lustig et al., 2001; this study), it is not expressed in TH^{+} neurons or and does not appear to be expressed on potential Rax^{+} median eminence astrocytes. Therefore, the loss in these populations must be an indirect effect. One possibility is that both *Rax*$^{+}$ astrocytes and TH^{+} neurons arise from NrCAM^{+} RGCs or from NrCAM^{+} tanycytes; in support of this, evidence in zebrafish shows that tanycytes can generate both *Rax*$^{+}$ parenchymal cells and TH^{+} ARC-like neurons (S. Brown, submitted). Whatever the mechanism, loss of these cell types appears to be specific to the hypothalamus: In the NrCAM$^{-/-}$ mouse, the ARC A12 TH^{+} neurons were decreased but the thalamus-derived zona incerta A13 TH^{+} population that is found dorsolateral to the 3V (Andrews et al., 2003; Puelles and Verney, 1998) showed no decrease. Together these results show that NrCAM$^{-/-}$ causes a specific decrease in the hypothalamic A12 TH^{+} population which is not common to TH^{+} neurons globally.

The tentative idea that loss of TH^{+} and *Rax*$^{+}$ parenchymal cells occurs due to the misregulation/loss of an NrCAM^{+} RGC or tanycyte stem-like cell is further supported by the finding that loss of NrCAM results in a subtle decrease in expression of *Rax*, *Fgf10* and, potentially, *Shh* in tanycytes. Intriguingly, levels are especially decreased in the PME, and in the α-tanycyte domain of the ME, regions implicated as harbouring a stem-like population (Robins et al., 2013; this study). This raises the possibility that loss of NrCAM results in the loss of a hypothalamic stem-like cell in the PME. Certainly, these studies suggest that NrCAM is acting upstream of *Rax*, *Fgf10* and *Shh* for either the generation or

Figure 5.10 TH expression and quantification along the anterior-posterior axis of the hypothalamus for wild type and NrCAM KO adult mice.

Images at 10x magnification of coronal sections showing TH (green) expression by immunofluorescence in the ARC along the A-P axis with nuclear DAPI staining (blue) in adult wild type (A-F) and NrCAM KO (G-L) mice. Scale bars 100µm. Images representative of the n=3 pairs of mice investigated.

M – Quantification of TH^+ cells along the A-P axis of the ARC in three pairs of wild type and NrCAM KO adult mice. Each icon represents a single measurement, collected as described in Chapter 2.2.5.2. Bars show 1 SD either side of the mean value. Analysis by unpaired t-test with Welch's correction showed a significant reduction of TH^+ cells in the ARC of NrCAM KO adult mice ($P<0.0001$).

N – Quantification of TH^+ cells in the ARC in A, AME, ME, PME, and P subregions, in three pairs of wild type and NrCAM KO adult mice. Each icon represents a single measurement, collected as described in Chapter 2.2.5.2. Bars show 1 SD either side of the mean value. Analysis by unpaired t-test with Welch's correction showed significant reductions of TH^+ cells in the ARC in NrCAM KO adult mice in A, AME, ME, and PME subregions (A $P<0.0001$; AME $P<0.0001$; ME $P<0.0001$; PME $P=0.0158$). No significant difference was seen the P subregion where ARC TH^+ cells are least populous ($P=0.2865$).

Images at 10x magnification of coronal sections showing TH (red) expression by immunofluorescence in the dorsal AME Zona Incerta (A13) population with nuclear DAPI staining (blue) in adult wild type (O) and NrCAM KO (P) mice. Scale bars 100µm. n=3 mice.

Q – Quantification of TH^+ cells in the dorsal AME Zona Incerta (A13) population in three pairs of wild type and NrCAM KO adult mice. Each icon represents a single measurement, collected as described in Chapter 2.2.5.2. Bars show 1 SD either side of the mean value. Analysis by unpaired t-test showed no significant difference of TH^+ cells in dorsal AME Zona Incerta (A13) population between wild type and NrCAM KO adult mice ($P=0.2543$).

Figure 5.10

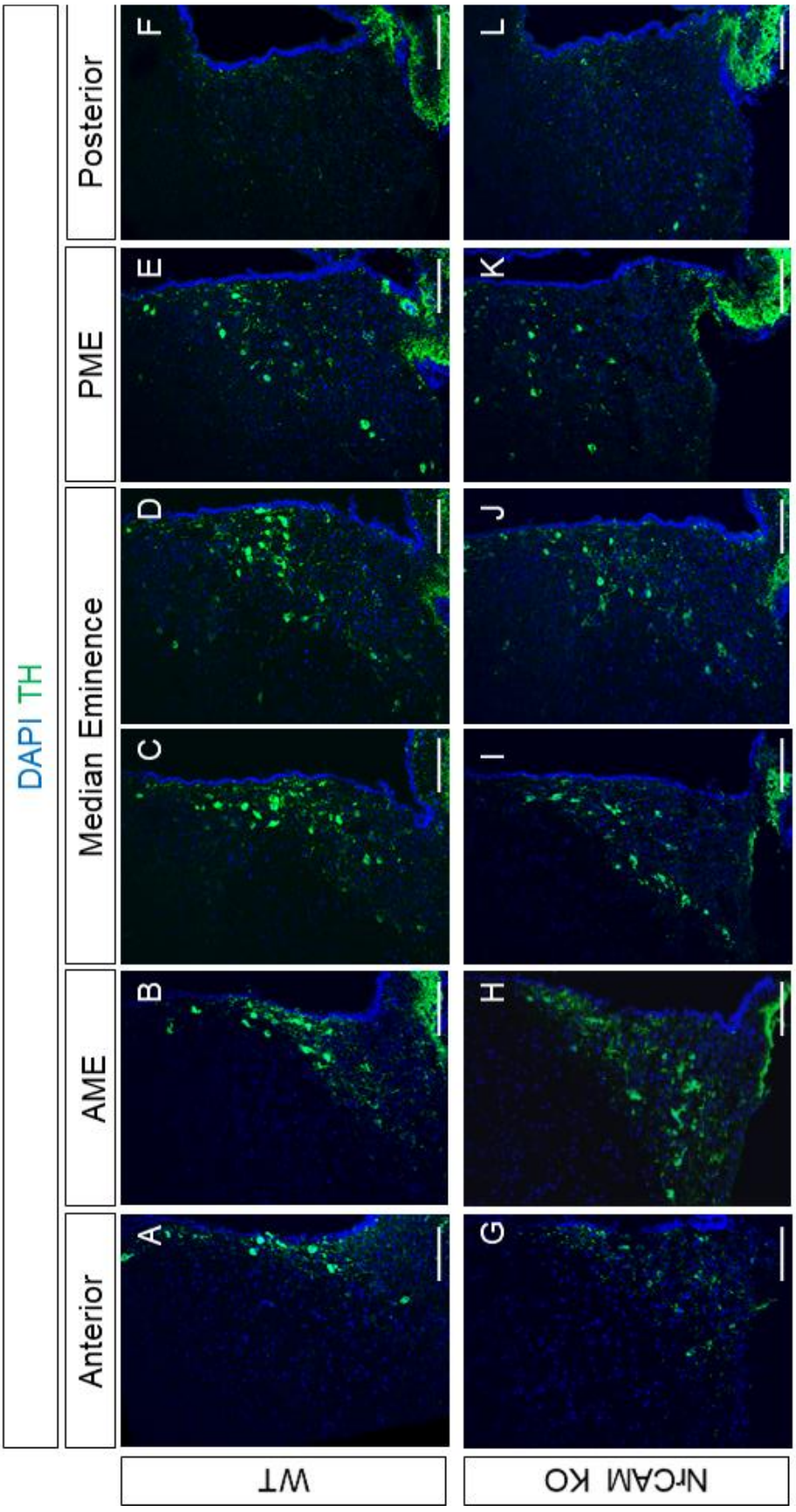
DAPI TH
Anterior
AME
Median Eminence
PME
Posterior
WT
Nr-CAM KO
A
B
C
D
E
F
G
H
I
J
K
L

Figure 5.10

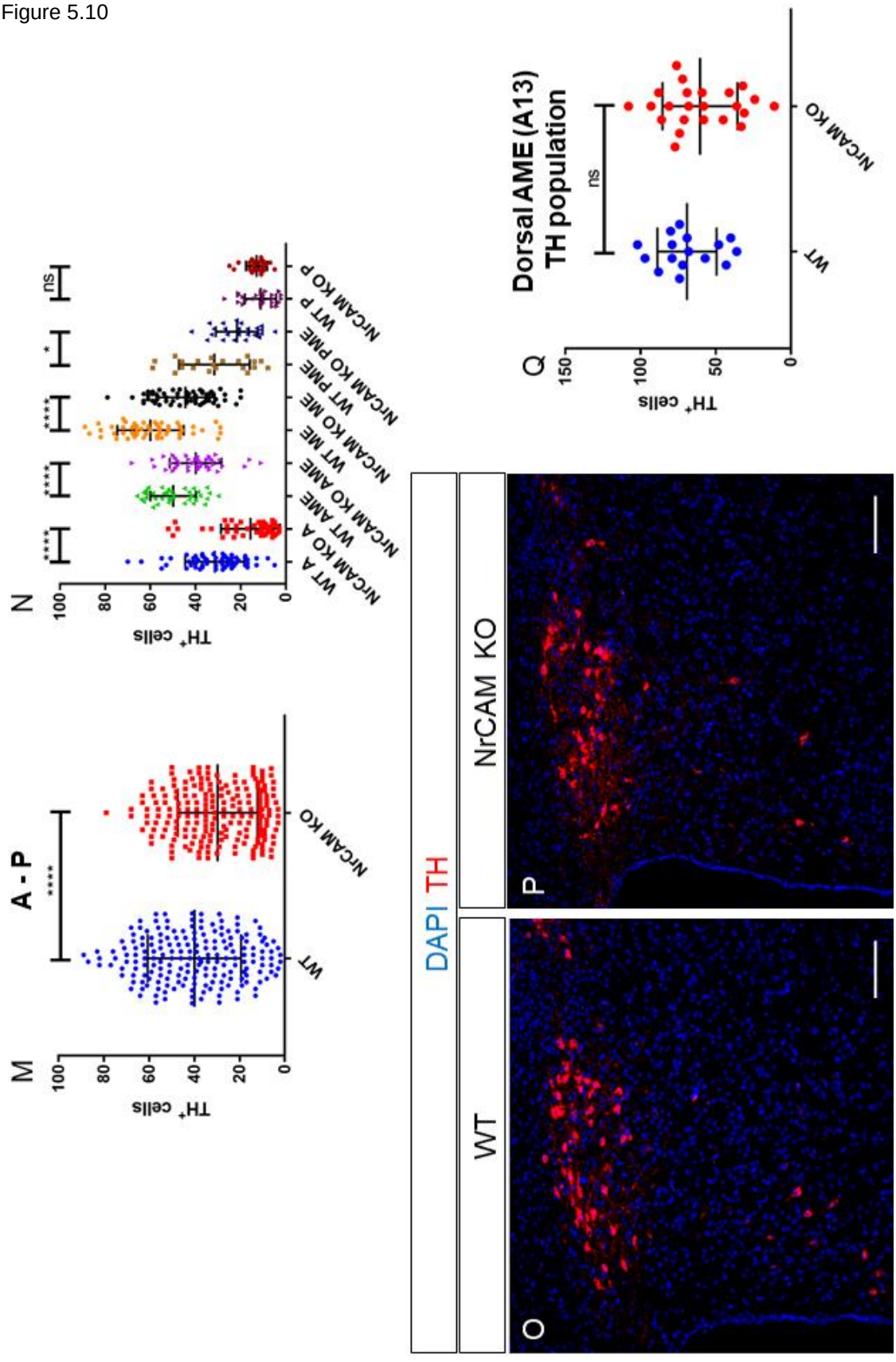
DAPI TH
WT
NrCAM KO
O
P
Q
Dorsal AME (A13)
TH population
TH+ cells
ns
WT
NrCAM KO
M
A - P
****
N
WT A
NrCAM KO A
WT AME
NrCAM KO AME
WT ME
NrCAM KO ME
WT PME
NrCAM KO PME
WT P
NrCAM KO P
*
ns

maintenance of PME-located tanycytes.

Attention should also be granted to the discrepancies in the A-P changes between the various markers I have used. While Nestin appears uniformly reduced in tanycytes along the A-P axis, reductions in *Rax* and *Fgf10* are most prominent posteriorly, and TH^+ neurons are reduced anteriorly. The mild *Rax* reduction across the A-P axis of the hypothalamus is likely indicative of the reduced number of tanycytes labelled by $Nestin^+$ processes. However, the PME/P subregion where both *Rax* and *Fgf10* are strongly reduced, is where *Rax* is most strongly expressed. Our hypothesis from Chapter 4 suggested that this PME/P subregion where we see the strong expression of a variety of stem-associated factors all together may be the region which harbours potential stem cells (Figs 4.9 and 4.10). We suggest proliferation in this region may yields cells that migrate and establish themselves more anteriorly, accounting for the concentric rings of tanycytes extending anteriorly from this point, with each ring expressing fewer tanycyte and stem cell-markers at weaker intensity (Fig 4.10). Reduction of *Rax* and *Fgf10* in this region in the NrCAM KO may have a negative impact on the neurogenic capacity of the hypothalamus, which in turn leads to the reduction of tanycytes throughout, and a reduction in TH^+ neurons in the more anterior subregions where they are most abundant.

The consequences of these reductions are is unclear. No overt phenotype is observed in the NrCAM KO mice that could easily be associated with mild disruption of the hypothalamus. It is possible that reduction of the TH^+ neurons may have effect on the regulation of prolactin secretion (Ben-Jonathan and Hnasko, 2001), however no difference has been immediately apparent in the ability of NrCAM KO mice to nurse pups in the litters we have raised. Similarly, the reduction of tanycytes may have effects on the local nuclei through changes in barrier properties (Holmes et al., 2016; Miranda-Angulo et al., 2014), and also through loss of projections to these nuclei, including the ARC where the reduced A12 TH^+ neurons reside, and also the median eminence. These projections play important roles in nutrient transport, neuronal support, and control of signalling (Balland et al., 2014; Fekete et al., 2014; Frayling et al., 2011; Langlet et al., 2013a, 2013b; Mullier et al., 2010). Further investigation of how a diminished tanycyte population affects these processes is required.

The results I have described point to one major question that must be addressed: Is this subtle but interesting phenotype a product of abnormal development, or an adult onset phenotype caused by impaired progenitor behaviour or survival? Chapter 6 of my thesis will investigate RGC markers, signals, and neuronal populations in the mouse embryo, to address whether the irregularities caused by loss of NrCAM are a product of abnormal development. I will investigate the developing mouse brain at E16 to ask whether the changes observed have occurred by E16, or occur at a later time. In Chapter 7 I will discuss two *ex vivo* approaches that have been tried to investigate adult hypothalamic progenitor proliferation and differentiation competency.

CHAPTER 6: NRCAM KO AND THE DEVELOPING HYPOTHALAMUS

6.1 Introduction

Following my investigation of NrCAM KO on the adult hypothalamus, I wished to determine whether the reduction in tanycytes and A12 dopaminergic neurons was a developmental or adult-onset phenotype. NrCAM is expressed in the presumptive hypothalamus by E11[6], and at E16 it appears to be expressed by RGCs, the tanycyte precursors known to populate the region (Edwards et al., 1990; Lustig et al., 2001b). Like tanycytes, RGCs are bipolar cells whose cell bodies are located at the VZ, and whose long processes extend to the pial surface (J. Everitt et al., 1986). They are routinely labelled using RC2 (an epitope of Nestin) (Park et al., 2009), and have been described as developmental CNS progenitors (Noctor et al., 2001; Sild and Ruthazer, 2011; Tamamaki et al., 2001). As yet, no study has examined the effect of loss of function of NrCAM in the developing hypothalamus, including effects on expression of Rax and Shh, both known to play a role in hypothalamic stem/progenitor cell differentiation in the embryonic mouse.

Rax expression in the presumptive hypothalamus begins at E7.5 and it has a role in the maintenance of early Shh expression and specification of the hypothalamic region (Furukawa et al., 1997; Lu et al., 2013; Orquera et al., 2016). The greatest period of hypothalamic neurogenesis occurs from E11-E14, and at this time Rax is necessary for the proper patterning of ARC and VMN neurons (Lu et al., 2013; Shimada and Nakamura, 1973). During this period Rax initiates expression of Lhx2 at E12.5, and both become restricted to the VZ where they are expressed into adulthood (Salvatierra et al., 2014). Lhx2 binds the regulatory zone of Rax where it acts to maintain its expression, which in turn specifies tanycyte differentiation (Salvatierra et al., 2014).

[6] Allen Developing Mouse Brain Atlas – NrCAM http://developingmouse.brain-map.org/gene/show/106439

Figure 6.1 Atlas of coronal sections from anterior to posterior through the E16 hypothalamus

Images at 20x magnification of coronal cross-sections, labelled with DAPI to show cell nuclei, centred on the base of the 3V and the ME. 15µm sections displayed in order from anterior to posterior with labels describing the position of the sections as Anterior, Anterior Median Eminence (AME), Median Eminence (ME), and Posterior. Every section along the axis has been collected and displayed, including those that are damaged or folded which are marked by white asterisks. The AME-P region is 420µm long (28x15µm sections). Green arrowhead, AME nuclei-dense pial region/pars tuberalis; purple arrowhead, infundibular recesses; grey arrowhead, bulbous median eminence out-pocketing; white arrowhead, ME forms the pituitary stalk and 3V tapers to a point. Scale bars 50µm. Atlas representative of all embryonic mice investigated.

Figure 6.1

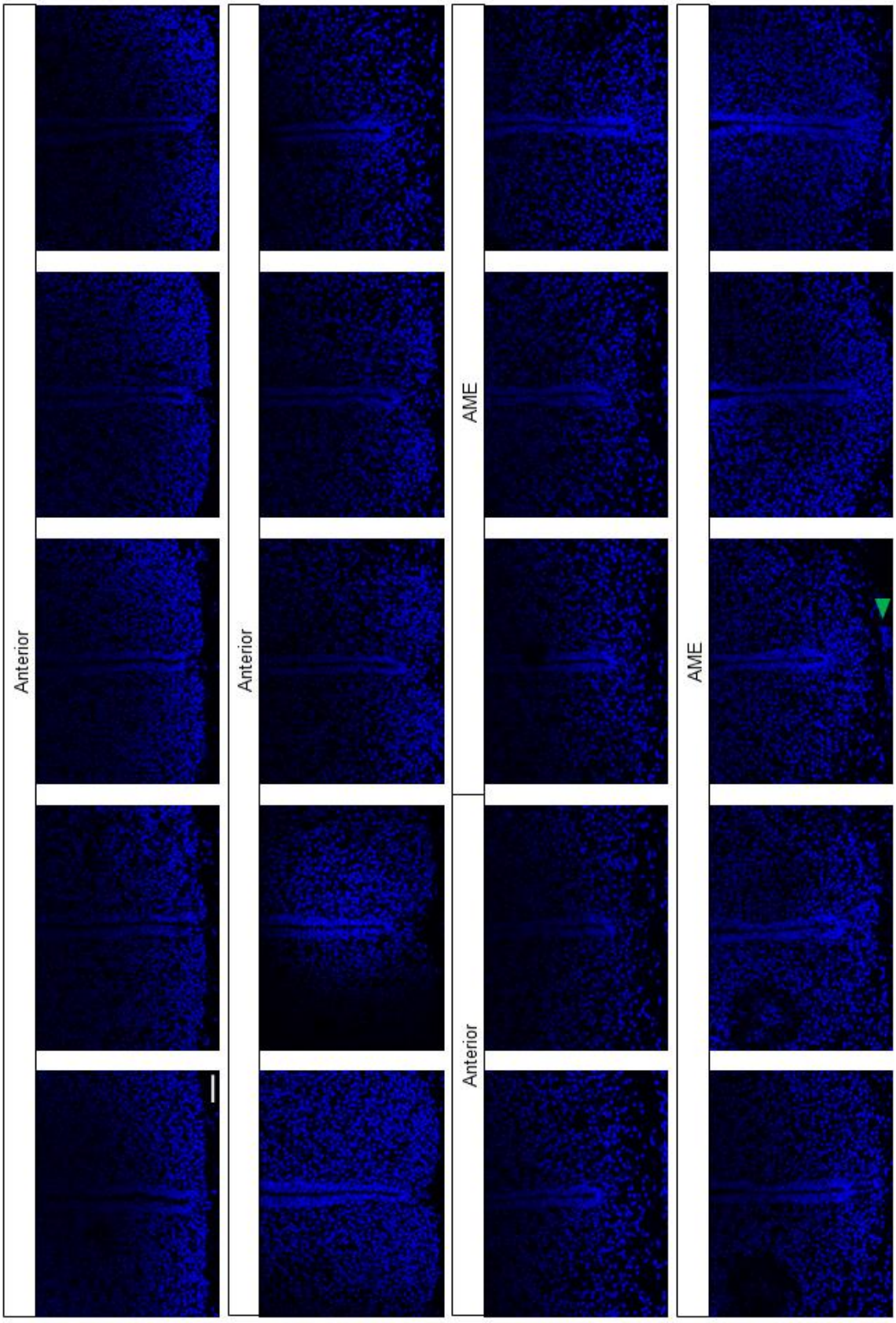

Figure 6.1

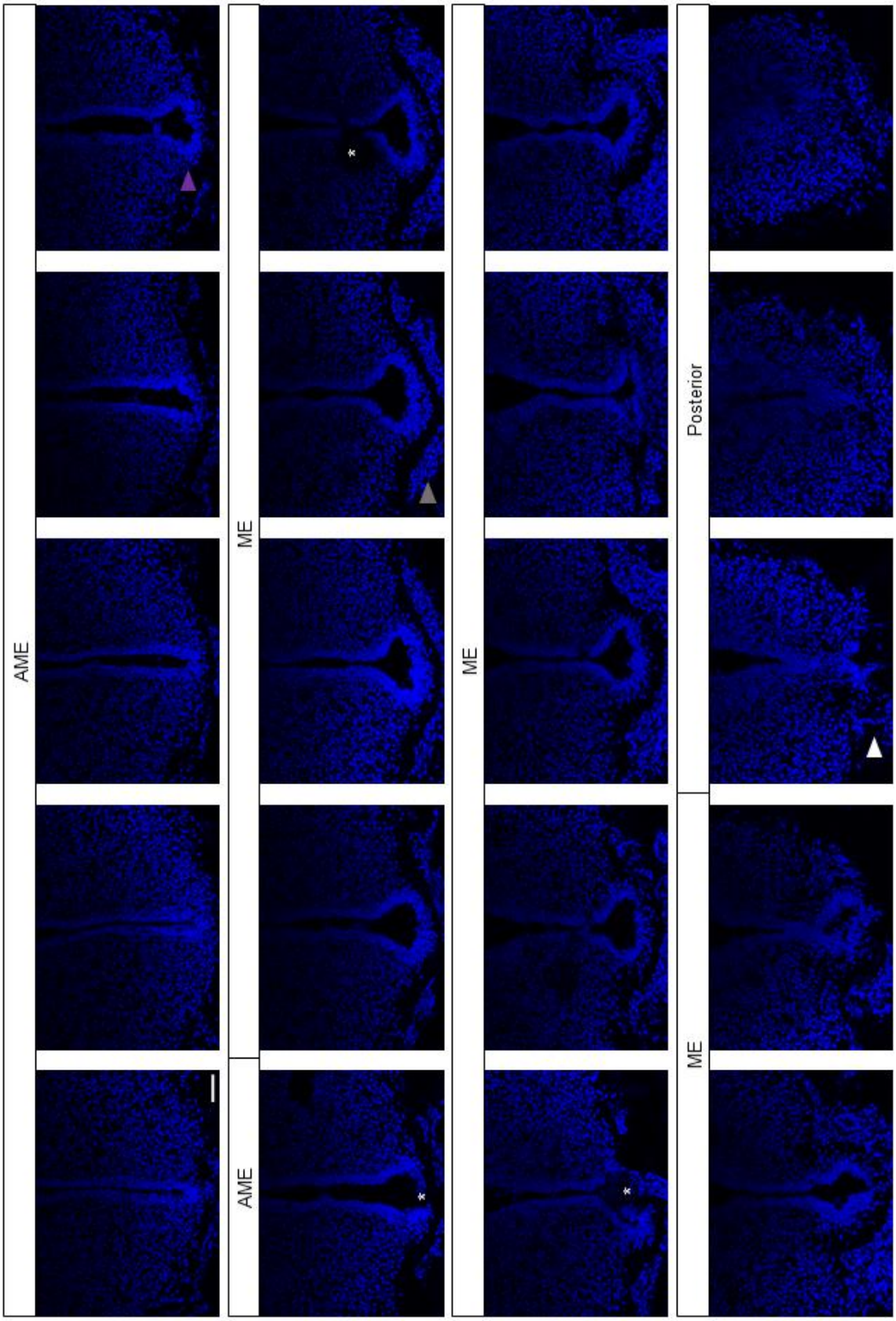

As loss of NrCAM causes reductions in tanycytes, and of expression of these well-established developmental signals, I wished to investigate whether this is caused by aberrant hypothalamic development. I therefore set out to examine NrCAM$^{-/-}$ mice at E16, immediately following the specification and expansion of the hypothalamus (Fu et al., 2017; Shimada and Nakamura, 1973), and the embryonic period that begins to mark the transition of RCGs to tanycyte specification (Salvatierra et al., 2014).

6.2 Results

6.2.1 Ventricle and ME morphology along the A-P axis of the E16 hypothalamus

To begin to compare the wild type and NrCAM KO hypothalamus at E16, I first determined the morphology of the hypothalamus along the A-P axis and defined discrete subregions, as I had done in adulthood. Figure 6.1 shows an atlas of every 15µm section collected through the hypothalamus, beginning anterior to the region containing the median eminence, and continuing posteriorly through the median eminence-containing region until the 3V tapers off and disappears entirely.

The Anterior (A) region includes a long thin 3V and no median eminence, but unlike the adult A subregion, it contains many Nestin^{+}NrCAM^{-} RGCs extending from VZ (Fig 6.2A). The AME subregion follows on from the A, and as in the adult, the ventricle descends toward the thickening pial surface which will become the ME (green arrowhead). The transition from A to AME is subtle but can be defined by the changes in the RGCs: AME RGCs have stronger Nestin expression and express NrCAM (Fig 6.2B).

Through the AME the ventricle extends, the VZ expands, and the pial surface that will surround the median eminence thickens. The transition to the ME subregion sees the rounding and outpocketing of the ventricle into the IR (purple arrowhead). The thickened pial surface of the median eminence surrounds the protruding ventricle and extends laterally (grey arrowhead). As in the adult hypothalamus, the median eminence grows larger until it rounds off entirely, leaving the 3V tapering to a point (white arrowhead). I have not included a PME subregion as the domain over which the ventricle tapers is

brief, but I have included the two sections that might be considered PME in with the ME subregion for ease of classification and quantitative analysis. In the Posterior (P) subregion the ventricle recedes until it is lost entirely.

I will use the four subregions A, AME, ME, and P, with additional anterior/posterior descriptors such as ME^{A} and ME^{P}, to help describe, compare, and quantitate the RGCs, markers, and TH^{+} A12 population in wild type and $NrCAM^{-/-}$ embryonic mice.

6.2.2 Nestin and NrCAM as RGC markers

Based on the observation of NrCAM in the E16 hypothalamus by Lustig et al. (2001), I began by comparing expression of NrCAM and the RGC marker Nestin. In the anterior hypothalamus, Nestin is expressed weakly on RGCs and NrCAM is absent (Fig 6.2 A,Ai,Aii). This changes at the transition to the AME, where NrCAM and Nestin are both expressed strongly on RGCs and the lining of the pial surface/forming ME (Fig 6.2 B,Bi,Bii). As in tanycytes, NrCAM is expressed in both the VZ and on the extending processes, whilst Nestin expression is limited to the processes only. The co-expression of NrCAM and Nestin continues through the ME and P (Fig 6.2 C-E). Unlike in the tanycytes of the adult hypothalamus, the expression of NrCAM and Nestin does not appear to increase in strength in more posterior sections, and may actually decrease.

These findings suggest that NrCAM is expressed on RGCs over the same AME-P subregions that contain $NrCAM^{+}$ tanycytes in the adult hypothalamus. The RGCs of the A subregion, and the rest of the neural tube, are lost toward the end of the development, whilst the $NrCAM^{+}$ subpopulation of the AME-P subregions are retained in the form of tanycytes.

6.2.3 Comparison of Nestin in wild type and $NrCAM^{-/-}$ mice

Following the observation that NrCAM KO leads to fewer tanycytes in adult mice, I next investigated whether the RGC population is compromised at E16 in $NrCAM^{-/-}$ mice. $Nestin^{+}$ RGCs are present throughout the hypothalamus in both the wild type and $NrCAM^{-/-}$ mice (Fig 6.3 A-J). In mice of both genotypes, Nestin expression is noticeably weaker in the A subregion (Fig 6.3 A,F). Qualitative assessment of RGCs in the AME-P subregions, that normally express NrCAM and are retained as tanycytes, suggests there are fewer RGCs in the

Figure 6.2 NrCAM and Nestin expression in the E16 tuberal hypothalamus along the anterior-posterior axis

Image composites (A-E) at 20x magnification of coronal cross-sections showing Nestin (green) and NrCAM (red) expression by immunofluorescence in relation to the 3V, ME, and hypothalamic parenchyma along the A-P axis with nuclear DAPI staining (blue) in a E16 wild type mouse. Corresponding separate channel images (Ai/Aii-Ei/Eii). NrCAM expression co-labels Nestin$^+$ processes from the AME-P (B-E). Scale bars for all images 50µm. Images representative of the n=3 mice investigated.

Figure 6.3 Comparison and quantification of Nestin expression in Radial-Glial Cells along the anterior-posterior axis of the hypothalamus of E16 wild type and NrCAM KO mice

Image composites at 20x magnification of coronal cross-sections showing Nestin (red) expression by immunofluorescence with nuclear DAPI staining (blue) in E16 wild type (A-E) and NrCAM KO littermates (F-J). Scale bars for all images 50µm. Images representative of the n=3 pairs of mice investigated.

K – Quantification of Nestin$^+$ process density of RGCs from AME-P in three pairs of E16 wild type and NrCAM KO mice. Each icon represents a single measurement, collected as described in Chapter 2.2.5.2. Bars show 1 SD either side of the mean value. Analysis by unpaired t-test showed a significant reduction of Nestin$^+$ tanycyte density in E16 NrCAM KO mice relative to wild type littermates ($P<0.0001$).

L – Quantification of Nestin$^+$ process density of RGCs in AME, ME, and P subregions in three pairs of E16 wild type and NrCAM KO littermates. Each icon represents a single measurement, collected as described in Chapter 2.2.5.2. Bars show 1 SD either side of the mean value. Analysis by unpaired t-test showed significant reductions of Nestin$^+$ RGC density in E16 NrCAM KO mice in every A-P subregion (AME $P<0.0001$; ME $P<0.0001$; P $P=0.0052$).

Figure 6.2

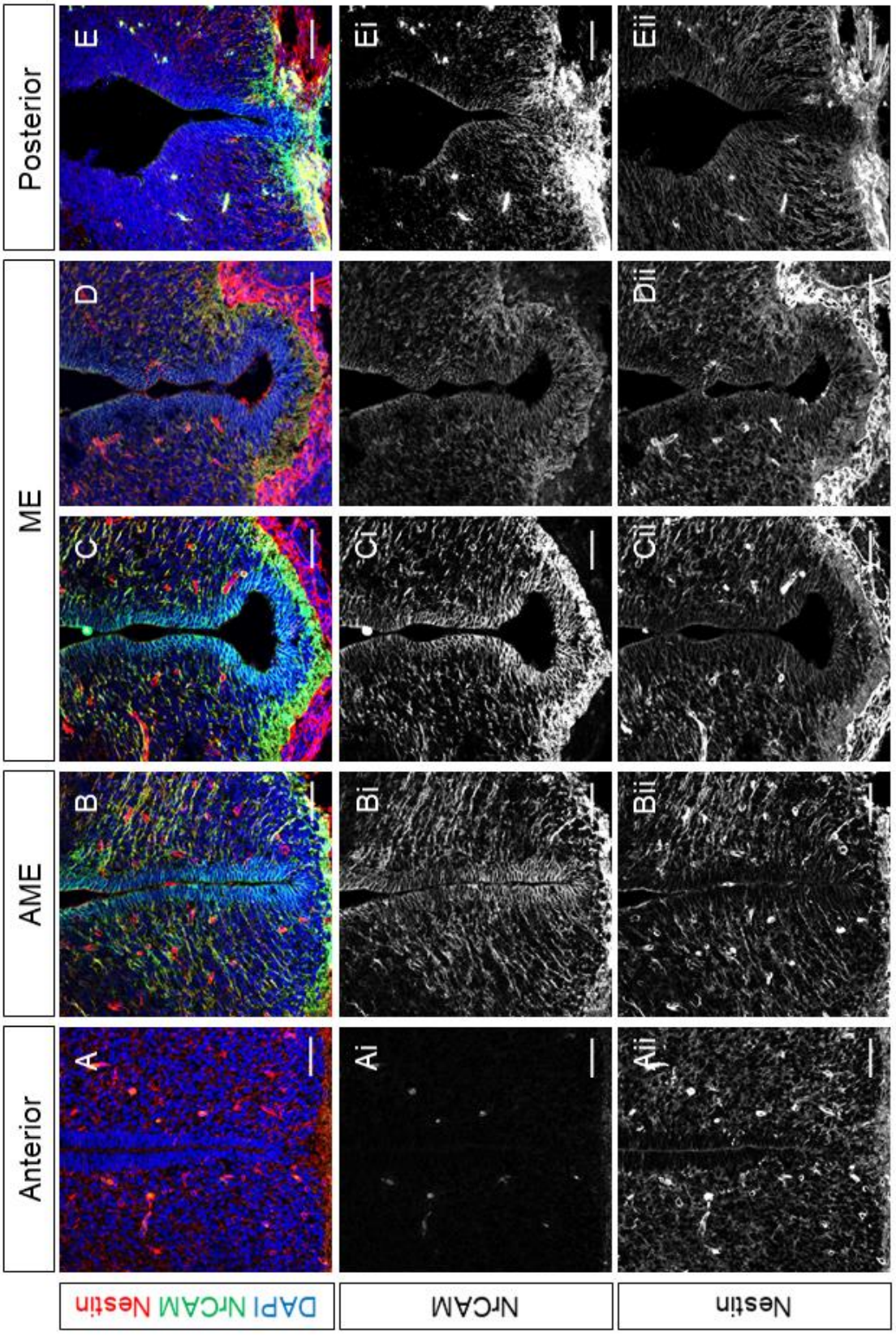
Anterior
AME
ME
Posterior
A
B
C
D
E
Ai
Bi
Ci
Di
Ei
Aii
Bii
Cii
Dii
Eii
DAPI NrCAM Nestin
NrCAM
Nestin

Figure 6.3

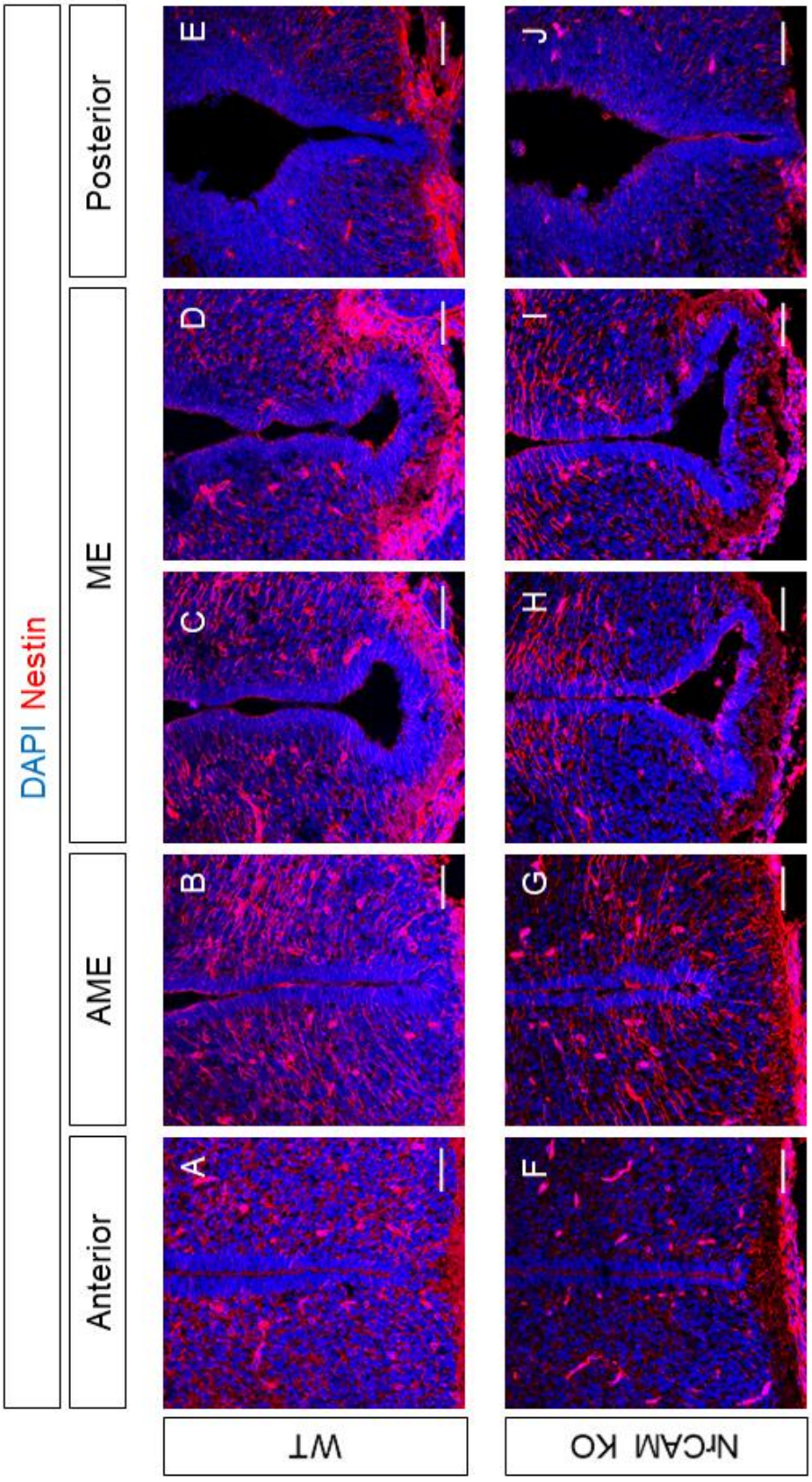
DAPI Nestin
Anterior
AME
ME
Posterior
WT
NrCAM KO
A
B
C
D
E
F
G
H
I
J

Figure 6.3

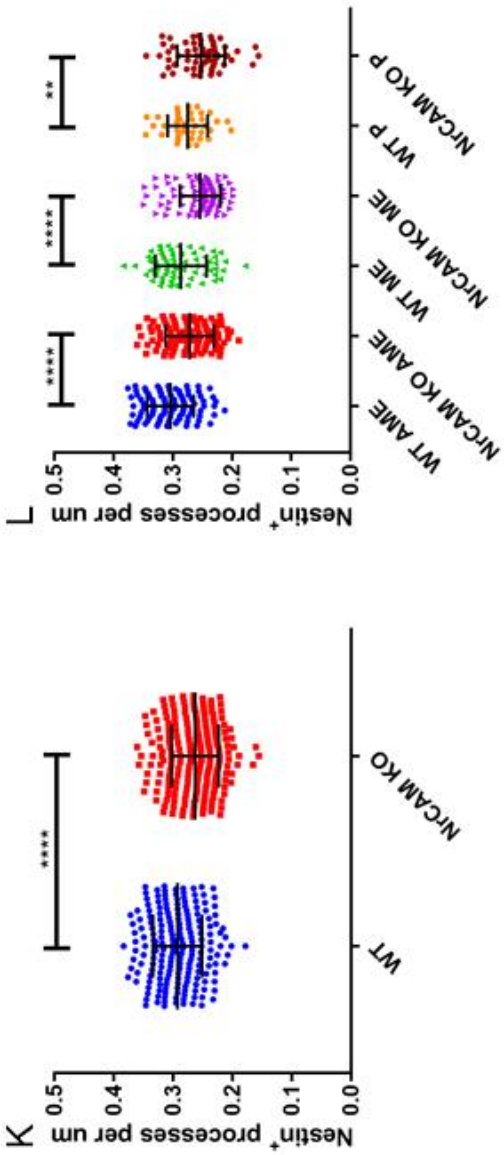
L
Nestin+ processes per um
0.0
0.1
0.2
0.3
0.4
0.5
WT AME
NrCAM KO AME
WT ME
NrCAM KO ME
WT P
NrCAM KO P
****
****
**
K
Nestin+ processes per um
0.0
0.1
0.2
0.3
0.4
0.5
WT
NrCAM KO
****

NrCAM$^{-/-}$ (Fig 6.3 B-E,G-J). Quantitative analysis shows that Nestin^{+} RGC processes are ~10% less densely packed across the AME-P subregions in the NrCAM$^{-/-}$ mice, and this result is consistent in each of the AME, ME, and P subregions (Fig 6.3 K,L). Thus, the reduction in tanycytes in the adult hypothalamus of NrCAM$^{-/-}$ mice is preceded by a reduction in the ancestral RGC population by E16.

6.2.4 Rax

By E16, *Rax* is restricted to the VZ where it is responsible for tanycyte specification (Salvatierra et al., 2014). I detect *Rax* expression through the entirety of the AME-P in both wild type and NrCAM$^{-/-}$ mice (Fig 6.4 A-J). Like the expression of *Rax* in tanycytes, at E16 *Rax* is expressed over the same hypothalamic region as NrCAM. Unlike in the adult, at this earlier timepoint the anterior-most expression is initiated approximately 70µm dorsal to the ventral tip of the 3V (Fig 6.4 A,F). Through the AME, the dorsal *Rax* domain expands and *Rax* expression is also initiated in the ventral tip of the 3V (Fig 6.4 B,G). These domains of expression expand toward each other and meet at the AME/ME^{A} boundary. Through the ME and P subregions the expression of *Rax* is similar to that seen in tanycytes (Fig 6.4 C-E,H-J). *Rax* is not seen in the median eminence parenchymal cells I have observed in adult mice. Generating comparable sections, with good labelling and little damage, to demonstrate the difference between wildtype and NrCAM KO mice was more difficult when using the embryonic hypothalamus than the adult hypothalamus. The A-P length of the embryonic hypothalamus is far shorter, and as a consequence the number of sections for each subregion is far smaller, and the morphological differences between adjacent sections was larger. This was compounded by difficulty recreating the identical plane of section between brains, and the necessity of using serial sections to label for different markers (*Rax*/*Fgf10*/*Shh*) so that their localisation may be directly compared. These complications are why I present wildtype and NrCAM$^{-/-}$ sections with slight differences in morphology in the P subregion, not because there are distinct morphological differences between genotypes. The sections best represent the labelling in the subregion.

The expression pattern I have described is the same in wild type and NrCAM$^{-/-}$ mice. There was no significant difference observed in either the length

Figure 6.4 Comparison and quantification of Rax expression along the anterior-posterior axis of the hypothalamus in E16 wild type and NrCAM KO littermates.

Image composites at 20x magnification of coronal cross-sections showing Rax mRNA expression (purple) by in situ hybridisation in relation to the 3V, ME, and hypothalamic parenchyma along the A-P axis in E16 wild type (A-E) and NrCAM KO (F-J) mice. Scale bars 50µm. Images representative of the n=3 pairs of mice investigated.

K – A graph comparing the length of the Rax-expressing domain round the ventral 3V in adult wild type (blue) and NrCAM KO (red) mice. The plotted value at each marked position is the mean of three biological replicates, with the bars showing the range. Using the Wilcoxon signed rank test, no significant difference was observed when values across the whole Rax-expressing domain in the wild type and NrCAM KO were compared. When the AME, ME, and P subregions were individually assessed, no significant difference was seen.

L – A graph comparing the chromogenic signal intensity of the Rax-expressing domain round the ventral 3V in adult wild type (blue) and NrCAM KO (red) mice. The plotted value at each marked position is the mean of three biological replicates, with the bars showing the range. The mean gray value gives a readout between 0 (black) and 256 (white) that represents the chromogenic signal intensity, and has been normalised against the background. A lower mean gray value (closer to black) represents a stronger signal strength. Using the Wilcoxon signed rank test, no significant difference was observed when values across the whole Rax-expressing domain in the wild type and NrCAM KO were compared. When the AME, ME, and P subregions were individually assessed, no significant difference was seen.

M – A graph comparing the percentage change in relative Rax signal strength in the NrCAM KO when compare to the wild type at each position along the A-P axis. The plotted value at each marked position is the mean of three biological replicates, with the bars showing the range. For each replicate, the normalised mean gray value for Rax in an NrCAM KO section was subtracted from the normalised mean gray value in the paired wild type section and converted to a percentage.

Figure 6.4

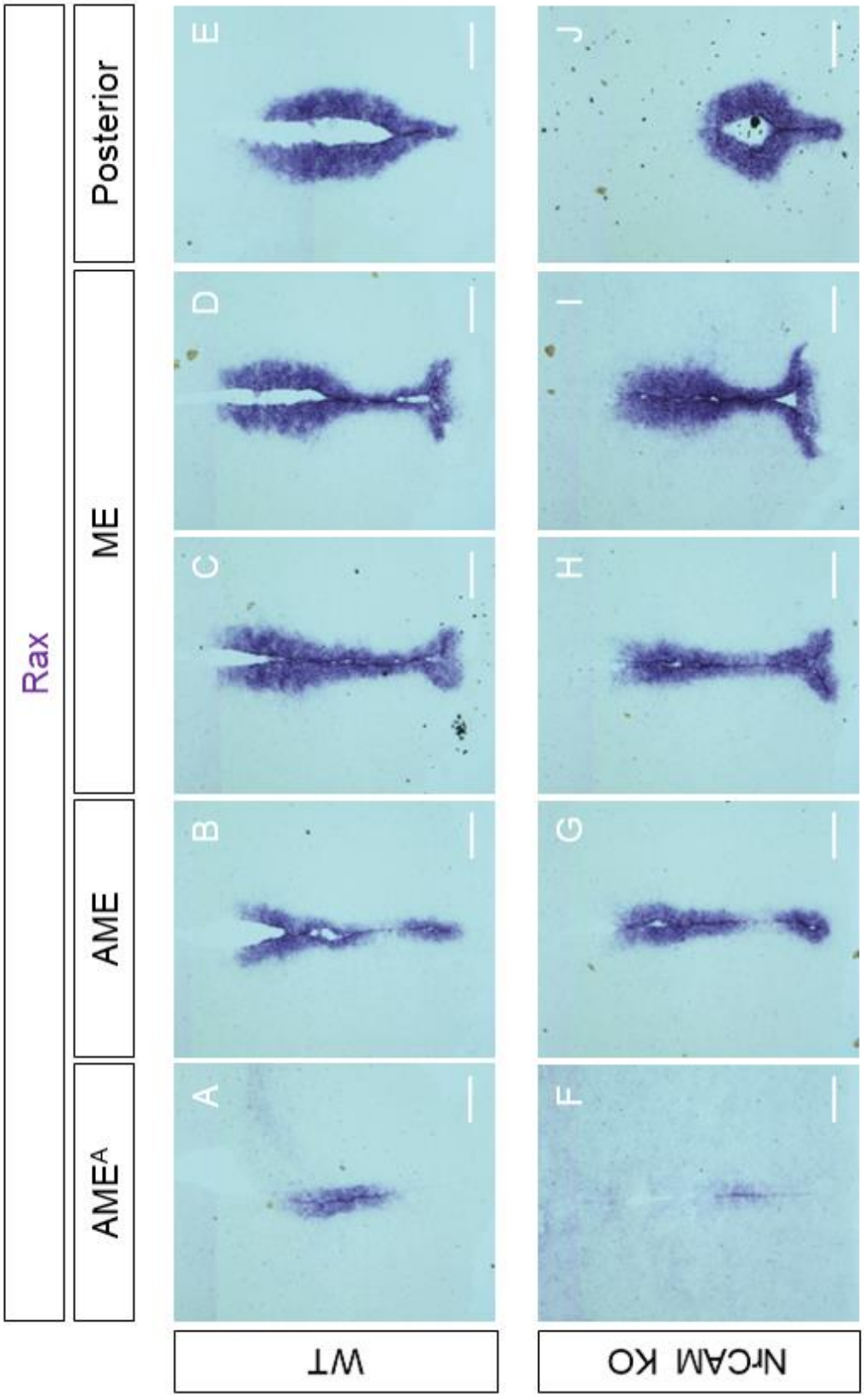

Figure 6.4

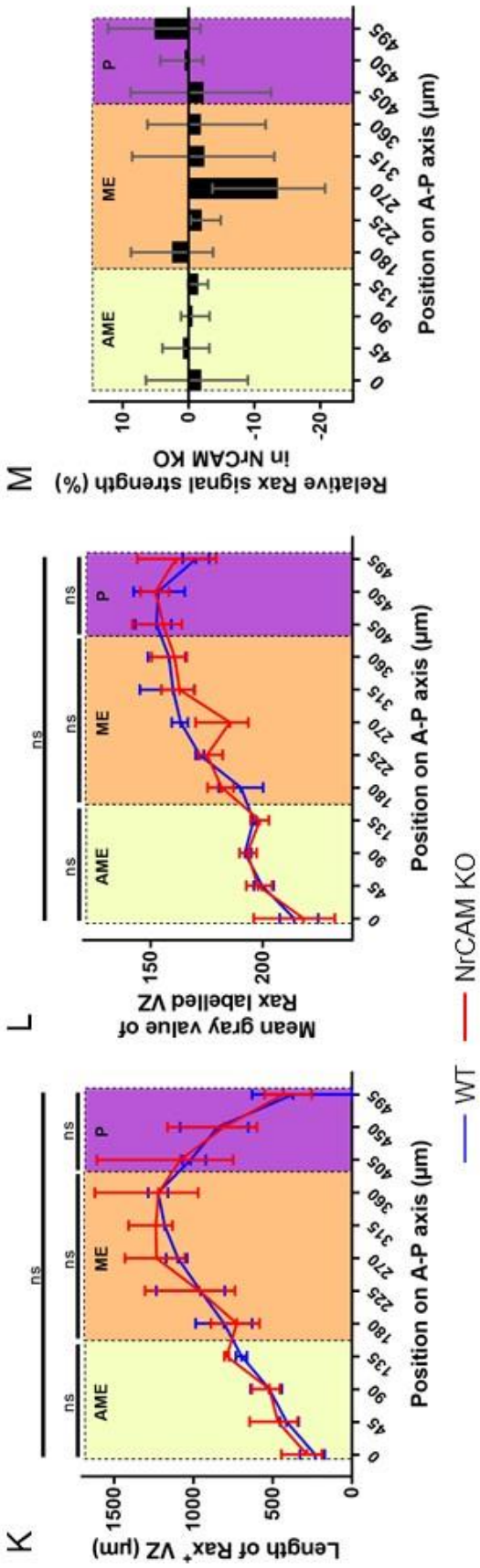
K
Length of Rax+ VZ (µm)
1500
1000
500
0
AME
ME
P
ns
Position on A-P axis (µm)
0
45
90
135
180
225
270
315
360
405
450
495
WT
NrCAM KO
L
Mean gray value of Rax labelled VZ
150
200
M
Relative Rax signal strength (%) in NrCAM KO
10
0
-10
-20

of the *Rax*$^{+}$ VZ domain (Fig 6.4 K), or in the intensity of the Rax chromogenic signal (Fig 6.4 L,M).

6.2.5 Fgf10

In the wild type mouse, *Fgf10* expression initiates in the final section of the AME^{P}, where it expressed weakly in two distinct domains (Fig 6.5 A). These domains appear analogous to the *Rax*$^{+}$ domains of the AME^{P} (Fig 6.4 B). Expression in the NrCAM$^{-/-}$ initiates at the same A-P coordinates, but is seen in the dorsal domain before the tip (Fig 6.5 E). Through the ME^{A} the expression increases in both domains which extend toward each other. The dorsal domain is lost in the ME^{P}, while expression in the base of the 3V gets stronger (Fig 6.5 B,C,F,G). Expression is retained into the P subregion (Fig 6.5 D,H). As explained in section 6.2.4, the morphological differences replicating the plane of section between brains, and wishing to use sections with the clearest labelling.

Expression in the NrCAM$^{-/-}$ mouse is lower in the AME, but broadly mirrors the expression in the wild type through the ME, with no differences in *Fgf10*$^{+}$ VZ domain length or label intensity (Fig 6.5 I-K). However, the Fgf10 mRNA signal intensity is significantly lower in the P subregion of NrCAM$^{-/-}$ mice, and qualitative analysis suggests this decrease begins in the final sections of the ME^{P}/PME subregion. This decrease mirrors the decrease observed in posterior tanycytes in the adult.

6.2.6 Shh

Shh is expressed in the VZ from AME^{A}-ME^{P} in both wild type and NrCAM$^{-/-}$ mice (Fig 6.6 A-H). Similar to *Rax*, *Shh* expression begins in two separate domains which merge at the ME^{A} (Fig 6.6 A-C), however the ventral expression is then lost, leaving only the dorsal expression domain in the ME^{P} (Fig 6.6 D). This dorsal domain is also lost before the transition to the P subregion. Expression in the NrCAM KO is weaker in the initial AME^{A} section (Fig 6.6 E), and its expression in the ventral tip of the 3V of the AME^{P} is reduced in length and intensity (Fig 6.6 F). Expression of *Shh* through the ME appears similar in both genotypes (Fig 6.6 C,D,G,H). Quantitative analysis of the length of the *Shh*$^{+}$ VZ domain and the intensity of the *Shh* signal shows no significant difference between the wild type and the NrCAM$^{-/-}$ mice (Fig 6.6 I-K). However, the data do

Figure 6.5 Comparison and quantification of Fgf10 expression along the anterior-posterior axis of the hypothalamus in E16 wild type and NrCAM KO littermates.
Image composites at 20x magnification of coronal cross-sections showing Fgf10 mRNA expression (purple) by in situ hybridisation in relation to the 3V, ME, and hypothalamic parenchyma along the A-P axis in E16 wild type (A-D) and NrCAM KO (E-H) mice. Scale bars 50µm. Images representative of the n=3 pairs of mice investigated.

I – A graph comparing the length of the Fgf10-expressing domain round the ventral 3V in adult wild type (blue) and NrCAM KO (red) mice. The plotted value at each marked position is the mean of three biological replicates, with the bars showing the range. Using the Wilcoxon signed rank test, no significant difference was observed when values across the whole Fgf10-expressing domain in the wild type and NrCAM KO were compared. No significant difference was seen in the ME and P subregions. The AME contains too few Fgf10+ sections to conduct statistical analysis.

J – A graph comparing the chromogenic signal intensity of the Fgf10-expressing domain round the ventral 3V in adult wild type (blue) and NrCAM KO (red) mice. The plotted value at each marked position is the mean of three biological replicates, with the bars showing the range. The mean gray value gives a readout between 0 (black) and 256 (white) that represents the chromogenic signal intensity, and has been normalised against the background. A lower mean gray value (closer to black) represents a stronger signal strength. Using the Wilcoxon signed rank test, no significant difference was observed across the whole Fgf10 domain in wild type and NrCAM KO E16s. Individual assessment of the ME, and P subregions, showed the mean gray value was significantly lower in the P subregion (P=0.0313) but not the ME subregion. AME contains too few Fgf10+ sections for statistical analysis.

K – A graph comparing the percentage change in relative Fgf10 signal strength in the NrCAM KO when compare to the wild type at each position along the A-P axis. The plotted value at each marked position is the mean of three biological replicates, with the bars showing the range. For each replicate, the normalised mean gray value for Fgf10 in an NrCAM KO section converted to a percentage of the normalised mean gray value in the paired wild type section.

Figure 6.5

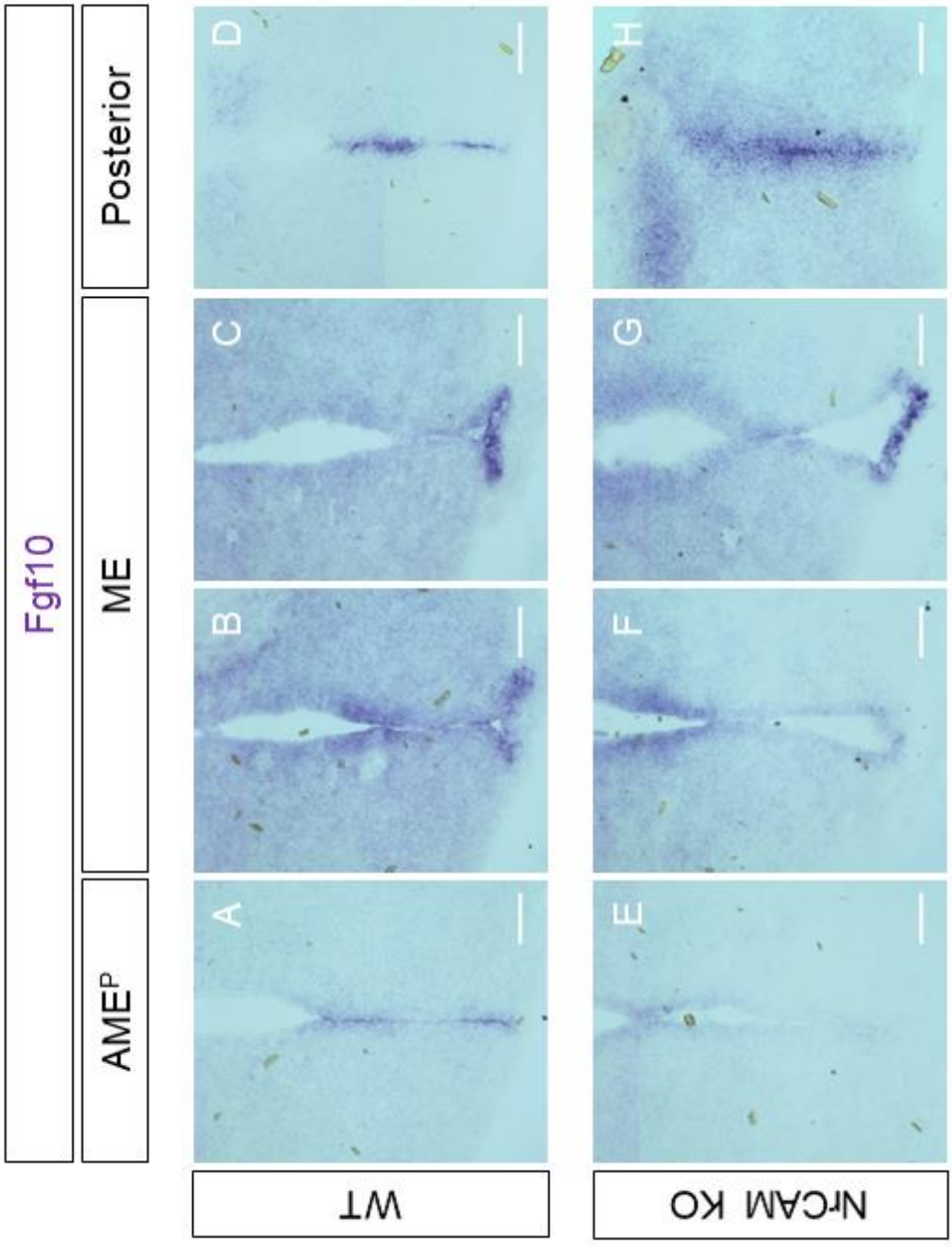

Figure 6.5

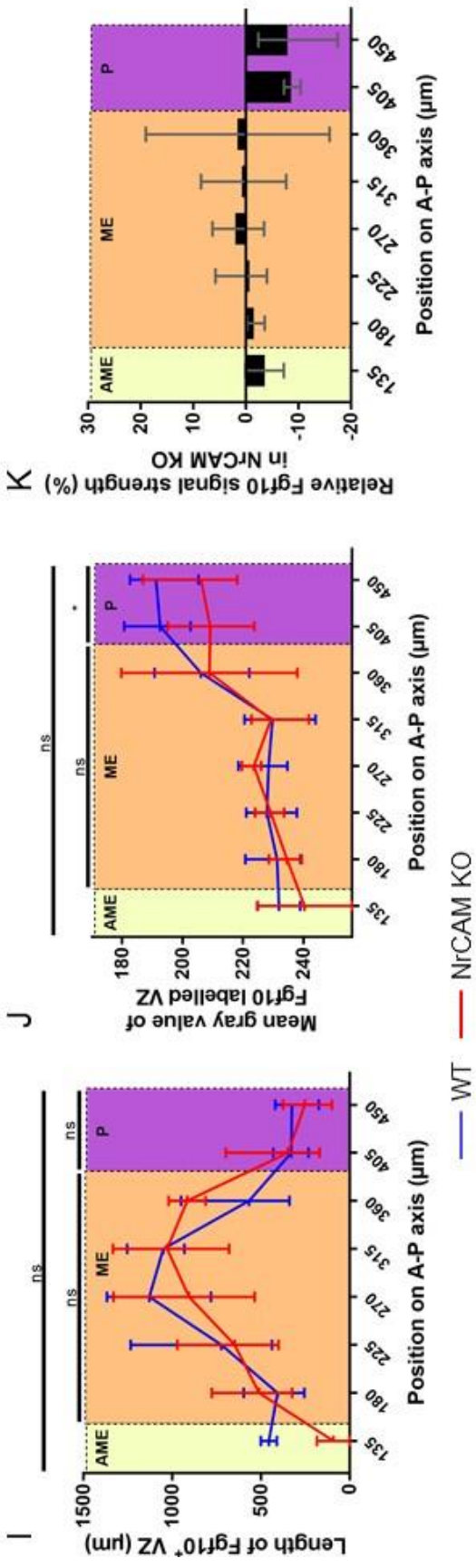
K
Relative Fgf10 signal strength (%) in NrCAM KO
30
20
10
0
-10
-20
AME
ME
P
135
180
225
270
315
360
405
450
Position on A-P axis (µm)
J
Mean gray value of Fgf10 labelled VZ
180
200
220
240
ns
ns
*
AME
ME
P
Position on A-P axis (µm)
I
Length of Fgf10+ VZ (µm)
1500
1000
500
0
ns
ns
ns
AME
ME
P
Position on A-P axis (µm)
WT
NrCAM KO

show a trend that approaches significance for reduced *Shh*$^{+}$ VZ domain length in the NrCAM$^{-/-}$ mice over the AME^{P} subregion where the expression in the ventral tip of the 3V is reduced (Fig 6.6 I). As explained in section 6.2.4, the morphological differences replicating the plane of section between brains, and wishing to use sections with the clearest labelling

6.2.7 TH

Expression of TH at E16 was too low to quantitate, so to examine the embryonic TH^{+} ARC population I used E18 mice. As in the adults, both wild type and NrCAM$^{-/-}$ mice have TH^{+} neurons in the ARC from A-P through the hypothalamus (Fig 6.7 A-H). These are most numerous in the AME subregion, where they are found throughout the ARC (Fig 6.7 B,F). The ME subregion also has many TH^{+} neurons, though here they are found predominantly along the dorsal border of the ARC (Fig 6.7 C,G). Quantitative analysis of all ARC TH^{+} neurons across the whole A-P region showed no significant difference between the wild type and the NrCAM$^{-/-}$ mice (Fig 6.7 I), however, a significant increase in TH^{+} neurons was seen in both the AME and ME subregions of NrCAM$^{-/-}$ mice (Fig 6.7 J). This contrasts with my observations from adult mice, as at this later timepoint the NrCAM$^{-/-}$ mice have fewer ARC TH^{+} neurons. No significant difference was observed in the zona incerta A13 TH^{+} population (Fig 6.7 K-M). This suggests that in the embryo, there is an early increase in TH^{+} ARC A12 neurons, specifically those located in the AME-ME subregions.

6.3 Discussion

These results show that the diminished tanycyte population I observed in adult NrCAM$^{-/-}$ mice is a consequence, at least in part, of abnormal development. A reduction in the quantity of RGCs in the AME-P region suggests that NrCAM is required for the normal development and/or maintenance of this population. *Rax* expression is normal in the NrCAM$^{-/-}$ mice, which suggests NrCAM is not acting upstream of *Rax* at this stage of development. Similarly, *Shh* expression appears mostly normal, though qualitative analysis suggests its expression at the tip of the 3V in the AME^{P} is reduced. It is unclear what effect this might have, and further replicates are required to determine whether this is different from the wild type expression. Expression of *Fgf10* in the 3V tip is also reduced

Figure 6.6 Comparison and quantification of Shh expression along the anterior-posterior axis of the hypothalamus in E16 wild type and NrCAM KO littermates.

Image composites at 20x magnification of coronal cross-sections showing Shh mRNA expression (purple) by in situ hybridisation in relation to the 3V, ME, and hypothalamic parenchyma along the A-P axis in E16 wild type (A-D) and NrCAM KO (E-H) mice. Scale bars 50µm. Images representative of the n=3 pairs of mice investigated.

I – A graph comparing the length of the Shh-expressing domain round the ventral 3V in adult wild type (blue) and NrCAM KO (red) mice. The plotted value at each marked position is the mean of three biological replicates, with the bars showing the range. Using the Wilcoxon signed rank test, no significant difference was observed when values across the whole Shh-expressing domain in the wild type and NrCAM KO were compared. When the AME and ME subregions were individually assessed, no significant difference was seen. Comparison of the AMEP-MEA subregion (90µm-180µm) approached significance (p=0.0547).

J – A graph comparing the chromogenic signal intensity of the Shh-expressing domain round the ventral 3V in adult wild type (blue) and NrCAM KO (red) mice. The plotted value at each marked position is the mean of three biological replicates, with the bars showing the range. The mean gray value gives a readout between 0 (black) and 256 (white) that represents the chromogenic signal intensity, and has been normalised against the background. A lower mean gray value (closer to black) represents a stronger signal strength. Using the Wilcoxon signed rank test, no significant difference was observed when values across the whole Shh-expressing domain in the wild type and NrCAM KO were compared. When the AME and ME subregions were individually assessed, no significant difference was seen.

K – A graph comparing the percentage change in relative Shh signal strength in the NrCAM KO when compare to the wild type at each position along the A-P axis. The plotted value at each marked position is the mean of three biological replicates, with the bars showing the range. For each replicate, the normalised mean gray value for Shh in an NrCAM KO section converted to a percentage of the normalised mean gray value in the paired wild type section.

Figure 6.6

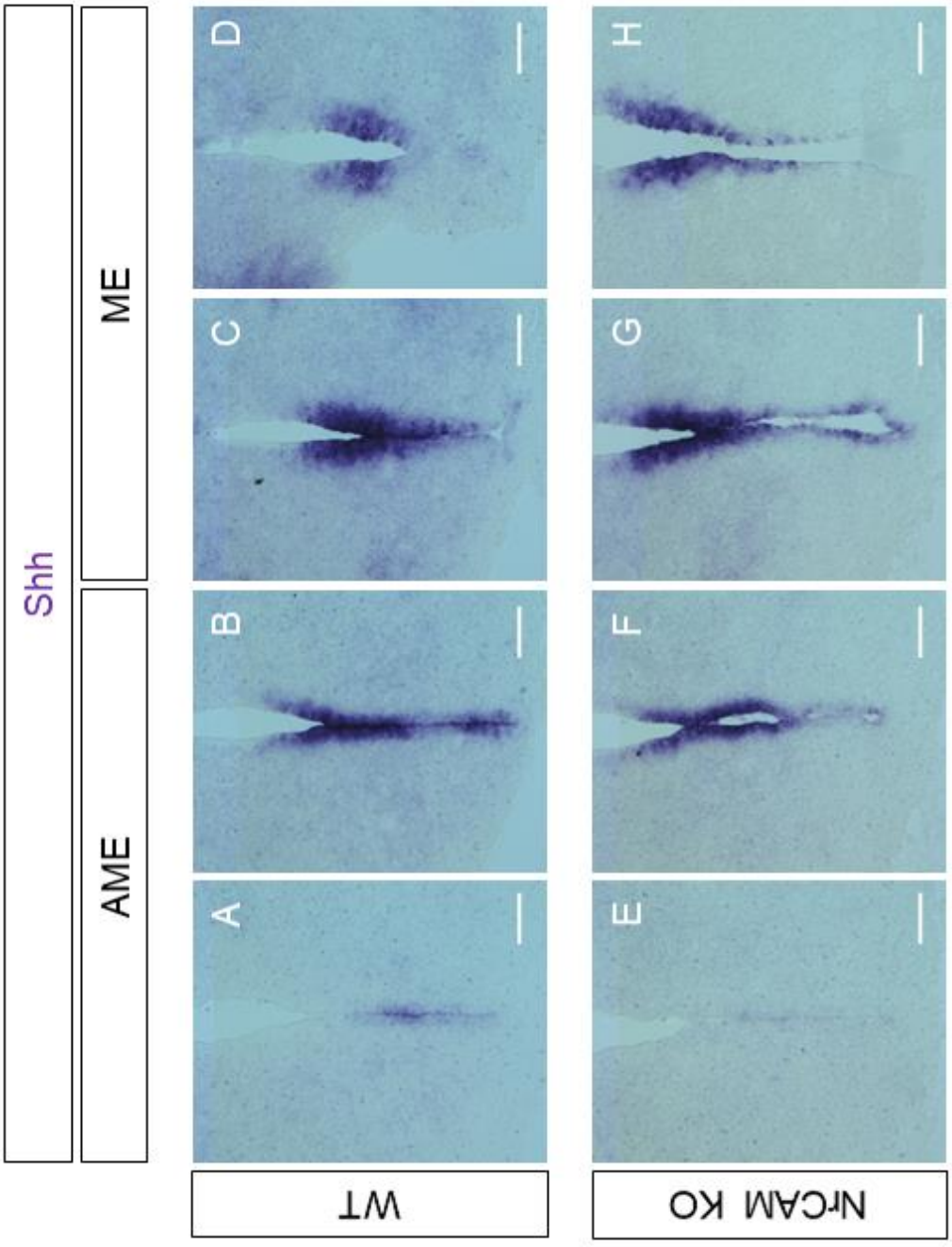

Figure 6.6

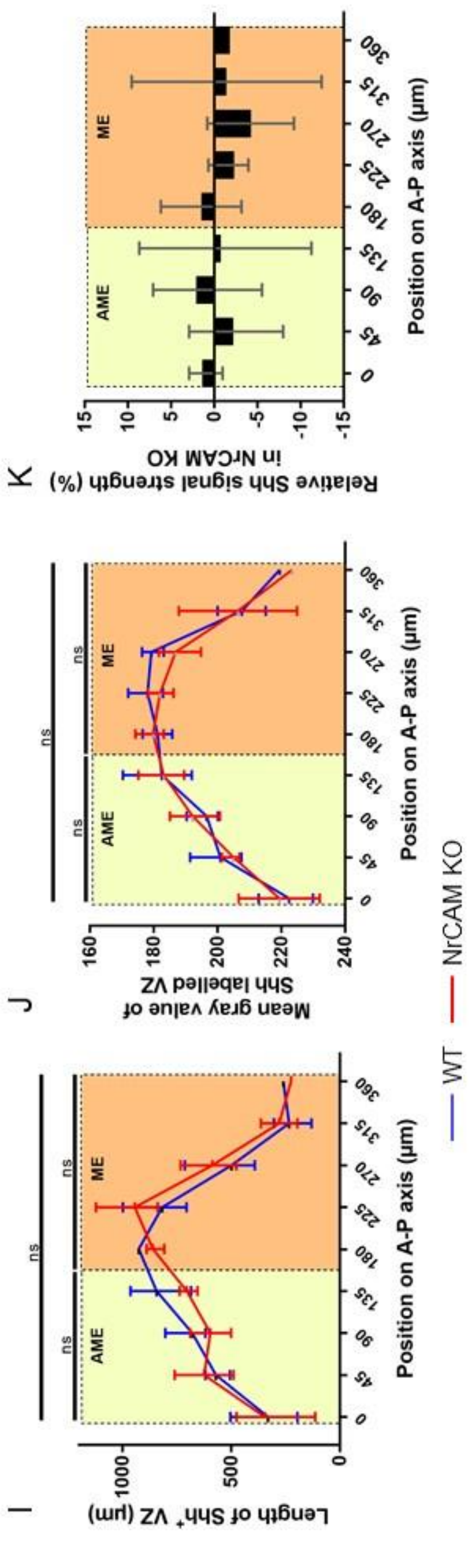
I
Length of Shh+ VZ (µm)
AME
ME
ns
Position on A-P axis (µm)
J
Mean gray value of Shh labelled VZ
K
Relative Shh signal strength (%) in NrCAM KO
WT
NrCAM KO

in the single AME section in which I detect expression, though this sample is not large enough to analyse statistically. Unlike *Rax* and *Shh*, *Fgf10* is significantly reduced in the P subregion of E16 NrCAM$^{-/-}$ mice. This correlates with the reduction of *Fgf10* in the PME/P subregions in adult NrCAM$^{-/-}$ mice. This suggests that NrCAM is acting upstream of *Fgf10* expression at E16.

While several studies have linked *Shh* and *Rax* to hypothalamic progenitors, and shown *Rax* localisation in the VZ, none have explicitly linked these signals to hypothalamic RGC specification and maintenance prior to tanycyte maturation (Lu et al., 2013; Muthu et al., 2016; Orquera et al., 2016; Salvatierra et al., 2014). As a consequence, I cannot directly tie losses of these RGCs to abnormalities in *Rax* and *Shh* signalling pathways. However, if *Rax* and *Shh* are important for specifying and/or maintain these RGCs, one may hypothesise that NrCAM may be acting downstream or in parallel to these signals, with NrCAM KO causing disruption to the normal specification or maintenance of RGCs.

To further complicate things, little is known about A-P (R-C) dynamics of hypothalamic proliferation and development in mouse. In the chick, the Fgf10^{+} tuberal region gives rise to both the anterior and mammillary progenitors, as well as the infundibulum (Fu et al., 2017). I have observed that the length AME-P region is consistent between wild type and NrCAM$^{-/-}$ mice, and there are more TH^{+} A12 neurons in the NrCAM$^{-/-}$ mice, so loss of NrCAM is not grossly impacting this early expansion. However, it has not been shown whether this Fgf10^{+} domain continues to contribute to further anterior or posterior domain later in hypothalamic expansion. A second hypothesis suggests the early Fgf10^{+} progenitors of the tuberal hypothalamus are retained in the ME/P subregions, and the decrease of *Fgf10* in the P subregion of NrCAM$^{-/-}$ mice leads to reduced proliferation of RGC precursors and fewer AME-P RGCs.

In a further hypothetical scenario, NrCAM could be involved in regulating the balance of proliferation and differentiation in AME-P RGCs. If loss of NrCAM leads to an imbalance in proliferation/differentiation in AME-P RGCs, where it is normally expressed, this could result in fewer RGCs and more TH^{+} neurons. To extrapolate upon this hypothesis further, fewer RGCs may then mean a smaller multipotent tanycyte population in postnatal mice, which in turn may lead to lower turnover of new tanycytes and TH^{+} neurons, converting the initial excess

of TH^+ neurons into a deficit, and further diminishing the tanycytes.

A further observation of interest is that in E16 mice, NrCAM and Nestin labelling intensity appears to reduce posteriorly, which is in direct contrast to adult mice where the expression of these markers increases posteriorly. We have hypothesised that in adult mice the neural stem cells may sit posteriorly (in the PME) (Figs 4.9 and 4.10), and that this localisation is linked to the increase in strength of tanycyte markers. The diminished expression at E16 may be for a variety of reasons. One possibility is that RGCs located posteriorly in the embryo are, or have recently been, highly proliferative, or proliferating at a higher rate than anterior RGCs, and as a consequence the otherwise high expression of NrCAM and Nestin has been diluted. An alternative hypothesis is that temporal differences in tanycyte differentiation may lead to differences in marker expression from A-P. As the anterior hypothalamus develops before the posterior hypothalamus (Fu et al., 2017; Muthu et al., 2016), it is possible that the anterior RGCs are initiating expression of these markers earlier, which manifests as an increase in these markers relative to their more posterior counterparts.

To determine whether any of these hypotheses are accurate, either separately or in combination, further analysis at a greater array of timepoints is required. Firstly, it is crucially important to determine when expression of NrCAM begins in the pre-hypothalamic neuroepithelium. Effects on earlier processes can be investigated, and progenitor populations can be examined after this point to deduce when the reductions in RGCs and P subregion *Fgf10* first emerge. Further investigation of tanycytes, *Rax*, *Shh*, *Fgf10*, and TH^+ neurons at P14 and P45 will provide information on the transition from the phenotype observed in the embryo, to that seen in adult, whilst keeping the work comparable to previous investigations on *Rax* and tanycytes in the postnatal period (Miranda-Angulo et al., 2014; Salvatierra et al., 2014). Finally, analysis at late life timepoints can describe whether the loss of tanycytes and TH^+ neurons in $NrCAM^{-/-}$ is progressive after maturation.

To examine these embryonic mice, I subdivided the hypothalamus into anterior, AME, ME, and P based on the morphological characteristics, deliberately omitting the PME region I describe in adult mice. This was not because the

transition zone from ME to P is not present, but because this transition zone in the embryo contains few sections. It would be difficult to accurately make meaningful qualitative comparisons of this diminutive region between mice, and quantitative analysis would not be statistically robust. Instead, I added the sections that may be classed as PME to the ME region on the basis that they still contain the median eminence. Overall, I believe this was the most effective way to analyse these sections, however one particular exception has arisen.

In Figure 6.7 J it is clear that both wildtype and NrCAM$^{-/-}$ ME sections can be split into two distinct subgroups, those with high quantities of TH^{+} cells, and those with low quantities of TH^{+} cells. In the adult mouse, sections from the ME subregion contains many TH^{+} cells, whilst sections from the PME contain few TH^{+} cells. The two subgroups that appear to be present in the embryonic ME subregion may be a consequence of including PME sections in the ME subregion. On this basis, one could argue that the embryonic ME and PME should be split into separate subregions, however I concluded that this would illicit more complications than the problems it solved, as it may make analysis of the other markers I have investigated weaker. An alternative would be to include PME sections in the P subregion, however this means grouping sections containing median eminence-projecting RGCs with regions that only have RGCs projecting to the parenchyma, which may obscure the special nature of the RGC/median eminence relationship. As the grouping of subregions along a spectrum is an arbitrary exercise in forcing simplicity onto a complex phenomenon to allow analysis, and no simplistic grouping will sufficiently describe the true variation across the spectrum, I decided to maintain the inclusion of PME sections in the ME subregion to bolster the majority of my analyses.

With this examination of NrCAM$^{-/-}$ mice during the late embryonic period, I have shown that abnormalities exhibited in adult NrCAM$^{-/-}$ are initiated in development. I have not, however, addressed whether the adult hypothalamic progenitor population has been impacted by loss of NrCAM. In Chapter 7 I will examine the capacity of adult hypothalamic tissue from NrCAM$^{-/-}$ mice to proliferate and differentiate.

Figure 6.7 Comparison and quantification of TH expression along the anterior-posterior axis of the hypothalamus in E18 wild type and NrCAM KO littermates.

Images at 20x magnification of coronal sections showing TH (red) expression by immunofluorescence in the ARC along the A-P axis with nuclear DAPI staining (blue) in adult wild type (A-D) and NrCAM KO (E-H) mice. Scale bars 50µm. Images representative of the n=3 pairs of mice investigated.

I – Quantification of TH^+ cells along the A-P axis of the ARC in three pairs of E18 wild type and NrCAM KO littermates. Each icon represents a single measurement, collected as described in Chapter 2.2.5.2. Bars show 1 SD either side of the mean value. Analysis by unpaired t-test showed no significant difference of TH^+ cells between the wild type and the NrCAM KO.

J – Quantification of TH^+ cells in the ARC in A, AME, ME, and P subregions, in three pairs of E18 wild type and NrCAM KO mice. Each icon represents a single measurement, collected as described in Chapter 2.2.5.2. Bars show 1 SD either side of the mean value. Analysis by unpaired t-test showed significant increases of TH^+ cells in the ARC of NrCAM KO mice in the AME and ME subregions (AME P=0.0044; ME P=0.0390). No significant difference was seen in the A or P subregions.

Images at 10x magnification of coronal sections showing TH (red) expression by immunofluorescence in the dorsal AME Zona Incerta (A13) population with nuclear DAPI staining (blue) in E18 wild type (K) and NrCAM KO (L) littermates. Scale bars 50µm. n=3 mice.

R – Quantification of TH^+ cells in the dorsal AME Zona Incerta (A13) population in three pairs of E18 wild type and NrCAM KO littermates. Each icon represents a single measurement, collected as described in Chapter 2.2.5.2. Bars show 1 SD either side of the mean value. Analysis by unpaired t-test showed no significant difference of TH^+ cells in dorsal AME Zona Incerta (A13) population between E18 wild type and NrCAM KO mice (P=0.7339).

Figure 6.7

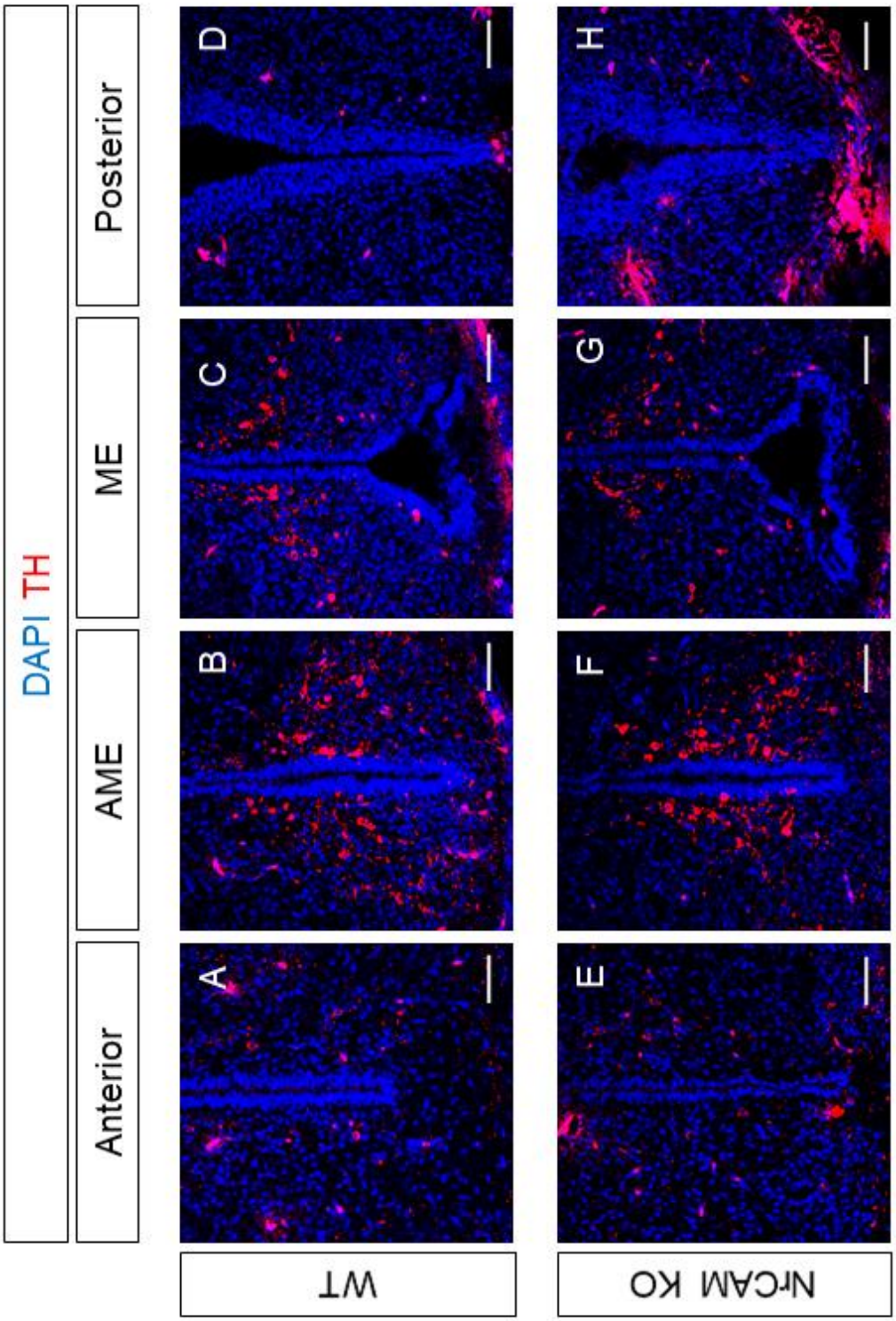

Figure 6.7

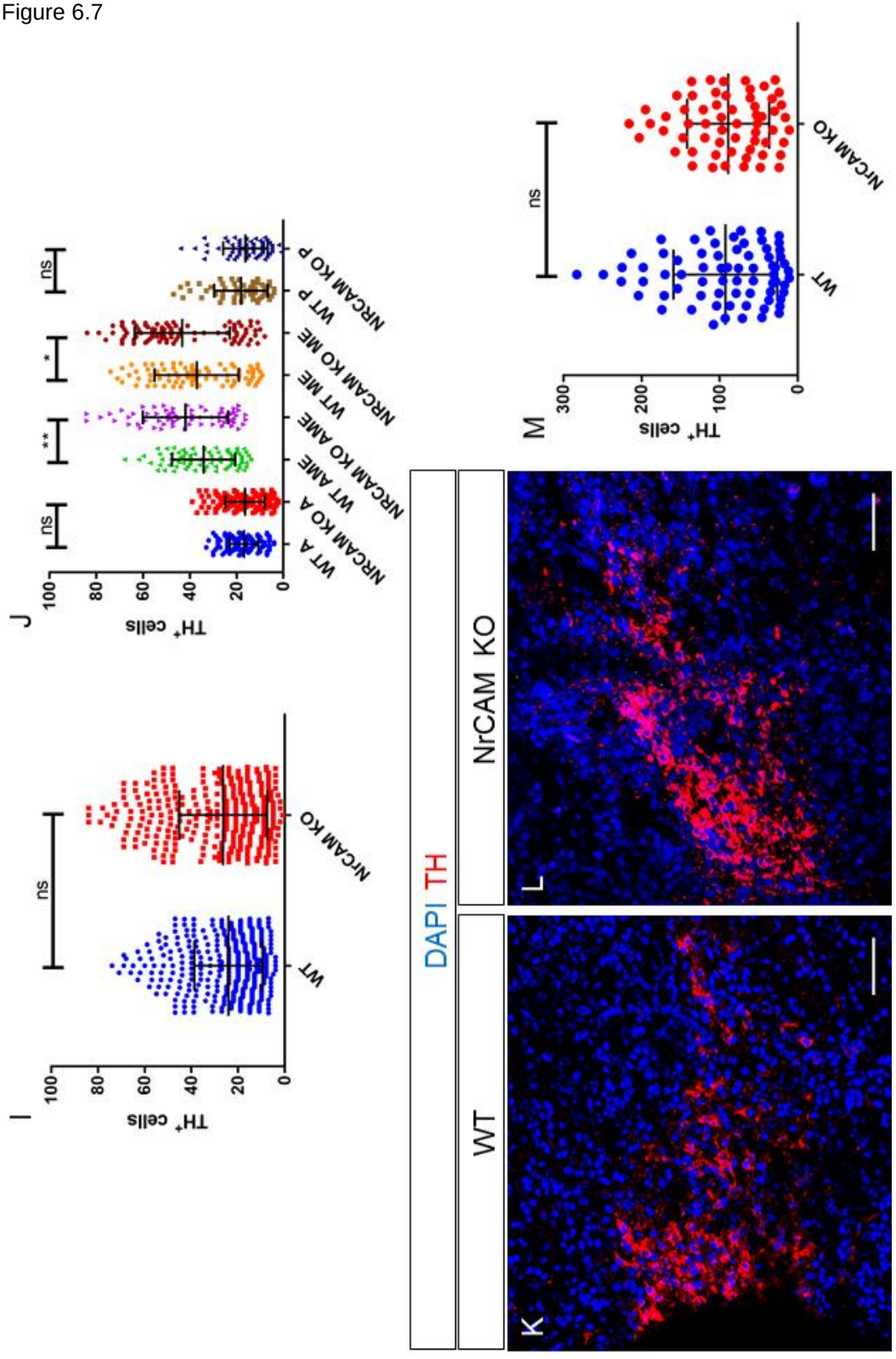
DAPI TH
WT
NrCAM KO
K
L
M
TH+ cells
ns
WT
NrCAM KO
I
J
WT A
NRCAM KO A
WT AME
NRCAM KO AME
WT ME
NRCAM KO ME
WT P
NRCAM KO P
*
**

CHAPTER 7: *EX VIVO* INVESTIGATION OF HYPOTHALAMIC NEUROGENESIS

7.1 Introduction

A variety of recent studies have described neurogenesis in the adult mouse hypothalamus (Haan et al., 2013; Kokoeva et al., 2005, 2007; Lee et al., 2014; Li et al., 2012; Pierce and Xu, 2010; Robins et al., 2013b, 2013a; Wang et al., 2012; Yulyaningsih et al., 2017). This has been accomplished using a range in *in vivo* and *in vitro* techniques. Each of these methods has its own strengths and weaknesses, and as a result, published studies may use a combination in arguing their conclusions.

While a recent study described a method for live-imaging neurogenesis in adult mouse hippocampus (Pilz et al., 2018), such techniques have not yet been utilised in hypothalamus. As a consequence, no one has directly observed neurogenesis in the hypothalamus. Instead, studies which show *in vivo* neurogenesis use inducible or injectable labels that mark dividing cells and their progeny, which can then be viewed after sacrifice of the animal (Haan et al., 2013; Kokoeva et al., 2007; Lee et al., 2014; Pierce and Xu, 2010; Robins et al., 2013b, 2013a; Yulyaningsih et al., 2017). An alternative *in vitro* technique that allows direct observation of proliferative capacity is the neurosphere assay (Reynolds and Weiss, 1992). This assay takes single cells dissociated from neural tissue and grows them in suspension. Cells capable of proliferation generate floating spherical colonies, and repeated successful passaging and dissociation of neurosphere cultures indicates a competent self-renewing population. This assay has been used to investigate proliferative potential of adult hypothalamic tissue (Li et al., 2012; Robins et al., 2013a; Xu et al., 2005b). Careful dissection of the ependymal region has suggested that the hypothalamic tanycytes are neurospherogenic (Robins et al., 2013a).

One criticism of the neurosphere assay is that dissociation to single-cells and growth in culture media removes the local signals and support provided by the niche a progenitor may occupy. The capability of a cell to divide under the conditions of such an assay may not represent a predisposition for that cell to

undergo proliferative behaviour *in vivo*. Given the distinct radial-glial morphology of tanycytes and their localisation at the ventricular zone, one may question whether dissociating and growing tanycytes in suspension is a useful way to test their proliferative capacity. Neurogenesis has also been investigated in postnatal hypothalamic tissue using slice cultures and other explant techniques which retain tissue integrity (Decourtye et al., 2017; Robins et al., 2013a).

I have shown that adult NrCAM$^{-/-}$ mice have fewer tanycytes, which are thought to include a progenitor population (Haan et al., 2013; Hendrickson et al., 2018; Lee et al., 2014; Li et al., 2012; Robins et al., 2013a). Furthermore, I have shown that NrCAM$^{-/-}$ mice have more ARC TH^{+} neurons during neurogenesis, but fewer in adulthood. I have hypothesised that the depleted tanycyte population may be a cause and/or consequence of diminished or unbalanced postnatal proliferation, which in turn leads to a reduced ARC TH^{+} neuron population. Previous studies from our lab have shown that hypothalamic neurospheres express NrCAM (Chapter 1.4.2, Fig 1.5B). In this chapter I will describe initial investigations into the proliferative capacity of the adult NrCAM$^{-/-}$ mouse hypothalamus using the neurosphere assay and explant culture.

7.2 Results

7.2.1 Investigation of proliferation and differentiation using the neurosphere assay

To investigate whether adult NrCAM$^{-/-}$ mice retain a self-renewing tanycyte population observed in wild type mice (Li et al., 2012; Robins et al., 2013a; Xu et al., 2005b), I established long-term neurosphere cultures. Previous studies investigating neural stem cells and progenitors have suggested that tissue without stem cells or progenitors should not survive after the first passage, and that tissues with only short-lived progenitors may survive 2-3 passages before the culture fails (Reynolds and Rietze, 2005; Reynolds and Weiss, 1992; Seaberg and van der Kooy, 2002). Wild type hypothalamic tissue

Figure 7.1 Comparison of the competency for adult wild type and NrCAM$^{-/-}$ mouse hypothalamic tissue to yield sustainable neurosphere cultures

A – Comparison of the number of neurospheres yielded per well of 10000 cells, 6 days after passaging. Both wild type and NrCAM$^{-/-}$ mouse adult hypothalamic tissue was capable of yielding neurosphere cultures that could be maintained across >10 passages. Wide variation in the number of neurospheres yielded for each replicate was observed in both wild type and NrCAM$^{-/-}$ tissue cultures. Analysis by 2-way ANOVA showed no significant difference in the number of neurospheres per well between wild type and NrCAM$^{-/-}$ tissue across the 2-11 passage period that was analysed. N=4 pairs of cultures, with each culture derived from the hypothalamus of two mice.

B – The concentration of dissociated cells after passaging was recorded as a proxy measurement for the total number of cells produced over the inter-passage period. A greater cell concentration may be indicative of a higher rate of proliferation within a culture. Wide variation in the cell concentration for each replicate was observed in both wild type and NrCAM$^{-/-}$ tissue cultures. Analysis by 2-way ANOVA showed no significant difference in the number of neurospheres per well between wild type and NrCAM$^{-/-}$ tissue across the 2-11 passage period that was analysed. N=4 pairs of cultures, with each culture derived from the hypothalamus of two mice.

A

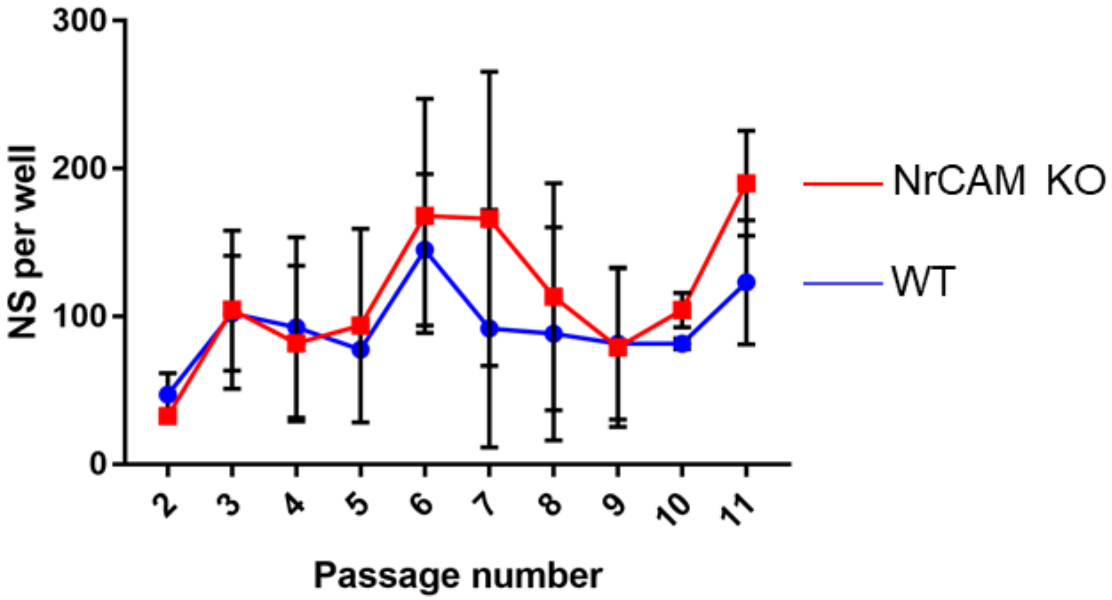
300
200
100
0
NS per well
2
3
4
5
6
7
8
9
10
11
Passage number
NrCAM KO
WT

B

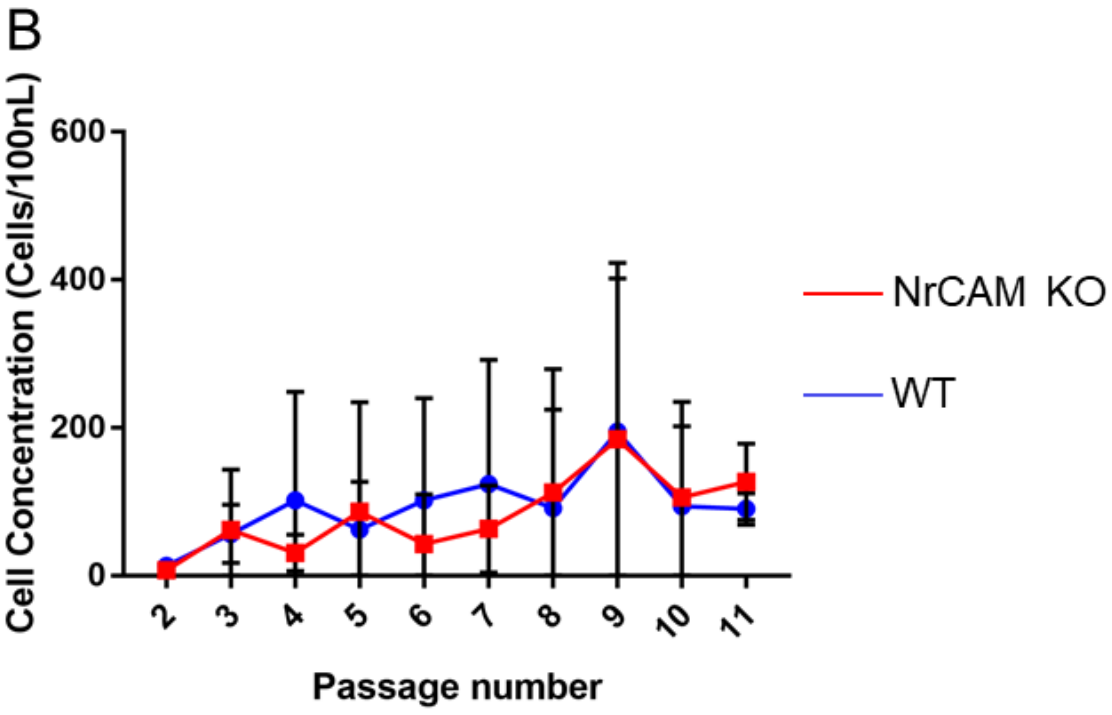
600
400
200
0
Cell Concentration (Cells/100nL)
2
3
4
5
6
7
8
9
10
11
Passage number
NrCAM KO
WT

from ventral VZ/SVZ domain of the central/ME hypothalamic subregion has been shown to support neurosphere cultures lasting beyond 10 passages (Robins et al., 2013a). These neurospheres broadly express Sox2, Nestin, Vimentin, and GFAP, which label tanycytes *in vivo*. Unpublished experiments from our lab have shown that neurospheres from adult wild type hypothalamic tissue broadly express NrCAM, which further supports the hypothesis that tanycytes include a self-renewing $NrCAM^{+}$ population (Fig 1.5 B).

Dissociated cells from adult wild type and $NrCAM^{-/-}$ mouse hypothalamic tissue were therefore cultured side by side and passaged every 6 days. Cultures from both wild type and $NrCAM^{-/-}$ mice were maintained beyond 10 passages with no sign of losing the competence to self-renew (Fig 7.1). The latest passage observed was passage 14. The number of neurospheres and the quantity of cells yielded over each inter-passage period varied greatly between replicates of both wild type and $NrCAM^{-/-}$ tissue cultures, but no significant difference was seen between the cultures of each genotype (Fig 7.1 A,B). These data show that both wild type and $NrCAM^{-/-}$ adult mice retain a hypothalamic population capable of self-renewal under the conditions of the neurosphere assay.

The neurospheres were then used to investigate the capacity of the self-renewing cells to produce daughters that can differentiate into a variety of hypothalamic cell types, in line with previous research that differentiated neurospheres derived from central hypothalamic tissue (Robins et al., 2013a). Both wild type and $NrCAM^{-/-}$ neurosphere cultures yielded $Nestin^{+}$ cells (Fig 7.2 A,B), which in the wild type included a subpopulation of $Nestin^{+}NrCAM^{+}$ cells (Fig 7.2 A). This subpopulation may be analogous to the tanycytes. MAP2 was used to label neuronal cells, and its expression saw wide overlap with the ARC neuronal markers NPY and GHRH in wild type and $NrCAM^{-/-}$ cultures (Fig 7.2 C-F). Six3 was seen in nuclei scattered through both cultures, and its expression did not overlap with the few cells labelled by the RIP antibody, which is known to label CNP in mature oligodendrocytes (Fig 7.2 G-H). The astrocyte and tanycyte marker GFAP was seen widely throughout wild type and $NrCAM^{-/-}$ cultures (Fig 7.2 I,J). No TH neurons were identified in wild type or $NrCAM^{-/-}$ cultures (not shown), though unpublished experiments using from others in our lab using adult wild type hypothalamic tissue have suggested TH^{+} neurons can be generated during neurosphere differentiation. This discrepancy

Figure 7.2 Comparison of progeny from differentiated neurospheres from adult wild type and NrCAM$^{-/-}$ mouse hypothalamic tissue cultures

Neurospheres from 8th passage wild type and NrCAM$^{-/-}$ cultures were plated and differentiated for 21 days before immunofluorescence and DAPI labelling (blue). Wild type and NrCAM$^{-/-}$ cultures both showed labelling for Nestin (A,B 20x), but NrCAM labelling was only seen on wild type cultures on a subset Nestin^{+} cells. Comparable labelling was seen in wild type and NrCAM$^{-/-}$ cultures labelled for NPY/MAP2 (C,D 20x MIP), GHRH/MAP2 (E,F 20x MIP), Six3/RIP (G,H 40x MIP), and GFAP (I,J 40x MIP). No TH labelled cells were identified in wild type or NrCAM$^{-/-}$ cultures. 14 day and 28 day cultures yielded cells expressing the same range of markers shown. Differentiation for each of the three durations (14, 21, and 28 days) was conducted once (n=1 biological replicate), with 8 technical replicates consisting of wells containing a single neurosphere. Scale bars 50µm.

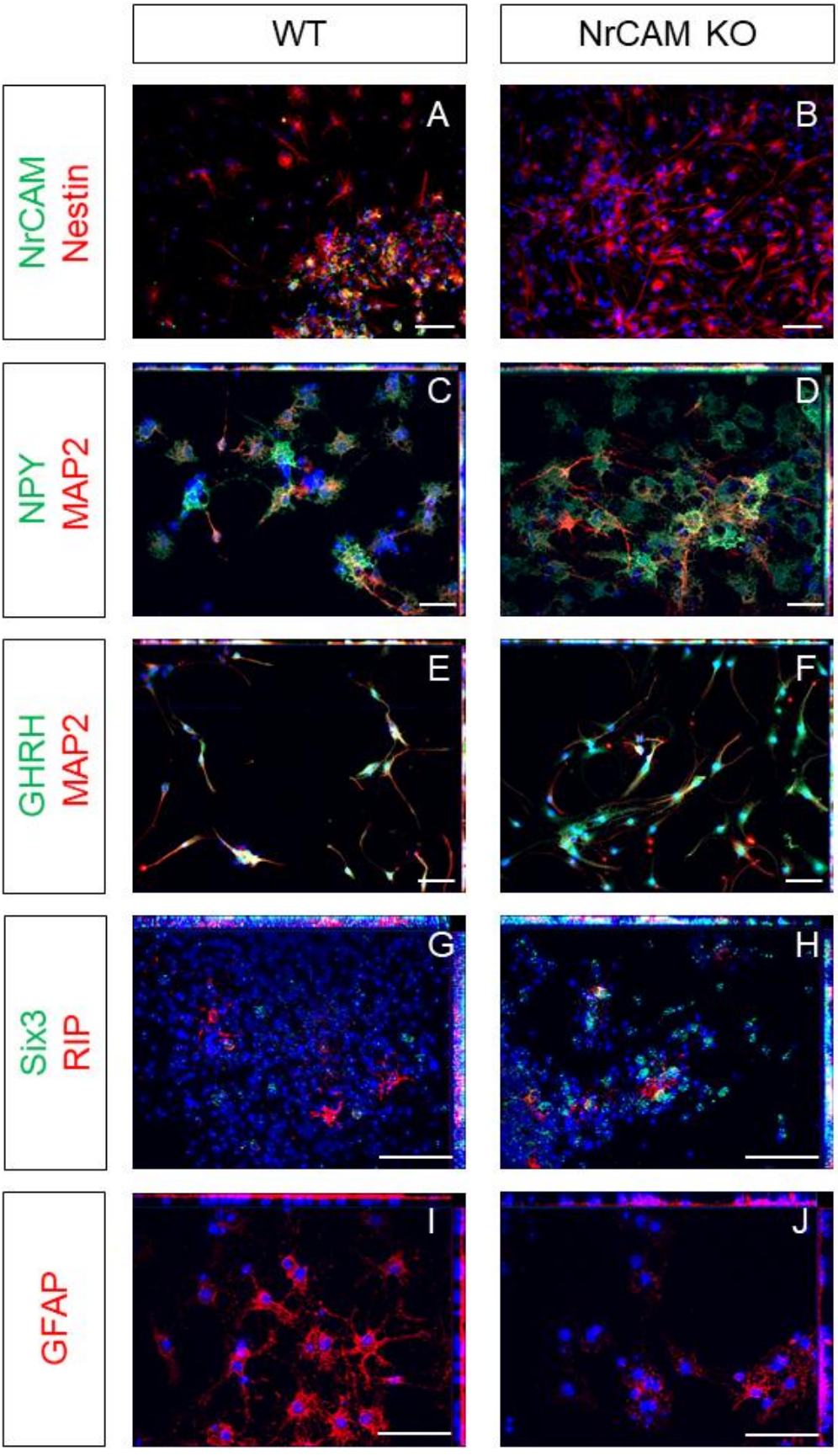
WT
NrCAM KO
NrCAM
Nestin
NPY
MAP2
GHRH
MAP2
Six3
RIP
GFAP
A
B
C
D
E
F
G
H
I
J

may have arisen because I differentiated late-passage (8th) neurospheres, while they used early-passage (2nd) neurospheres. These data show that late-passage neurospheres from both wild type and NrCAM$^{-/-}$ mouse adult hypothalamic tissue can undergo multipotent differentiation into a variety of cell types found within the hypothalamus.

7.2.2 Investigation of proliferation and differentiation of hypothalamic explant cultures

The neurosphere cultures I have described were derived from a large quantity of tissue from the ME-containing hypothalamus, and, therefore, do not no specifically show that the tanycyte population was responsible for the expansion of the culture. Additionally, the neurosphere assay takes cells out of their local niche to grow in suspension. Stem cells are known to interact with cells and signals from the local environment of their niche, and these will not be present in this experiment. In an attempt to overcome these limitations, we dissected the ventral VZ and SVZ domain from anterior, ME, and posterior subregions of the adult hypothalamus, and cultured these explants embedded in a collagen matrix for 7 days. Explants were created from adult wild type, NrCAM$^{+/-}$, and NrCAM$^{-/-}$ mouse hypothalamus. Over the culture period, the explants of all genotypes showed significant outgrowth (Fig 7.3 C,D), indicating that the VZ/SVZ domain of wild type, NrCAM$^{+/-}$, and NrCAM$^{-/-}$ all contain cells capable of proliferation.

Labelling of uncultured wild type control explants with TH did not show any TH^{+} cells, indicating the dissected tissue did not contain TH^{+} neurons from the adjacent ARC prior to culture (Fig 7.4 A). By contrast, after culturing explants for 7 days, wild type, NrCAM$^{+/-}$, and NrCAM$^{-/-}$ explants contained TH^{+} cells, suggesting these were progeny of the cells contained within the explants (Fig 7.4 B-E). Co-labelling NrCAM$^{+/-}$ and NrCAM$^{-/-}$ explants for TH and HuC/D, which specify neuronal identity and maturation (Fig 7.4 D,Di,Dii)(Akamatsu et al., 2005), showed that the majority of TH^{+} cells also expressed HuC/D, and were indeed TH^{+} neurons (Fig 7.4 F). Approximately half of HuC/D^{+} neurons were TH^{+}, indicating that explants contained other TH^{-} neurons (Fig 7.4 G). The observations were similar in explants from all three subregions, and no significant difference was seen between NrCAM$^{+/-}$ and NrCAM$^{-/-}$ explants.

Figure 7.3 Growth of VZ explant cultures from hypothalamic tissue

A – Ventral view of an adult mouse brain. The boxed region contains hypothalamic tissue collected for neurospheres and explants. Scale bar 1mm.

B – Coronal section through the ME subregion collected using a tissue chopper. Scale bar 400µm.

C – VZ/SVZ dissected from the section in panel. This tissue is ready to be embedded in a collagen matrix for explant culture. Scale bar 200µm.

D – The VZ/SVZ explants from panel C after 7 days culture. Explant growth has established bubble-like formations and neurite-like protrusions. Scale bar 200µm.

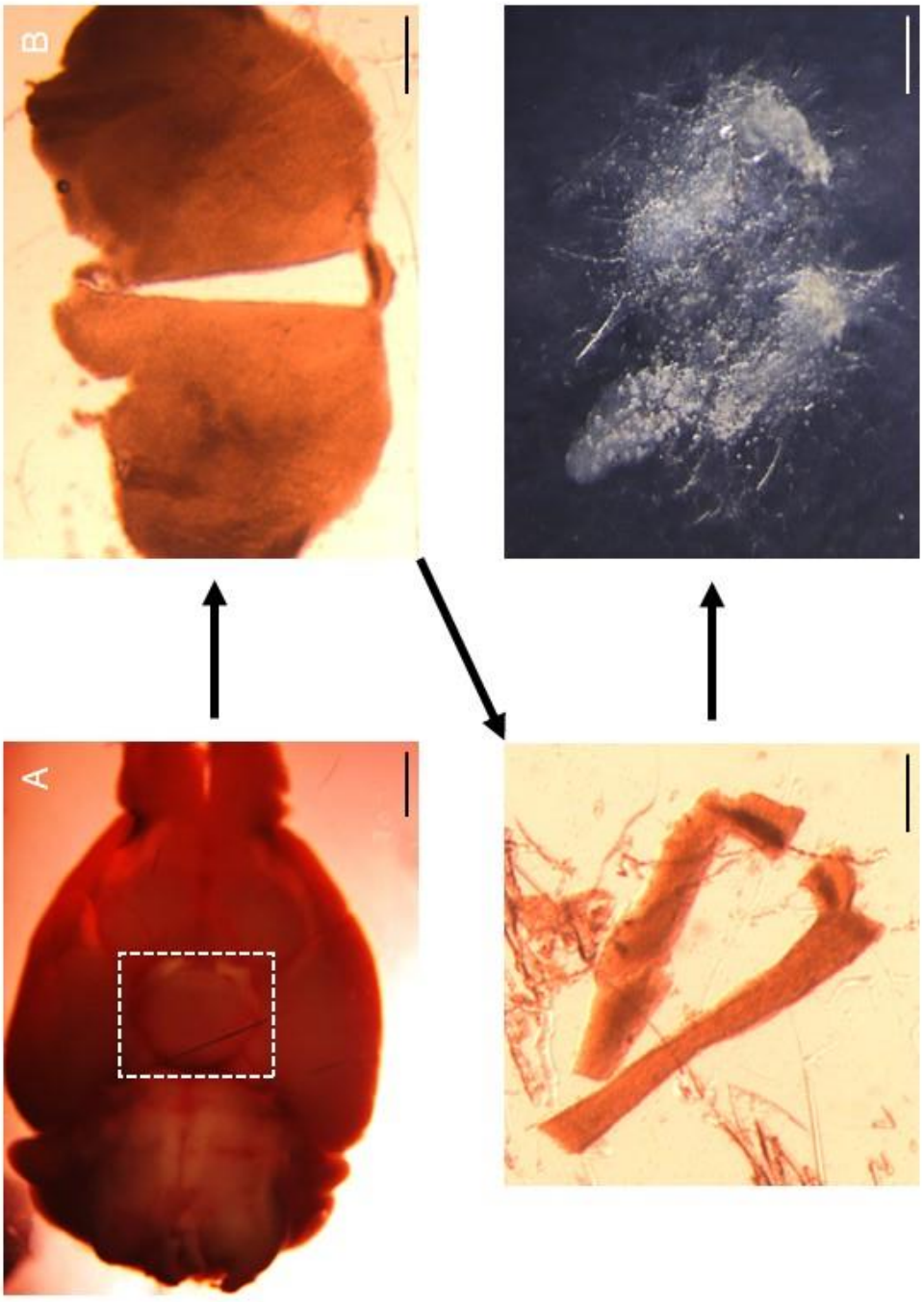
B
A

NrCAM$^{+/-}$ and NrCAM$^{-/-}$ explants were also co-labelled for TH and phosphor-Histone 3 (pH3), which labels mitotic cells (Hans and Dimitrov, 2001; Wei et al., 1998) (Fig 7.4 C,Ci,Cii). pH3 was expressed broadly through the explants, confirming that proliferation was occurring in the cultured tissue. A significant minority of TH^{+} cells were pH3^{+} (Fig 7.4 H), and a minority of pH3^{+} cells expressed TH. No significant difference was seen between NrCAM$^{+/-}$ and NrCAM$^{-/-}$ explants. Together, these results show that proliferation is occurring within the cultured explants, and neurogenic cells give rise to TH^{+} neurons that were absent from uncultured explants.

7.3 Discussion

The results in this chapter confirm that the adult NrCAM$^{-/-}$ mouse retains a hypothalamic population capable of long-term self-renewal and multipotent differentiation *in vitro*. As such, the loss of NrCAM, which causes a reduction in the tanycyte and ARC TH^{+} neuron populations, does not remove all capability of tanycytes to proliferate and differentiate. Indeed, between my explant experiments and the differentiation of early passage neurospheres by others in our lab, we have identified the TH^{+} neurons can be produced *de novo* by adult hypothalamic tissue, ostensibly from the ventral VZ/SVZ region inhabited by tanycytes, and this capability is retained in tissue from NrCAM$^{-/-}$ mice. These experiments do not, however, inform us whether loss of NrCAM causes a change in the rate of proliferation, or an imbalance in differentiation, particularly in an *in vivo* context.

The neurosphere experiments I conducted determined the quantity of neurospheres and total number of cells produced in both wild type and NrCAM$^{-/-}$ cultures are not significantly different. However, large variations in both these outputs were seen between replicates, and this inter-replicate variability may mask any changes in the rate of proliferation. As a consequence we cannot rule out the hypothesis that the loss of NrCAM reduces the turnover of the hypothalamic stem or progenitor population.

Differentiating late-passage neurospheres showed that both wild type and NrCAM$^{-/-}$ adult hypothalamic stem-like cells can give rise to a variety of hypothalamic cells types. However, I have not investigated the proportion of

Figure 7.4 Immunofluorescence analysis of VZ explant cultures from adult hypothalamic tissue

VZ and adjacent parenchyma was dissected from adult wild type, NrCAM$^{+/-}$, and NrCAM$^{-/-}$ mice and prepared for explant culture. Wild type tissue prepared for immunofluorescenct analysis on the day of dissection and used as a no-culture did not label for TH (A), demonstrating that ARC tissue was not included in the dissected VZ tissue. After 7 days of culture, wild type explants were shown to contain TH^{+} cells (B). N=1 one mouse used to derive multiple explants. 20x magnification, scale bars 50µm.

Co-labelling cultured explants with TH and pH3 (C,Ci,Cii) showed TH^{+}pH3^{-} cells (red arrow head), TH^{+}pH3^{+} cells (yellow arrow head), TH^{-}pH3^{+} cells (green arrowhead), and TH^{-}pH3^{-} cells (DAPI only). Co-labelling cultured explants with TH and HuCD (D,Di,Dii) showed TH^{+}HuCD^{-} cells (red arrow head), TH^{+}HuCD^{+} cells (yellow arrow head), TH^{-}HuCD^{+} cells (green arrowhead), and TH^{-}HuCD^{-} cells (DAPI only). N=4 mice used to derive multiple explants. 20x magnification, scale bars 50µm.

Anterior hypothalamus (Ant), ME hypothalamus (ME), and posterior hypothalamus (Post) cultured explants from adult NrCAM$^{+/-}$ and NrCAM$^{-/-}$ mice were compared for TH, pH3, and HuCD labelling. Quantitative analysis of the total number of TH^{+} cells per explant showed no significant difference between the NrCAM$^{+/-}$ and NrCAM$^{-/-}$ explants in any of the three subregions (E). The proportion of TH^{+} cells that were also HuCD^{+} (F), and HuCD^{+} cells that were also TH^{+} (G), were assessed, and no significant difference was seen between the NrCAM$^{+/-}$ and NrCAM$^{-/-}$ explants. The proportion of TH^{+} cells that were also pH3^{+} (H), and pH3^{+} cells that were also TH^{+} (I), were assessed, and no significant difference was seen between the NrCAM$^{+/-}$ and NrCAM$^{-/-}$ explants. No NrCAM$^{-/-}$ Anterior explants were assessed for pH3 and TH. N=2 pairs of NrCAM$^{+/-}$ and NrCAM$^{-/-}$ used to derive multiple explants for comparison.

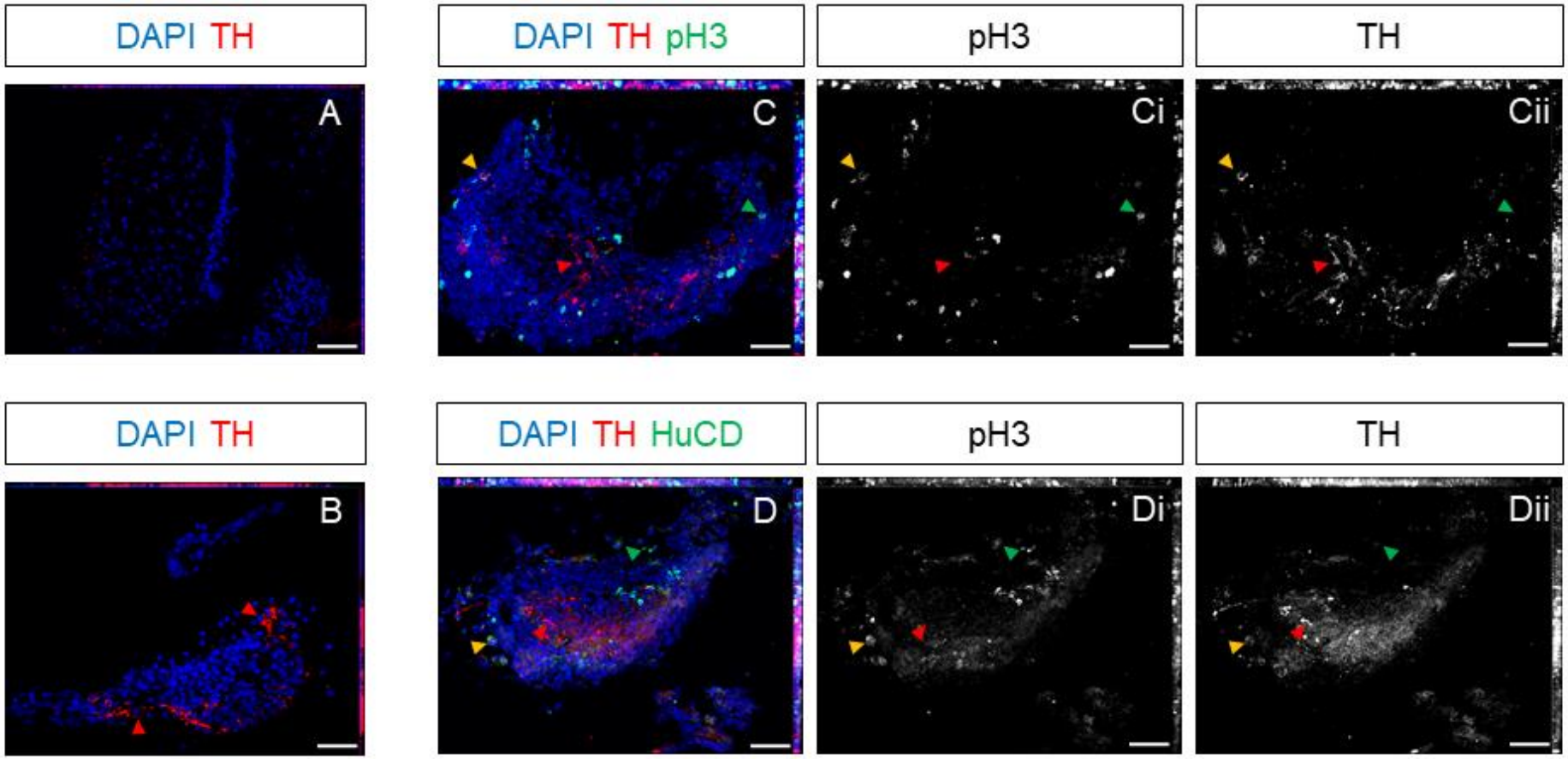
DAPI TH
A
DAPI TH pH3
C
pH3
Ci
TH
Cii
DAPI TH
B
DAPI TH HuCD
D
pH3
Di
TH
Dii

TH+ cells per explant section
HuCD+ cells that are TH+ (%)
TH+ cells that are HuCD+ (%)
TH+ cells that are pH3+ (%)
pH3+ cells that are TH+ (%)
NrCAM Het Ant
NrCAM KO Ant
NrCAM Het ME
NrCAM KO ME
NrCAM Het Post
NrCAM KO Post

cells labelled by the range of hypothalamic markers, and as a consequence I cannot use these results to address the hypothesis that loss of NrCAM causes an imbalance of differentiation and selection of different cell fates. In addition, the failure to yield TH^+ neurons from late passage neurospheres, when TH^+ neurons have been generated from primary explant cultures or in early-passage neurosphere differentiation cultures conducted by others, suggests long-term neurosphere culture may induce changes in differentiation competency. Research on embryonic stem cells and induced pluripotent stem cells has found that long term culture can induce chromosomal and transcriptional changes that confer a growth advantage, and may come at the expense of other patterns of differentiation (Amps et al., 2011; Gokhale et al., 2015). From this, one may hypothesise that long-term neurosphere culture inhibits the selection of a TH^+ neuron fate in differentiated cultures. Alternatively, the capacity to produce TH^+ neurons from primary explants and early-passage neurosphere cultures may be due to the presence of short-lived progenitors which can yield TH^+ neurons, but cannot self-renew over the long-term, and are not replaced by self-renewing stem-like cells.

Culturing ventral VZ/SVZ explants from confirmed that cells this region from this region could proliferate (pH3-labelling) and differentiate into HuC/D^+ and TH^+ cells. Due to tissue scarcity I was only able use wild type hypothalamic tissue for my initial explant experiments that demonstrated explant growth and TH^+ cell differentiation. For the follow up experiment, quantitating TH, pH3, and HuC/D in the explants, I was limited to $NrCAM^{+/-}$ mice for comparison against $NrCAM^{-/-}$ mice. As I have not previously assessed whether $NrCAM^{+/-}$ mice are phenotypically abnormal, I am unable to draw any solid conclusions about potential differences between wild type and $NrCAM^{-/-}$ mice. In addition to this, the low numbers of samples used meant that the pH3/TH-labelled anterior subregions had too few explants to statistically compare. Where sufficient sections were present for observation, the statistical analysis I carried out was of limited use. Quantitating the total number of TH^+ cells per explant section is not a useful metric without also quantitating the total number of cells per explant section. This additional measurement could be used to establish the overall proportion of proliferating ($pH3^+$), and *de novo* differentiating (TH^+ and/or HuC/D^+) cells in wild type and $NrCAM^{-/-}$ explants. Such data can address

whether loss of NrCAM causes any change in the rate of proliferation or neuronal differentiation. Despite these experimental flaws, this preliminary experiment successfully demonstrates that wild type, NrCAM$^{+/-}$, and NrCAM$^{-/-}$ adult hypothalamic VZ/SVZ tissue can proliferate and differentiate, and establishes this culture method for further exploring hypothalamic stem and progenitor behaviour *in vitro*.

While these preliminary *in vitro* experiments failed to allow for strong conclusions to be drawn about the potential effects of NrCAM KO on the rate of adult hypothalamic stem/progenitor cell proliferation and differentiation, both culture techniques may contribute to our overall understanding of whether NrCAM impacts adult and embryonic hypothalamic stem/progenitor behaviour by supplementing other experiments. Improvements may include analysing wild type and NrCAM$^{-/-}$ explants with a wider array of tanycyte and ARC markers, comparing the proportions of these markers relative to the total number of cells per explant, and incorporating a BrdU-chase or lineage-tracing to track progeny. Using this culture technique in combination with *in vivo* analysis of proliferation and differentiated through lineage-tracing and BrdU-Chase experiments could provide robust evidence for further investigating the effects of NrCAM KO in both adult and embryonic mice, and assessing the ability of tanycytes to produce TH^{+} ARC neurons.

CHAPTER 8: DISCUSSION

8.1 Experimental outcomes and hypotheses

In my research I set out with the dual aims of investigating tanycytes and the neurogenic niche along the A-P axis of the hypothalamus, and beginning to evaluate the presence and role of NrCAM on tanycytes. I approached the first aim by characterising a range of tanycyte markers, signals, and neuronal populations across the A-P axis, and have created models detailing my findings. I have confirmed NrCAM as a tanycyte-specific marker in the hypothalamus, and I have conducted comparisons of NrCAM KO mouse hypothalamus in adulthood, development, and *in vitro* to establish the effects that occur when it is lost. I will discuss my findings in detail below.

8.1.1 Anterior-posterior positioning defines tanycyte subsets

The first key outcome of my research is that tanycytes do not reside neatly in the widely used α and β subset domains normally defined in the DV axis adjacent to the medium eminence (Fig 1.1 B) (Rodríguez et al., 2005), but instead, within the AME, ME, PME, and P subregions that I have defined (Fig 4.9), the dorso-ventral localisation of tanycytes and their various markers go through significant changes (discussed in Chapter 4.3). For example, the tanycytes located in the ventral AME subregion are more similar in expression pattern to the more dorsal of the ME subregion, which previous research has described as α2-tanycytes. Most similarity is seen between Figure 1.1B and Figure 4.9 in the panel that represents a section through the ME^{P}, as this section includes 4 distinct subsets of tanycytes. Despite this, the model I propose does not match entirely, as classically the α2-tanycytes have been described as projecting to the ARC, whilst I show two distinct populations with ARC projections. This suggests that the defining tanycyte subsets by their projections is insufficient, and that a greater emphasis must be on using combinations of tanycyte markers to describe their localisation. A ventral population of the ME^{P} subregion appears to lack many of the markers expressed by the surrounding tanycytes, such as *Rax*, *Fgf10*, and Six3, and this may be analogous to the β2-tanycyte population which has been described in some previous research as

including a neurogenic population (Lee et al., 2012, 2014).

Whilst the majority of research investigating tanycytes shows their location in ME sections, tanycytes are most densely packed within the PME and P subregions. This coincides with increased expression of the pan-tanycyte markers Nestin, NrCAM, and *Rax* in these posterior regions (Chapter 4), and of highest expression of markers that are associated with neural stem/progenitor populations (Six3, Fgf10, Rax, Nestin) (Hendrickson et al., 2018; Muthu et al., 2016; Orquera et al., 2016; Park et al., 2010; Xenaki et al., 2011). From my analysis of marker expression I have proposed a model in which different tanycyte subsets occupy nested arcs that extend anteriorly from the PME/P subregions (Fig 4.10).

8.1.2 Do the newly identified Shh$^+$ cells of the PME constitute a stem cell population?

The second novel outcome of my research is my observation of *Shh* expression in the adult mouse hypothalamus (Fig 3.8). Previously undescribed, *Shh* appears to be expressed in a handful of ventral tanycytes in the ME^P/PME^A subregion. This expression coincides with the ventral ME^P population of tanycytes in which neither *Fgf10*, *Rax*, nor Six3 can be detected (or are detected at very low level), potentially the β2-tanycyte subset (Fig 4.9). The important exception to this observation is in the PME subregion, where *Shh* expression appears to coincide with expression of *Fgf10*, *Rax*, Six3, and GFAP. The concentration of this array of markers associated with stemness may indicate a link to the embryonic *Shh*$^+$*Fgf10*$^+$ cells hypothesised to drive hypothalamic growth (Fu et al., 2017)(discussed in Chapter 1.3.1). Indeed, the *Shh*$^+$*Fgf10*$^+$ embryonic stem cells give rise to *Shh*$^+$*Fgf10*$^-$ progenitors that reside directly anterior and adjacent to the stem cells (Fig 1.4 C), in a location that may be analogous to the *Shh*$^+$*Fgf10*$^-$ cells of the ventral ME^P tanycyte domain. Based on these observations, we hypothesise that *Shh*$^+$*Fgf10*$^+$ stem cells that drive embryonic growth are retained ventrally in the PME/P of adult mice, and that these cells give rise to the more anterior tanycytes arranged in nested arcs, with those proximal to the PME/P expressing a greater number of the stem/progenitor-associated tanycyte markers (Fig 4.10). While these tentative hypotheses are certainly interesting, they are currently based upon extrapolation from limited data. Further co-localisation analysis of markers, lineage-tracing of *Shh*$^+$*Fgf10*$^+$ cells, and assessment of the A-P

dynamics of proliferation within the hypothalamus (as described below) are required to see if this hypothesis stands up to scrutiny.

8.1.3 NrCAM is a tanycyte-specific marker within the hypothalamus

The third outcome of this research is the establishment of NrCAM as a marker of all tanycyte (Chapter 4). Its expression within the hypothalamus is specific to tanycytes and it appears to be expressed on all tanycyte subsets. These qualities suggest it is a superior marker of tanycyte identity when compared to the other tanycyte markers which are either not expressed in all tanycytes (GFAP/Six3/*Fgf10*/*Shh*), or are not specific to tanycytes (Nestin/*Rax*/Sox2/GFAP/Six3) (Fig 4.9). It is also superior to the widely used tanycyte marker Vimentin which, though strongly expressed in tanycytes, is also expressed in the dorsal ependymocytes of the 3V (Robins et al., 2013a). No antibodies to mouse Rax are widely available, and as a consequence it can only be detected by ISH, limiting the cellular resolution of analysis. Compared to Nestin, NrCAM also has the added advantage of being a cell surface marker, rather than an intermediate filament marker, which in this circumstance allows improved visualisation of process and cell body morphology. As a cell surface marker, NrCAM has future utility in live cell selection, while the internal markers Nestin and Rax do not. In addition to labelling tanycytes, in the E16 mouse hypothalamus NrCAM specifically labels the RGCs of the AME-P region neuroepithelium (Fig 6.2), widely believed to be tanycyte precursors (Salvatierra et al., 2014; Wang et al., 2012). This provides scope for using NrCAM as a label for investing tanycytes and their precursors from late embryonic development, through the juvenile period and into adulthood.

8.1.4 Loss of NrCAM causes reductions in tanycytes and TH^+ neurons following abnormal development

Finally, I have investigated the effect of NrCAM KO on the mouse hypothalamus (Chapters 5-7). Loss of NrCAM was confirmed using an anti-NrCAM antibody. $NrCAM^{-/-}$ adult mice have a uniform reduction of $Nestin^+$ tanycytes throughout AME-P domains (Fig 5.2). This is coupled to reduced ARC TH^+ neuron populations that differentiate in the parenchyma in proximity to tanycytes (Fig 5.10). As these neurons do not express NrCAM (Fig 5.9), the loss in this population must be caused by an indirect effect of loss of NrCAM. No reduction of TH^+ neurons is seen in the

nearby thalamic zona incerta A13 TH^+ population (Fig 5.10), a population outside the hypothalamus, indicating that reduction is specific to the hypothalamus, and not part of a global reduction of TH^+ neurons. The length of the tanycyte-containing domain (i.e. AME-P domain) is not reduced in NrCAM KO mice, suggesting that the reductions I have observed are not due to a universal reduction in growth of the hypothalamus.

In addition, I have identified decreases in *Fgf10* and *Rax* expression in the PME/P subregions (Fig 5.3-5.6), decreases in the number of *Rax*$^+$ cells of the median eminence parenchyma (Fig 5.3, 5.4), and a trend towards a reduction of *Shh*$^+$ cells in the ME^P/PME subregion (Fig 5.7, 5.8). If the PME subregion is indeed the site of the adult hypothalamic stem cells, as we have suggested in section 8.1.2, one may hypothesise that the reductions in these markers may be linked to a reduction in stem cell activity, leading to the loss of tanycytes and neurons. However, as shown in chapter 7, the NrCAM KO mouse retains hypothalamic cells capable of self-renewing and differentiating *in vitro*, so it is clear that NrCAM KO does not remove all cells with stem/progenitor capability. The effect of losing NrCAM must be subtle, such as a reduced stem/progenitor population, reduced survival, or an imbalance in proliferation and differentiation.

The hypothalamic phenotype of the $NrCAM^{-/-}$ mouse appears to emerge at least in part from developmental abnormalities. At E16 I have identified a reduction in the density of Nestin$^+$ RGCs of the AME-P region (Fig 6.3).This indicates that the loss of tanycytes in not purely an adult onset phenotype. Furthermore, a reduction in *Fgf10* expression is seen in the P subregion (Fig 6.5), and I have also observed a potential decrease in ventral *Shh* (Fig 6.6, discussed Chapter 6.3). These data are comparable to the reductions I saw in the expression of the same genes in adult NrCAM KO mice, suggesting that NrCAM may be acting upstream of these signals from late developmental stages through until adulthood. However, the loss of NrCAM does not interfere with early hypothalamic specification and growth, as hypothalamic length, morphology, and early markers such as Rax are unaffected (Chapter 6). It is therefore unlikely that NrCAM is acting upstream of Rax prior to E10 when hypothalamic specification is occurring (Fu et al., 2017; Lu et al., 2013; Manning et al., 2006).

In contrast to adult mice, E18 NrCAM$^{-/-}$ mice have increased numbers of TH^{+} neurons in the AME and ME subregions (Fig 6.7). Together these data show that from embryo to adulthood in NrCAM$^{-/-}$ mice there is a progression from an increased to decreased ARC TH^{+} population, and from normal *Rax* expression to reduced expression of *Rax* in the PME/P. From this we can surmise that the NrCAM KO hypothalamic phenotype begins during development, and may progress after the embryonic period to give the phenotype observed in adult NrCAM$^{-/-}$ mice if these are causally linked.

In support of this, I have observed that *Rax*$^{+}$ median eminence parenchymal cells (Chapter 4.3) cannot be detected in wild type and NrCAM$^{-/-}$ mice at E16 (Fig 6.4), but have been produced by the adult time point. The populations produced in the NrCAM$^{-/-}$ mice are significantly reduced by comparison to the adult wild type mice (Fig 5.3, 5.4), but the production of these cells after the late embryonic period in both the wild type and NrCAM$^{-/-}$ mice shows that NrCAM$^{-/-}$ mice must also retain at least some cells capable of producing new cells in late development. This is supported by my *in vitro* experiments showing that both wild type and NrCAM$^{-/-}$ adult tissue is capable of proliferating and differentiating as neurospheres and explants (Chapter 7).

8.1.5 Hypotheses addressing mechanisms leading to the NrCAM KO hypothalamic phenotype

To address potential mechanisms for the hypothalamic phenotypes of NrCAM$^{-/-}$ mice, I have generated a set of hypotheses to explore (Fig 8.1). In the first hypothesis, loss of NrCAM causes reduced production of RGCs from pre-RGC progenitor cells. So far there is limited data to support or dispute this hypothesis, because it is unclear exactly when NrCAM expression begins in the hypothalamus, i.e. whether NrCAM is already expressed in a pre-RGC progenitor. This hypothesis could account for the reduction in AME-P RGCs at E16, but does not explain why we see an increase in ARC TH^{+} neurons which then decrease in the postnatal period. Any effect on a prior progenitor population must be limited to the tuberal hypothalamus, as the thalamic zona incerta TH^{+} neurons are unaffected, and it must have no effect on the overall growth of the tuberal hypothalamus, which appears the same in wild type and NrCAM$^{-/-}$ mice.

Figure 8.1 – Effect of NrCAM KO on RGCs and tanycytes

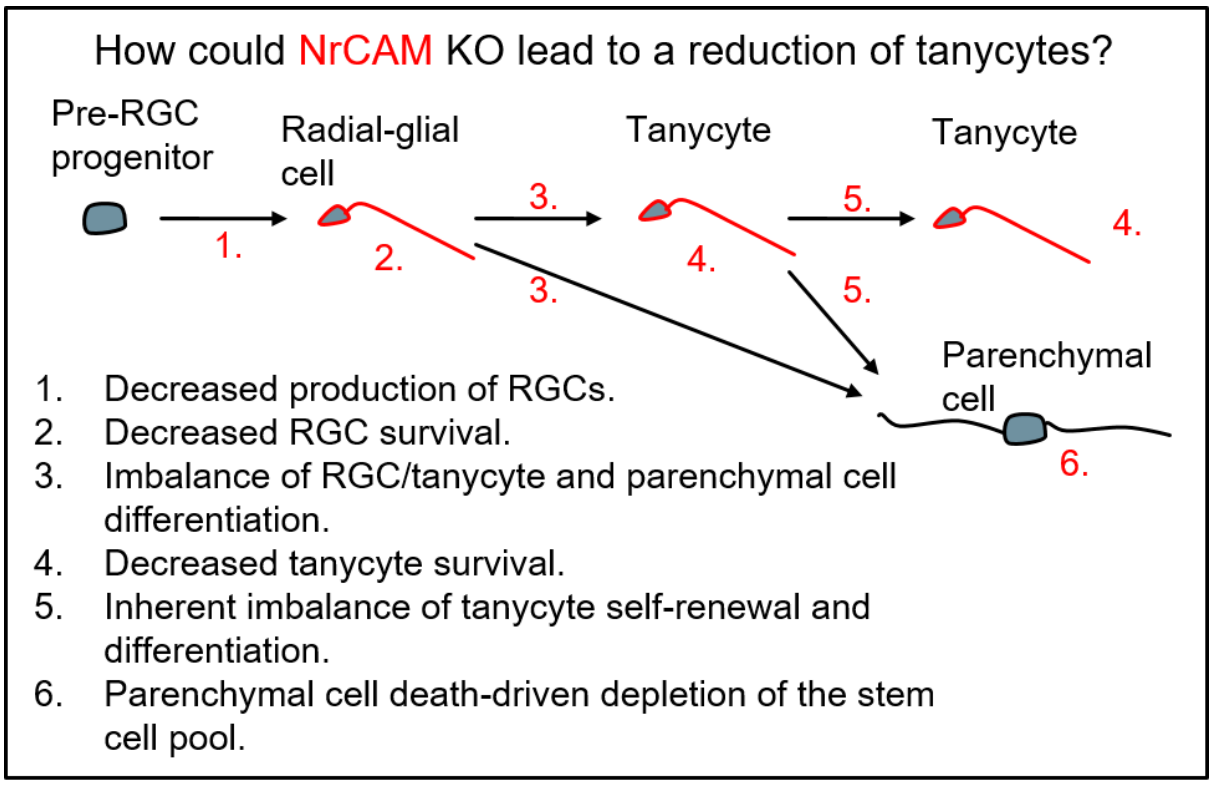

A second possibility is that NrCAM is required for RGC survival. In such a scenario, hypothalamic growth and generation of RGCs occurs normally, but the AME-P RGCs which would normally express NrCAM show reduced survival. I have not investigated markers of cell death, so I do not have direct evidence to support or dispute this hypothesis. In the developing cerebellum, loss of NrCAM and L1 reduces survival of GNPs and a consequent reduction in cerebellar lobe size (Sakurai et al., 2001), suggesting a similar mechanism could be at play here. However, this hypothesis does not provide an explanation for the increased ARC TH^+ neuron population at E18, suggesting a lack of RGC survival cannot alone account for my observations.

In a third scenario, NrCAM modulates the decision for RGCs to proliferate and differentiate. This may occur in two ways: it may affect the rate of proliferation, or it may bias RGCs to produce a greater quantity of parenchymal daughters at the expense of self-renewing. Under the first option, over-proliferation of RGCs may lead to early senescence, and a reduced population capable of sustained division. This does not fit with my observations, as in this instance we might expect to see a developmental increase in RGCs followed by a subsequent decrease; what I actually see is a developmental population of RGCs that is reduced in number. The second

option appears more likely, as if too many parenchymal cells, such as TH^+ neurons, are produced at the expense of self-renewing, that would result in a reduced RGC population and an increased TH^+ population: this matches my observations. Such an outcome could be achieved by changes in asymmetric/symmetric division, either through abnormal adhesion, or through changes in response to signals such as Shh and Fgf10. Precedent for IgSF CAMs eliciting such effects has been shown in research into the role of F3/contactin in the cortex, where its overexpression leads to a delay in progenitor commitment and changes in the proportions of cortical layers (Bizzoca et al., 2012). NrCAM, F3/contactin, and TAG1 also have established roles modulating the Shh pathway in the development of the cerebellum (Xenaki et al., 2011), whilst L1 and another IgSF CAM, NCAM, interact with FGF receptors (discussed below) (Cavallaro et al., 2001; Herron et al., 2009; Kiselyov et al., 2005; Kulahin et al., 2008; Maness and Schachner, 2007). The second option also allows for the progressive phenotype I have suggested, as the reduced RGC/tanycyte population may be insufficient to produce sufficient *Rax*$^+$ parenchymal cells, or maintain sufficient tanycytes and TH^+ neurons in adulthood. To investigate these options further, markers of proliferation and differentiation need to be compared between wild type and $NrCAM^{-/-}$ embryonic mice.

A fourth hypothesis suggests that NrCAM KO leads to a reduction in tanycyte survival. This hypothesis cannot be mutually exclusive to the hypotheses above, as it would not account for the differences in the embryonic mouse. It could, however, provide a partial explanation for reduction of tanycytes and their potential ARC TH^+ neurons progeny. As with hypothesis two, analysis of cell cycle markers is required.

The fifth hypothesis is similar to the third, and suggests that an imbalance in proliferation or differentiation may lead to the reductions observed in adulthood. Like hypothesis 4, this is not sufficient to explain the differences in embryonic mice. However, this hypothesis is plausible when combined with one of the previous hypotheses that address the embryonic phenotype, and if shown to be true it may be an extension of hypothesis three: an imbalance in proliferation/differentiation in RGCs that continues in tanycytes.

In a final scenario, loss of NrCAM leads to increased parenchymal cell death, which in turn causes over-proliferation and subsequent reduction of the RGC/tanycyte

populations. This hypothesis does not account for the initial increase in TH^+ neurons, and is weakened by the RGC/tanycyte-specific expression of NrCAM which excludes autonomous cell death of parenchymal cells. Non-autonomous cell death, triggered by a lack of NrCAM on tanycytes that contact the parenchymal cells is possible but seems unlikely. This hypothesis could be addressed using markers of cell death.

Weighing up these scenarios, none can be directly excluded without further research. However, the current evidence suggests that the phenotypes I observe are most likely caused by a change or imbalance in proliferation behaviour in the embryo (hypothesis three). Such an imbalance could continue in the adult neurogenic population (hypothesis five), particularly when one considers that the adult neurogenic population may be a remnant of the RGC neurogenic population. These imbalances could be caused by changes in signalling, either through the Shh or Fgf10 pathways as I have suggested, or by modulating other pathways I have not yet investigated, such as the Wnt or Notch pathways that are known to be active during development (described below). Alternatively, loss of NrCAM may cause changes in cell-surface signalling, through the loss of interactions between NrCAM and molecules on the surface of neighbouring cells. An additional possibility is that NrCAM may play a role is the morphological changes necessary for tanycyte division, either by modulating signalling, or through physical interactions consisting of surface binding and its intracellular link to the cytoskeleton (Bennett and Baines, 2001). The related molecules F3/contactin and TAG1 are modulate neuronal precursor proliferation during development, through changes to apico-basal positioning and nuclear migration, or through changes in the Notch signalling pathway (Bizzoca et al., 2012; Okamoto et al., 2013). NrCAM may be acting through similar mechanisms, or others I've listed, to modulate RGC and tanycyte proliferation and the progeny that are produced.

8.2 Future Work

Several key steps are needed to continue this work. Our model of a PME stem cell population is compelling but requires substantiation. Analysis of proliferation, differentiation, and migration across the A-P axis of the hypothalamus using mitotic markers, BrdU pulse-chase, or inducible lineage tracing lines can provide data showing the localisation of dividing cells and their progeny, and may inform us

whether the reductions in Rax, Fgf10, and Shh mRNA in the posterior hypothalamic region of the hypothalamus of NrCAM$^{-/-}$ mice lead to changes in postnatal proliferation. A mouse line with GFP under a tamoxifen inducible Shh-promoter, or specifically in Shh^{+}Fgf10^{+} cells , would be ideal for lineage-tracing the proposed PME stem cells, as the Shh^{+} population in the adult hypothalamus is so limited. This could be used in conjunction with a BrdU pulse-chase study to both identify whether the Shh^{+}Fgf10^{+} cells are proliferative, and if so what offspring they produce. Analysis of ratios of tanycyte, glia, and neuronal progeny in wild type and NrCAM$^{-/-}$ mice can address the hypothesis of that loss of NrCAM leads to an imbalance in proliferation/differentiation. This research in the adult can be complemented by similar analyses of proliferation, migration, and differentiation in the embryo, to investigate the A-P dynamics during development.

While my work provides a useful starting point for re-evaluating tanycyte subtypes, further comparisons of markers are needed to make my conclusions robust. Repeating these marker characterisations to get higher sample sizes, and including various double and triple immunolabelling and ISH marker comparisons, will help to show which markers truly co-localise. Double ISH to determine whether Fgf10 and Shh co-localise in the PME and abut in the ME^{P} is a priority.

To further investigate the effect of NrCAM KO, analysis of further timepoints will be important. My study confirms previous work by Lustig et al. (2001) showing expression of NrCAM in the hypothalamus by E16, and establishes that it is expressed by Nestin^{+} RGCs. In the NrCAM KO, RGCs are reduced in number by E16, and to understand how this occurs we must look earlier in development. It is unclear when NrCAM is initiated in the mouse hypothalamus, though ISH analysis by the Allen Institute shows NrCAM mRNA expression in the hypothalamus by E11.5[7] (the earliest timepoint they analyse). It is unclear from this experiment which hypothalamic cells are NrCAM^{+}, but it highlights that investigation of NrCAM at this timepoint and earlier may help elucidate the early roles of NrCAM in the hypothalamus, and allow us to pinpoint the first time at which NrCAM$^{-/-}$ could be causing disturbances to the hypothalamus.

[7] Allen Developing Mouse Brain Atlas – NrCAM http://developingmouse.brain-map.org/gene/show/106439

This investigation of early expression can be supplemented by assessing the markers I have used at additional embryonic and juvenile timepoints, with the aim of determining when the observed phenotypes are first exhibited, and how they progress into adulthood. Analysis of tanycytes in aged wild type and NrCAM$^{-/-}$ mice will complement this research. Limited research on tanycyte aging in rats suggests tanycyte number and/or morphology is lost later in life, so this analysis will contribute to our understanding of age-related tanycyte changes in wild type mice, and outline whether the NrCAM KO losses of tanycytes and TH^{+} neurons progress at a faster rate (Koopman et al., 2017; Zoli et al., 1995). Use of a conditional/inducible NrCAM KO mouse line would provide greater clarity about the onset and progression of the observed phenotypes, and could be used to assess whether NrCAM loss in adult mice has detrimental effects after a normal development.

Investigating the effects of NrCAM KO can ultimately lead us toward understanding the role/function of NrCAM on hypothalamic RGCs and tanycytes. The presence of NrCAM on the surface of tanycytes raises the question of its purpose in this population. One potential utility maybe be as a signal modulator, in which NrCAM modulates receptor localisation, trafficking, or activity. In the cerebellar granule neuron progenitors, NrCAM works in tandem with the other CAMs F3 and TAG1 as a binding partner to modulate Shh signalling output governing proliferation and differentiation choices (Xenaki et al., 2011). Further investigation of Shh and NrCAM in the hypothalamus, may reveal whether NrCAM has any role in managing what function Shh serves.

While NrCAM has not previously been linked to FGF signalling, other IgSF CAMs have. L1 and NCAM have been implicated in binding and activating FGFR1 and FGFR4 respectively (Cavallaro et al., 2001; Herron et al., 2009; Kiselyov et al., 2005; Kulahin et al., 2008; Maness and Schachner, 2007). In both cases, receptor activation lead to changes in the adhesive properties of cells. FGFR1 is expressed in tanycytes and has been shown to modulate feeding behaviour through TSH signalling (Samms et al., 2015). FGFR2 is also known to be expressed in the hypothalamus (Hajihosseini et al., 2008), and both have been shown to respond to Fgf10 in other tissues (Zhang et al., 2006). Neither receptor complex has been investigated in relation to hypothalamic neurogenesis, but given that both respond to

Fgf10, and Fgf10 has been linked to tanycyte neurogenesis, it is possible that such behaviour may be mediated by the FGFR complexes. As an L1-like CAM, NrCAM may also possess the ability to bind FGFRs. Further investigation of NrCAM and FGFRs in tanycytes is required to determine whether such interactions occur, and if they do, then whether there is any effect on adhesion, enzymatic regulation, neurogenesis, or other tanycyte functions.

In this thesis I have not begun to look at the roles of other signalling pathways in either the developing or adult hypothalamus. Wnt family members have roles in the development of the hypothalamus, including establishing expression of foxd1 and the RDVM as presumptive hypothalamus, and during neurogenesis (Lagutin et al., 2003; Lavado et al., 2008; Lee et al., 2006; Manning et al., 2006; Martinez-Ferre et al., 2013; Shimogori et al., 2010). Furthermore, Wnts have been directly linked to tanycyte neurogenesis (Wang et al., 2012). NrCAM is a target of the Wnt effectors β-catenin/LEF-1, and it is through this pathway that NrCAM is upregulated in a variety of tumours, increasing motility and promoting further tumourigenesis (Chan et al., 2011; Conacci-Sorrell et al., 2002, 2005; Górka et al., 2007). The connections between Wnts, NrCAM, and proliferation make studying these targets in the hypothalamus of interest.

A further signal that should be further analysed is the Notch and its effectors Hes1 and Hes5. Notch1, Notch2 are expressed in tanycytes (Salvatierra et al., 2014; Shimogori et al., 2010), as is the Notch effector Hes5 (unpublished), and these expression patterns appear specific to tanycytes. During development, Notch is upstream of Ascl1/Mash1 which drives hypothalamic neurogenesis (Aujla et al., 2011, 2013; Ratié et al., 2013). There is also crosstalk between tcf3 and Hesx1, Wnt and Notch pathway components, in the developing forebrain (Andoniadou et al., 2011). No clear link has been made between NrCAM and the Notch pathway, though its cousin and binding partner F3/contactin acts as a Notch ligand in oligodendrocyte maturation (Hu et al., 2003). It is not known whether F3 is expressed in the hypothalamus, but as NrCAM, Notch1, and Notch2 are expressed on tanycytes, and all three are ligands for F3, it may be worth investigating a link between NrCAM and the Notch pathway in tanycytes.

In addition to investigating the role of NrCAM in tanycytes and the broader

hypothalamus, NrCAM expression and knock-out may be useful for exploring the broader functions of tanycytes within the hypothalamus, including roles such as neuronal modulation/communication, and acting as a barrier/selective-transporter between the CSF and the hypothalamic parenchyma. As knocking out NrCAM diminishes the tanycyte population without completely removing them, this model can allow investigators to investigate how tanycyte reductions effect the hypothalamus *in vivo*, without initiating widespread death of tanycytes (or other cells) and the complications this may cause. One recent paper showed that knocking out *Gnasxl*, a variant of $G\alpha_s$ which is expressed by hypothalamic neurons associated with feeding behaviour but not tanycytes, leads not only to a lean, hypermetabolic state, but also to a reduction α-tanycytes postnatally (Holmes et al., 2016). It is not clear why this occurs, or what impact this reduction has, however it appears as though this reduction is caused by neuronal changes. This result is similar but opposite of my finding of reduced TH^+ neurons following a reduction of RGCs/tanycytes, and results such as these suggest that more work is required to determine what effect disruption of tanycyte/neuron communication has.

8.3 Conclusion

Overall, I believe the research I have described constitutes and important contribution to the study of hypothalamic tanycytes. The three dimensional model of tanycytes I have presented (Fig 4.9), that describes their position based on an array of markers from A-P as well as from D-V within the hypothalamus, shows the need for future work to carefully address the specific localisation of the tanycytes that are being investigated. This will, by necessity, add an additional level of complexity to studying tanycytes, however this more rigorous analysis may provide improved clarity on aspects of tanycyte function that were previously described by contradictory research papers.

Furthermore, I have described NrCAM as a strongly expressed marker of all tanycytes which is also specific to tanycytes within the hypothalamus, properties that will make it useful for future investigations of tanycytes. This utility is bolstered by my research that identifies NrCAM as an important factor for determining the quantity of both tanycytes and the arcuate TH-neuron population in adult and embryonic mice, which may suggest a role for NrCAM in specifying tanycyte identity, or as a

contributing factor to tanycyte and/or RGC neurogenesis. These observations open avenues for further researching tanycyte function and neurogenesis.

CHAPTER 9: APPENDIX

This section describes the statistical reanalysis I discussed in Chapter 2.6. Based on discussions with a biostatistician I have begun to reanalyse the data in my thesis for publication. I aim to improve the robustness of the analysis, and assess the differences between each of the biological replicates (wildtype and NrCAM KO mouse pairs), conducting and reporting statistical analysis on each pair of mice.

I have first checked for normal distribution in our data. Where data is normally distributed and unpaired, I have used an unpaired t-test with Welch's correction. I have used this correction, as prior to analysis I have not assumed that the variance of the datasets are equal. If the data are not normally distributed for at least one of the unpaired data sets being compared, I have used the non-parametric Mann-Whitney U-test to compare ranks. For normally distributed paired data, I have used a paired t-test, and the non-parametric Wilcoxon matched-pairs signed rank test when they are not normally distributed. Included with these statistical analyses are scatter plots showing each data point and bars for mean and standard deviation. I have also included histograms showing frequency distribution for measurements in each subregion. Examples are included below.

Reanalysis of $Nestin^+$ processes in adult mice (Fig 9.1, see Chapter 5) shows broadly the same pattern as previous statistical analysis, with a reduction in $Nestin^+$ processes in NrCAM KO mice when the hypothalamus is taken as a whole. Additionally, I observed a trend for reduced $Nestin^+$ processes in each subregion in the NrCAM KO mice, with most analyses showing a significant difference.

Reanalysis of TH^+ cells in wildtype and NrCAM KO E18 mice was mixed (Fig 9.2, see Chapter 6). Over the whole hypothalamus, one of the three NrCAM KO E18 mice had more TH^+ cells relative to its wildtype littermate, while the other two were not significantly different (as was reported in Chapter 6). The A subregion had more TH^+ cells in one NrCAM KO E18 mouse relative to its wildtype littermate, whilst the other two NrCAM KO mice were significantly

reduced. When these data were pooled in Chapter 6, no significant difference was found. In Chapter 6 I described an increase in TH^+ cells in the AME and ME subregions of NrCAM KO E18 mice. These significant differences were seen in two of 3 NrCAM KO E18 mice, with the non-significant results for AME and ME arising in different mouse pairs. The overall trend was consistent with the previously reported analysis.

Figure 9.1 Reanalysis of Nestin expression along the anterior-posterior axis of the hypothalamus for wild type and NrCAM KO adult mice.

A – Quantification of Nestin$^+$ process density for β1 and α2 tanycytes in all tanycyte containing sections along the A-P axis of the tuberal hypothalamus in three pairs of wild type and NrCAM KO adult mice (graphs i-iii). Each icon represents a single measurement, collected as described in Chapter 2.2.5.2. Bars show 1 SD either side of the mean value. Analysis by unpaired t-test with Welch's correction (Pair 1), or Mann-Whitney test (Pairs 2 and 3) shows a significant reduction of Nestin$^+$ tanycyte density in NrCAM KO adult mice (Pair 1, P<0.0001; Pair 2, P<0.0001; Pair 3, P<0.0001).

B – Quantification of Nestin$^+$ process density for β1 and α2 tanycytes in AME, ME, PME, and P subregions in three pairs of wild type and NrCAM KO adult mice (graphs i-iii). Each icon represents a single measurement, collected as described in Chapter 2.2.5.2. Bars show 1 SD either side of the mean value. While the AME and ME are not significantly different in Pair 2, and the PME is not significantly different in Pair 1 (despite approaching significance), all analyses show a downward trend in Nestin$^+$ process density in the NrCAM KO mice relative to the widltype, and this difference is significant in the majority of analyses for each subregion.

Bi – Pair 1: AME (Mann-Whitney P<0.0001), ME (Welch's t-test P<0.0001), PME (Mann-Whitney P=0.0571 ns), P (Welch's t-test P<0.0001)

Bii – Pair 2: AME (Welch's t-test P=0.2817 ns), ME (Welch's t-test P=0.4931 ns), PME (Mann-Whitney P=0.0173), P (Welch's t-test P<0.0001)

Biii – Pair 3: AME (Welch's t-test P<0.0001), ME (Welch's t-test P=0.0004), PME (Welch's t-test P=0.0141), P (Mann-Whitney P=0.0448)

C – Histograms comparing the distribution of measurements for each subregion of each mouse pair. Pair 1 i-iv, Pair 2 v-viii, Pair 3 ix-xii. WT – blue, NrCAM KO – red.

Figure 9.1

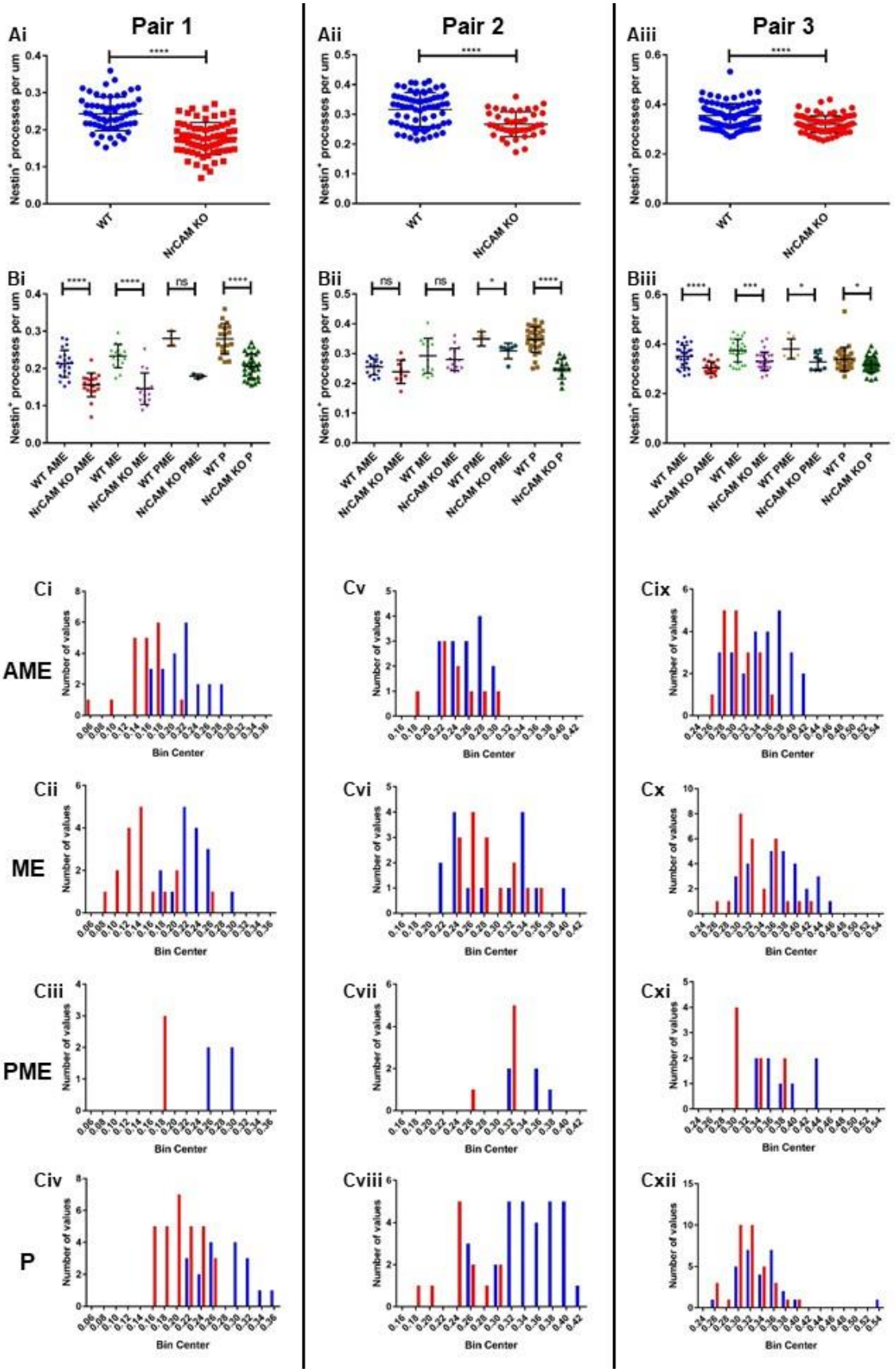
Pair 1
Pair 2
Pair 3
Ai
Aii
Aiii
Nestin+ processes per um
WT
NrCAM KO
****
Bi
Bii
Biii
ns
*
***
WT AME
NrCAM KO AME
WT ME
NrCAM KO ME
WT PME
NrCAM KO PME
WT P
NrCAM KO P
Ci
Cii
Ciii
Civ
Cv
Cvi
Cvii
Cviii
Cix
Cx
Cxi
Cxii
AME
ME
PME
P
Number of values
Bin Center

Figure 9.2 Reanalysis of TH expression along the anterior-posterior axis of the hypothalamus for wild type and NrCAM KO E18 mice.

A – Quantification of TH^+ cells along the A-P axis of the ARC in three pairs of E18 wild type and NrCAM KO littermates (graphs i-iii). Each icon represents a single measurement, collected as described in Chapter 2.2.5.2. Bars show 1 SD either side of the mean value. Analysis by Mann-Whitney test shows a significant reduction of TH^+ cells across the embryonic hypothalamus in the NrCAM KO E18 mouse from pair 1 relative to its wildtype littermate (Pair 1, P=0.0057); but no significant difference was seen in Pair 2 (P=0.3469) or Pair 3 (P=0.2738).

B – Quantification of TH^+ cells in A, AME, ME, and P subregions in three pairs of wild type and NrCAM KO E18 littermates (graphs i-iii). Each icon represents a single measurement, collected as described in Chapter 2.2.5.2. Bars show 1 SD either side of the mean value. While the A TH^+ cells are significantly higher in the NrCAM KO E18 littermate of pair 1, the ME TH^+ cells are not significantly different in Pair 2, and the AME TH^+ cells are not significantly different in Pair 3 (despite approaching significance), the majority of analyses for each of the A, AME, and ME subregions are significantly different between the wildtype and NrCAM KO mice. The majority of analyses for the A subregion show a significant decrease in the NrCAM KO mice, whilst the AME and ME show a significant increase in the NrCAM KO mice. No significant difference is seen in the P subregion.

Bi – Pair 1: A (Welch's t-test P<0.0001), AME (Welch's t-test P<0.0001), ME (Welch's t-test P=<0.0001), P (Mann-Whitney P=0.6376)

Bii – Pair 2: A (Welch's t-test P=0.0271), AME (Welch's t-test P=0.0269), ME (Welch's t-test P=0.9151), P (Welch's t-test P=0.1044)

Biii – Pair 3: A (Mann-Whitney P<0.0001), AME (Mann-Whitney P=0.0553), ME (Welch's t-test P=0.0395), P (Welch's t-test P=0.8331)

C – Histograms comparing the distribution of measurements for each subregion of each mouse pair. Pair 1 i-iv, Pair 2 v-viii, Pair 3 ix-xii. WT – blue, NrCAM KO – red.

Figure 9.2

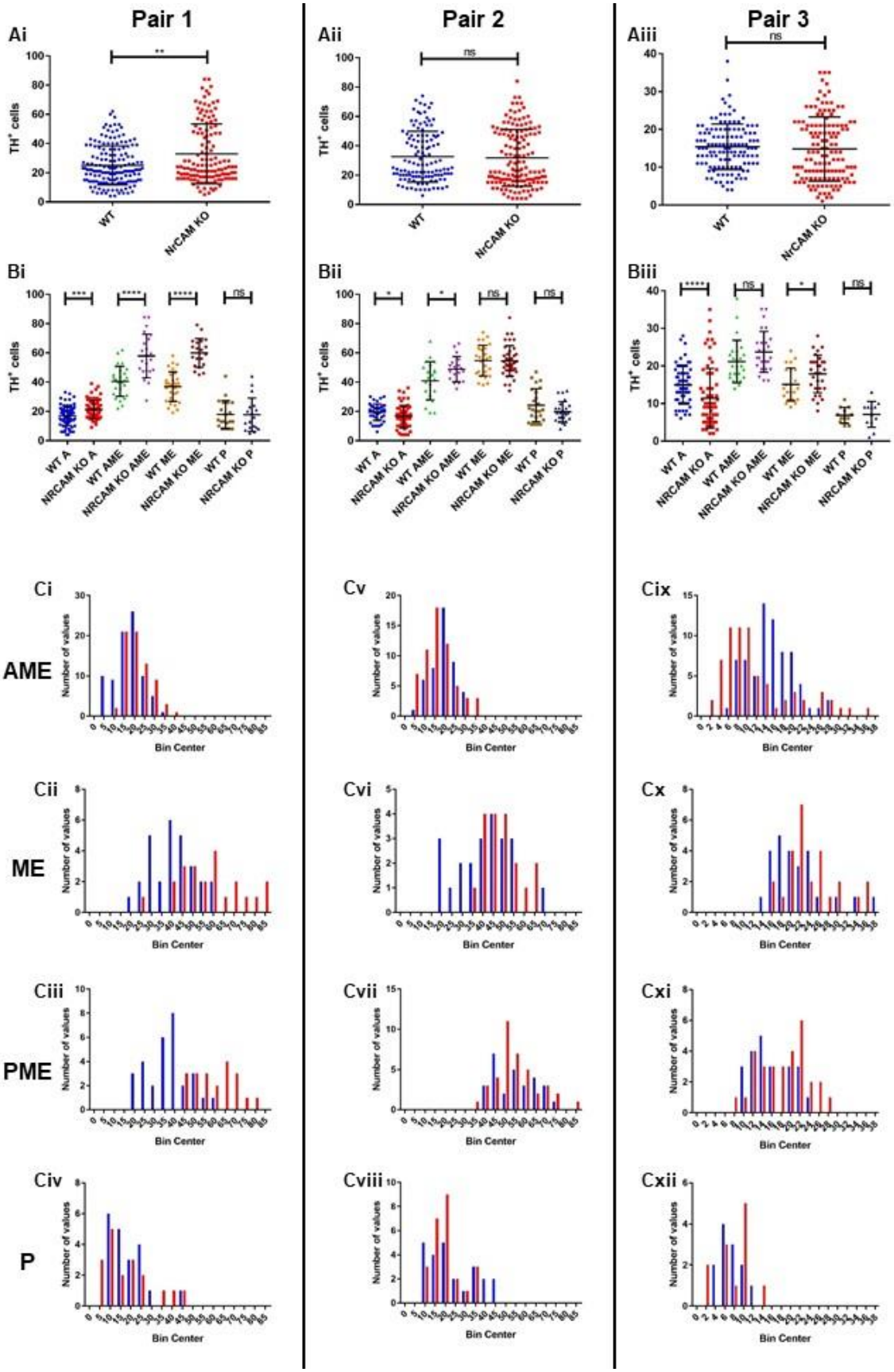
Pair 1
Pair 2
Pair 3
Ai
Aii
Aiii
Bi
Bii
Biii
TH+ cells
WT
NrCAM KO
WT A
NRCAM KO A
WT AME
NRCAM KO AME
WT ME
NRCAM KO ME
WT P
NRCAM KO P
Ci
Cii
Ciii
Civ
Cv
Cvi
Cvii
Cviii
Cix
Cx
Cxi
Cxii
AME
ME
PME
P
Number of values
Bin Center

REFERENCES

Ahlgren, S., Vogt, P., and Bronner-fraser, M. (2003). Excess FoxG1 Causes Overgrowth of the Neural Tube ABSTRACT : J. Neurobiol. *57*, 337–349.

Akamatsu, W., Fujihara, H., Mitsuhashi, T., Yano, M., Shibata, S., Hayakawa, Y., Okano, H.J., Sakakibara, S.-I., Takano, H., Takano, T., et al. (2005). The RNA-binding protein HuD regulates neuronal cell identity and maturation. Proc. Natl. Acad. Sci. U. S. A. *102*, 4625–4630.

Alvarez-Bolado, G., Paul, F.A., and Blaess, S. (2012). Sonic hedgehog lineage in the mouse hypothalamus: From progenitor domains to hypothalamic regions. Neural Dev. *7*.

Alvarez-Buylla, A., and Lim, D.A. (2004). For the long run: Maintaining germinal niches in the adult brain. Neuron *41*, 683–686.

Alvarez-Buylla, A., Theelen, M., and Nottebohm, F. (1990a). Proliferation “hot spots” in adult avian ventricular zone reveal radial cell division. Neuron *5*, 101–109.

Alvarez-Buylla, A., Kirn, J.R., and Nottebohm, F. (1990b). Birth of Projection Neurons in Adult Avian Brain May Be Related to Perceptual or Motor Learning. Science (80-.). 360–360.

Amps, K., Andrews, P.W., Anyfantis, G., Armstrong, L., Avery, S., Baharvand, H., Baker, J., Baker, D., Munoz, M.B., Beil, S., et al. (2011). Screening ethnically diverse human embryonic stem cells identifies a chromosome 20 minimal amplicon conferring growth advantage. Nat. Biotechnol. *29*, 1132–1144.

Andoniadou, C.L., Signore, M., Young, R.M., Gaston-Massuet, C., Wilson, S.W., Fuchs, E., and Martinez-Barbera, J.P. (2011). HESX1- and TCF3-mediated repression of Wnt/β-catenin targets is required for normal development of the anterior forebrain. Development *138*, 4931–4942.

Andrews, G.L., Yun, K., Rubenstein, J.L.R., and Mastick, G.S. (2003). Dlx transcription factors regulate differentiation of dopaminergic neurons of the

ventral thalamus. Mol. Cell. Neurosci. *23*, 107–120.

Anthony, T.E., Klein, C., Fishell, G., and Heintz, N. (2004). Radial Glia Serve as Neuronal Progenitors in All Regions of the Central Nervous System. Neuron *41*, 881–890.

Aponte, Y., Atasoy, D., and Sternson, S.M. (2011). AGRP neurons are sufficient to orchestrate feeding behavior rapidly and without training. Nat. Neurosci. *14*, 351–355.

Aujla, P.K., Bora, A., Monahan, P., Sweedler, J. V., and Raetzman, L.T. (2011). The Notch effector gene Hes1 regulates migration of hypothalamic neurons, neuropeptide content and axon targeting to the pituitary. Dev. Biol. *353*, 61–71.

Aujla, P.K., Naratadam, G.T., Xu, L., and Raetzman, L.T. (2013). Notch/Rbpjκ signaling regulates progenitor maintenance and differentiation of hypothalamic arcuate neurons. Development *3521*, 3511–3521.

Balland, E., Dam, J., Langlet, F., Caron, E., Steculorum, S., Messina, A., Rasika, S., Trinquet, E., Jockers, R., Bouret, S.G., et al. (2014). Hypothalamic Tanycytes Are an ERK-Gated Conduit for Leptin into the Brain. Cell Metab. *19*, 293–301.

Barnabé-Heider, F., Göritz, C., Sabelström, H., Takebayashi, H., Pfrieger, F.W., Meletis, K., and Frisén, J. (2010). Origin of new glial cells in intact and injured adult spinal cord. Cell Stem Cell *7*, 470–482.

Baroncini, M., Allet, C., Leroy, D., Beauvillain, J., Francke, J., and Prevot, V. (2007). Morphological Evidence for Direct Interaction Between Gonadotrophin-Releasing Hormone Neurones and Astroglial Cells in the Human Hypothalamus Neuroendocrinology. J. Neuroendocrinol. *19*, 691–702.

Batailler, M., Droguerre, M., Baroncini, M., Fontaine, C., Prevot, V., and Migaud, M. (2014). DCX-expressing cells in the vicinity of the hypothalamic neurogenic niche: A comparative study between mouse, sheep, and human tissues. J. Comp. Neurol. *522*, 1966–1985.

Batailler, M., Derouet, L., Butruille, L., and Migaud, M. (2016). Sensitivity to the photoperiod and potential migratory features of neuroblasts in the adult sheep

hypothalamus. Brain Struct. Funct. *221*, 3301–3314.

Ben-Jonathan, N., and Hnasko, R. (2001). Dopamine as a prolactin (PRL) inhibitor. Endocr. Rev. *22*, 724–763.

Bennett, V., and Baines, A.J. (2001). Spectrin and Ankyrin-Based Pathways : Metazoan Inventions for Integrating Cells Into Tissues. Physiol. Rev. *81*, 1353–1392.

Bennett, L., Yang, M., Enikolopov, G., and Iacovitti, L. (2009). Circumventricular organs: A novel site of neural stem cells in the adult brain. Mol. Cell. Neurosci. *41*, 337–347.

Berglund, E.O., Murai, K.K., Fredette, B., Sekerkova, G., Marturano, B., Weber, L., Mugnaini, E., Ranscht, B., and Diego, S. (1999). Ataxia and Abnormal Cerebellar Microorganization in Mice with Ablated Contactin Gene Expression. Neuron *24*, 739–750.

Bizzoca, A., Virgintino, D., Lorusso, L., Buttiglione, M., Yoshida, L., Polizzi, A., Tattoli, M., Caginao, R., Rossi, F., Kozlov, S., et al. (2003). Transgenic mice expressing F3/contactin from the TAG-1 promoter exhibit developmentally regulated changes in the differentiation of cerebellar neurons. Development *130*, 29–43.

Bizzoca, A., Corsi, P., Polizzi, A., Pinto, M.F., Xenaki, D., Furley, A.J.W., and Gennarini, G. (2012). F3/Contactin acts as a modulator of neurogenesis during cerebral cortex development. Dev. Biol. *365*, 133–151.

Bless, E.P., Yang, J., Acharya, K.D., Nettles, S.A., Vassoler, F.M., Byrnes, E.M., and Tetel, M.J. (2016). Adult neurogenesis in the female mouse hypothalamus: Estradiol and high fat diet alter the generation of newborn neurons expressing estrogen receptor a. ENeuro *3*.

Bloch, B., Brazeau, P., Ling, N., Bohlen, P., Esch, F., Wehrenberg, W.B., and Benoit, R. (1983). Immunohistochemical Detection of Growth Hormone-Releasing Factor in Brain. Nature *301*, 607–608.

Bolborea, M., and Dale, N. (2013). Hypothalamic tanycytes: Potential roles in the control of feeding and energy balance. Trends Neurosci. *36*, 91–100.

Bouyer, K., Loudes, C., Robinson, I.C.A.F., Epelbaum, J., and Faivre-Bauman, A. (2007). Multiple co-localizations in arcuate GHRH-eGFP neurons in the mouse hypothalamus. J. Chem. Neuroanat. *33*, 1–8.

Brümmendorf, T., and Lemmon, V. (2001). Immunoglobulin superfamily receptors : cis-interactions , intracellular adapters and alternative splicing regulate adhesion. Curr. Opin. Cell Biol. *13*, 611–618.

Brümmendorf, T., and Rathjen, F.G. (1996). Structure / function relationships of axon-associated adhesion receptors of the immunoglobulin superfamily Thomas BrOmmendorf 1 and Fritz G Rathjen 2. Curr. Opin. Neurobiol. *6*, 584–593.

Buchstaller, A., Kunz, S., Berger, P., Kunz, B., Ziegler, U., Rader, C., and Sonderegger, P. (1996). Cell Adhesion Molecules NgCAM and Axonin-1 Form Heterodimers in the Neuronal Membrane and Cooperate in Neurite Outgrowth Promotion. J. Cell Biol. *135*, 1593–1607.

Butruille, L., Batailler, M., Mazur, D., Prévot, V., and Migaud, M. (2018). Seasonal reorganization of hypothalamic neurogenic niche in adult sheep. Brain Struct. Funct. *223*, 91–109.

Campbell, J.N., Macosko, E.Z., Fenselau, H., Pers, T.H., Lyubetskaya, A., Tenen, D., Goldman, M., Verstegen, A.M., Resch, J.M., McCarroll, S.A., et al. (2017). A Molecular Census of Arcuate Hypothalamus and Median Eminence Cell Types. Nat. Neurosci. *20*, 484–496.

Castellani, V., Falk, J., and Rougon, G. (2004). Semaphorin3A-induced receptor endocytosis during axon guidance responses is mediated by L1 CAM. Mol. Cell. Neurosci. *26*, 89–100.

Cavallaro, U., Niedermeyer, J., Fuxa, M., and Christofori, G. (2001). N-CAM modulates tumour-cell adhesion to matrix by inducing FGF-receptor signalling. Nat. Cell Biol. *3*, 650–657.

Chaker, Z., George, C., Petrovska, M., Caron, J.B., Lacube, P., Caille, I., and Holzenberger, M. (2016). Hypothalamic neurogenesis persists in the aging brain and is controlled by energy-sensing IGF-I pathway. Neurobiol. Aging *41*, 64–72.

Chan, J.Y., Ong, C.W., and Salto-Tellez, M. (2011). Overexpression of neurone

glial-related cell adhesion molecule is an independent predictor of poor prognosis in advanced colorectal cancer. Cancer Sci. *102*, 1855–1861.

Chen, S., and Yang, J. (2018). Emerging Roles of Sonic Hedgehog in Adult Neurological Diseases: Neurogenesis and Beyond. Int. J. Mol. Sci. *19*.

Conacci-Sorrell, M.E., Ben-Yedidia, T., Shtutman, M., Feinstein, E., and Einat, P. (2002). Nr-CAM is a target gene of the B-catenin/LEF-1 pathway in melanoma and colon cancer and its expression enhances motility and confers tumorigenesis. Genes Dev. *1*, 2058–2072.

Conacci-Sorrell, M.E., Kaplan, A., Raveh, S., Gavert, N., Sakurai, T., and Ben-Ze'ev, A. (2005). The shed ectodomain of Nr-CAM stimulates cell proliferation and motility, and confers cell transformation. Cancer Res. *65*, 11605–11612.

Conte, I., Morcillo, J., and Bovolenta, P. (2005). Comparative analysis of Six3 and Six6 distribution in the developing and adult mouse brain. Dev. Dyn. *234*, 718–725.

Coppola, A., Liu, Z., Andrews, Z., Paradis, E., Roy, M., Friedman, M., Ricquier, D., Richard, D., Horvath, T.L., Gao, X., et al. (2008). A Central Thermogenic-like Mechanism in Feeding Regulation: an Interplay Between Arcuate Nucleus T3 and UCP2. Cell Metab. *5*, 21–33.

Dang, P., Smythe, E., and Furley, A.J.W. (2012). TAG1 regulates the endocytic trafficking and signalling of the Semaphorin3A receptor complex. J. Neurosci. *32*, 10370–10382.

Decimo, I., Bifari, F., Krampera, M., and Fumagalli, G. (2012). Neural Stem Cell Niches in Health and Diseases. Curr. Pharm. Des. *18*, 1755–1783.

Decourtye, L., Mire, E., Clemessy, M., Heurtier, V., Ledent, T., Robinson, I.C., Mollard, P., Epelbaum, J., Meaney, M.J., Garel, S., et al. (2017). IGF-1 Induces GHRH Neuronal Axon Elongation during Early Postnatal Life in Mice. PLoS One 1–19.

Demyanenko, G.P., Mohan, V., Zhang, X., Brennaman, L.H., Dharbal, K.E.S., Tran, T.S., Manis, P.B., and Maness, P.F. (2014). Neural Cell Adhesion Molecule NrCAM Regulates Semaphorin 3F-Induced Dendritic Spine

Remodeling. J. Neurosci. *34*, 11274–11287.

Deng, W., Aimone, J.B., and Gage, F.H. (2010). New neurons and new memories: How does adult hippocampal neurogenesis affect learning and memory? Nat. Rev. Neurosci. *11*, 339–350.

Doetsch, F. (2003). A niche for adult neural stem cells. Curr. Opin. Genet. Dev. *13*, 543–550.

Doetsch, F., Caillé, I., Lim, D.A., García-Verdugo, J.M., and Alvarez-Buylla, A. (1999). Subventricular zone astrocytes are neural stem cells in the adult mammalian brain. Cell *97*, 703–716.

Dzhashiashvili, Y., Zhang, Y., Galinska, J., Lam, I., Grumet, M., and Salzer, J.L. (2007). Nodes of Ranvier and xon initial segments are ankyrin G-dependent domains that assemble by distinct mechanisms. J. Cell Biol. *177*, 857–870.

Ebling, F.J.P., and Lewis, J.E. (2018). Tanycytes and hypothalamic control of energy metabolism. Glia 1176–1184.

Ebling, F.J.P., Arthurs, O.J., Turney, B.W., and Cronin, A.S. (1998). Seasonal neuroendocrine rhythms in the male Siberian hamster persist after monosodium glutamate-induced lesions of the arcuate nucleus in the neonatal period. J. Neuroendocrinol. *10*, 701–712.

Edwards, M.A., Yamamoto, M., and caviness, V.S. (1990). Organization of radial glia and related cells in the developing murine CNS. An analysis based upon a new monoclonal antibody marker. Neuroscience *36*, 121–144.

El-Yazbi, A.F., Cho, W.J., Cena, J., Schulz, R., and Daniel, E.E. (2008). Smooth muscle NOS, colocalized with caveolin-1, modulates contraction in mouse small intestine. J. Cell. Mol. Med. *12*, 1404–1415.

Ellis, P.S., Burbridge, S., Soubes, S., Ohyama, K., Ben-haim, N., Chen, C., Dale, K., Shen, M.M., Constam, D., and Placzek, M. (2015). ProNodal acts via FGFR3 to govern duration of Shh expression in the prechordal mesoderm. Development *142*, 3821–3832.

Fekete, C., Lechan, R.M., Introduction, I., and Axis, H. (2014). Central

Regulation of Hypothalamic-Pituitary-Thyroid Axis Under Physiological and Pathophysiological Conditions. Endocr. Rev. *35*, 159–194.

Felding-habermann, B., Silletti, S., Mei, F., Siu, C., Yip, P.M., Brooks, P.C., Cheresh, D.A., Toole, T.E.O., Ginsberg, M.H., and Montgomery, A.M.P. (1997). A Single Immunoglobulin-like Domain of the Human Neural Cell Adhesion Molecule L1 Supports Adhesion by Multiple Vascular and Platelet Integrins. J. Cell Biol. *139*, 1567–1581.

Frayling, C., Britton, R., and Dale, N. (2011). ATP-mediated glucosensing by hypothalamic tanycytes. J. Physiol. *589*, 2275–2286.

Fu, T., Towers, M., and Placzek, M. (2017). Fgf10 + progenitors give rise to the chick hypothalamus by rostral and caudal growth and differentiation. Development dev.153379.

Fuller, M.T., and Spradling, A.C. (2007). Germline Stem Cells : Two Versions of Immortality. Germ Cells *316*, 402–405.

Furukawa, T., Kozak, C.A., and Cepko, C.L. (1997). Rax, a Novel Paired-Type Homeobox Gene, Shows Expression in the Anterior Neural Fold and Developing Retina. Proc. Natl. Acad. Sci. *94*, 3088–3093.

Gage, F.H., Kempermann, G., Palmer, T.D., Peterson, D.A., and Ray, J. (1998). Multipotent progenitor cells in the adult dentate gyrus. J Neurobiol *36*, 249–266.

Geng, X., Speirs, C., Lagutin, O., Inbal, A., Liu, W., Solnica-Krezel, L., Jeong, Y., Epstein, D.J., and Oliver, G. (2008). Haploinsufficiency of Six3 Fails to Activate Sonic hedgehog Expression in the Ventral Forebrain and Causes Holoprosencephaly. Dev. Cell *15*, 236–247.

Gleeson, J.G., Peter T, L., Flanagan, L.A., and Walsh, C.A. (1999). Doublecortin is a microtubule-associated protein and is expressed widely by migrating neurons. Neuron *23*, 257–271.

Gokhale, P.J., Au-Young, J.K., Dadi, S.V., Keys, D.N., Harrison, N.J., Jones, M., Soneji, S., Enver, T., Sherlock, J.K., and Andrews, P.W. (2015). Culture adaptation alters transcriptional hierarchies among single human embryonic stem cells reflecting altered patterns of differentiation. PLoS One *10*, 1–13.

Goldman, S. a, and Nottebohm, F. (1983). Neuronal production, migration, and differentiation in a vocal control nucleus of the adult female canary brain. Proc. Natl. Acad. Sci. U. S. A. *80*, 2390–2394.

Goodman, T., and Hajihosseini, M.K. (2015). Hypothalamic tanycytes — masters and servants of metabolic, neuroendocrine, and neurogenic functions. Front. Neurosci. *9*, 1–9.

Górka, B., Skubis-Zegadło, J., Mikula, M., Bardadin, K., Paliczka, E., and Czarnocka, B. (2007). NrCAM, a neuronal system cell-adhesion molecule, is induced in papillary thyroid carcinomas. Br. J. Cancer *97*, 531–538.

Gouazé, A., Brenachot, X., Rigault, C., Krezymon, A., Rauch, C., Nédélec, E., Lemoine, A., Gascuel, J., Bauer, S., Pénicaud, L., et al. (2013). Cerebral Cell Renewal in Adult Mice Controls the Onset of Obesity. PLoS One *8*.

Gould, E. (2007). How widespread is adult neurogenesis in mammals? Nat. Rev. Neurosci. *8*, 481–488.

Gulisano, W., Bizzoca, A., Gennarini, G., Palmeri, A., and Puzzo, D. (2017). Role of the adhesion molecule F3/Contactin in synaptic plasticity and memory. Mol. Cell. Neurosci. *81*, 64–71.

Haan, N., Goodman, T., Najdi-samiei, A., Stratford, C.M., Rice, R., Agha, E. El, Bellusci, S., and Hajihosseini, M.K. (2013). Fgf10-Expressing Tanycytes Add New Neurons to the Appetite/Energy-Balance Regulating Centers of the Postnatal and Adult Hypothalamus. J. Neurosci. *33*, 6170–6180.

Hahn, T.M., Breininger, J.F., Baskin, D.G., and Schwartz, M.W. (1998). Coexpression of Agrp and NPY in fasting-activated hypothalamic neurons. Nat. Neurosci. *1*, 271–272.

Hajihosseini, M.K., Langhe, S. De, Lana-Elola, E., Morrison, H., Sparshott, N., Kelly, R., Sharpe, J., Rice, D., and Bellusci, S. (2008). Localization and fate of Fgf10-expressing cells in the adult mouse brain implicate Fgf10 in control of neurogenesis. Mol. Cell. Neurosci. *37*, 857–868.

Hall, P.E., Lathia, J.D., Miller, N.G.A., Caldwell, M.A., and Ffrench-Constant, C. (2006). Integrins are markers of human neural stem cells. Stem Cells *24*, 2078–

2084.

Hans, F., and Dimitrov, S. (2001). Histone H3 phosphorylation and cell division. Oncogene *20*, 3021–3027.

Haubst, N., Georges-labouesse, E., Arcangelis, A. De, Mayer, U., and Götz, M. (2006). Basement membrane attachment is dispensable for radial glial cell fate and for proliferation , but affects positioning of neuronal subtypes. Development *133*, 3245–3254.

Hendrickson, M.L., Zutshi, I., Wield, A., and Kalil, R.E. (2018). Nestin expression and in vivo proliferative potential of tanycytes and ependymal cells lining the walls of the third ventricle in the adult rat brain. Eur. J. Neurosci. *47*, 284–293.

Hendzel, M.J., Wei, Y., Mancini, M.A., Van Hooser, A., Ranalli, T., Brinkley, B.R., Bazett-Jones, D.P., and Allis, C.D. (1997). Mitosis-specific phosphorylation of histone H3 initiates primarily within pericentromeric heterochromatin during G2 and spreads in an ordered fashion coincident with mitotic chromosome condensation. Chromosoma *106*, 348–360.

Herron, L.R., Hill, M., Davey, F., and Gunn-Moore, F.J. (2009). The intracellular interactions of the L1 family of cell adhesion molecules. Biochem. J. *419*, 519–531.

Heyden, A., Angenstein, F., Sallaz, M., Seidenbecher, C., and Montag, D. (2008). Abnormal Axonal Guidance And Brain Anatomy In Mouse Mutants For The Cell Recognition Molecules Close Homolog Of L1 And Ngcam-Related Cell Adhesion Molecule. Neuroscience *155*, 221–233.

Hill, A.S., Sahay, A., and Hen, R. (2015). Increasing Adult Hippocampal Neurogenesis is Sufficient to Reduce Anxiety and Depression-Like Behaviors. Neuropsychopharmacology *40*, 2368–2378.

Hiney, J.K., Srivastava, V., Nyberg, C.L., Ojeda, S.R., and Dees, W.L. (1996). Insulin-Like Growth Factor I of Peripheral Origin Acts Centrally to Accelerate the Initiation of Feamle Puberty. Endocrinology *137*.

Holmes, A.P., Wong, S.Q., Pulix, M., Johnson, K., Horton, N.S., Thomas, P.,

Magalhães, J.P. De, and Plagge, A. (2016). Reductions in hypothalamic Gfap expression, glial cells and α-tanycytes in lean and hypermetabolic Gnasxl - deficient mice. Mol. Brain *9*, 1–13.

Hu, Q.D., Ang, B.T., Karsak, M., Hu, W.P., Cui, X.Y., Duka, T., Takeda, Y., Chia, W., Sankar, N., Ng, Y.K., et al. (2003). F3/contactin acts as a functional ligand for notch during oligodendrocyte maturation. Cell *115*, 163–175.

Hynes, R.O. (2002). Integrins: Bidirectional, allosteric signaling machines. Cell *110*, 673–687.

Ishiguro, H., Liu, Q., Gong, J., Hall, F.S., Ujike, H., Morales, M., Sakurai, T., Grumet, M., and Uhl, G.R. (2006). NrCAM in Addiction Vulnerability : Positional Cloning , and Altered Drug Reward in Knockout Mice. 572–584.

J. Everitt, B., Meister, B., Hökfelt, T., Melander, T., Terenius, L., Rökaeus, Å., Theodorsson-Norheim, E., Dockray, G., Edwardson, J., Cuello, C., et al. (1986). The hypothalamic arcuate nucleus-median eminence complex: Immunohistochemistry of transmitters, peptides and DARPP-32 with special reference to coexistence in dopamine neurons. Brain Res. Rev. *11*, 97–155.

Jeong, Y., Leskow, F.C., El-Jaick, K., Roessler, E., Muenke, M., Yocum, A., Dubourg, C., Li, X., Geng, X., Oliver, G., et al. (2008). Regulation of a remote Shh forebrain enhancer by the Six3 homeoprotein. Nat. Genet. *40*, 1348–1353.

Jin, Z., Kirilly, D., Weng, C., Kawase, E., Song, X., Smith, S., and Schwartz, J. (2008). Article Differentiation-Defective Stem Cells Outcompete Normal Stem Cells for Niche Occupancy in the Drosophila Ovary. Cell Stem Cell *2*, 39–49.

Junghans, D., Hack, I., Frotscher, M., Taylor, V., and Kemler, R. (2005). β-Catenin – Mediated Cell-Adhesion Is Vital for Embryonic Forebrain Development. Dev. Dyn. 528–539.

Kadowaki, M., Nakamura, S., Machon, O., Krauss, S., Radice, G.L., and Takeichi, M. (2007). N-cadherin mediates cortical organization in the mouse brain. Dev. Biol. *304*, 22–33.

Kamiguchi, H., Long, K.E., Pendergast, M., Schaefer, A.W., Rapoport, I., Kirchhausen, T., and Lemmon, V. (1998). The Neural Cell Adhesion Molecule

L1 Interacts with the AP-2 Adaptor and Is Endocytosed via the Clathrin-Mediated Pathway. J. Neurosci. *18*, 5311–5321.

Katidou, M., Vidaki, M., Strigini, M., and Karagogeos, D. (2008). The immunoglobulin superfamily of neuronal cell adhesion molecules : Lessons from animal models and correlation with human disease. 1564–1580.

Kiselyov, V. V., Soroka, V., Berezin, V., and Bock, E. (2005). Structural biology of NCAM homophilic binding and activation of FGFR. J. Neurochem. *94*, 1169–1179.

Kobayashi, D., Kobayashi, M., Matsumoto, K., Ogura, T., and Nakafuku, M. (2002). Early subdivisions in the neural plate define distinct competence for inductive signals. Development *129*, 83–93.

Kokoeva, M. V, Yin, H., Flier, J.S., and Balance, E. (2005). Neurogenesis in the hypothalamus of adult mice: potential role in energy balance. Science *310*, 679–683.

Kokoeva, M. V, Yin, H., and Flier, J.S. (2007). Evidence for Constitutive Neural Cell Proliferation in the Adult Murine Hypothalamus. J. Comp. Neurol. *505*, 209–220.

Koopman, A.C.M., Taziaux, M., and Bakker, J. (2017). Age-related changes in the morphology of tanycytes in the human female infundibular nucleus/median eminence. J. Neuroendocrinol. *29*, 1–9.

Kosodo, Y., Ro, K., Marzesco, A., Corbeil, D., and Huttner, W.B. (2004). Asymmetric distribution of the apical plasma membrane during neurogenic divisions of mammalian neuroepithelial cells. EMBO J. *23*, 2314–2324.

Kuhn, H., Dickinson-Anson, H., and Gage, F. (1996). Neurogenesis in the dentate gyrus of the adult rat: age-related decrease of neuronal progenitor proliferation. J. Neurosci. *16*, 2027–2033.

Kulahin, N., Li, S., Hinsby, A., Kiselyov, V., Berezin, V., and Bock, E. (2008). Fibronectin type III (FN3) modules of the neuronal cell adhesion molecule L1 interact directly with the fibroblast growth factor (FGF) receptor. Mol. Cell. Neurosci. *37*, 528–536.

Kunz, S., Spirig, M., Ginsburg, C., Buchstaller, A., Berger, P., Lanz, R., Rader, C., Vogt, L., Kunz, B., and Sonderegger, P. (1998). Neurite Fasciculation Mediated by Complexes of Axonin-1 and Ng Cell Adhesion Molecule. J. Cell Biol. *143*, 1673–1690.

Lagutin, O. V., Zhu, C.C., Kobayashi, D., Topczewski, J., Shimamura, K., Puelles, L., Russell, H.R.C., McKinnon, P.J., Solnica-Krezel, L., and Oliver, G. (2003). Six3 repression of Wnt signaling in the anterior neuroectoderm is essential for vertebrate forebrain development. Genes Dev. *17*, 368–379.

Langlet, F., Mullier, A., Bouret, S.G., Prevot, V., and Dehouck, B. (2013a). Tanycyte-like cells form a blood-cerebrospinal fluid barrier in the circumventricular organs of the mouse brain. J. Comp. Neurol. *521*, 3389–3405.

Langlet, F., Levin, B.E., Luquet, S., Mazzone, M., and Messina, A. (2013b). Tanycytic VEGF-A Boosts Blood-Hypothalamus Barrier Plasticity and Access of Metabolic Signals to the Arcuate Nucleus in Response to Fasting. Cell Metab. *17*, 607–617.

Lavado, A., Lagutin, O. V., and Oliver, G. (2008). Six3 inactivation causes progressive caudalization and aberrant patterning of the mammalian diencephalon. Development *135*, 441–450.

Lee, D.A., Bedont, J.L., Pak, T., Wang, H., Song, J., Miranda-Angulo, A., Takiar, V., Charubhumi, V., Balordi, F., Takebayashi, H., et al. (2012). Tanycytes of the hypothalamic median eminence form a diet-responsive neurogenic niche. Nat. Neurosci. *15*, 700–702.

Lee, D.A., Yoo, S., Pak, T., Salvatierra, J., Velarde, E., Aja, S., and Blackshaw, S. (2014). Dietary and sex-specific factors regulate hypothalamic neurogenesis in young adult mice. Front. Neurosci. *8*, 1–11.

Lee, J.E., Wu, S.-F., Goering, L.M., and Dorsky, R.I. (2006). Canonical Wnt signaling through Lef1 is required for hypothalamic neurogenesis. Development *133*, 4451–4461.

Li, L., and Xie, T. (2005). Stem Cell Niche: Structure and Function. Annu. Rev. Cell Dev. Biol. *21*, 605–631.

Li, J., Tang, Y., and Cai, D. (2012). IKK β / NF- κ B disrupts adult hypothalamic neural stem cells to mediate a neurodegenerative mechanism of dietary obesity and pre-diabetes. Nat. Cell Biol. *14*, 999–1012.

Lin, S., Storlien, L.H., and Huang, X.F. (2000). Leptin receptor, NPY, POMC mRNA expression in the diet-induced obese mouse brain. Brain Res. *875*, 89–95.

Lois, C., and Alvarez-Buylla, A. (1993). Proliferating subventricular zone cells in the adult mammalian forebrain can differentiate into neurons and glia. Proc. Natl. Acad. Sci. U. S. A. *90*, 2074–2077.

Lois, C., and Alvarez-Buylla, A. (1994). Long-distance neuronal migration in the adult mammalian brain. Sci. (New York, NY) *264*, 1145–1148.

Lomet, D., Cognié, J., Chesneau, D., Dubois, E., Hazlerigg, D., and Dardente, H. (2018). The impact of thyroid hormone in seasonal breeding has a restricted transcriptional signature. Cell. Mol. Life Sci. *75*, 905–919.

Loulier, K., Lathia, J.D., Marthiens, V., Relucio, J., Mughal, M.R., Tang, C., Coksaygan, T., Hall, P.E., Chigurupati, S., Patton, B., et al. (2009). β1 Integrin Maintains Integrity of the Embryonic Neocortical Stem Cell Niche. PLoS Biol. *7*.

Lu, F., Kar, D., Gruenig, N., Zhang, Z.W., Cousins, N., Rodgers, H.M., Swindell, E.C., Jamrich, M., Schuurmans, C., Mathers, P.H., et al. (2013). Rax is a selector gene for mediobasal hypothalamic cell types. J. Neurosci. *33*, 259–272.

Lustig, M., Zanazzi, G., Sakurai, T., Blanco, C., Levinson, S.R., Lambert, S., Grumet, M., and Salzer, J.L. (2001a). Nr-CAM and neurofascin interactions regulate ankyrin G and sodium channel clustering at the node of Ranvier. Curr. Biol. *11*, 1864–1869.

Lustig, M., Erskine, L., Mason, C.A., Grumet, M., and Sakurai, T. (2001b). Nr-CAM expression in the developing mouse nervous system: Ventral midline structures, specific fiber tracts, and neuropilar regions. J. Comp. Neurol. *434*, 13–28.

Ma, M.S., Brouwer, N., Wesseling, E., Raj, D., van der Want, J., Boddeke, E., Balasubramaniyan, V., and Copray, S. (2015). Multipotent stem cell factor

UGS148 is a marker for tanycytes in the adult hypothalamus. Mol. Cell. Neurosci. *65*, 21–30.

Maness, P.F., and Schachner, M. (2007). Neural recognition molecules of the immunoglobulin superfamily: signaling transducers of axon guidance and neuronal migration. Nat. Neurosci. *10*, 19–26.

Manning, L., Ohyama, K., Saeger, B., Hatano, O., Wilson, S.A., Logan, M., and Placzek, M. (2006). Regional Morphogenesis in the Hypothalamus: A BMP-Tbx2 Pathway Coordinates Fate and Proliferation through Shh Downregulation. Dev. Cell *11*, 873–885.

Marin, F., Herrero, M.T., Vyas, S., and Puelles, L. (2005). Ontogeny of tyrosine hydroxylase mRNA expression in mid- and forebrain: Neuromeric pattern and novel positive regions. Dev. Dyn. *234*, 709–717.

Marthiens, V., and Ffrench-Constant, C. (2009). Adherens junction domains are split by asymmetric division of embryonic neural stem cells. EMBO Rep. *10*, 515–520.

Marthiens, V., Kazanis, I., Moss, L., Long, K., and Ffrench-Constant, C. (2010). Adhesion molecules in the stem cell niche--more than just staying in shape? J. Cell Sci. *123*, 1613–1622.

Martinez-Ferre, A., Navarro-Garberi, M., Bueno, C., and Martinez, S. (2013). Wnt Signal Specifies the Intrathalamic Limit and Its Organizer Properties by Regulating Shh Induction in the Alar Plate. J. Neurosci. *33*, 3967–3980.

Matsuzaki, K., and Katakura, M. (2009). Proliferation of neuronal progenitor cells and neuronal differentiation in the hypothalamus are enhanced in heat-acclimated rats. Integr. Physiol. *458*, 661–673.

Matsuzaki, K., Katakura, M., Sugimoto, N., Hara, T., Hashimoto, M., and Shido, O. (2017). Neural progenitor cell proliferation in the hypothalamus is involved in acquired heat tolerance in long-term heat-acclimated rats. PLoS Genet. 1–16.

McNay, D.E.G., Briançon, N., Kokoeva, M., Maratos-flier, E., and Flier, J.S. (2012). Remodeling of the arcuate nucleus energy- balance circuit is inhibited in obese mice. J. Clin. Invest. *122*, 142–152.

Meister, B., Hökfelt, T., Vale, W., Sawchenko, P., Swanson, L., and Goldstein, M. (1986). Coexistence of tyrosine hydroxylase and growth hormone-releasing factor in a subpopulation of tubero-infundibular neurons of the rat. Neuroendocrinology *42*, 237–247.

Messina, A., and Giacobini, P. (2013). Semaphorin signaling in the development and function of the gonadotropin hormone-releasing hormone system. Front. Endocrinol. (Lausanne). *4*, 1–12.

Migaud, M., Batailler, M., Pillon, D., Franceschini, I., and Malpaux, B. (2011). Seasonal changes in cell proliferation in the adult sheep brain and pars tuberalis. J. Biol. Rhythms *26*, 486–496.

Migaud, M., Butrille, L., and Batailler, M. (2015). Seasonal regulation of structural plasticity and neurogenesis in the adult mammalian brain: Focus on the sheep hypothalamus. Front. Neuroendocrinol. *37*, 146–157.

Millhouse, O.E. (1971). A Golgi study of third ventricle tanycytes in the adult rodent brain. Zeitschrift Für Zellforsch. Und Mikroskopische Anat. *121*, 1–13.

Millington, G.W. (2007). The role of proopiomelanocortin (POMC) neurones in feeding behaviour. Nutr. Metab. (Lond). *4*, 18.

Ming, G.-L., and Song, H. (2011). Adult neurogenesis in the mammalian brain: significant answers and significant questions. Neuron *70*, 687–702.

Miranda-Angulo, A.L., Byerly, M.S., Mesa, J., Wang, H., and Blackshaw, S. (2014). Rax regulates hypothalamic tanycyte differentiation and barrier function in mice. J. Comp. Neurol. *522*, 876–899.

Mirzadeh, Z., Kusne, Y., Duran-Moreno, M., Cabrales, E., Gil-Perotin, S., Ortiz, C., Chen, B., Garcia-Verdugo, J.M., Sanai, N., and Alvarez-Buylla, A. (2017). Bi- and uniciliated ependymal cells define continuous floor-plate-derived tanycytic territories. Nat. Commun. *8*, 13759.

Moraes, J.C., Coope, A., Morari, J., Cintra, D.E., Roman, E.A., Pauli, J.R., Romanatto, T., Carvalheira, J.B., Oliveira, A.L.R., Saad, M.J., et al. (2009). High-fat diet induces apoptosis of hypothalamic neurons. PLoS One *4*.

Moré, M.I., Kirsch, F., and Rathjen, F.G. (2001). Targeted ablation of NrCAM or ankyrin-B results in disorganized lens fibers leading to cataract formation. J. Cell Biol. *154*, 187–196.

Mukouyama, Y. -s., Deneen, B., Lukaszewicz, A., Novitch, B.G., Wichterle, H., Jessell, T.M., and Anderson, D.J. (2006). Olig2+ neuroepithelial motoneuron progenitors are not multipotent stem cells in vivo. Proc. Natl. Acad. Sci. *103*, 1551–1556.

Mullier, A., Bouret, S.G., and Prevot, V. (2010). Differential Distribution of Tight Junction Proteins Suggests a Role for Tanycytes in Blood-Hypothalamus Barrier Regulation in the Adult Mouse Brain. J. Comp. Neurol. *518*, 943–962.

Muthu, V., Eachus, H., Ellis, P., Brown, S., and Placzek, M. (2016). Rx3 and Shh direct anisotropic growth and specification in the zebrafish tuberal / anterior hypothalamus. Development *143*, 2651–2663.

Nascimento, L.F.R., Souza, G.F.P., Morari, J., Barbosa, G.O., Solon, C., Moura, R.F., Victório, S.C., Ignácio-Souza, L.M., Razolli, D.S., Carvalho, H.F., et al. (2016). N-3 fatty acids induce neurogenesis of predominantly POMC-expressing cells in the hypothalamus. Diabetes *65*, 673–686.

Neuwelt, E.A., Bauer, B., Fahlke, C., Fricker, G., Donnell, M.E.O., Povlishock, J.T., Saunders, N.R., Sharp, F., Stanimirovic, D., Watts, R.J., et al. (2011). Engaging neuroscience to advance translational research in brain barrier biology. Nat. Rev. Neurosci. *12*, 169–182.

Newman, E.A., Kim, D.W., Wan, J., Wang, J., Qian, J., and Blackshaw, S. (2018). Foxd1 is required for terminal differentiation of anterior hypothalamic neuronal subtypes. Dev. Biol. *439*, 102–111.

Niwa, A., Nishibori, M., Hamasaki, S., Kobori, T., Liu, K., Wake, H., Mori, S., Yoshino, T., and Takahashi, H. (2016). Voluntary exercise induces neurogenesis in the hypothalamus and ependymal lining of the third ventricle. Brain Struct. Funct. *221*, 1653–1666.

Noctor, S.C., Flint, A.C., Weissman, T.A., Dammerman, R.S., and Kriegstein, A.R. (2001). Neurons derived from radial glial cells establish radial units in

neocortex. Lett. to Nat. *409*, 714–720.

Norsted, E., Gömüç, B., and Meister, B. (2008). Protein components of the blood-brain barrier (BBB) in the mediobasal hypothalamus. J. Chem. Neuroanat. *36*, 107–121.

Nottebohm, F. (1980). Testosterone triggers growth of brain vocal control nuclei in adult female canaries. Brain Res. *189*, 429–436.

O'Reilly, A.M., Lee, H., and Simon, M.A. (2008). Integrins control the positioning and proliferation of follicle stem cells in the. J. Cell Biol. *182*, 801–815.

Ohyama, K., Ellis, P., Kimura, S., and Placzek, M. (2005). Directed differentiation of neural cells to hypothalamic dopaminergic neurons. Development *132*, 5185–5197.

Ohyama, K., Das, R., and Placzek, M. (2008). Temporal progression of hypothalamic patterning by a dual action of BMP. Development *135*, 3325–3331.

Okamoto, M., Namba, T., Shinoda, T., Kondo, T., Watanabe, T., Inoue, Y., Takeuchi, K., Enomoto, Y., Ota, K., Oda, K., et al. (2013). TAG-1-assisted progenitor elongation streamlines nuclear migration to optimize subapical crowding. Nat. Neurosci. *16*, 1556–1566.

Oliver, G., Mailhos, A., Wehr, R., Copeland, N.G., Jenkins, N.A., and Gruss, P. (1995). Six3 , a murine homologue of the sine oculis gene , demarcates the most anterior border of the developing neural plate and is expressed during eye development. Development *121*, 4045–4055.

Orquera, D.P., Low, M.J., Rubinstein, M., and de Souza, F.S.J. (2016). Essential function of the transcription factor Rax in the early patterning of the mammalian hypothalamus. Dev. Biol. *416*, 212–224.

Palmer, T.D., Takahashi, J., and Gage, F.H. (1997). The adult rat hippocampus contains primordial neural stem cells. Mol. Cell. Neurosci. *8*, 389–404.

Palmer, T.D., Willhoite, A.R., and Gage, F.H. (2000). Vascular niche for adult hippocampal neurogenesis. J. Comp. Neurol. *425*, 479–494.

Park, D., Xiang, A.P., Zhang, L., Mao, F.F., Walton, N.M., Choi, S.S., and Lahn, B.T. (2009). The radial glia antibody RC2 recognizes a protein encoded by Nestin. Biochem. Biophys. Res. Commun. *382*, 588–592.

Park, D., Xiang, A.P., Mao, F.F., Zhang, L., Di, C.G., Liu, X.M., Shao, Y., Ma, B.F., Lee, J.H., Ha, K.S., et al. (2010). Nestin is required for the proper self-renewal of neural stem cells. Stem Cells *28*, 2162–2171.

Parkash, J., Messina, A., Langlet, F., Cimino, I., Loyens, A., Mazur, D., Gallet, S., Balland, E., Malone, S.A., Pralong, F., et al. (2015). Semaphorin7A regulates neuroglial plasticity in the adult hypothalamic median eminence. Nat. Commun. *6*, 6385.

Pearson, C.A., Ohyama, K., Manning, L., Aghamohammadzadeh, S., Sang, H., and Placzek, M. (2011). FGF-dependent midline-derived progenitor cells in hypothalamic infundibular development. Development *138*, 2613–2624.

Pegram, C.N., Eng, L.F., Wikstrand, C.J., McComb, R.D., Lee, Y.-L., and Bigner, D.D. (1983). Monoclonal antibodies reactive with epitopes restricted to glial fibrillary acidic proteins of several species. Neurochem. Pathol. *3*, 119–138.

Pellegrino, G., Trubert, C., Terrien, J., Pifferi, F., Leroy, D., Loyens, A., Migaud, M., Baroncini, M., Maurage, C.-A., Fontaine, C., et al. (2017). A comparative study of the neural stem cell niche in the adult hypothalamus of human, mouse, rat and grey mouse lemur (Microcebus murinus). J. Comp. Neurol. 1419–1443.

Pencea, V., Bingaman, K.D., Wiegand, S.J., and Luskin, M.B. (2001). Infusion of brain-derived neurotrophic factor into the lateral ventricle of the adult rat leads to new neurons in the parenchyma of the striatum, septum, thalamus, and hypothalamus. J. Neurosci. *21*, 6706–6717.

Pérez-Martín, M., Cifuentes, M., Grondona, J.M., López-Ávalos, M.D., Gómez-Pinedo, U., García-Verdugo, J.M., and Fernández-Llebrez, P. (2010). IGF-I stimulates neurogenesis in the hypothalamus of adult rats. Eur. J. Neurosci. *31*, 1533–1548.

Peruzzo, B., Pastor, F.E., Blázquez, J.L., Schöbitz, K., Peláez, B., Amat, P., and Rodríguez, E.M. (2000). A second look at the barriers of the medial basal

hypothalamus. Exp. Brain Res. *132*, 10–26.

Pierce, A. a, and Xu, A.W. (2010). De novo neurogenesis in adult hypothalamus as a compensatory mechanism to regulate energy balance. J. Neurosci. *30*, 723–730.

Pilz, G., Bottes, S., Betizeau, M., Jörg, D.J., Carta, S., Simons, B.D., Helmchen, F., and Jessberger, S. (2018). Live imaging of neurogenesis in the adult mouse hippocampus. Science (80-.). *359*, 658–662.

Placzek, M., and Dale, K. (1999). Tissue Recombinations in Collagen Gels. In: Sharpe P.T., Mason I. (eds) Molecular Embryology. Methods in Molecular Biology™. Sharpe P.T., Mason I. Mol. Embryol. Methods Mol. Biol. *97*.

Placzek, M., Jessell, T.M., and Dodd, J. (1993). Induction of floor plate differentiation by contact-dependent , homeogenetic signals. Development *117*, 205–218.

Prevot, V., Bouret, S., Croix, D., Takumi, T., Jennes, L., Mitchell, V., Beauvillain, J., Inserm, U., and Cedex, L. (2000). Evidence That Members of the TGF b Superfamily Play a Role in Regulation of the GnRH Neuroendocrine Axis : Expression of a Type I Serine – Threonine Kinase Receptor for TGF b and Activin in GnRH Neurones and Hypothalamic Areas of the Female Rat. J. Neuroendocrinol. *12*, 665–670.

Prevot, V., Cornea, A., Mungenast, A., Smiley, G., and Ojeda, S.R. (2003). Activation of erbB-1 Signaling in Tanycytes of the Median Eminence Stimulates Transforming Growth Factor 1 Release via Prostaglandin E 2 Production and Induces Cell Plasticity. J. Neurosci. *23*, 10622–10632.

Prevot, V., Hanchate, N.K., Bellefontaine, N., Sharif, A., Parkash, J., Estrella, C., Allet, C., de Seranno, S., Campagne, C., d'Anglemont de Tassigny, X., et al. (2010). Function-related structural plasticity of the GnRH system. A role for neuronal-glial-endothelial interactions. Front. Neuroendocrinol. *31*, 241–258.

Prevot, V., Dehouck, B., Sharif, A., Ciofi, P., Giacobini, P., and Clasadonte, J. (2018). The versatile tanycyte: a hypothalamic integrator of reproduction and energy metabolism. Endocr. Rev. 333–368.

Puelles, L., and Verney, C. (1998). Early neuromeric distribution of tyrosine-hydroxylase-immunoreactive neurons in human embryos. J. Comp. Neurol. *394*, 283–308.

Puzzo, D., Bizzoca, A., Privitera, L., Furnari, D., Giunta, S., Girolamo, F., Pinto, M., Gennarini, G., and Palmeri, A. (2013). F3/Contactin promotes hippocampal neurogenesis, synaptic plasticity, and memory in adult mice. Hippocampus *23*, 1367–1382.

Puzzo, D., Bizzoca, A., Loreto, C., Guida, C. a., Gulisano, W., Frasca, G., Bellomo, M., Castorina, S., Gennarini, G., and Palmeri, A. (2015). Role of F3/contactin expression profile in synaptic plasticity and memory in aged mice. Neurobiol. Aging *36*, 1702–1715.

Radakovits, R., Barros, C.S., Belvindrah, R., Patton, B., and Mu, U. (2009). Regulation of Radial Glial Survival by Signals from the Meninges. J. Neurosci. *29*, 7694–7705.

Ratié, L., Ware, M., Barloy-hubler, F., Romé, H., Gicquel, I., Dubourg, C., David, V., and Dupé, V. (2013). Novel genes upregulated when NOTCH signalling is disrupted during hypothalamic development Novel genes upregulated when NOTCH signalling is disrupted during hypothalamic development. Neural Dev. *8*, e1-13.

Ray, J., Peterson, D. a, Schinstine, M., and Gage, F.H. (1993). Proliferation, differentiation, and long-term culture of primary hippocampal neurons. Proc. Natl. Acad. Sci. U. S. A. *90*, 3602–3606.

Reddy, A.B., Cronin, A.S., Ford, H., and Ebling, F.J.P. (1999). Seasonal regulation of food intake and body weight in the male Siberian hamster: Studies of hypothalamic orexin (hypocretin), neuropeptide Y (NPY) and pro-opiomelanocortin (POMC). Eur. J. Neurosci. *11*, 3255–3264.

Reynolds, B.A., and Rietze, R.L. (2005). Neural stem cells and neurospheres - Re-evaluating the relationship. Nat. Methods *2*, 333–336.

Reynolds, B.A., and Weiss, S. (1992). Generation of neurons and astrocytes from isolated cells of the adult mammalian central nervous system. Science (80-

.). *255*, 1707–1710.

Richards, L.J., Kilpatrick, T.J., and Bartlett, P.F. (1992). De novo generation of neuronal cells from the adult mouse brain. Proc. Natl. Acad. Sci. U. S. A. *89*, 8591–8595.

Robins, S.C., Stewart, I., McNay, D.E., Taylor, V., Giachino, C., Goetz, M., Ninkovic, J., Briancon, N., Maratos-Flier, E., Flier, J.S., et al. (2013a). α-Tanycytes of the adult hypothalamic third ventricle include distinct populations of FGF-responsive neural progenitors. Nat. Commun. *4*, 2049.

Robins, S.C., Trudel, E., Rotondi, O., Liu, X., Djogo, T., Kryzskaya, D., Bourque, C.W., and Kokoeva, M. V (2013b). Evidence for NG2-glia Derived , Adult-Born Functional Neurons in the Hypothalamus. PLoS One *8*.

Rodriguez, E.M., Gonz, C.B., and Delannoy, L. (1979). Cell and Tissue Cellular Organization of the Lateral and Postinfundibular Regions of the Median Eminence in the Rat *. Cell Tissue Res. *408*, 377–408.

Rodríguez, E.M., Blázquez, J.L., Pastor, F.E., Peláez, B., Peña, P., Peruzzo, B., and Amat, P. (2005). Hypothalamic tanycytes: A key component of brain-endocrine interaction. Int. Rev. Cytol. *247*, 89–164.

Rogers, M.C., Silverman, A.J., and Gibson, M.J. (1997). Gonadotropin-releasing hormone axons target the median eminence: In vitro evidence for diffusible chemoattractive signals from the mediobasal hypothalamus. Endocrinology *138*, 3956–3966.

Rougon, G., and Hobert, O. (2003). New insights into the diversity and function of Neuronal Immunoglobulin Superfamily Molecules. Annu. Rev. Neurosci. *26*, 207–238.

Ruxton, C., Reed, S., Simposon, M., and Millington, K. (2007). The health benefits of omega-3 polyunstaurated fatty acids: a review of the evidence. J. Hum. Nutr. Diet. *20*, 275–285.

Sahay, A., and Hen, R. (2007). Adult hippocampal neurogenesis in depression. Nat. Neurosci. *10*, 1110–1115.

Sakurai, T. (2012). The role of NrCAM in neural development and disorders — Beyond a simple glue in the brain. Mol. Cell. Neurosci. *49*, 351–363.

Sakurai, T., Lustig, M., Babiarz, J., Furley, A.J.W., Tait, S., Brophy, P.J., Brown, S.A., Brown, L.Y., Mason, C.A., and Grumet, M. (2001). Overlapping functions of the cell adhesion molecules Nr-CAM and L1 in cerebellar granule cell development. J. Cell Biol. *154*, 1259–1273.

Sakurai, T., Ramoz, N., Reichert, J.G., Corwin, T.E., Kryzak, L., Smith, C.J., Silverman, J.M., Hollander, E., and Buxbaum, J.D. (2006). Association analysis of the NrCAM gene in autism and in subsets of families with severe obsessive – compulsive or self-stimulatory behaviors. 251–257.

Salvatierra, J., Lee, D.A., Zibetti, C., Duran-Moreno, M., Yoo, S., Newman, E.A., Wang, H., Bedont, J.L., de Melo, J., Miranda-Angulo, A.L., et al. (2014). The LIM homeodomain factor Lhx2 is required for hypothalamic tanycyte specification and differentiation. J. Neurosci. *34*, 16809–16820.

Salzer, J.L. (2003). Polairsed Domains of Myelinated Axons. Neuron *40*, 297–318.

Samms, R.J., Lewis, J.E., Lory, A., Fowler, M.J., Cooper, S., Warner, A., Emmerson, P., Adams, A.C., Luckett, J.C., Perkins, A.C., et al. (2015). Antibody-Mediated Inhibition of the FGFR1c Isoform Induces a Catabolic Lean State in Siberian Hamsters. Curr. Biol. *25*, 2997–3003.

Sanchez-Arrones, L., Stern, C.D., Bovolenta, P., and Puelles, L. (2012). Sharpening of the anterior neural border in the chick by rostral endoderm signalling. Development *139*, 1034–1044.

Sanchez, E., Vargas, M.A., Singru, P.S., Pascual, I., Romero, F., Fekete, C., Charli, J.L., and Lechan, R.M. (2009). Tanycyte pyroglutamyl peptidase II contributes to regulation of the hypothalamic-pituitary-thyroid axis through glial-axonal associations in the median eminence. Endocrinology *150*, 2283–2291.

Saper, C.B., and Lowell, B.B. (2014). The hypothalamus. Curr. Biol. *24*, 1111–1116.

Seaberg, R.M., and van der Kooy, D. (2002). Adult rodent neurogenic regions:

the ventricular subependyma contains neural stem cells, but the dentate gyrus contains restricted progenitors. J. Neurosci. *22*, 1784–1793.

Seranno, S. De, Tassigny, A. De, Estrella, C., Loyens, A., Kasparov, S., Ojeda, S.R., Beauvillain, J., and Prevot, V. (2010). Role of Estradiol in the Dynamic Control of Tanycyte Plasticity Mediated by Vascular Endothelial Cells in the Median Eminence. Neuroendocrinology *151*, 1760–1772.

Seri, B., García-Verdugo, J.M., McEwen, B.S., and Alvarez-Buylla, A. (2001). Astrocytes give rise to new neurons in the adult mammalian hippocampus. J. Neurosci. *21*, 7153–7160.

Seri, B., García-Verdugo, J.M., Collado-Morente, L., McEwen, B.S., and Alvarez-Buylla, A. (2004). Cell types, lineage, and architecture of the germinal zone in the adult dentate gyrus. J. Comp. Neurol. *478*, 359–378.

Shimada, M., and Nakamura, T. (1973). Time of neuron origin in mouse hypothalamic nuclei. Exp. Neurol. *41*, 163–173.

Shimogori, T., Lee, D.A., Miranda-Angulo, A., Yang, Y., Wang, H., Jiang, L., Yoshida, A.C., Kataoka, A., Mashiko, H., Avetisyan, M., et al. (2010). A genomic atlas of mouse hypothalamic development. Nat. Neurosci. *13*, 767–775.

Shors, T.J., Miesegaes, G., Beylin, A., Zhao, M., Rydel, T., and Gould, E. (2001). Neurogenesis in the adult is involved in the formation of trace memories. Nature *410*, 372–376.

Sild, M., and Ruthazer, E.S. (2011). Radial Glia: Progenitor, Pathway, and Partner. Neurosci. *17*, 288–302.

Silletti, S., Mei, F., Sheppard, D., and Montgomery, A.M.P. (2000). Plasmin-sensitive Dibasic Sequences in the Third Fibronectin-like Domain of L1 – Cell Adhesion Molecule (CAM) Facilitate Homomultimerization and Concomitant Integrin Recruitment. J. Cell Biol. *149*, 1485–1501.

Silva-Vargas, V., Crouch, E.E., and Doetsch, F. (2013). Adult neural stem cells and their niche: A dynamic duo during homeostasis, regeneration, and aging. Curr. Opin. Neurobiol. *23*, 935–942.

Silva-Vargas, V., Maldonado-Soto, A.R., Mizrak, D., Codega, P., and Doetsch, F. (2016). Age-Dependent Niche Signals from the Choroid Plexus Regulate Adult Neural Stem Cells. Cell Stem Cell *19*, 643–652.

Smith, R.G., Ploeg, L.H.T. Van der, Howard, A.D., Feighner, S.D., Cheng, K., Hickey, G.J., Matthew J. Wyvratt, J., Fisher, M.H., Nargund, R.P., and Patchett, A.A. (1997). Peptidomimetic Regulation of Growth Hormone Secretion. Endocr. Rev. *18*, 621–645.

Song, X., and Xie, T. (2002). DE-cadherin-mediated cell adhesion is essential for maintaining somatic stem cells in the Drosophila ovary. Proc. Natl. Acad. Sci. *99*, 14813–14818.

Song, H., Stevens, C.F., and Gage, F.H. (2002). Astroglia induce neurogenesis from adult neural stem cells. Nature *417*, 39–44.

Suhonen, J.O., Peterson, D.A., Ray, J., and Gage, F.H. (1996). Differentiation of adult hippocampus-derived progenitors into olfactory neurons in vivo. Lett. to Nat. *383*, 624–627.

Szilvásy-Szabó, A., Varga, E., Beliczai, Z., Lechan, R.M., and Fekete, C. (2017). Localization of connexin 43 gap junctions and hemichannels in tanycytes of adult mice. Brain Res. *1673*, 64–71.

Tamamaki, N., Nakamura, K., Okamoto, K., and Kaneko, T. (2001). Radial glia is a progenitor of neocortical neurons in the developing cerebral cortex. Neurosci. Res. *41*, 51–60.

Tanentzapf, G., Devenport, D., Godt, D., and Brown, N.H. (2007). Integrin-dependent anchoring of a stem-cell niche. Nat. Cell Biol. *9*.

Tompkins, M.M., Basgall, E.J., Zamrini, E., and Hill, W.D. (1997). Apoptotic-like changes in Lewy-body-associated disorders and normal aging in substantia nigral neurons. Am. J. Pathol. *150*, 119–131.

Traiffort, E., and Charytoniuk, D. (1999). Discrete Localization of Hedgehog Signalling Components in the Developing and Adult Rat Nervous System. Eur. J. … *11*, 3199–3214.

Trowe, M., Zhao, L., Weiss, A., Christoffels, V., Epstein, D.J., and Kispert, A. (2013). Inhibition of Sox2-dependent activation of Shh in the ventral diencephalon by Tbx3 is required for formation of the neurohypophysis. Development *140*, 2299–2309.

Tsuchida, T., Ensini, M., Morton, S.B., Baldassare, M., Edlund, T., Jessell, T.M., and Pfaff, S.L. (1994). Topographic organization of embryonic motor neurons defined by expression of LIM homeobox genes. Cell *79*, 957–970.

Wang, X., Kopinke, D., Lin, J., McPherson, A.D., Duncan, R.N., Otsuna, H., Moro, E., Hoshijima, K., Grunwald, D.J., Argenton, F., et al. (2012). Wnt Signaling Regulates Postembryonic Hypothalamic Progenitor Differentiation. Dev. Cell *23*, 624–636.

Wataya, T., Ando, S., Muguruma, K., Ikeda, H., Watanabe, K., Eiraku, M., Kawada, M., Takahashi, J., Hashimoto, N., and Sasai, Y. (2008). Minimization of exogenous signals in ES cell culture induces rostral hypothalamic differentiation. Proc. Natl. Acad. Sci. *105*, 11796–11801.

Wei, L.C., Shi, M., Chen, L.W., Cao, R., Zhang, P., and Chan, Y.S. (2002). Nestin-containing cells express glial fibrillary acidic protein in the proliferative regions of central nervous system of postnatal developing and adult mice. Dev. Brain Res. *139*, 9–17.

Wei, Y., Mizzen, C.A., Cook, R.G., Gorovsky, M.A., and Allis, C.D. (1998). Phosphorylation of histone H3 at serine 10 is correlated with chromosome condensation during mitosis and meiosis in Tetrahymena. Proc. Natl. Acad. Sci. *95*, 7480–7484.

Xenaki, D., Martin, I.B., Yoshida, L., Ohyama, K., Gennarini, G., Grumet, M., Sakurai, T., and Furley, A.J.W. (2011). F3/contactin and TAG1 play antagonistic roles in the regulation of sonic hedgehog-induced cerebellar granule neuron progenitor proliferation. Development *138*, 519–529.

Xu, A.W., Kaelin, C.B., Morton, G.J., Ogimoto, K., Stanhope, K., Graham, J., Baskin, D.G., Havel, P., Schwartz, M.W., and Barsh, G.S. (2005a). Effects of hypothalamic neurodegeneration on energy balance. PLoS Biol. *3*, 1–9.

Xu, Q., Cobos, I., De La Cruz, E., Rubenstein, J.L., and Anderson, S. (2004). Origins of Cortical Interneuron Subtypes. J. Neurosci. *24*, 2612–2622.

Xu, Y., Tamamaki, N., Noda, T., Kimura, K., Itokazu, Y., Matsumoto, N., Dezawa, M., and Ide, C. (2005b). Neurogenesis in the ependymal layer of the adult rat 3rd ventricle. Exp. Neurol. *192*, 251–264.

Yamamura, T., Yasuo, S., Hirunagi, K., Ebihara, S., and Yoshimura, T. (2006). T3 implantation mimics photoperiodically reduced encasement of nerve terminals by glial processes in the median eminence of Japanese quail. Cell Tissue Res. *324*, 175–179.

Yamashita, Y.M., Jones, D.L., and Fuller, M.T. (2003). Orientation of Asymmetric Stem Cell Division by the APC Tumor Suppressor and Centrosome. Science (80-.). *301*, 1547–1551.

Yamashita, Y.M., Mahowald, A.P., Perlin, J.R., and Fuller, M.T. (2007). Asymmetric Inheritance of Mother Versus Daughter Centrosome in Stem Cell Division. Science (80-.). *315*, 518–522.

Yan, R.T., Ma, W.X., and Wang, S.Z. (2001). Neurogenin2 Elicits the Genesis of Retinal Neurons From Cultures of Nonneural Cells. Proc. Natl. Acad. Sci. U. S. A. *98*, 15014–15019.

Yee, C.L., Wang, Y., Anderson, S., Ekker, M., and Rubenstein, J.L.R. (2009). Arcuate nucleus expression of NKX2.1 and DLX and lineages expressing these transcription factors in neuropeptide Y+, proopiomelanocortin+, and tyrosine hydroxylase+ neurons in neonatal and adult mice. J. Comp. Neurol. *517*, 37–50.

Yin, W., and Gore, A.C. (2010). The Hypothalamic Median Eminence and its Role in Reproductive Aging. 113–122.

Yoo, S., and Blackshaw, S. (2018). Regulation and function of neurogenesis in the adult mammalian hypothalamus. Prog. Neurobiol. 0–1.

Yulyaningsih, E., Rudenko, I.A., Valdearcos, M., Dahlén, E., Vagena, E., Chan, A., Alvarez-Buylla, A., Vaisse, C., Koliwad, S.K., and Xu, A.W. (2017). Acute Lesioning and Rapid Repair of Hypothalamic Neurons outside the Blood-Brain Barrier. Cell Rep. *19*, 2257–2271.

Zhang, J., Niu, C., Ye, L., Huang, H., He, X., Harris, S., Wiedemann, L.M., Mishina, Y., and Li, L. (2003). Identification of the haematopoietic stem cell niche and control of the niche size. Nature *425*, 0–5.

Zhang, X., Ibrahimi, O.A., Olsen, S.K., Umemori, H., Mohammadi, M., and Ornitz, D.M. (2006). Receptor specificity of the fibroblast growth factor family: The complete mammalian FGF family. J. Biol. Chem. *281*, 15694–15700.

Zhao, L., Zevallos, S.E., Rizzoti, K., Jeong, Y., Lovell-Badge, R., and Epstein, D.J. (2012). Disruption of SoxB1-Dependent Sonic hedgehog Expression in the Hypothalamus Causes Septo-optic Dysplasia. Dev. Cell *22*, 585–596.

Zoli, M., Ferraguti, F., Frasoldati, A., Biagini, G., and Agnati, L.F. (1995). Age-Related Alterations in Tanycytes of the Mediobasal Hypothalamus of the Male Rat. Neurobiol. Aging *16*, 77–83.

Zonta, B., Desmazieres, A., Rinaldi, A., Tait, S., Sherman, D.L., Nolan, M.F., and Brophy, P.J. (2011). Article A Critical Role for Neurofascin in Regulating Action Potential Initiation through Maintenance of the Axon Initial Segment. Neuron *69*, 945–956.